FATIGUE CHARACTERIZATION OF AM60B MAGNESIUM ALLOY SUBJECTED TO CONSTANT AND VARIABLE AMPLITUDE LOADING WITH POSITIVE AND NEGATIVE STRESS RATIOS

by

Morteza Mehrzadi

Submitted in partial fulfilment of the requirements
for the degree of Doctor of Philosophy

at

Dalhousie University
Halifax, Nova Scotia
April 2013

DALHOUSIE UNIVERSITY

DEPARTMENT OF CIVIL AND RESOURCE ENGINEERING

The undersigned hereby certify that they have read and recommend to the Faculty of Graduate Studies for acceptance a thesis entitled "FATIGUE CHARACTERIZATION OF AM60B MAGNESIUM ALLOY SUBJECTED TO CONSTANT AND VARIABLE AMPLITUDE LOADING WITH POSITIVE AND NEGATIVE STRESS RATIOS" by Morteza Mehrzadi in partial fulfilment of the requirements for the degree of Doctor of Philosophy.

Dated: April 22, 2013

External Examiner: ______________________________

Research Supervisor: ______________________________

Examining Committee: ______________________________

____

Departmental Representative: ______________________________

DALHOUSIE UNIVERSITY

DATE: April 22, 2013

AUTHOR: Morteza Mehrzadi

TITLE: FATIGUE CHARACTERIZATION OF AM60B MAGNESIUM ALLOY SUBJECTED TO CONSTANT AND VARIABLE AMPLITUDE LOADING WITH POSITIVE AND NEGATIVE STRESS RATIOS

DEPARTMENT OR SCHOOL: Department of Civil and Resource Engineering

DEGREE: Ph.D. CONVOCATION: October YEAR: 2013

Signature of Author

I dedicate this dissertation to my parents,
Laya and Ebrahim
And to my lovely wife,
Laleh

TABLE OF CONTENTS

LIST OF TABLES

LIST OF FIGURES

ABSTRACT

AM60B magnesium alloy is being increasingly used in auto industry in applications that usually involve various formats of cyclic loading scenarios. Therefore, the fatigue response of this alloy is investigated in this thesis. Our investigation is focused on characterization of the influence of compressive stress cycles within a given cyclic loading scenario on alloy's crack propagation response.

In the first part of this dissertation, fatigue crack growth rate (FCGR) of AM60B alloy subject to cyclic loadings with various stress ratios (both positive and negative) is investigated and a modified model is proposed to predict the FCGR under a wide range of stress ratios. Subsequently, using the modified model, the experimental results of the crack propagation tests are condensed into a single line in a logarithmic scale and the integrity of a proposed FCGR model is investigated. The investigation is continued by studying the influence of compressive stress cycle (CSC) on FCGR. Constant and random amplitude loadings with several magnitudes of CSCs are applied, leading to considerable acceleration in FCGR. The stress distribution ahead of the crack tip is also studied using the finite element method. The tensile residual stress and plastic zone are characterized upon the removal of the CSCs. The acceleration in the crack propagation is shown to be governed by the tensile zone ahead of the crack tip.

Furthermore, application of an overload within an otherwise constant amplitude loading (CAL) has been known to retard the crack propagation, thus increase the fatigue life. This retardation would be a function of the affected zone and retardation magnitude. It is shown in this thesis that the affected zone would be influenced by the "sensitivity" of the material to overload. Moreover, it is also demonstrated that the nature of baseline CAL loading would also affect the retardation response and dimension of the affected zone. Therefore, modification to the Wheeler model is proposed, thereby enabling the model to account for material's sensitivity and nature of the baseline loading. The integrity of the proposed model is verified by the experimental results obtained in this project, as well as those reported by other investigators for other alloys.

ACKNOWLEDGEMENTS

Foremost, it is with immense gratitude that I acknowledge my supervisor, Dr. Farid Taheri for his continuous support and help. This thesis would not have been possible without his guidance and kind advices. I would also like to thank my other supervisory committee members Dr. Koko and Dr. Jarjoura.

This research is financially supported by Auto21 Network of Centers of Excellence, an automotive research and development program. All of the specimens used in our research were provided by Meridian Technologies Inc. (Strathroy, Ontario). All of their supports is gratefully appreciated.

CHAPTER 1 Introduction

1.1 Introduction to AM60B magnesium alloy

Development of magnesium alloys has traditionally been driven by the automobile and light truck industries requirements for lightweight materials to address operations under increasingly demanding conditions. Due to these alloys relatively low density (a quarter that of steel and two thirds that of aluminum), magnesium alloys have been found attractive by automotive engineers and designers. In fact, applications of magnesium alloys in auto industry dates back to early 70s, when the Volkswagen Group of companies and some other manufacturers utilized the alloys in various components. For instance, in 1971, 42000 tons of magnesium alloys was used by Volkswagen [1]. Moreover, the use of magnesium alloys in racing cars was also incepted in 1920.

High-pressure die-casting (HPDC) is an efficient and cost-effective manufacturing process for producing magnesium alloy components. As a result, cast magnesium alloys are finding incremental use in automotive industry due to their high specific strength, lighter weight and excellent castability and machinability. However, to further increase the use of the alloys in various applications, more knowledge about their fracture and fatigue properties and responses should be gained.

The magnesium alloy used in this investigation is AM60B, which is increasingly being used to produce various automotive parts. The Meridian Technologies Inc. (Strathroy, Ontario), which is one of the largest producers of magnesium alloys auto parts in Canada, provided the AM60B alloy used in our investigation. The chemical composition of the alloy is shown in Table 1.1.

Table 1.1 Chemical composition of the AM60B alloy in % weight [2]

Mg	Al	Mn	Si	Zn	Fe	Cu	Ni	Other
Bal.	5.5-6.5	0.25 min	0.1 max	0.22 max	0.005 max	0.01 max	0.002 max	0.003 max (total)

Mechanical response of the alloy could be defined using a bilinear stress-strain curve with properties shown in Table 1.2.

Table 1.2 Mechanical & physical properties of AM60B

Yield stress (σ_y)	150 MPa
Modulus of elasticity (E)	40 GPa
Plastic Modulus (E_T)	2.5 GPa
Density	1800 Kg/m^3

The micro-mechanical properties of the alloy have already been investigated by some researchers. For instance, the mechanical response of the "skin" and "core" sections of AM60B Mg alloy was investigated and reported by Lu et al. [2]. They showed that the microstructures of the alloy varied from the skins to core layer with respect to grain size and porosity ratio. The researchers expanded their work to further study the influence of porosity on fatigue life of the alloy [3]. They showed that pores could act as stress riser and as locations for initiation of cracks. Moreover, they illustrated that the pores' size, shape, configuration and their spatial distance could significantly affect the fatigue life of the alloy.

The influence of temperature on fatigue response of the alloy was subsequently investigated by Nur Hossein and Taheri [4 & 5]. They observed a longer fatigue life at when the alloy was tested at cold temperature and shorter fatigue life when tested at elevated temperature (in comparison to fatigue life evaluated at room temperature). The crack propagation rate of the alloy for a small range of stress ratios [R = 0, 0.1 and 0.2] was also investigated [5], but more investigation is required to include the influence of a wider range of the stress ratios.

In this thesis the fatigue response of the alloy was studied without any emphasis on its micro-mechanical properties.

1.2 Thesis objectives

As mentioned above, the main application of this material is in auto industry where cyclic loading is a dominant type of loading. Therefore, more research in fatigue and fracture properties of the alloy is required. In general, several models have been proposed for predicting the crack growth rate (FCGR) in metals. Nevertheless, as stated earlier, the compressive stress cycles within a cyclic loading are usually dismissed in fatigue life assessment, while as will be demonstrated, they would have significant effect on FCGR.

The main objective of this thesis is therefore the investigation of the influence of the compressive stress cycles (CSC) present within a cyclic loading on crack propagation rate. Beside the fact that all the experimental investigations were carried out on AM60B magnesium alloy, nevertheless, the proposed modifications on FCGR models have also been verified by applying the developed models to other metallic alloys as well, thus verifying the integrity of the models and their applicability to a wide range of metallic alloys.

The objectives and goals of this study could be summarized as;

- To develop a model for predicting crack propagation in the alloy for a wide range of positive and negative stress ratios with a good accuracy.
- To study the influence of CSCs present within a cyclic loading on the alloy’s crack propagation rate.
- To study the stress distribution and plastic deformation ahead of crack tips in order to better understand the physics of crack propagation acceleration due to a compressive underload.
- To study the influence of the interaction of compressive underload within a cyclic loading on crack propagation rate.
- To assess the retardation in crack propagation due to overload and modify a suitable model for predicting the phenomenon more accurately.

- To investigate the retardation response due to applied overload within a baseline constant amplitude loading (CAL) with a negative stress ratio.

1.3 Thesis layout

This dissertation contains eight chapters, including the present chapter, which is the introduction to the project and its main objectives. The second chapter contains some literature reviews on crack propagation, as well as discussion of some basic concepts of fracture mechanics. Several fatigue crack growth (FCG) models are briefly reviewed in chapter two. Our initial attempt to detect the damage in material due to application of cyclic loading is presented in chapter three. In this approach, the degradation of alloy's properties under a cyclic loading up to the fracture stage is assessed by a vibration-based methodology. The natural frequency and damping capacity of fatigue specimen were thereby evaluated. Chapters four to seven are the journal papers compiled based on the results obtained in this project, which are either published or under review for publication.

In chapter four, FCGR of the alloy under constant amplitude loading (CAL), with various stress ratios is investigated. The Paris equation [6] is the most well-known model used for predicting FCGR with respect to the stress intensity factor range, however, the influence of the stress ratio is not considered in that model. Walker [7] proposed his model in 1970 for predicting FCGR under various stress ratios by adding one extra parameter to Paris' model. However, it has been shown experimentally that the model is not capable of doing accurate FCGR prediction for a wide range of stress ratios. This shortfall of the model would be attributed to two fundamental flawed assumptions. Firstly, the negative or compressive portion of a cyclic loading was completely dismissed in the model. Secondly, the slope of the curve (line) of FCGR versus stress intensity factor range plotted on a logarithmic scale was assumed to be identical for all stress ratios. Therefore, Walker's model has been modified so as to condense the scattered FCGR data obtained over a wide range of stress ratios by a single line when plotted in the logarithmic scale. Moreover, the integrity of the modified model was verified by FCGR experimental data of other materials.

The significance of CSCs within constant and random amplitude cyclic loadings is presented in chapter five. In this chapter, several scaled magnitudes of CSCs were applied within both random and constant amplitude loading scenarios and the acceleration in crack propagation rate was studied. An in-depth finite element analysis was also carried out to study the stress distribution ahead of crack tip at various far-field loading stages. The plastic zone dimension was evaluated at the end of the tension and compression loading. A new parameter was defined to better reflect the influence of the compressive portion of a cyclic loading on FCGR. Various FCGR models were used to estimate the fatigue life of the specimens subject to random amplitude loading. Moreover it has been demonstrated that the application of a certain number of compressive underload would affect the FCGR of the alloy. The influence of the presence and interaction of the underload is investigated and discussed.

Most structural components experience various magnitudes of tensile or compressive stress cycles during their service life. AM60B magnesium alloy is currently used in auto industry or manufacturing various automotive components (such as engine cradle, front end carrier, instrument panel, lifegate inner structure and radiator support, to name a few). These components are usually subject to cyclic loading; they also become sometimes subjected to sudden loading spikes, as well as impact loads (e.g., due to uneven pavements, pot-holes, accidental collisions, etc.). Such loads in turn produce tensile overloads or compressive underload in the components. Therefore, investigation into the influence of overload and underload on crack propagation rate of the alloy is an ongoing useful and important task. In chapter six, the retardation in crack propagation due to the application of an overload applied within an otherwise CAL is investigated. The Wheeler model [8] was initially employed to predict the retardation response of the alloy. Wheeler proposed his model based on defining the affected zone dimension and magnitude of retardation. The affected zone dimension is a function of the current and overload plastic zones. A three dimensional finite element analysis has been carried out to evaluate the plastic zone dimension with respect to various stress intensity factors. Applying the evaluated plastic zone dimensions in the Wheeler model, confirms that the model is not capable of predicting the affected zone, either for AM60B magnesium alloy, or for other materials. Analysis of the experimental results, showed that in some materials, the affected zone would be larger than that predicted by the Wheeler model, and in some other cases would be smaller. Therefore, Wheeler's model was modified by adding a "sensitivity parameter" to it. The magnitude of this parameter was found to be less than one for AM60B magnesium alloy, which confirms the lower sensitivity of this material to overload. Additionally, the influence of overload was studied within a random amplitude loading scenario by using "clipping level" concept.

The influence of overload on FCGR is usually reported for specimens tested under baseline loadings with positive stress ratios. Lack of information on retardation due to overload in baseline loadings with negative stress ratios, motivated us to implement a new series of experimental investigation, whose results are presented in chapter seven. In that investigation, the overload was applied within CAL baselines with various stress ratios (both positive and negative). It was observed that the presence of CSCs within such baseline loadings significantly altered the trend in retardation response of the alloy. For instance, a significant acceleration was observed when the stress ratio of the baseline loading was negative, leading to a significant reduction in retardation. Moreover, the sequence of overload and underload was proved to have a noticeable effect in the retardation of FCGR. Finally, the variation in the fracture surface roughness of specimens subjected to cyclic loading with various stress ratios was also evaluated. In the end, chapter eight presents the overall summary and conclusions of the thesis.

1.4 References

[1] Watarai, H., Sci. Technol. Trends Quart, Rev. 18, p. 84, 2006.

[2] Lu, Y., Taheri, F., Gharghouri, M., "Monotonic and Cyclic Plasticity Response of Magnesium Alloy. Part II. Computational Simulation and Implementation of a Hardening Model", Strain (International Journal for Experimental Mechanics), 47, pp. e25- e33, 2008.

[3] Lu, Y., Taheri, F., Gharghouri, M., “Study of Fatigue Crack Incubation and Propagation Mechanisms in a HPDC AM60B Magnesium Alloy”, Journal of Alloys and Compounds, 2008, 466, pp. 214-227.

[4] Nur-Hossain, M.; Taheri, F., “Fatigue and fracture characterization of HPDC AM60B magnesium alloy at cold temperature”. *J. Mater. Eng. Perform.*, *20*, 1684–1689, 2011.

[5] Nur Hossain, Md. and Taheri, F., "Influence of elevated temperature and stress ratio on the fatigue response of AM60B magnesium alloy”, Accepted for publication in the Journal of Materials Engineering and Performance, July, 2011.

[6] Paris, P. & Erdogan, F., “A Critical Analysis of Crack Propagation Laws”, Journal of Basic Engineering, 85, pp.528- 534, 1963.

[7] Walker, K., “The Effect of Stress Ratio during Crack Propagation and Fatigue for 2024-T3 and 7075-T69 Aluminum”, ASTM STP 462, pp.1-14, 1970.

[8] Wheeler, O.E., “Spectrum Loading and Crack Growth”, Journal of Basic Engineering, 94, pp.181-86, 1972.

CHAPTER 2 Literature Review

2.1 Introduction

Application of a cyclic loading on any industrial component (with loading amplitude above a certain magnitude, yet below the yield strength of the material) would cause degradation of the material properties, finally causing their fracture. A typical stress versus number of cycles graph, better known as the "S-N" curve is shown in Figure 2.1. The curve would guide engineers in safe design of structural components against fatigue loading. These curves could be obtained from fatigue tests on un-notched specimens.

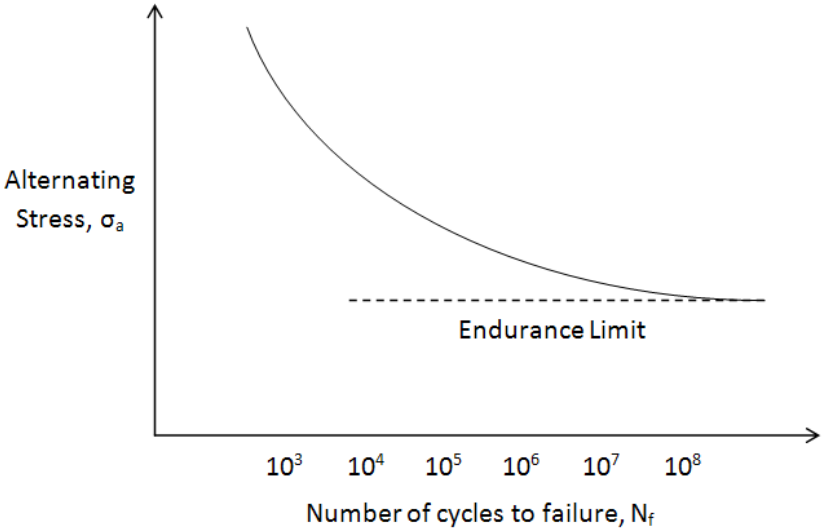

Figure 2.1 Schematic graph of S-N curve

As can be seen in Figure 2.1, application of higher levels of stress would shorten the fatigue life of the specimens. Some materials, like steel, show a stress limit, below which the fatigue life would be theoretically infinite; that limit is known as the "endurance limit". Some materials, however, do not have an endurance limit (e.g. aluminum).

A typical constant amplitude cyclic loading is shown in Figure 2.2. A cyclic loading could be characterized by the stress range, $\Delta\sigma$, and stress ratio, R, expressed by equations 2.1 and 2.2.

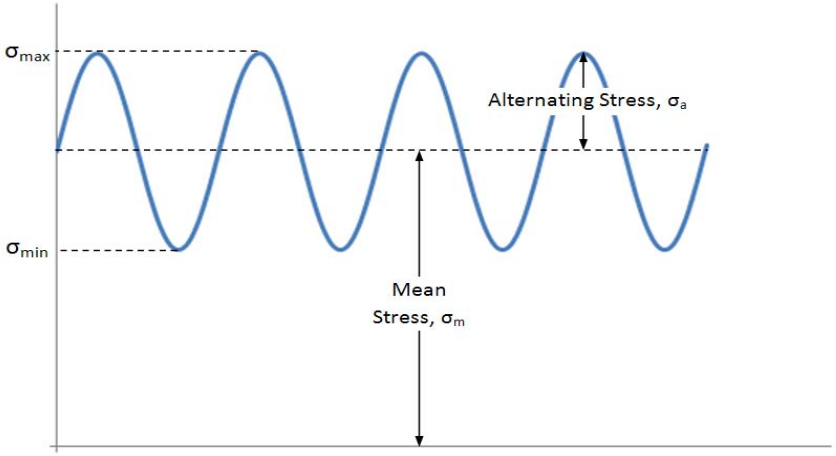

Figure 2.2 Schematic graph of a cyclic loading

$$\Delta\sigma = \sigma_{\max} - \sigma_{\min} \tag{2.1}$$

$$R = \frac{\sigma_{\min}}{\sigma_{\max}} \tag{2.2}$$

The mean stress has a significant effect on the fatigue life of the specimens as shown in Figure 2.3 [1]. This figure shows that higher mean stress levels have detrimental effect on fatigue life, while lower mean stress levels would result in longer fatigue life.

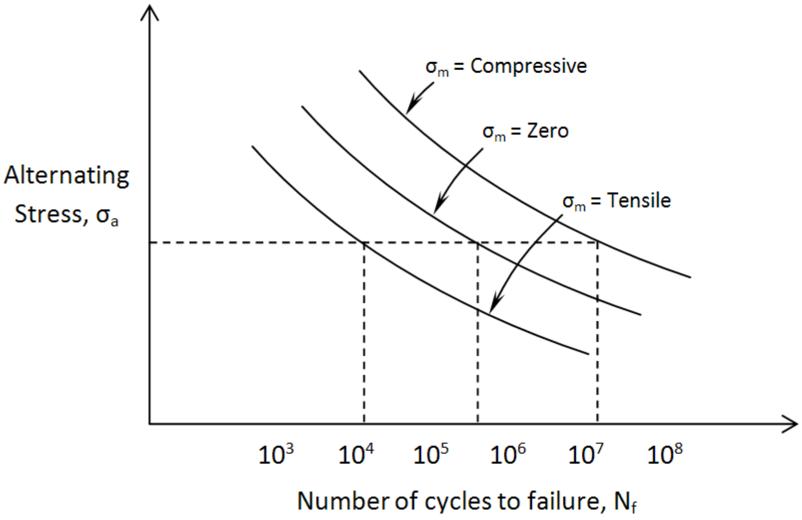

Figure 2.3 S-N curve for various mean stresses [1]

For a cracked specimen, the results would usually be illustrated as a function of fracture properties of the specimen; therefore, in the next part some basic concepts of fracture are presented.

2.2 Fracture mechanics

A crack may exist in materials due to manufacturing related anomalies. A crack can also be developed within any man-made structure due to application of stress levels higher than the material's strength of the component, which in turn may lead to fracture of the component. A crack can experience three different types of loading as illustrated in Figure 2.4. These loadings would force a crack to displace in different modes. The opening mode or mode I would occur when the load is applied in a direction perpendicular to the crack plane. Second and third modes correspond to in plane and out of plane shear loading, which result in sliding and tearing respectively. A crack can also be subject to a combination of the above loading modes.

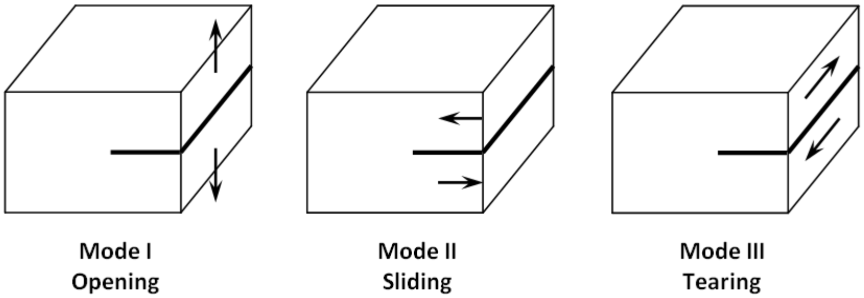

Figure 2.4 Three modes of fracture

The stress distribution ahead of the crack tip could be characterized using a single parameter, K, which is known as the stress intensity factor. The stress intensity factor in an infinite plate is a function of the far-field applied stress, σ and half crack length, a. A geometry dependent parameter, *Y*, would be added when the crack is hosted by a finite dimension plate, mathematically represented by the following equation [2-4].

$$K = Y \sigma \sqrt{\pi a} \tag{2.3}$$

The geometry dependent parameter, *Y*, could be evaluated using finite element analysis. For instance, the results for a center crack are presented using a polynomial function as shown in equation 2.4 [5].

$$Y = \left[\sec\left(\frac{\pi a}{2W}\right)\right]^{1/2} \left[1 - 0.025\left(\frac{a}{W}\right)^2 + 0.06\left(\frac{a}{W}\right)^4\right] \tag{2.4}$$

where a and W are half crack length and half width of a center cracked plate, respectively. Crack could be subjected to a mixed mode loading, which usually occurs when the crack is angled. In such cases the global energy release would consist of the sum of the energy released by each contributing mode. Crack propagation rate is usually presented with respect to the stress intensity factor range. Some of the crack propagation model is presented in next part.

2.3 Crack propagation models

Figure 2.5 shows a typical crack propagation rate with respect to the stress intensity factor range in a logarithmic scale. This graph can be divided into three regions. Crack propagation rate in region I is in the order of 10^{-9} m/cycle or less. The main feature of this region is the threshold value, ΔK_{th}. A crack would not propagate under the stress intensity factor range lower than ΔK_{th}. The threshold stress intensity factor range is practically defined as the stress intensity factor range corresponding to the propagation rate of 10^{-10} m/cycle. Several equations (see for example [6, 7]) are suggested for predicting ΔK_{th} as a function of the stress ratio or Young's modulus of materials. Crack propagation rate in this region is affected by the microstructure of the material, environmental conditions and cyclic loading properties. It has been observed that the stress ratio of a cyclic loading is the most important parameter that affects the threshold stress intensity factor [8]. The second region of the crack propagation is a linear function of the stress intensity factor range in a logarithmic scale. This region would continue, reaching to the third region, which corresponds to fast crack growth and the eventual fracture of the specimen.

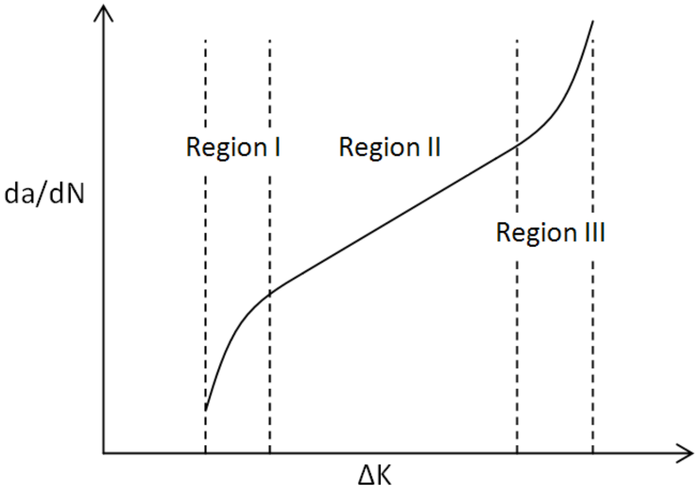

Figure 2.5 Crack propagation rate versus stress intensity factor range

2.3.1 Crack propagation models under constant amplitude loading (CAL)

Several models have been proposed for predicting the crack propagation rate under CAL as a function of the stress intensity factor range (ΔK). Stress intensity factor range at any constant amplitude loading is a function of stress range and crack length, as shown in equation 2.5.

$$\Delta K = Y\left(\Delta\sigma\right)\sqrt{\pi a} = Y\left(\sigma_{\max} - \sigma_{\min}\right)\sqrt{\pi a} \tag{2.5}$$

where $\sigma_{\max}$ and $\sigma_{\min}$ are the maximum and minimum stresses in the CAL. For CAL with negative stress ratio, some standards suggest the dismissal of the compressive stress cycles (CSC) (e.g. [9]); in other words, the stress range would include the maximum stress and $\sigma_{\min} = 0$. In the following section, some of the crack propagation models will be briefly introduced.

2.3.1.1 Paris model

Paris and Erdogan [10] proposed their model in 1963, which is known as the Paris model, expressed by the following equation.

$$\frac{da}{dN} = C_p\left(\Delta K\right)^{m_p} \tag{2.6}$$

where C_p and m_p are curve fitting coefficients that have to be established experimentally. For instance, these parameters were experimentally evaluated by Yuen and Taheri [11] as; $C_p = 1.66 \times 10^{-13}$ and $m_p = 4.06$ for 350WT steel alloy when the stress intensity factor range (ΔK) was less than 26.5 $MPa.m^{½}$.

Paris' model essentially describes the straight line portion of the FCGR curve shown in Figure 2.5 (region II), with m_p representing the slope and C_p being the intercept of the line. Thus, the model can predict FCGR only in the second region. The other limitation of this model is that the effect of stress ratio cannot be accounted for.

2.3.1.2 Walker model

Walker [12] considered the influence of the stress ratio in his model, presented in 1970. He improved Paris' model to become capable of predicting the crack propagation rate for various stress ratios, by the use of a single equation. His model is presented in equation 2.7.

$$\frac{da}{dN} = C_w \left(\frac{\Delta K}{(1-R)^{1-\gamma_w}} \right)^{m_w} \tag{2.7}$$

However, in order to use this model, three curve fitting parameters should be experimentally evaluated. At zero stress ratio, C_w and m_w would be equal to C_p and m_p in Paris' equation. For other stress ratios one extra parameter must be evaluated. That parameter could be found by trial and error using the experimental data obtained for various stress ratios. The $(1-R)^{1-\gamma_w}$ parameter governs shifting of the FCGR curve to either left or right. However, the slope of these lines is supposed to be identical.

2.3.1.3 Forman model

The Forman model [13] can account for the second and third regions (see Figure 2.5) of the FCGR curve. As shown in equation 2.8, a parameter, K_C, is added to the previous model, which represents the critical stress intensity factor or fracture toughness of the material.

$$\frac{da}{dN}=\frac{C_F\left(\Delta K\right)^{m_y}}{\left(1-R\right)K_C-\Delta K}=\frac{C_F\left(\Delta K\right)^{m_y}}{\left(1-R\right)\left(K_C-K_{\max}\right)} \tag{2.8}$$

Equation 2.8 shows that, when the maximum stress intensity factor value reaches the fracture toughness, the crack propagation rate would increase to infinity. This model is also capable of describing the crack propagation rate in the second region and considers the effect of the stress ratio. Similar to Walker's model, this model also assumes that the slopes of the FCGR lines would be identical for various stress ratios (i.e. the lines would be parallel to one another).

Hartman and Shijve [14] added the threshold stress intensity factor to Forman's equation to cover the crack propagation rate for all regions showed in Figure 2.5. As can be seen in equation 2.9, when the stress intensity factor range approaches to the threshold value, the FCGR reduces to zero.

$$\frac{da}{dN}=\frac{C_{HS}\left(\Delta K-\Delta K_{th}\right)^{m_{HS}}}{\left(1-R\right)K_C-\Delta K} \tag{2.9}$$

2.3.1.4 Frost, Pook and Denton model

Frost and Pook [15] related the crack propagation rate to the stress intensity factor range and Young's modulus of the material. This model is supposed to be applicable to various materials. They proposed two separate equations, one for plane stress and another for plane strain condition as shown in the following equations.

$$\frac{da}{dN}=\frac{9}{\pi}\left(\frac{\Delta K}{E}\right)^2 \qquad \textit{Plane stress} \tag{2.10}$$

$$\frac{da}{dN}=\frac{7}{\pi}\left(\frac{\Delta K}{E}\right)^2 \qquad \textit{Plane strain} \tag{2.11}$$

2.3.1.5 Zhang and Hirt model

This model was initially introduced by Lal and Weiss [16], and subsequently modified by Zheng and Hirt [17,18]. They applied a linear fracture analysis and assumed that a crack would propagate within a distance, at the end of which the normal stress becomes equal to the critical fracture stress, σ_{ff}, as shown in Figure 2.6.

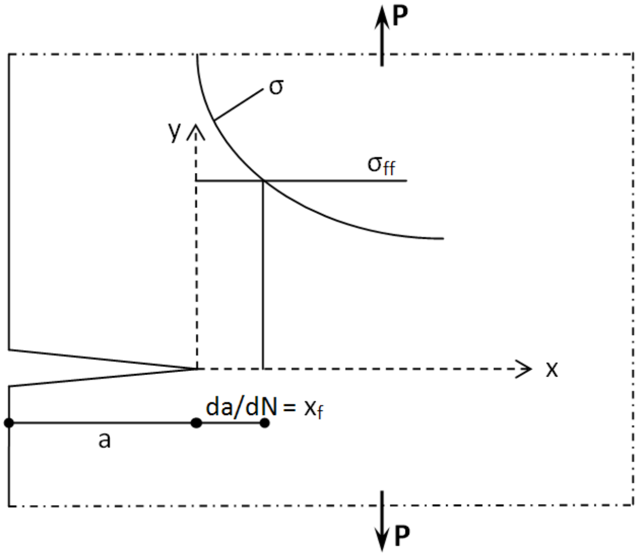

Figure 2.6 Stress distribution and crack propagation in one cycle [17]

Using the normal stress distribution ahead of the crack tip and equating it to the critical fracture stress yields equation 2.12. It should be noted that the effective stress intensity factor range, ΔK_{eff}, has been included in this equation to account for the influence of the threshold stress intensity factor.

$$\begin{aligned} &\frac{da}{dN} = B\,\Delta K_{eff}^2 = \frac{1}{2\pi\sigma_{ff}^2}\left(\Delta K - \Delta K_{th}\right)^2 \\ &where \quad \sigma_{ff} = \sqrt{E\sigma_f \varepsilon_f} \end{aligned} \tag{2.12}$$

In the above equation, σ_f and ε_f are the stress and strain at the failure stage of the un-cracked material. The fracture stress of the material is taken as the ultimate strength of the material. Yuen and Taheri [19] proposed some modification to the above equation, specifically in relation to the way the fracture stress is evaluated and obtained better agreement with their experimental data. They proposed that the true fracture stress should be used in the Zheng and Hirt model instead of the engineering stress.

2.3.1.6 Dowling and Begley model

Dowling and Begley [20] presented the crack propagation rate data with respect to ΔJ (the J-integral range) instead of ΔK in a gross plasticity ahead of the crack tip as shown in the following equation.

$$\frac{da}{dN} = C_{BD}\,\Delta J^{m_{BD}} \tag{2.13}$$

They carried out a set of experimental investigation on A533B steel. Displacement controlled cyclic loading was applied in a way to produce large scale yielding around the crack tip. As shown in equation 2.13, C_{BD} and m_{BD} are model's parameters. In the case of large plastic deformation, the concept of linear fracture mechanics would not be valid and a new parameter referred to as the J integral was introduced by Rice [21] to extend the application of the fracture mechanics concept. Furthermore, the J integral is shown to be a unique parameter, characterizing the stress distribution ahead of crack tip in an elastic-plastic material [22, 23].

2.3.1.6 Elber Model

This model is based on the crack closure concept, introduced by Elber [24, 25]. He observed that the crack faces remain closed even at some levels of tensile loading. The stress level at which crack faces start to be open is known as the opening stress (σ_{op}), which corresponds to the opening stress intensity factor. The portion of a cyclic loading which is greater than the opening stress is assumed as a driving force for crack propagation; therefore, he replaced the stress intensity factor range by the effective stress intensity factor range. The effective stress intensity factor range is the difference between the maximum and opening stress intensity factors as expressed by equation 2.14.

$$\Delta K_{eff} = \left(K_{\max} - K_{op}\right) = Y\left(\sigma_{\max} - \sigma_{op}\right)\sqrt{\pi a} \tag{2.14}$$

The opening stress should be evaluated experimentally by measuring the crack opening displacement as depicted in Figure 2.7 [24]. The load-displacement graph of a cracked specimen consisted of three regions (AB, BC and CD). Region AB represents the fully closed crack faces, which has the same slope as that of the uncracked specimen. Crack faces are fully open when the load increases from point C to D. Region BC is a transition region (from fully closed to fully open status) and the stress level at point C is the opening stress. In light of the abovementioned discussion, this model requires an extra set of experiments to establish the opening stress. Several attempts (e.g. [26]) have been made to formulate the opening stress level within cyclic loadings.

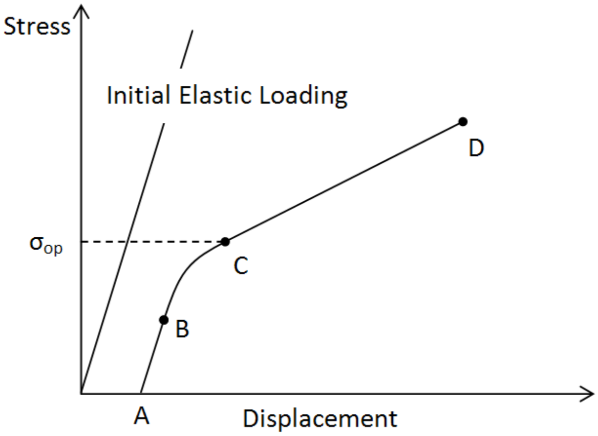

Figure 2.7 Experimental results for opening stress evaluation [24]

2.3.2 Crack propagation models under variable amplitude loading (VAL)

There is no guaranty that structural or industrial components would experience only constant amplitude cyclic loading during their life. Therefore the crack propagation under variable amplitude loading ought to be investigated. In a variable amplitude loading, loading sequence and its magnitude would significantly affect the crack propagation rate. Application of a tensile overload in an otherwise constant amplitude loading is a simplest scenario for VAL. The influence of an applied tensile overload is schematically shown in the following figure.

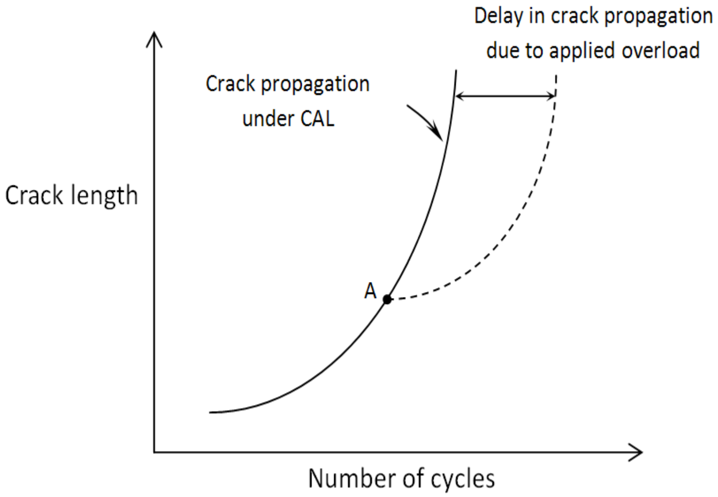

Figure 2.8 Delay in crack propagation due to overload

Figure 2.8 evidences some increase in the fatigue life as a result of the retardation in crack propagation due to the application of the tensile overload. Point A in that graph represents the crack length at which the overload is applied. The amount of retardation depends on the overload ratio (OLR) and the nature of the baseline loading. On the other hand, application of a compressive underload within a CAL would accelerate the crack propagation.

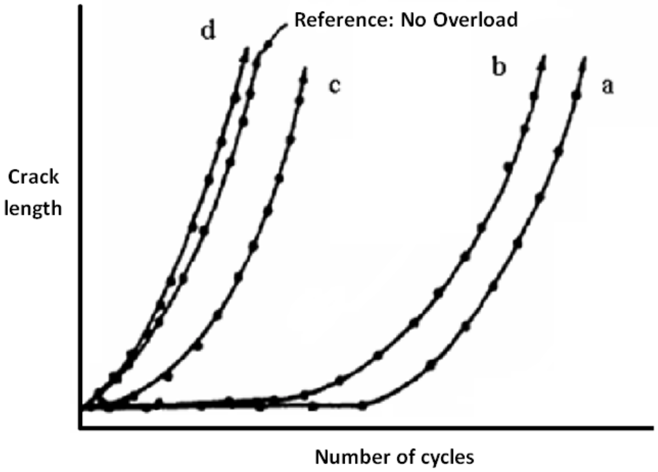

Figure 2.9 Crack propagation after application of (a) a tensile overload (b) a compressive underload followed by a tensile overload (c) a tensile overload followed by a compressive underload (d) a compressive underload [27]

Interaction of tensile overload and compressive underload is graphically shown in Figure 2.9 [27]. Graphs (a) and (d) in Figure 2.8 illustrate the retardation and acceleration in crack propagation due to application of the tensile overload and compressive underload, respectively. A significant reduction in the amount of retardation would be observed when a tensile overload is followed by a compressive underload (graph c), while the reverse sequence does not produce noticeable reduction in retardation of crack propagation (graph b).

2.3.2.1 Wheeler model

Wheeler [28] added a reduction factor, Φ_R, to the steady state crack propagation rate. He also defined an affected zone that the crack propagation would be retarded. The affected zone is a function of the current and overload plastic zone dimensions, as represented mathematically by the following equations.

$$\frac{da}{dN} = \Phi_R \left(\frac{da}{dN} \right)_{CAL} \tag{2.15}$$

where: $$\Phi_R = \begin{cases} \left[\dfrac{r_{p,i}}{a_{OL} + r_{p,OL} - a_i} \right]^m & \text{when} \quad a_i + r_{p,i} \langle a_{OL} + r_{p,OL} \\ 1 & \text{when} \quad a_i + r_{p,i} \rangle a_{OL} + r_{p,OL} \end{cases} \tag{2.16}$$

where $r_{p,i}$ and $r_{p,OL}$ are the “current” and “overload” plastic zones, respectively. The current crack length and the crack length at which the overload was applied are represented by a_i and a_{OL} in equation 2.16. The reduction factor is effective over the length through which the boundary of the current plastic zone reaches the boundary of overload’s plastic zone. Wheeler assumed that crack propagation would be retarded immediately upon the application of an overload, however there would be some delay in retardation and even initial acceleration have been observed under some baseline loading conditions. Wheeler’s original crack propagation model is schematically shown in Figure 2.10. This model has been modified and further discussed in Chapter six.

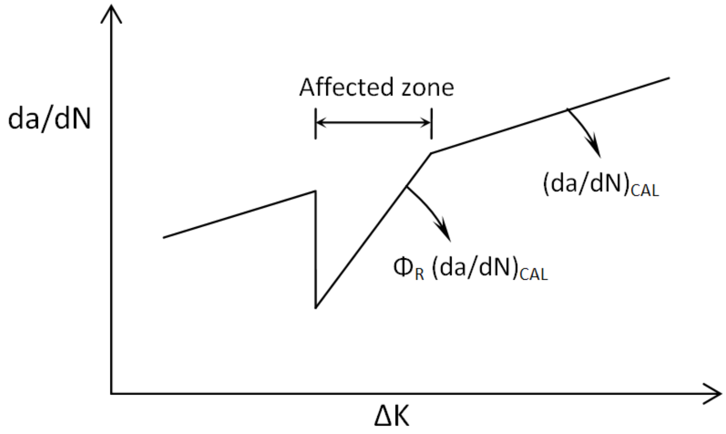

Figure 2.10 Wheeler retardation model

2.3.2.2 Willenborg model

Willenborg et al. [29] used Wheeler's assumption and proposed the reduction in crack propagation by introducing an effective stress intensity factor. The stress intensity factor that produces a plastic zone to reach the boundary of overload plastic zone is called K_{req} and was used to define the reduction in stress intensity factor (K_{red}). The reduction in stress intensity factor, K_{red}, was modified by Gallagher [30] to be presented as a function of crack length as expressed by the following equation.

$$K_{red} = K_{req} - K_{\max,i} = K_{\max,OL}\sqrt{1 - \frac{a - a_{OL}}{R_{y,OL}}} - K_{\max,i} \tag{2.17}$$

where $K_{max,i}$, $K_{max,OL}$, a, a_{OL} and $R_{y,OL}$ are the current maximum stress intensity factor, overload maximum stress intensity factor, current crack length, the crack length at which the overload is applied and the overload plastic zone dimension, respectively. The K_{red} would be then subtracted from the current maximum and minimum stress intensity factors to define the effective stress intensity factors. The effective parameters shown in equation 2.18 could be applied in a crack propagation model to predict the retardation of crack propagation.

$$
\begin{aligned}
K_{\max,eff} &= K_{\max} - K_{red} \\
K_{\min,eff} &= K_{\min} - K_{red} \\
R_{eff} &= \frac{K_{\min,eff}}{K_{\max,eff}}
\end{aligned}
\tag{2.18}
$$

where $K_{max,eff}$ and $K_{min,eff}$ are the maximum and minimum effective stress intensity factor and R_{eff} is the effective stress ratio.

2.3.2.3 Equivalent parameters

Barsom [31] proposed the equivalent stress intensity factor range be employed within an appropriate crack propagation model. The root mean square technique was applied to define the equivalent stress intensity factor range, ΔK_{rms}, as shown in equation 2.19.

$$
\Delta K_{rms} = \sqrt{\frac{\sum_{i=1}^{n} \Delta K_i^2}{n}}
\tag{2.19}
$$

where ΔK_i is the stress intensity factor range at the ith cycle and n is the total number of cycles. It should be noted that the influence of the loading sequence and the stress ratio are not considered by this model. Having the equivalent stress intensity factor range, a Paris like crack propagation model can be presented by:

$$
\frac{da}{dN} = C_B \left(\Delta K_{rms} \right)^{m_B}
\tag{2.20}
$$

where C_B and m_B are the model's coefficients that could be evaluated using the experimental data. In order to consider the effect of stress ratio predicting the crack propagation under variable amplitude loading, Hudson [32] defined the equivalent maximum and minimum stress as shown in equation 2.21.

$$
\sigma_{\max(or\ \min),rms} = \sqrt{\frac{\sum_{i=1}^{n} \sigma^2_{\max(or\ \min),i}}{n}}
\tag{2.21}
$$

These equivalent stresses could be used to define the stress intensity range and ratio and employed in a crack propagation model to predict the fatigue life of the components.

2.4 Summary and conclusion

Some of the most common fatigue crack propagation models have been reviewed in this chapter. Crack propagation rate under constant amplitude loading (CAL) would typically be presented as a function of the stress intensity factor range. For predicting the fatigue life under variable amplitude scenarios, one should also consider the loading sequence effect. The stress ratio and loading amplitude are the main parameters controlling the crack propagation under constant amplitude cyclic loading.

The crack propagation trend as a result of cyclic loading is customarily described in three regions; in the first region, propagation would start when the stress intensity factor range becomes greater than the threshold value. This is followed by a stable crack growth in the second region. This region would have a linear relation with respect to the stress intensity factor range in a logarithmic scale. In the third region, the crack propagation rate takes a faster rate, leading to specimen's fracture. Several models are proposed to predict the crack propagation under CAL. All the models require some coefficients that must be evaluated using experimental results. Each model has been proposed based on a specific requirement; for instance, some of them are formulated such to consider the effect of the stress ratio and some are developed to consider and predict the crack propagation in the third region of the FCGR curve.

Loading sequence also has a significant effect on FCGR under variable amplitude loading. Application of a tensile overload results in retardation in FCGR while the existence of a compressive underload would yield to a faster FCGR. Some crack propagation models were reviewed that can account for the loading sequence effect. Most of them, as noted, are based on the size of plastic zone developed ahead of a crack tip.

2.5 References

[1] Stephens, R. L., Fatemi, A., Stephens, R. R., and Funchs, H. O., "Metal Fatigue in Engineering", Second Edition, WILEY-INTERSCIENCE, John Wiley & Sons, Inc., Professional/Trade Division, 605 Third Avenue, New York, NY, 10158-0012, 2001.

[2] Anderson, T. L., “Fracture Mechanics, Fundamentals and Applications”, Third Edition, CRC Press, Taylor & Francis Group, Boca Raton, FL 33487-2742, 2005.

[3] Bannantine, J. A., Commer, J. J., Handrock, J. L., “Fundamental of Metal Fatigue Analysis”, Prentice Hall, Englewood Cliffs, New Jersey, 07632, 1989.

[4] Broek, D., “The Practical Use of Fracture Mechanics”, FractuREsarch Inc., Galena, OH, USA, Kluwer Academic Publisher, P. O. Box 17, 3300 AA Dordrecht, The Netherland, 1988.

[5] Tada, H., Paris, P. C. & Irwin, G. R., “The Stress Analysis of Crack Handbook”, Second Edition, Paris Productions Inc., St. Louis, 1985.

[6] Barsom, J. M. & Rolfe, S. T., “Fracture and Fatigue Control in Structures, Application of Fracture Mechanics”, Third Edition, ASTM, 100 Bar Harbor Drive, West Conshohocken, PA, 1999.

[7] Wason, J. and Heier, E., “Fatigue Crack Growth Threshold- The Influence of Young’s Modulus and Fracture Surface Roughness”, International Journal of Fatigue, 20, pp. 737-742, 1998.

[8] Dowling, N. E., “Mechanical Behavior of Materials, Engineering Methods for Deformation, Fracture and Fatigue”, Second Edition, PRENTICE HALL, Upper Saddle River, New Jersey 07458, 1999.

[9] ASTM E647-08, "Standard Test Method for Measurement of Fatigue Crack Growth Rates”, ASTM International, PA, USA, 2009.

[10] Paris, P. and Erdogan, F., “A Critical Analysis of Crack Propagation Laws”, Journal of Basic Engineering, 85, pp.528- 534, 1963.

[11] Yuen, B.C.K. & Taheri, F., "Proposed Modification to the Wheeler Retardation Model for Multiple Overloading Fatigue Life Prediction", *International Journal of Fatigue*, 28, pp.1803-19, 2006.

[12] Walker, K., "The Effect of Stress Ratio during Crack Propagation and Fatigue for 2024-T3 and 7075-T69 Aluminum", ASTM STP 462, pp.1-14, 1970.

[13] Forman, R. G., "Study of Fatigue Crack Initiation from Flaws Using Fracture Mechanics Theory", Engineering Fracture Mechanics, 4, pp. 333- 345, 1972.

[14] Hartman, A. and Shijve, J., "The Effect of Environment and Load Frequency on the Crack Propagation Law for Macro Fatigue Crack Growth in Aluminum Alloys", Engineering Fracture Mechanics, 1, pp. 615- 631, 1970.

[15] Frost, N. E., Pook, L. P. and Denton, K., "A Fracture Mechanics Analysis of Fatigue Crack Growth Data for Various Materials", Engineering Fracture Mechanics, 3, pp. 109-126, 1971.

[16] Lal, D. N. and Wiess, V., "A Notch Analysis of Fracture Approach to Fatigue Crack Propagation", Metallurgical Transactions, 9A, pp. 413- 425, 1978.

[17] Zheng, X. and Hirt, M. A., "Fatigue Crack Propagation in Steels", Engineering Fracture Mechanics, 18, pp. 965- 973, 1983.

[18] Zheng X., "A Simple Formula for Fatigue Crack Propagation and a New Method for Determining of ΔK_{th}", Engineering Fracture Mechanics, 27, pp. 465- 475, 1987.

[19] Yuen, B. K. C. and Taheri, F., "Proposed Modification to the Zheng and Hirt Fatigue Model", Journal of Material Engineering and Performance, 13, pp. 226- 231, 2004.

[20] Dowling, N. E. and Begley, J. A., “Fatigue Crack Growth during Gross Plasticity and the J-Integral”, Mechanics of Crack Growth, ASTM STP 590, American Society for Testing and Materials, Philadelphia, PA, pp. 82- 105, 1976.

[21] Rice, J. R., “A Path Independent Integral and the Approximate Analysis of Strain Concentration by Notches and Cracks”, Journal of Applied Mechanics, 35, pp. 379- 386, 1968.

[22] Hutchinson, J. W., “Singular Behavior at the End of a Tensile Crack Tip in a Hardening Material”, Journal of the Mechanics and Physics of Solids, 16, pp. 13- 31, 1968.

[23] Rice, J. R. and Rosengren, G. F., “Plane Strain Deformation near a Crack Tip in a Power Law Hardening Material”, Journal of the Mechanics and Physics of Solids, 16, pp. 1- 12, 1968.

[24] Elber W., “Fatigue Crack Closure under Cyclic Tension”, Engineering Fracture Mechanics, 2, pp. 37- 45, 1970.

[25] Elber, W., “The Significance of Fatigue Crack Closure”, Damage Tolerance in Aircraft Structures, ASTM STP 486, American Society for Testing and Materials, Philadelphia, PA, pp. 230- 242, 1972.

[26] Newman, J. C., “A Crack Opening Stress Equation for Fatigue Crack Growth”, International Journal of Fracture, 24, pp. R131- R135, 1984.

[27] Funchs, H. O. and Stephens, R., “Metal Fatigue in Engineering”, John Wiely and Sons, New York, 1980.

[28] Wheeler, O. E., “Spectrum Loading and Crack Growth”, Journal of Basic Engineering, 94, pp. 181- 186, 1972.

[29] Willenborg, J., Engle, R. M. and Wood, H. A., 1971. “A Crack Growth Retardation Model Using an Effective Stress Concept”. Air Force Flight Dynamic Laboratory, Dayton, Report AFFDL-TR71-1, 1971.

[30] Gallagher, J. P., “A Generalized Development of Yield-zone Models”, AFFDL-TM-74-28, Air Force Flight Dynamics Laboratory, Wright-Patterson Air Force Base, Ohio, 1974.

[31] Barsom, J. M., “Fatigue Crack Growth under Variable Amplitude Loading in Various Bridge Steels”, In Fatigue Crack Growth under Spectrum Loads, ASTM STP 595, American Society for Testing and Materials, Philadelphia, PA, pp.217-235, 1976.

[32] Hudson, C. M., “A Root-Mean-Square Approach for Predicting Fatigue Crack Growth under Random Loading”, Methods and Models for Predicting Fatigue Crack Growth under Random Loading, ASTM STP 748. J. B. Chang and C .M. Hudson, Eds., American Society for Testing and Materials, pp. 41-52, 1981.

CHAPTER 3 Evaluation of fatigue damage in HPDC AM60B

In earlier efforts expended by some members of our research group, the special distribution of porosity that is an inherent result of high pressure die-casting were carefully identified and the resulting influence on the performance of materials, both under monotonic and cyclic loading conditions were systematically investigated.

The project outlined in this thesis was initiated by an attempt to see whether the influence of porosity that exists within high pressure die cast (HPDC) AM60B could be quantified by a relatively simple vibration method. Moreover, as alluded earlier, since the alloy is often used in applications subject to cyclic loading and vibration, evaluation of the dynamic properties of the alloy was also desirable.

In this section, the dynamic response of the alloy during a cyclic loading was investigated. The natural frequency and damping capacity of the alloy were evaluated in certain cyclic intervals, up to the failure stage of the specimens. To evaluate a material's dynamic response, beam-type specimens were clamped at one end and excited at their free end.

Since the dynamic properties of materials change as a result of the applied loading cycles, the change is postulated to provide a measurable criterion for assessing the extent of damage in materials. In this case, an approximate variation of 5% in the natural frequency and a 60% change in the damping capacity of the alloy were observed at the failure stage. Additionally, the influence of porosity was evaluated by taking micrographs of the material's cross section.

3.1 Introduction

The degree of damage in a material subject to fatigue loading is a function of the applied loading cycles. Thus, as the cycle number increases, the material property degrades, reaching a critical limit, after which failure becomes eminent. In most real situations where a component undergoes cyclic loading, there would neither be a loading history record, nor could one guarantee that the material would always be subject to a cyclic loading with a constant amplitude in its lifetime. Therefore, it would be desirable to develop a methodology by which one could monitor the performance of the materials throughout their service life when subject to fatigue loading. To that extent, one should monitor the integrity of the material as it undergoes cyclic loading (or vibration).

Detection of structural damage through changes in a material's natural frequency has been reviewed by Salawu [1]. He showed that a structural component's dynamic parameters could be obtained easily and cost-effectively from the recorded vibration response of the component, and that the changes in the properties could be used to monitor a component's health in real-time. Hsieh et al. [2], used the change in a material's natural frequency as a nondestructive means for monitoring the health of a cyclic loaded nickel titanium rotary component. They considered the natural frequency as an effective parameter for evaluating the microstructural changes in materials. Furthermore, the effect of fatigue loading on the dynamic response frequency of spot-welded joints was studied by Shang et al. [3, 4]. They found a detectable change in material's natural frequency that was most noticeable after 60% of the fatigue life of the component.

The main objective of this study is to evaluate damage propagation in AM60B magnesium alloy specimens that include various levels of porosities as a result of cyclic loading by using the dynamic property of the alloy. As such, the natural frequency and damping capacity of the alloy are considered as the varying material properties in this part.

3.2 Material porosity

For evaluating the porosity ratio, several specimens were cut from different parts of a HPDC alloy plate. A reflected light microscope was used to capture the image of the microstructure in the specimens' cross section. The specimens were polished and prepared according to ASTM-E-1245 [5]. The total porosity areas was measured in each image (field) using an image analyzer software. Typical field images are shown in Figure 3.1. As can be seen, the porosity ratio varies significantly from field to field. The average value of the field-to-field porosity ratio in each specimen is taken as the surface porosity ratio of that specimen. The porosity ratios for eight of the specimens are presented in Table 3.1.

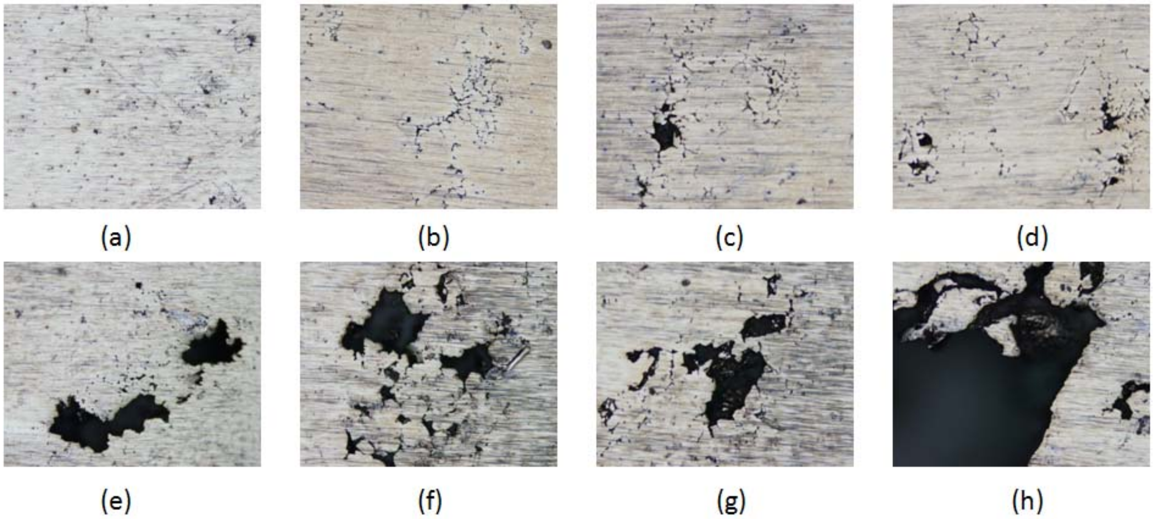

Figure 3.1 Surface porosity in each field, leading to the porosity ratio of a-1.88%, b-3.07%, c- 4.33%, d-3.35%, e-10.5%, f-14.72%, g-10.87%, h-54.25%.

Table 3.1 The average surface porosity ratio of the specimens

Specimen No.	**1**	**2**	**3**	**4**	**5**	**6**	**7**	**8**
Surface Porosity (%)	1.71	2.03	10.85	1.29	1.32	4.11	5.05	1.25

As seen, the porosity ratio in these specimens varied significantly from approximately 1% to 10%.

3.3 Test setup

Specimens were cut from the core section of HPDC AM60B alloy plates provided by the Meridian Technologies Inc. (Strathroy, Ontario). The top and bottom skin layers of the plate were removed in order to reach the core of the material, which was prepared with an appropriate surface-finishing operation. The dimensions of the specimens were established according to ASTM E-466 [6] to enable us to evaluate a large number of vibration modes. As such, various trials were done to establish the optimum dimensions of the specimens. The aim was to establish a geometry that could produce more than one mode of vibration, and be suitable for fatigue testing. It should be noted that the limitation in specimen dimensions were also a function of the fatigue machine test. The resulting specimen is shown in Figure 3.2.

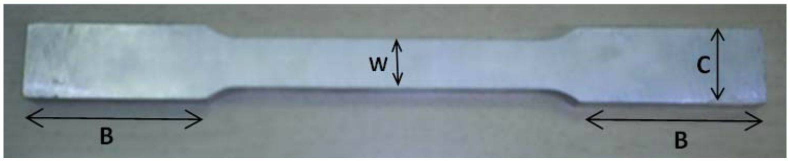

Figure 3.2 Total Length = 250 mm, c = 23 mm, w = 15 mm,
B = 60 mm, Thickness = 10 mm

Fatigue tests were conducted by an Instron servo-hydraulic universal test machine, controlled by a 8501 digital controller, under constant amplitude load control regime, with a maximum stress of 90 MPa and stress ratio of R=0.1. The cyclic loading was applied at a rate of 30 Hz. The fatigue loading setup is shown in Figure 3.3.

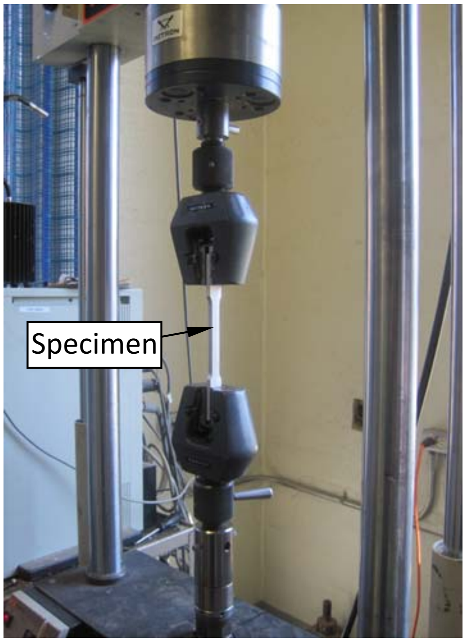

Figure 3.3 Fatigue test setup

3.4 Dynamic test procedure

In order to measure the vibration properties of each specimen, one end of the specimen was released from the end fixture after a certain number of cycles, thus leaving the specimen in the form of a cantilever beam. A small vibration hammer (model 5800B5, Dytran Inst., Chatsworth, CA) was used to excite the specimen at its free end and the vibration signal was acquired with a light weight accelerometer at the same point. The accelerometer was mounted onto the specimen using an appropriate wax. It should be noted that the vibration signal extracted at the same location of excitation would include a large number of higher frequency modes. Such data would however occupy only a small segment of the signal at the beginning of the time increment. This segment can be easily removed from the signal, leading to a purer signal. This procedure was repeated to the end of the specimen life. The data acquired through the accelerometer was then processed via LabVIEW software and stored in a personal computer.

A total of six specimens were tested. The data sampling rate for all specimens was at 25,000 Hz, which was at least twice the expected natural frequency of the specimen, thus conforming to the Nyquist theory.

In order to enhance the vibration excitation, three types of hammer tips (i.e., hard plastic, soft plastic and aluminum) were trial tested. Of the three, the aluminum tip could generate a more pronounced excitation, thus affecting the higher natural frequencies. The impact test setup and a sample of an acquired accelerometer signal are shown in Figures 3.4 and 3.5.

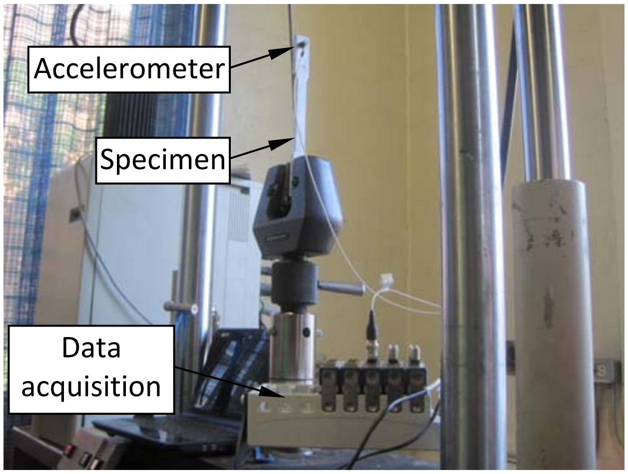

Figure 3.4 Vibration test set up

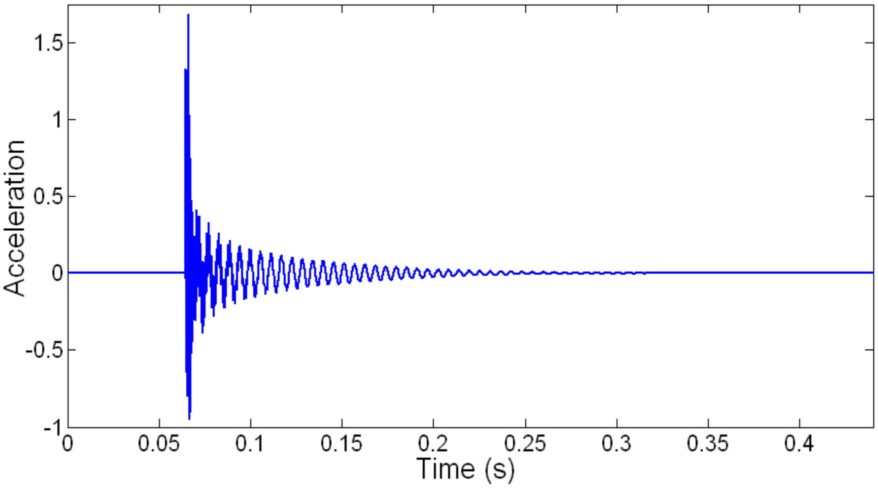

Figure 3.5 Typical acquired vibration signal

3.5 Data analysis

3.5.1 Natural frequency

Natural frequency is a property related to the stiffness and mass of the material. By transforming the vibration signal from the time domain to the frequency domain using the Fourier transform, one can obtain the natural frequency associated to the different modes of vibration. In this section, the objective was to evaluate the change in the natural frequency of AM60B as a result of applied cyclic loading after a certain number of loading cycles. The following defined parameters would aid us in analyzing the data. The cyclic life ratio is defined as [3]:

$$Cyclic\ life\ ratio = \frac{N_i}{N_f} \tag{3.1}$$

where N_i is the number of cycles at each loading stage and N_f is the total number of cycles leading to the failure of each specimen. As stated earlier, a cyclic loading generally causes an increase in the density of micro-cracks and void ratios within materials (due to void coalescence), thereby causing damage to the material. As a result, material's physical properties such as the natural frequency would be affected (degraded). The natural frequency change is defined as:

$$\Delta f = 1 - \frac{f_i}{f_0} \tag{3.2}$$

where f_i is the natural frequency evaluated upon completion of each loading stage and f_0 is the natural frequency of an undamaged specimen. As stated earlier, the first part of the vibration signal is affected by the impact; therefore the unwanted signals are eliminated and the free vibration part is transformed to the frequency domain using the Fast Fourier Transform (FFT) technique, as illustrated in Figure 3.6.

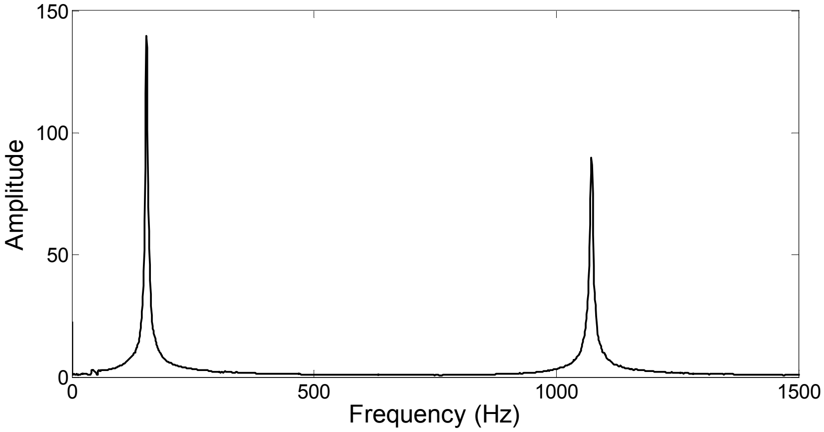

Figure 3.6 Free vibration signal in frequency domain

As can be seen, the second natural frequency is significantly greater than the first one; therefore, the change in the second natural frequency of vibration could be more detectable as a result of damage. Consequently, the change in the second natural frequency will be considered for all specimens. It should also be noted that each specimen was tested four times, and the mean value of the natural frequency of each specimen is reported in Table 3.2.

Table 3.2 Typical variation in the second natural frequency of vibration observed in the specimens

Number of Cycles	f2 (test 1)	f2 (test 2)	f2 (test 3)	f2 (test 4)	F2 (mean)	Cycles Ratio %	Frequency change %
0	1235	1237	1236	1232	1235	0	0
8942	1225	1226	1225	1226	1225.5	18.21	0.769
13976	1218	1220	1220	1221	1219.75	28.46	1.235
22607	1221	1221	1222	1222	1221.5	46.04	1.093
34576	1202	1202	1201	1200	1201.25	70.42	2.733
39598	1205	1206	1206	1206	1205.75	80.65	2.368
44616	1201	1201	1202	1202	1201.5	90.87	2.712
47519	1190	1189	1189	1189	1189.25	96.78	3.704
48809	1175	1176	1175	1173	1174.75	99.41	4.878
49099	Fail	**	**	**	**	100	**

3.5.2 Damping capacity evaluation

The logarithmic decrement method is used in order to evaluate the damping capacity of the material. In this method, the damping capacity is obtained from the ratio of the acceleration amplitude recorded at different cycles. The logarithm decrement is defined as [7]:

$$\delta = Ln\left(\frac{y_m}{y_{m+n}}\right) \tag{3.3}$$

where y_m and y_{m+n} are the peak amplitudes of vibration for cycles mth and (m+n)th, respectively. The damping capacity can then be calculated by [7]:

$$\xi = \left(\frac{\delta}{2\pi n}\right) \tag{3.4}$$

In general, if one assumes that the free vibration response of a system can be characterized by a periodic function (sine or cosine) in the time domain, as represented by Equation 3.5, the natural logarithm of the peak amplitude in each half-cycle would then be a function of the damping capacity.

$$y(t) = e^{-\xi\omega t} Cos\left(\omega t + \phi\right) \tag{3.5}$$

As shown in Equation 3.5, the natural logarithm of the peak amplitude would be a line with the slope of $-\xi\omega$. As we know, the vibration mode shape of any system is a combination of different mode shapes; however, the first mode shape has a significant role in the final outcome of the vibration; therefore, the output signals were filtered by a low pass filter, which eliminated frequencies higher than 500 Hz, so that only the first mode of vibration signals were included. The absolute value of the peak amplitude in each half-cycle was then identified, as shown by the stars in Figure 3.7. As can be seen, the magnitudes of these peak amplitudes gradually decrease, and the amplitude ratio of the last point to the first point is equal to 0.05.

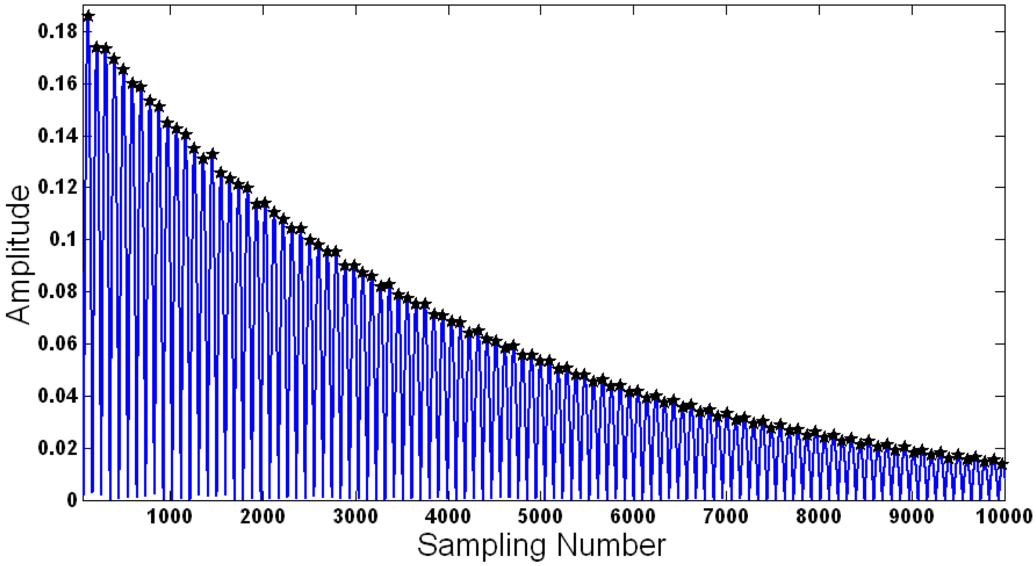

Figure 3.7 The absolute value of a signal at its peak in each half-cycle

A line is then fitted to the points established by the natural logarithm of the maximum amplitudes, as shown in Figure 3.8. The slope of the line passing through the data points would represent the product of the damping capacity and natural frequency. The evaluated damping capacity for each of the specimens is reported in Table 3.3. As seen, the damping capacity of this material is about 0.48%. However, because of the variation in porosity throughout the specimens, the data are somewhat scattered, indicating the variation in the void ratio of the specimens.

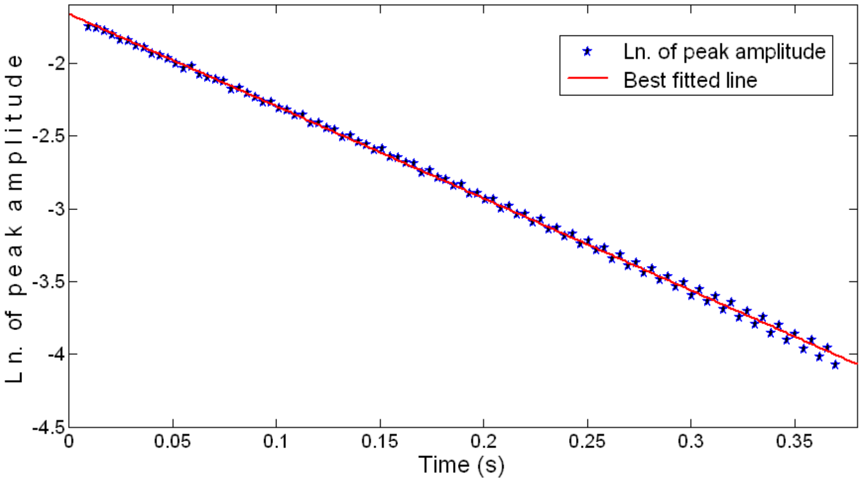

Figure 3.8 Best fitted line to the natural logarithm of the peak amplitude of each half-cycle

Table 3.3 Damping capacity of the specimens

Specimen No.	Damping Capacity (%) Test 1	Damping Capacity (%) Test 2	Damping Capacity (%) Test 3	Damping Capacity (%) Test 4	Mean Damping Capacity (%)
1	0.643	0.592	0.56	0.547	0.5855
2	0.482	0.544	0.474	0.463	0.49075
3	0.467	0.491	0.4	0.398	0.439
4	0.502	0.472	0.477	0.501	0.488
5	0.432	0.426	0.421	0.415	0.4235
6	0.451	0.458	0.438	0.467	0.4535

In order to establish damage progress in each specimen, the damping evaluation was performed for all the signals. The change in the damping capacity ratio, Δξ, is defined by:

$$\Delta\xi = \frac{\xi - \xi_0}{\xi_0} \tag{3.6}$$

where ξ is the damping capacity of the specimen after a certain number of fatigue loading cycles, and ξ_0 is the damping capacity of the virgin specimen. The calculated variation in the damping capacity as a function of the applied loading cycles (reported as % cycles ratio) of one of the specimens is reported in Table 3.4.

Table 3.4 Damping capacity change

Number of Loading Cycles	Damping Capacity (%)	Cycles Ratio (%)	Δξ (%)
0	0.439	0	0
11256	0.563	28.53	28.18
23636	0.538	59.91	22.53
32294	0.657	81.86	49.61
33443	0.686	84.77	56.33
35156	0.681	89.12	55.13
36984	0.667	93.75	51.94
38944	0.668	98.72	52.16
39450	Fail	Fail	Fail

3.6 Material's response during cyclic loading

The variations in the natural frequency and damping capacity of the alloy evaluated during the application of cyclic loading indicate that the cyclic loading had caused degradation in material's stiffness, which in turn affected the material's natural frequency. This change is depicted in Figure 3.9 for all specimens.

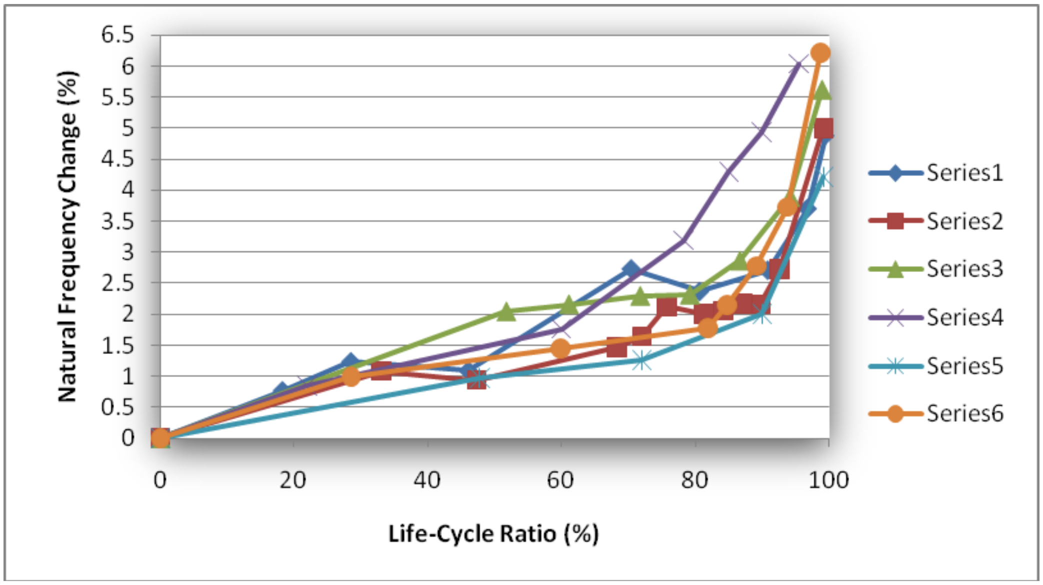

Figure 3.9 Variation of the natural frequency as a function of life cycles ratio

As reported in Table 3.4, an increase in the damping capacity was observed for all specimens as a result of the applied cyclic loading. The evaluated change in the damping capacity is illustrated for all the specimens in Figure 3.10.

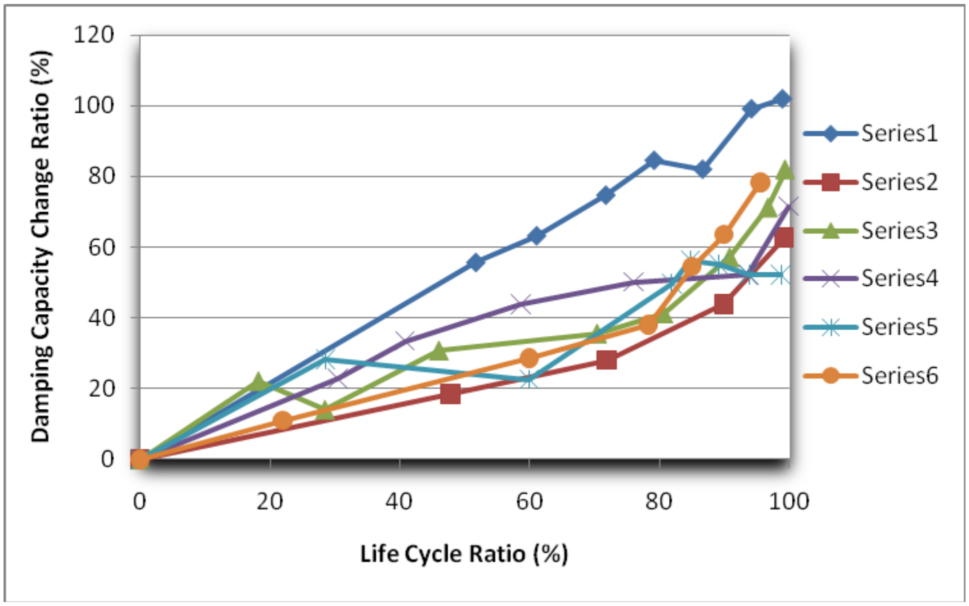

Figure 3.10 Variation of the damping capacity as a function of life cycles ratio

3.7 Summary and conclusions

Vibration characteristics of HPDC AM60B magnesium alloy were evaluated with the aim of establishing the damage progress in the alloy as a result of the applied cyclic loading and indirectly evaluate the influence of especial porosity within the alloy. The variation of the natural frequency and damping capacity of a material, as a result of applied cyclic loading, can be utilized as a means for evaluating damage progress in materials. This information can be used for estimating materials' life-cycles. This approach can be considered as an effective approach, which is independent of the loading amplitude, and the location of excitation and signal collection. However, our observations indicated that the results are quite sensitive to the test specimen's dimensions.

A frequency degradation of approximately 5% indicated excessive damage that could be considered as the failure of the material. This value was not however very consistent for all the tested specimens, as it ranged from 4% to 6%. The response in the degradation of an alloy's natural frequency was observed to follow two regimes. Through the first regime, which covered approximately the first 60% of the life cycle ratio of the material, the material degradation increased gradually. Within the second regime (i.e., from 60% life-cycle ratio to the end of the material's life-cycle), the material underwent abrupt and significant degradation, ended by the ultimate failure.

It was demonstrated that cyclic loading caused an increase in the damping capacity of the material. The values of this change to the failure ranged from 60% to 100%, which is a sizeable interval. Moreover, the variation in the damping capacity occurred within a wide range. This is believed to be in part due to the inherent nature of the HPDC alloy considered in this study, which had a large variation in its porosity. It could also be due to the method used in establishing the damping capacity, in that the method uses a curve fitting algorithm to establish the damping capacity. As a result, any error embedded in the experimental data could be grossly amplified and adversely affecting the outcropping damping capacity.

3.8 References

[1] Salawu, O.S., "Detection of Structural Damage through Change in Frequency; A Review", Engineering Structures, 19, pp. 718-723, 1997.

[2] Hsieh, S.-C., Lee, S.- Y., Ciou, C.- Y., Huang, H.- M., "Non-Destructive Natural Frequency Tests of Cyclic Fatigue-Loaded Nickel–Titanium Rotary Instruments", Med Biol Eng Comput, 48, pp. 555–560, 2010.

[3] Shang, D.- G., Barkey, M. E., Wang, Y., Lim, T. C., "Effect of Fatigue Damage on the Dynamic Response Frequency of Spot-Welded Joints", International Journal of Fatigue, 25, pp. 311– 316, 2003.

[4] Shang. D.-G. and Barkey, M.E., "Analysis of Fatigue Crack Behavior Based on Dynamic Response Simulations and Experiments for Tensile-Shear Spot-Welded Joints", Fatigue Fract Engng Mater Struct, 29, 23–30, 2006.

[5] ASTM E1245, “Standard Practice for Determining the Inclusion or Second-Phase Constituent Content of Metals by Automatic Image Analysis”, (Reapproved 2008).

[6] ASTM E466-07, “Standard Practice for Conducting Force Controlled Constant Amplitude Axial Fatigue Tests of Metallic Materials”.

[7] Smith, C. B. and Werely, N. M., “Composite Rotorcraft Flex Beams with Viscoelastic Damping Layers for Aeromechanical Stability Augmentation”, In M^3D III: Mechanics and Mechanisms of Material Damping, Edited by Volfenden and V.K.Kinra. American Society for Testing and Materials, ASTM STP 1304, West Conshohoken, Pa, pp. 62-67, 1997.

CHAPTER 4 The Influence of Negative and Positive Stress Ratios on Crack Growth Rate in AM60B Magnesium Alloy

Morteza Mehrzadi and Farid Taheri
Department of Civil and Resource Engineering, Dalhousie University, 1360 Barrington Street, Halifax, NS, B3J 1Z1, Canada

Published in the journal of Material Science and Engineering A., 545, 68- 77, 2012.

4.1 Abstract

In this paper, the effect of stress ratio on fatigue crack growth rate (FCGR) of AM60B magnesium alloy plates at room temperature is studied. The plates are loaded under a wide range of stress ratios (-1, -0.8, -0.6, -0.3, 0, 0.25, 0.5 and 0.75) and the behavior of the center crack is investigated. Most FCGR data available in the literature have been presented using various FCGR models that are mainly based on a positive stress intensity range as well as the entire stress intensity range. In this paper, a modified model, developed based on the Walker model, is proposed. The model condenses and presents the data obtained under the wide stress ratio range into a single line on a logarithmic scale. Finally, the variances in the FCGR data that were presented with different models from the best-fitted line to the zero stress ratio were calculated and compared to each other to clarify the efficiency of the model.

Keywords: Fatigue crack propagation rate, AM60B magnesium alloy, Walker model, Stress intensity range

4.2 Introduction

Magnesium alloys are increasingly being used in automobile and light truck industries due to their low density (a quarter that of steel and two-thirds that of aluminum), high specific strength, relatively lighter weight and excellent castability and machinability.

The use of Mg alloys in automotive components dates back to 1920, when they were being used in racing cars. However, in early 70s, Volkswagen Group of companies, along with other auto manufacturers (including DaimlerChrysler (Mercedes Benz), BMW, Ford and Jaguar), actively started using Mg alloys in various applications. As an example, in 1971, Volkswagen used nearly 42,000 tons of Mg alloys in various automobile applications [1]. Automobile components, however, are usually subjected to cyclic loading. As a result, the likelihood of failure due to fatigue becomes high. Failure caused by fatigue loading is usually catastrophic; therefore, there is an urgent need for better understanding of the fatigue and fracture behavior of Mg alloys, especially when subject to a wide range of stresses.

A few research works have been produced examining the mechanical behavior of AM60B. For instance, the monotonic and cyclic plasticity of the alloy in ambient temperature was studied by Lu et al. [2]. They discussed the influence of alloy's "skin-core" microstructure (which is the result of the non-equilibrium solidification of the molten alloy during the high-pressure die-casting process) on the fracture response of the alloy. It was observed that the microstructure of alloy's skin and core were quite different with respect to grain size and percentage of pores, and that the difference increased as the plate's thickness increased. Moreover, the pores act as a stress riser and initiates cracking in the material. The researchers presented the continuation of their investigations in a subsequent work [3], studying the fatigue life of AM60B under different maximum stress levels. Similarly, Nur Hossein and Taheri [4] studied the effect of the stress ratio on the fatigue crack growth rate of AM60B magnesium alloy and material fatigue behavior at various environmental temperatures. FCGR experimental data for specimens bearing an edge crack tested under three stress ratios (R=0, 0.1 and 0.2) was presented and compared to the results obtained by incorporating the Paris and Walker models. Their comparison showed the effectiveness of the Walker model. It is however worth noting that the stress ratios considered in that study were close to one another and, more importantly, they were close to R=0.

Zheng and Powell [5] also applied the Walker model in considering the effect of the stress ratio on the FCGR of the nickel-based superalloy Udimet720, highlighting the method used to determine the parameters of the Walker model.

Elber [6] was the first to introduce the crack closure concept. He defined a new model by substituting the effective stress intensity range for the stress intensity range appearing in the Paris model in order to account for the stress ratio effects on FCGR. He showed that, in a crack produced by cyclic loading, the load at which the crack is closed would be neither zero nor compressive, but would be tensile. He concluded that a crack would propagate at the opening portion of cyclic loading, and defined the effective stress intensity range as:

$$\Delta K_{eff} = (K_{\max} - K_{op}) \tag{4.1}$$

where ΔK_{eff} , K_{max} and K_{op} are the effective, maximum and opening (or closure) stress intensity factors. Other researchers have also applied the crack closure concept to define the FCGR and stress ratio effects for different materials [7, 8, 9].

Kujawski [10] described the difficulties with the proposed crack closure model of Elber and introduced the $(\Delta K^{+}\ K_{max})^{0.5}$ parameter as a driving force for FCGR when considering the stress ratio effect. This newly-defined parameter is based on the hypothesis that the compressive part of the loading does not have any effect on crack propagation. In subsequent papers, Kujawski [11, 12], modified $(\Delta K^{+}\ K_{max})^{0.5}$ to $K_{max}^{\alpha}\ (\Delta K^{+})^{1-\alpha}$, such that α is a material-dependent parameter. As in his previous paper, positive and maximum stress intensities were used to define crack propagation behavior without any contribution from the compressive part of fatigue loading. Kujawski demonstrated in his research how to determine his model's parameter (α).

Huang and Moan [13] reviewed several models, including Kujawski's, and proposed a new model as a function of stress ratio (R). Kujawski's model was modified to provide more accurate results, especially for negative and high stress ratios. Noroozi et al [14] proposed a unified two-parameter fatigue crack growth model for different stress ratios and related the crack propagation to the maximum stress intensity and total stress intensity range. Dimitriu and Bhadeshia [15] used the neural network to define a crack propagation model for a wide range of material and specimen conditions as well as stress ratios.

In this paper, the FCG behavior of AM60B Mg alloy subject to various stress ratios (both negative and positive) is investigated. The integrity of some of the available models in predicting the *FCGR* is also investigated, and their results are discussed. Finally, a new model, developed based on our experimental data, is proposed. The model is capable of accounting for a wide range of stress ratios effectively. The efficiency of the proposed model in comparison to the other FCGR models is also presented.

4.3 Material

The chemical composition of the magnesium alloy used in this project is shown in Table 4.1. The alloy was provided by Meridian Technologies Inc. (Strathroy, Ontario).

Table 4.1 Chemical composition of the AM60B alloy in weight. % [1]

Mg	Al	Mn	Si	Zn	Fe	Cu	Ni	Other
Bal.	5.5-6.5	0.25 min	0.1 max	0.22 max	0.005 max	0.01 max	0.002 max	0.003 max (total)

The plates from which the specimens were extracted were 3mm thick, as received and were cast by the Meridian. As mentioned previously, the volume of the micro-voids and porosity in a cast material is highly dependent on the thickness of the final product. Therefore, for specimens as thin as those used in this study, the porosity ratio was found to be much less than those observed in the specimens used in our previous studies [16]. The consistency observed in the experimental results indicates that the existence of the small porosity ratio in our specimens did not have any effect on the fatigue response of the material. The mechanical properties of the alloy are reported in Table 4.2.

Table 4.2 Material properties

Yield stress (σ_Y)	150 MPa
Modulus of elasticity (E)	40 GPa

4.4 Test setup

4.4.1 Specimen preparation

Specimens were cut from as-received high-pressure die-cast AM60B alloy plates provided by Meridian Technologies Inc. (Strathroy, Ontario), according to ASTM E-647-08 [17]. Grip holes were drilled on the top and bottom of the plate, along with a very small center hole (1 mm in diameter), which was used to initiate a 6 mm long starter notch, using a jeweler's saw (Figure 4.1).

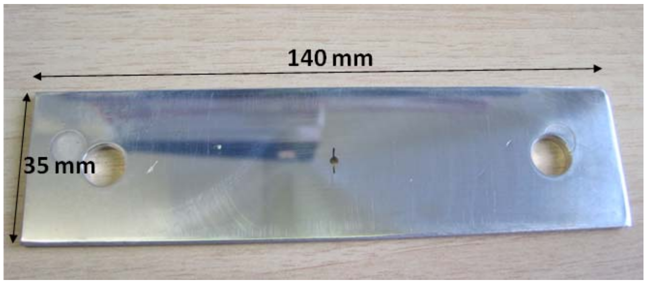

Figure 4.1 Geometry of the specimen

In order to obtain a clear view of the crack length and make an accurate measurement of it, the surface of the specimens were polished to a mirror-like sheen, according to recommendations in ASTM E1245 [18]. The polishing process involved using progressively finer abrasive papers (i.e., 320, 400 and 600 grit) before finally applying a suspension of 3-micron aluminum oxide on a rotary pad to produce the ultimate shine.

4.4.2 Fatigue loading

An Instron servo-hydraulic universal test machine, with a capacity of ±100 KN under dynamic, or 200 KN under static loading conditions, controlled by an 8501 digital controller, was used to apply constant-amplitude cyclic loading. The maximum stress of 55 MPa with a loading rate of 6 Hz was applied to all specimens. The sole variable in testing the specimens was the variation in the stress ratio, *R*, defined as:

$$R = \frac{\sigma_{\min}}{\sigma_{\max}} \tag{4.2}$$

where σ_{min} and σ_{max} are the minimum and maximum stresses in each cycle, respectively. An anti-buckling device was designed and fabricated to prevent the lateral buckling of the specimens when subjected to a negative stress ratio. Figure 4.2 shows the configuration of the anti-buckling device, which is attached to our test fixture grip. As shown in Figure 4.2, two roller bearings support each side of the specimen, thereby minimizing the contact force between the device and the specimen under the loading. The digital microscope, Dino-Lite AM-7013MZTL, with a magnification of 92X and resolution of 5 megapixel (2592×1944), mounted on a traveling micrometer, was used to measure the crack length. This microscope was equipped with 8 LEDs to illuminate the crack-tip region, and could be conveniently connected to a computer to record crack propagation. The entire test setup is shown in Figure 4.3.

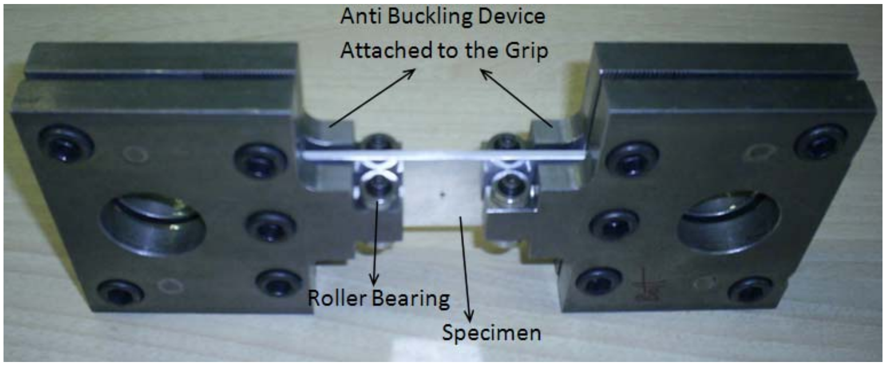

Figure 4.2 Anti-buckling device

As shown in Figure 4.3, the grip and anti-buckling device were held by machined fixed grips, connected to a load cell. After a certain number of cycles, the test was interrupted and the crack length was carefully measured; the procedure was repeated till specimen's failure was observed.

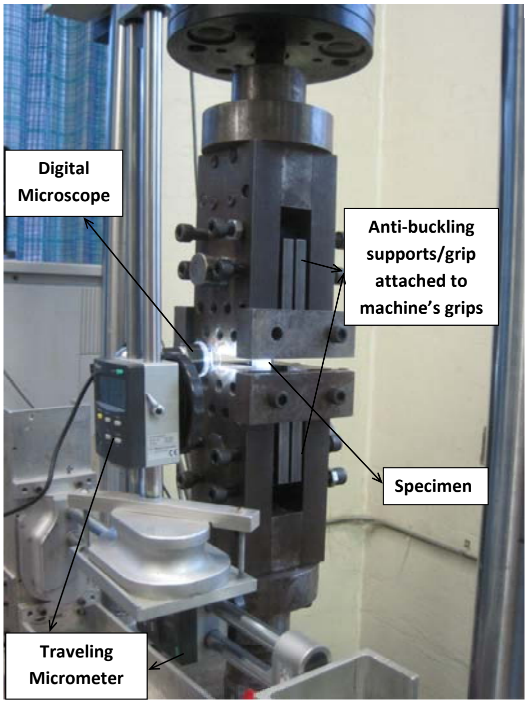

Figure 4.3 Test setup

All tests were conducted at room temperature. In order to obtain a sharp crack, the 6 mm notch was pre-cracked to a length of 8 mm and the subsequent FCG data was recorded with datum to this sharp crack tip. A maximum stress of 55 MPa with a stress ratio of zero was applied to the specimens at the pre-crack stage. An image of a crack captured with the digital microscope is illustrated in Figure 4.4.

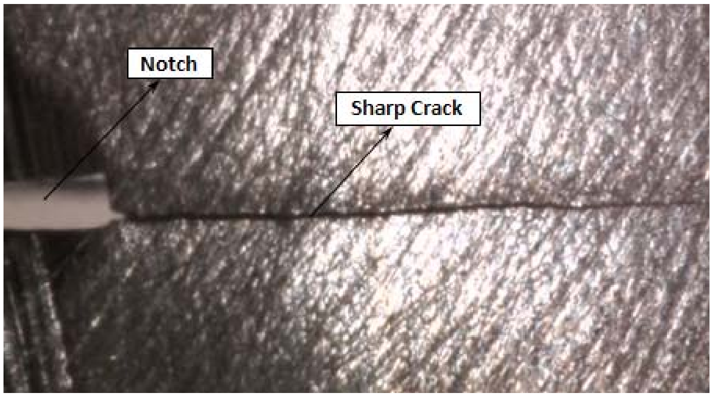

Figure 4.4 Image of the notch and crack

4.5 Results and analysis

4.5.1 Crack length versus number of cycles

As stated previously, different stress ratios, but maintaining the same maximum stress were applied to the specimens, and the incremental center crack lengths versus the number of the cycles were recorded. The considered cyclic loading scenarios are summarized in Table 4.3.

Table 4.3 Different cyclic loading properties

No.	R	Max. Stress (MPa)	Min. Stress (MPa)
1	-1	55	-55
2	-0.8	55	-44
3	-0.6	55	-33
4	-0.3	55	-16.5
5	0	55	0
6	0.25	55	13.75
7	0.5	55	27.5
8	0.75	55	41.25

As is widely known, a decreased stress ratio would shorten the life-cycle of a specimen, as it is subjected to a relatively larger magnitude of stress. The curves of crack length versus number of cycles are shown in Figure 4.5. For a better understanding of what occurs under a negative stress ratio range, data related to R=0, -0.3, -0.6, -0.8 and -1 are depicted on a separate graph (Figure 6). Several researchers [see, for instance, references 10, 11 and 12] have contended that a decrease in the stress ratio to a negative magnitude would have no effect on the resulting crack propagation rate. Their statement has been based on the hypothesis that when a crack in a material is subjected to compressive stress, it would be closed and thus would not grow. However, as shown in Figure 4.6, application of a negative stress ratio significantly decreased material's fatigue life. Further, as shown in Figures 4.5 and 4.6, specimen's fatigue life is highly dependent on the stress ratio. It should be noted that three tests were carried out for each stress ratio, and that the average values of the three curves are presented for each stress ratio.

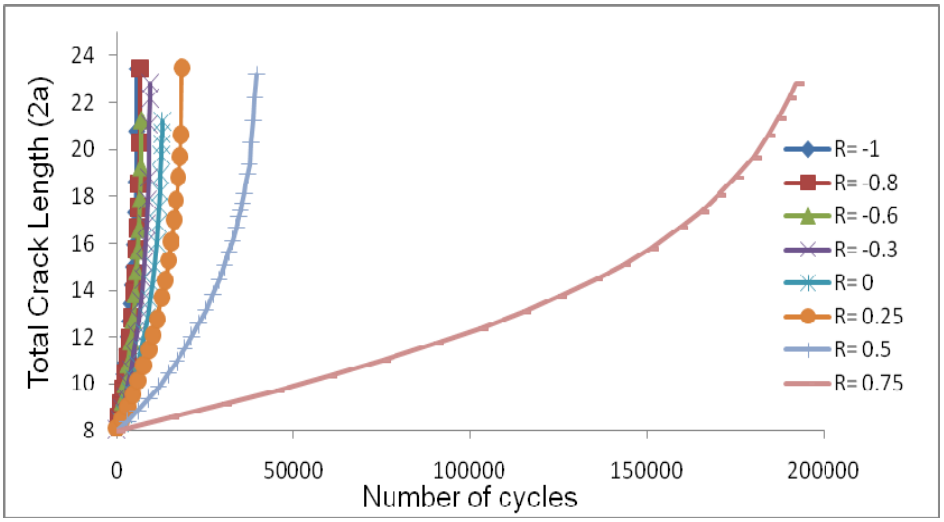

Figure 4.5 Crack propagation versus number of cycles for all stress ratios

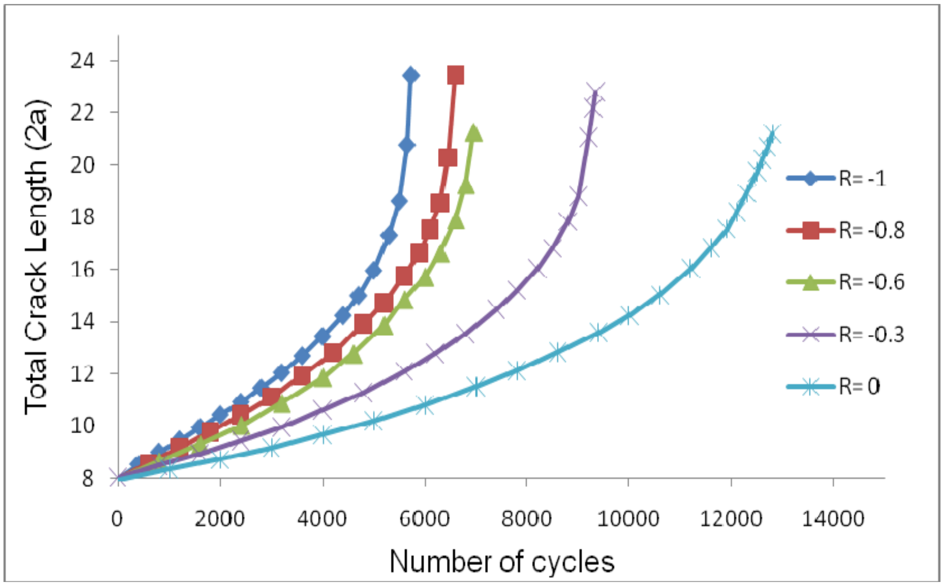

Figure 4.6 Crack propagation versus number of cycles for the negative stress ratios

4.5.2 Fatigue crack growth rate (FCGR)

In this section, the FCGR of the AM60B predicted by the use of some of the most commonly- used models are presented and compared with the experimental data.

4.5.2.1 The Paris model

The FCGR response of metals can be divided into three regions [19]. The first region covers the threshold portion, which consists of slow FCG. This region is followed by the second region, which represents the stable FCG, followed by the third region that contains the fast FCG response up to failure. In the second region, the FCGR follows a linear trend as a function of the increasing stress intensity range, when plotted on a logarithmic scale. In all of the FCGR tests in this study, data related to the first and third regions are eliminated, and only the data related to the second region is presented.

In 1963 Paris and Erdogan introduced their famous model, commonly referred as the Paris Model [20]. The model defines the material's FCGR behavior in the second region as a function of the stress intensity range, and is represented by the following mathematical relation:

$$\frac{da}{dN} = C_p(\Delta K)^{m_p} \tag{4.3}$$

where $\frac{da}{dN}$ and ΔK are the FCGR and stress intensity range, respectively, C_p and m_p are the Paris model coefficients, which are material-dependent.

According to the linear fracture mechanics theory, the crack tip stress intensity factor could be presented as a function of the applied far field stress, σ, half-crack length, a, and a geometry related coefficient, Y [21, 22], shown mathematically by:

$$K = Y\sigma\sqrt{\pi a} \tag{4.4}$$

where the geometry coefficient for a center crack in a finite plate obtained through a finite element analysis is represented by [21]:

$$Y = \left[\sec\left(\frac{\pi a}{2w}\right)\right]^{0.5}\left[1 - 0.025\left(\frac{a}{w}\right)^2 + 0.06\left(\frac{a}{w}\right)^4\right] \tag{4.5}$$

In the above equation, w is the half-plate width. ASTM E-647 08[16] also suggests the use of equation 4.6 for evaluation of the stress intensity range. In the following equation, only the positive (tensile) segment of the applied stress is used in calculating Δ*K*, and the compressive portion of the applied stress is ignored. In the following sections, FCGR behavior will be computed both as a function of the positive range of Δ*K* and also by considering the entire stress intensity factor range, pending the sense of stress ratio, R,

$$\begin{aligned} \Delta K &= (1-R)K_{\max} && R > 0 \\ \Delta K &= K_{\max} && R \le 0 \end{aligned} \tag{4.6}$$

4.5.2.1.1 Paris model's prediction when considering the positive stress intensity range (ΔK^+)

In this section, the positive portion of the cyclic loading is considered in establishing the stress intensity range (as defined by Equation 4.6). The graph of crack growth versus the positive stress intensity range, ΔK^+, for different stress ratios considered in our experimental work is presented in a logarithmic scale, in Figure 4.7.

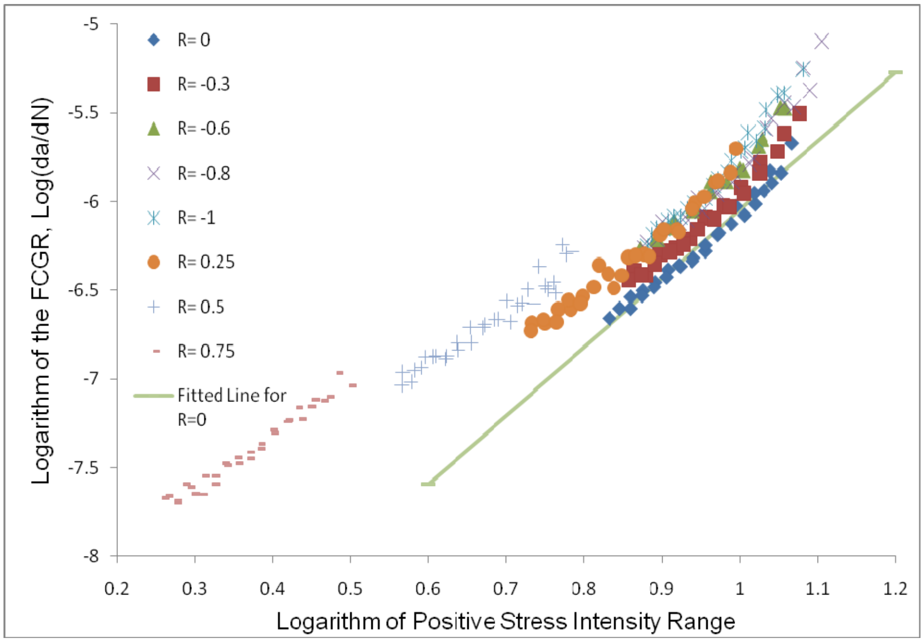

Figure 4.7 Crack growth behavior versus the positive stress intensity range, ΔK^+

As shown in the figure, the data are widely scattered and FCGR trend for each stress ratio is different from the others. The behaviour for each stress ratio, therefore, has to be represented by a separate line on the logarithmic scale. The best-fitted line to the FCGR data of plates tested at zero stress ratio is also shown in Figure 4.7; this line illustrate how widely the data for other stress ratios are scattered. As well, Figure 4.7 shows the strong dependency of the FCGR response to stress ratio. However, this dependency is not consistent for both positive and negative stress ratios. For instance, while an increase in the stress ratio in the positive part results in faster crack growth for a given positive stress intensity range, this trend is completely reversed in the case of negative stress ratios.

The next step for applying the Paris model is the evaluation of the Paris coefficients C_p and m_p. As mentioned before, the Paris model is applicable to the second region in which FCGR follows a linear trend when plotted in the logarithmic scale. Thus, by fitting a straight line to the plot of *da/dN* versus ΔK, the values of the Paris model's coefficient could easily be established. C_p would be the intercept of the best-fit line to the data, and m_p would be the slope of the line, as mathematically represented by the following equation;

$$Log\left(\frac{da}{dN}\right) = Log\ C_p + m_p \times Log(\Delta K^{+}) \tag{4.7}$$

Paris model's parameters for the FCGR data obtained at different stress ratios are calculated and reported in Table 4.4. It should be noted that these parameters are established based on the consideration of positive stress intensity range.

Table 4.4 Paris model parameters for different stress ratios

R	C_p	m_p	Log (C_p)
-1	2.50611E-11	4.9091	-10.601
-0.8	3.62243E-11	4.6915	-10.441
-0.6	1.09648E-10	4.1919	-9.96
-0.3	1.09749E-10	4.046	-9.9596
0	1.22603E-10	3.8666	-9.9115
0.25	5.55265E-10	3.4209	-9.2555
0.5	1.64097E-09	3.1128	-8.7849
0.75	3.08816E-09	3.0284	-8.5103

The variation of m_p and log (C_p) versus stress ratio are shown in Figures 4.8.a., 4.8.b. and 4.8.c. The relation between m_p and the stress ratios are divided into two categories (i.e., negative and positive stress ratios.) As shown in Table 4.4 and the following figures, the slope of the FCGR curves increase as the stress ratio decreases. While this relation could be defined by a polynomial function, separately, for the positive and negative stress ratios (as presented in Equation 4.8), the variation in the logarithmic value of C_p does not follow a distinct trend when plotted as a function of the stress ratio, R, such that it could be expressed by a single mathematical equation. It is believed that this is due to the adaptation of ΔK^+ instead of ΔK which is calculated based on the full range of the applied stress.

$$\begin{aligned} m_p &= 0.8839\,R^2 - 0.1915\,R + 3.8666 \qquad R \le 0 \\ m_p &= 1.2470\,R^2 - 2.1939\,R + 3.8666 \qquad R \ge 0 \end{aligned} \tag{4.8}$$

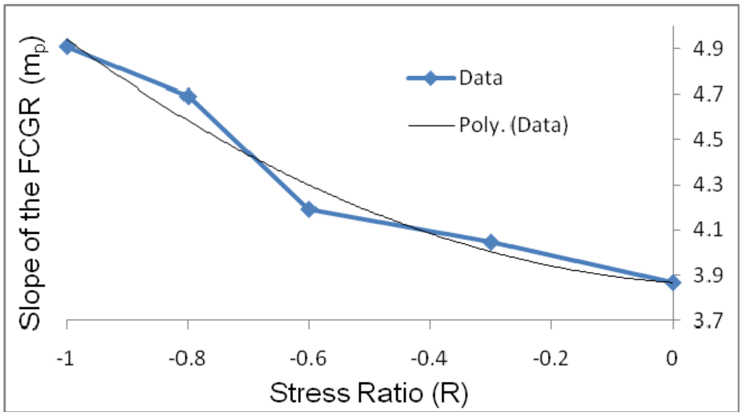

(a)

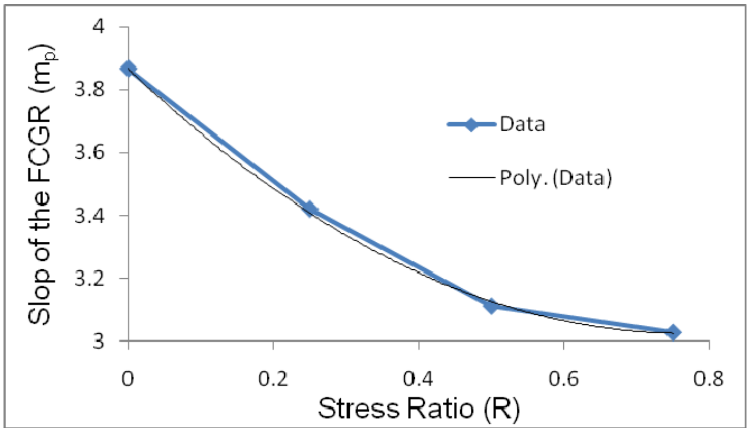

(b)

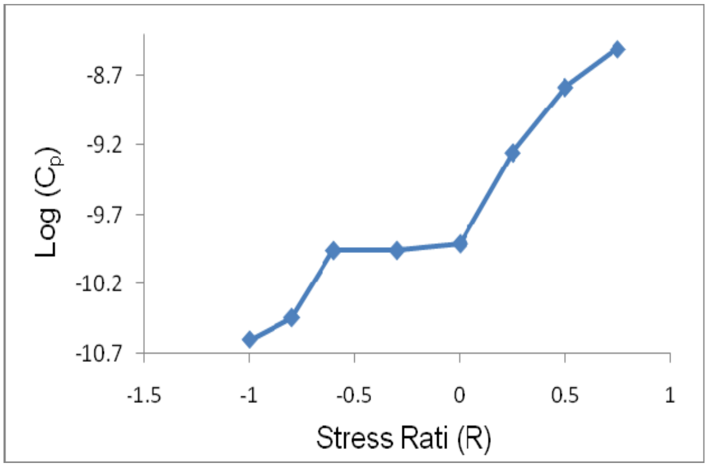

(c)

Figure 4.8 Graphs illustrating variation of (a) m_p versus positive stress ratio; (b) m_p versus negative stress ratio; (c) Log (C_p) versus stress ratio

4.5.2.1.2 Paris model's prediction when considering the full range of the stress intensity range (ΔK)

In the previous section, the positive portion of the stress range was considered in establishing ΔK and later in establishing Paris model's parameters. In this section, the entire stress range will be considered in calculating the stress intensity factor and its effect on Paris model's parameters will be investigated.

The full range stress intensity factor can be calculated by considering both the positive and negative stress ratios, using the following equation:

$$\Delta K = Y(\sigma_{\max} - \sigma_{\min})\sqrt{\pi a} = (1-R)K_{\max} \tag{4.9}$$

The plot of the resulting FCGR versus the full stress intensity range for various stress ratios on a logarithmic scale is shown in Figure 4.9. The resulting curves are now clearly separated from one to another and the influence of stress ratio is more distinctly evident. It can be seen that when the full range of the applied stress is considered, the increase in the stress ratio essentially moves the FCGR curve to the left, similar to the trend observed when using only the positive stress ratios as seen in Figure 4.7.

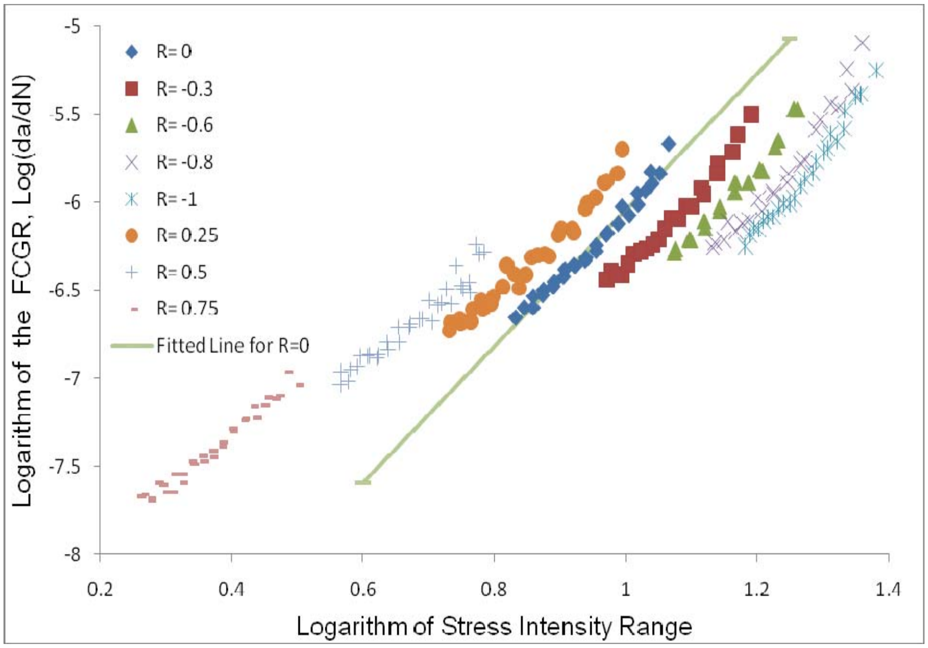

Figure 4.9 Crack propagation behavior versus the whole stress intensity rang (ΔK)

Moreover, the response, as plotted on the logarithmic scale, also follows a linear trend. It can be mathematically demonstrated that the slope of the best-fitted lines to the data would be similar to those established when using ΔK^+ (see Figure 4.7), and that the only change would occur in the value of the intersect of the best-fit lines (i.e., the values of C_p). The relationships for establishing the graph in negative stress ratio region are shown below.

$$\Delta K = (1-R)\,\Delta K^+ \quad \Rightarrow \quad \Delta K^+ = \frac{\Delta K}{(1-R)}$$

$$\frac{da}{dN} = C_p(\Delta K^+)^{m_p} = C_p\left(\frac{\Delta K}{1-R}\right)^{m_p} \tag{4.10}$$

$$Log\left(\frac{da}{dN}\right) = \left[Log\ C_p - m_p \times Log(1-R)\right] + m_p \times Log(\Delta K)$$

As shown in Equation 4.10, the slope of the line is represented by m_p, but the Log (C_p) as used earlier has been replaced by Log(C_p) - m_p × Log (1-R). The above parameters, calculated for the different stress ratios, are presented in Table 4.5.

Table 4.5 Paris model's parameters calculated based on the entire stress intensity range

R	C_p (New)	m_p	Log(C_p (New))
-1	8.34091E-13	4.9091	-12.07878635
-0.8	2.29821E-12	4.6915	-11.63861096
-0.6	1.5288E-11	4.1919	-10.81565056
-0.3	3.79652E-11	4.046	-10.4206148
0	1.22603E-10	3.8666	-9.9115
0.25	5.55265E-10	3.4209	-9.2555
0.5	1.64097E-09	3.1128	-8.7849
0.75	3.08816E-09	3.0284	-8.5103

The variation in the value of Log (C_p) as a function of the stress ratio has been plotted in Figure 4.10. It can be seen that Log (C_p) increases as R increases, and that this behavior can be defined by fitting a line through the data respectively yielding the following equation.

$$Log(C_p) = 2.1457\,R - 9.8173 \tag{4.11}$$

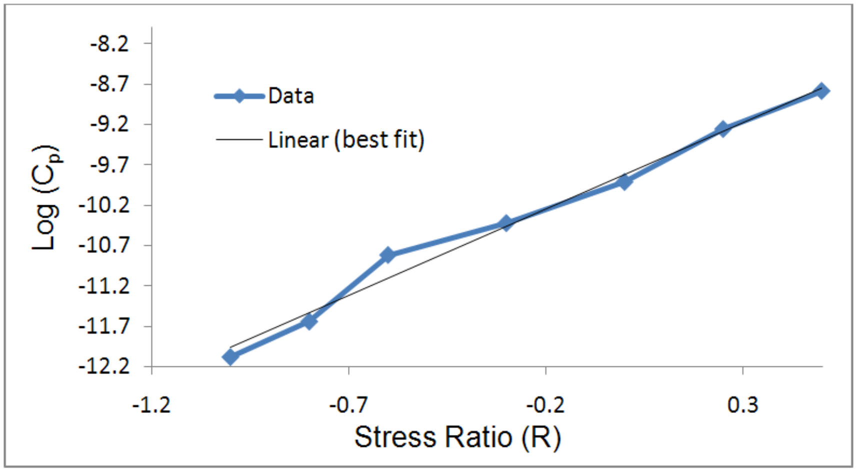

Figure 4.10 Variation in Log (C_p) versus stress ratios

The best-fitted line to the FCGR curve at the stress ratio of zero is also plotted in Figure 4.9. It can be seen that the data for various stress ratios are more scattered in this plot when compared to those plotted when the positive stress intensity range was used (see Figure 4.7); nevertheless, this time, the data scatter has a trend in itself (i.e., they are scattered as a function of the stress ratio). Furthermore, a unified and more logical trend is seen in the variation of the logarithm of C_p as a function of the stress ratio, and the variation could be represented by a linear function, as stated by Equation 4.11.

Presenting the data with the aid of the Paris model using the two different values for the stress intensity range (ΔK^+ and ΔK) indicates that beside the fact that Paris coefficient are material-dependent, they are R-dependent, and highly sensitive to the variation in the stress ratio. It can be concluded that the use of the entire portion of the cyclic stress range in calculating the stress intensity range would produce a better relationship between the Paris model's parameters and the stress ratio, such that the parameter can be effectively defined by polynomial equations.

4.5.2.2 The Walker model

Walker proposed his model in 1970 [23] with the aim of improving the shortfall of the Paris model by incorporating the effect of the stress ratio. In fact, Walker asserted that his model was capable of predicting FCGR behavior using just one equation by inclusion of a new stress intensity range parameter, namely, $\overline{\Delta K}$. Walker proposed the inclusion of the following stress intensity range, $\overline{\Delta K}$, instead of ΔK used in the Paris model:

$$\overline{\Delta K} = \frac{\Delta K}{(1-R)^{1-\gamma_w}} \tag{4.12}$$

Accordingly, the FCGR can be calculated by the following relationship:

$$\frac{da}{dN} = C_w(\overline{\Delta K})^{m_w} = C_w\left[\frac{\Delta K}{(1-R)^{1-\gamma_w}}\right]^{m_w} \tag{4.13}$$

where m_w, C_w and γ_w are Walker model's parameters. In the case of R=0, this model would yield the Paris model; so, m_w and C_w would equate to m_p and C_p. Walker defined his new model such that the FCGR data for different stress ratios could be condensed and represented by a single line, by suggesting the use of an extra parameter, γ_w. He tested the integrity of his model by evaluating FCGR for two aluminum alloys (2024-T3 and 7075-T6), adopting γ_w values of 0.5 and 0.425, respectively.

4.5.2.2.1 Evaluation of γ_w

In this section, two methods will be reviewed for evaluating the value of γ_w.

4.5.2.2.1.1 Method I

Some researchers [5, 24] used Paris model's parameter to establish the value of γ_w used in the Walker model. This approach is based on the assumption that the plot of FCGR versus the stress intensity range for all stress ratios would fall on lines parallel to one another in logarithmic scale. If this were true, it would mean that the value of m_w would be the same for all stress ratios. However, it has been shown that not only m_p is highly stress ratio dependent, but its variation as a function of stress ratio is not linear.

In showing the effect of non-parallel trend of FCGR for different stress ratios, the abovementioned approach will be applied to our FCGR data. Comparison of the Paris and Walker model indicates that:

$$C_p = \frac{C_w}{(1-R)^{m_w(1-\gamma_w)}} \tag{4.14}$$

Taking the logarithm of the above equation would yield:

$$Log\ C_p = Log\ C_w - \left[m_w(1-\gamma_w)\right] Log\,(1-R) \tag{4.15}$$

By plotting the Log (C_p) versus Log (1-R) and fitting a straight line to the data, the slope of the line would represent m_w (1-γ_w). As stated, according to the assumption, m_w should be constant and equate to $\mathrm{m_p}$, so the value of γ_w could be easily determined by comparing the FCGR for each stress ratio with the FCGR of R=0. The plot of FCGR versus Walker's model stress intensity range, $\overline{\Delta K}$, calculated by the use of γ_w as established based on the abovementioned approach, is plotted on the logarithmic scale, as shown in Figure 4.11.

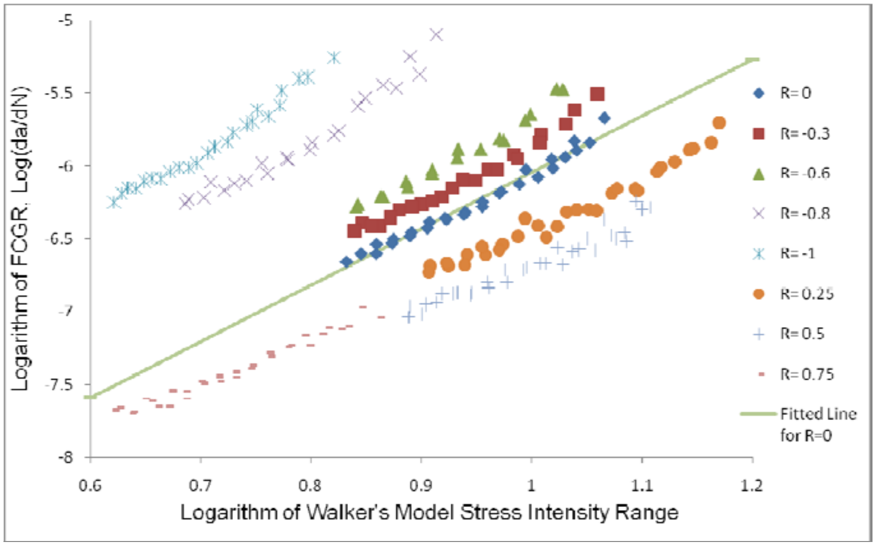

Figure 4.11 FCGR versus $\frac{\Delta K}{(1-R)^{1-\gamma_w}}$ in logarithmic scale

As seen in Figure 4.11, the Walker model could not condense the data on a single line (i.e. on the best-fit line to the data for *R*=0), due to the incorrect assumption with respect to the FCGR for different stress ratios having the same slope in logarithmic scale.

The role of $(1-R)^{1-\gamma_w}$ in the Walker model equation has been supposed to push the parallel curves to the right or left with respect to the best-fit line at *R*=0, in the logarithmic scale. The values of $Log\left[(1-R)^{1-\gamma_w}\right]$ for different stress ratios are presented in Table 4.6; the values are also plotted against the stress ratio (for both positive and negative values), separately in Figures 4.12.a. and 4.12.b.

Table 4.6 $Log\left[(1-R)^{1-\gamma_w}\right]$ for different stress ratios

R	$Log\left[(1-R)^{1-\gamma_w}\right]$
-1	0.560517136
-0.8	0.446677369
-0.6	0.233835789
-0.3	0.131668725
0	0
0.25	-0.17515205
0.5	-0.322837138
0.75	-0.36237889

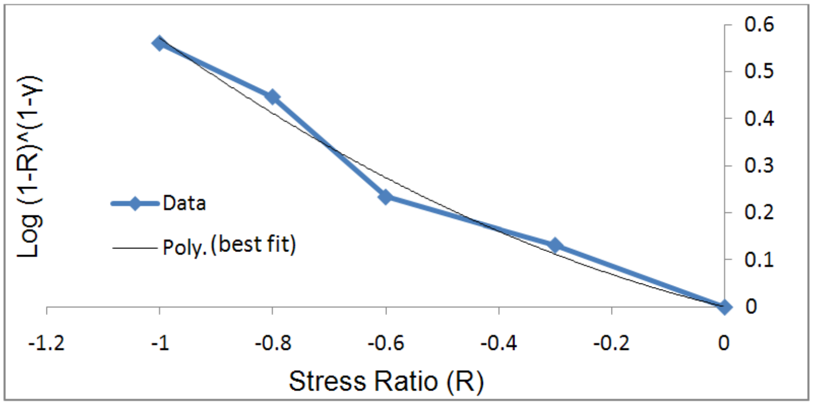

(a)

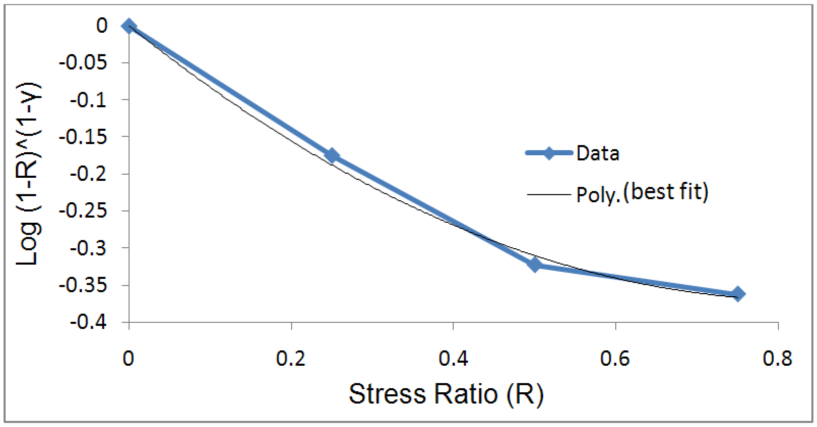

(b)

Figure 4.12 Variation in $Log\left[(1-R)^{1-\gamma_w}\right]$ as a function of the stress ratio (R); (a) For the negative stress ratios and (b) For the positive stress ratios

As seen, the variation of $Log\left[(1-R)^{1-\gamma_w}\right]$ as a function of the stress ratio can be defined by the following polynomial functions as:

$$Log\left[(1-R)^{1-\gamma_w}\right] = 0.2813\,R^2 - 0.2890\,R \qquad R \le 0$$
$$Log\left[(1-R)^{1-\gamma_w}\right] = 0.5255\,R^2 - 0.8829\,R \qquad R \ge 0 \qquad (4.16)$$

4.5.2.2.1.2 Method II

The other method for evaluating the value of γ_w has been presented by Kujawski [11], which was verified for positive stress ratios. Again, his method is applicable in cases where the FCGR obtained for different stress ratios in logarithmic scale follow a parallel trend with respect to one another. He extracted the γ_w by considering two FCGR curves, each for different stress ratios, $R_2 \geq R_1 \geq 0$, as:

$$\gamma_w = \frac{Log(\Delta K_1^+ / \Delta K_2^+)}{Log(1 - R_1/1 - R_2)} \tag{4.17}$$

where ΔK_1^+ and ΔK_2^+ are the stress intensity range corresponding to a constant crack growth rate (i.e. *da/dN* being constant). In this approach, the value of γ_w has to be calculated for different values of *da/dN* and their average value would be reported. The obtained values for γ_w using this method for different stress ratios are shown in Figure 4.13. As seen, the value of γ_w for each stress ratio is highly variable and could not be used in the Walker model.

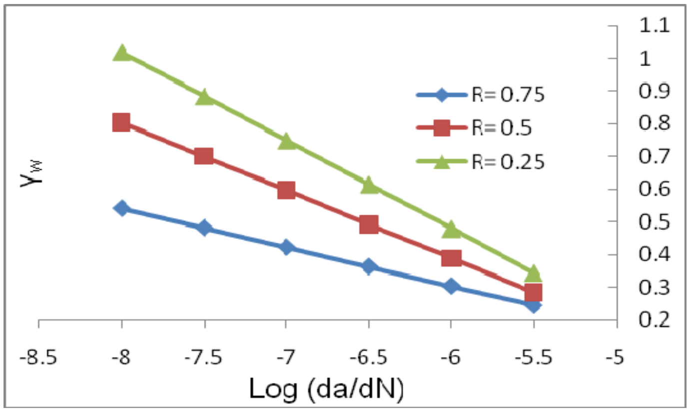

Figure 4.13 γ_w versus Log(da/dN) for different stress ratios

4.5.2.3 Kujawski's model

Kujawski initially proposed his model, which used $(\Delta K^+ K_{\max})^{0.5}$ for calculating FCGR [10]. He then improved his model and used $(K_{\max})^{\alpha}(\Delta K^+)^{1-\alpha}$ in calculating FCGR [11, 12]. Although he applied his model for cases with negative stress ratios, his modified model was however developed based on the assumption that the negative part of the cyclic loading would not have any effect on crack growth rate. Thus, when one applied his suggested expression for stress intensity factor for negative stress ratios, his parameter equals that appearing in the original Paris model (also see Figure 4.7); or mathematically:

$$(K_{\max})^{\alpha}(\Delta K^{+})^{1-\alpha} = \Delta K^{+} \; or \; K_{\max} \tag{4.18}$$

where α is a material dependent parameter. Noting that this model is not appropriate for consideration of negative stress ratios, it will not be discussed further in this paper.

4.5.2.4 The Huang and Moan model [13]

Huang and Moan reviewed different models, and finally came up with the following relationship:

$$\frac{da}{dN} = C(M \; \Delta K)^{m} \tag{4.19}$$

where

$$M = \begin{cases} (1-R)^{-\beta_1} & -5 \le R < 0 \\ (1-R)^{-\beta} & 0 \le R < 0.5 \\ (1.05 - 1.4R + 0.6R^2)^{-\beta} & 0.5 \le R < 1 \end{cases} \tag{4.20}$$

The modification factor was applied to the stress intensity range such to condense the data on a single line in the logarithmic scale. As seen, two new parameters β and β_1 were also defined in the model, which are dependent on the material and environment ($\beta \le \beta_1 \le 1$). The researchers used $\beta_1 = 1.2 \times \beta$, and $\beta=0.5$ and $\beta=0.7$ as a result of fitting their experimentally obtained FCGR data for Ti-6Al-4V and aluminum, respectively. While Huang and Moan mentioned in their paper that the same value of β could be used for similar materials, they however did not describe how β could be determined for other types of materials.

Huang and Moan's model was applied to our data by trying different values of β to fit the model to the experimental data. As seen from Figure 4.14, it was determined that β=0.5 produced the most favorable results, that is in terms of uniting all data obtained for various stress ratios near a single line.

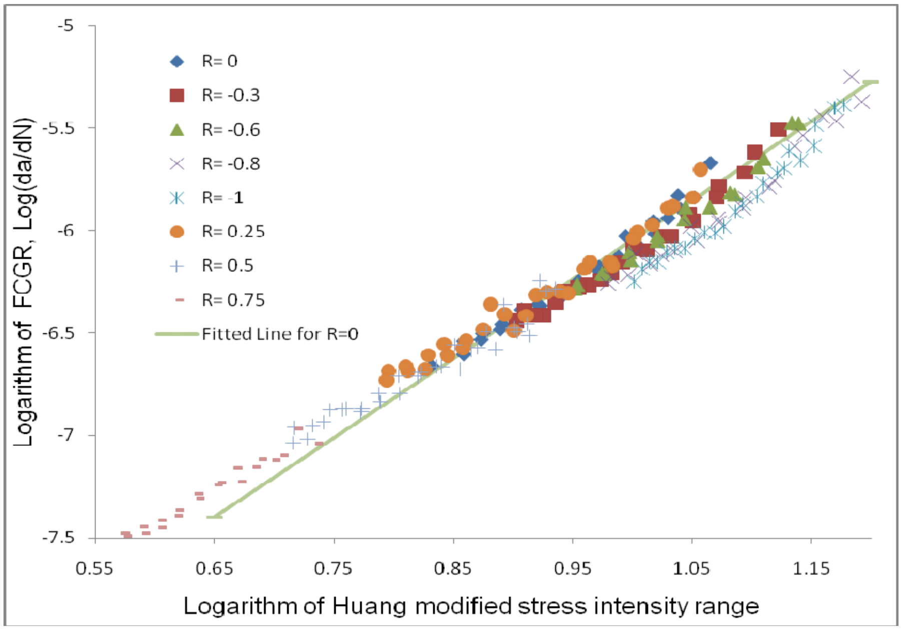

Figure 4.14 FCGR versus Huang modified ΔK in logarithmic scale ($R^2 = 0.981$)

As shown in Figure 4.14, this model provides better condensation of the data in comparison to Paris and Walker models.

4.5.2.5 Proposed Modified Walker model

As mentioned previously, the underlying assumption for establishing γ_w in Walker's model was that all the FCGR curves generated by Paris model for different stress ratios would be in parallel to one another. However, as discussed above, the data would not be in parallel, and the slope of the best-fit line to the data would be changing as a function of the stress ratio in a manner such that the slope would be decrease as the stress ratio increases.

Walker's model is a relatively simple, proven and a widely used model, requiring minimal parametric values. It would therefore be desirable if one could somehow arrange the data in such a way that they would align along the same slope, so that the Walker model could be used. To do so, a new form of the stress intensity range is proposed, which takes the following form:

$$\Delta K' = \Delta K^{\frac{(m_p)_{R_i}}{(m_p)_{R0}}} \tag{4.21}$$

where $(m_p)_{R_i}$ is the slope of the best-fit line of the data corresponding to stress ratio of "*i*", which was previously defined by Equation 4.8, and $(m_p)_{R0}$ is the slope of the FCGR data at *R*=0. Finally, $\Delta K'$ could be represented by:

$$\begin{aligned} \Delta K' &= \Delta K^{(0.2286R^2 - 0.0495R + 1)} \qquad R \le 0 \\ \Delta K' &= \Delta K^{(0.3691R^2 - 0.5674R + 1)} \qquad R \ge 0 \end{aligned} \tag{4.22}$$

Since the value of γ_w is not a unified value for all stress ratios, we recommend using the equivalent expression instead, as introduced in equations 4.16 (i.e., $Log\left[(1-R)^{1-\gamma_w}\right]$), which accounts for various variation in *R*. By incorporating the equivalent value and $\Delta K'$ (as per Equations 4.16 and 4.22, respectively) into the Walker model, the proposed modified Walker model can be presented by the following relationship:

$$\frac{da}{dN} = C_w(\Delta K_m)^{m_w} \tag{4.23}$$

in which:

$$\Delta K_m = \begin{cases} \dfrac{\Delta K^{(0.2286R^2 - 0.0495R + 1)}}{10^{(0.2813R^2 - 0.2980R)}} & R \le 0 \\ \dfrac{\Delta K^{(0.3691R^2 - 0.5674R + 1)}}{10^{(0.5255R^2 - 0.8829R)}} & R \ge 0 \end{cases} \tag{4.24}$$

ΔK_m is the modified stress intensity range, C_w and m_w could be found from the best-fitted line to the FCGR versus ΔK_m data plotted in the logarithmic scale, or from the best-fitted line to the FCGR versus stress intensity range for the case of *R*=0. In that particular case,

$C_w = (C_p)_{R=0}$ =1.22603E-10 and $m_w = (m_p)_{R=0}$ = 3.8666. The plot of FCGR obtained from the proposed model versus ΔK_m in the logarithm scale for various values of R is depicted in Figure 4.15.

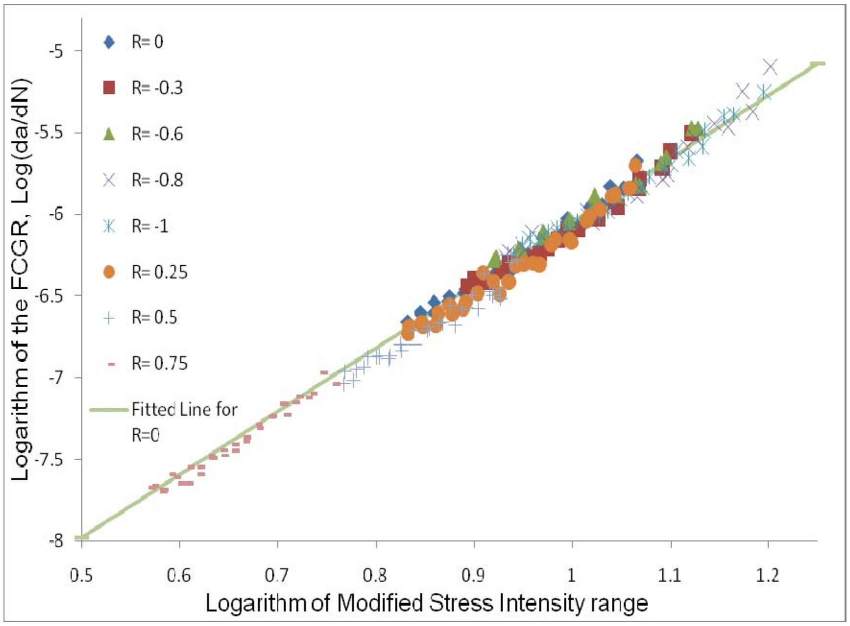

Figure 4.15 FCGR versus ΔK_m in a logarithmic scale ($R^2 = 0.989$)

As can be seen, this model best fits the experimental data.

4.5.2.6 Comparison of the predicted values obtained from different models

To show the accuracy of the proposed model in predicting FCGR response with a single equation, the variance of the data predicted by different models discussed earlier from the best-fitted line to the zero stress ratio is defined by the following mathematical relationship:

$$S = \sqrt{\frac{\left[Log\left(\frac{da}{dN}\right)_i - Log\left(\frac{da}{dN}\right)_{F.L.} \right]^2}{n}} \tag{4.25}$$

where s is the variance, $(\frac{da}{dN})_i$ is the individual values of the predicted FCGR at each stress ratio, $(\frac{da}{dN})_{F.L.}$ is the value of FCGR taken off of the best-fit line to the data at stress ratio of R=0, and n is the number of data points. The variances amongst the four models are calculated and presented in Figure 4.16.

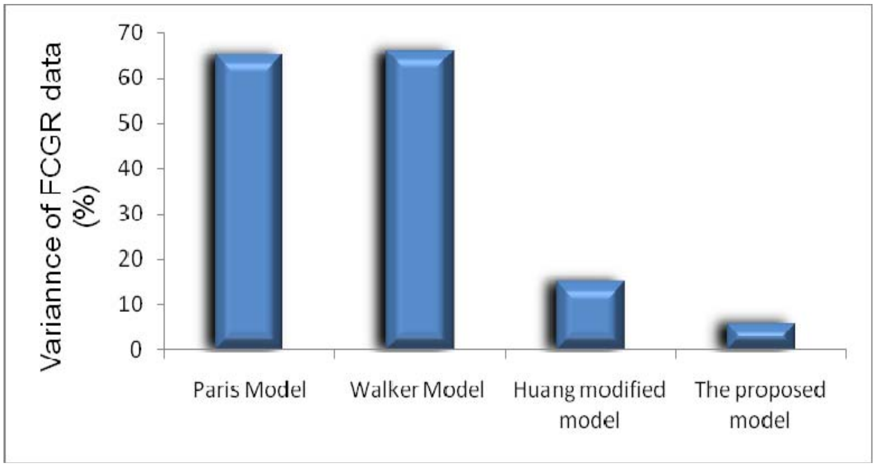

Figure 4.16 Variance of the FCGR data for different models

As seen from the figure, the proposed model produces the lowest variance compared to the other models.

4.5.2.7 Integrity of proposed model's prediction when considering FCGR of other materials

As a part of our continuing efforts, here we examine the integrity of the proposed model and its applicability to other materials. For the sake of comparison, we first illustrate the experimental FCGR data obtained by Ritchie et al [25] for another alloy (namely, Ti-6Al-4V). The data discloses FCG response of the alloy obtained from tests conducted at stress ratios of $0.1 \leq R \leq 0.92$, as illustrated in Figure 4.17. In addition, to illustrate the capability of our proposed model in better condensing the data (as illustrated in Figure 4.18(b)), we also have illustrated the FCGR response of the alloy as per ΔK suggested by

Huang and Moan's model (see Figure 4.18(a)). As seen from the figures, our model does a better job of condensing the data into a single curve.

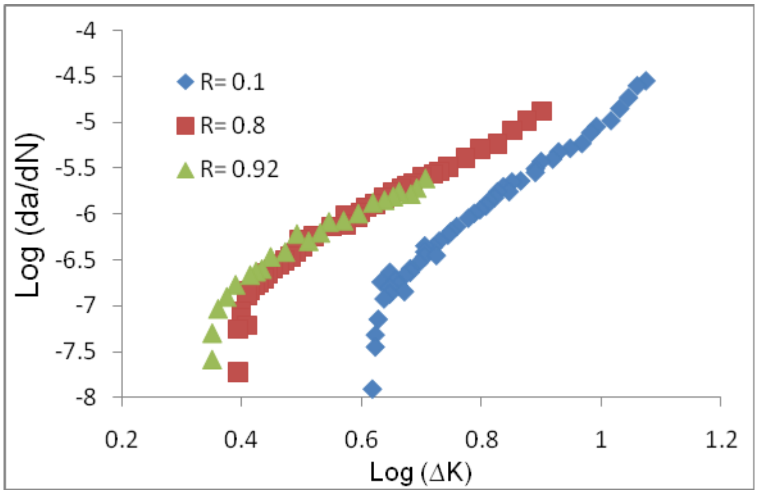

Figure 4.17 Experimental FCGR data of Ti-6Al-4V obtained at different stress ratios, obtained by Ritchie et al. [25]

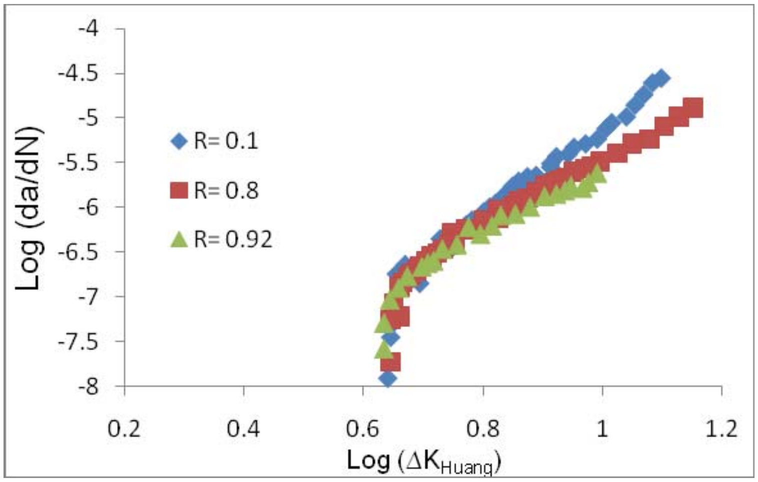

(a)

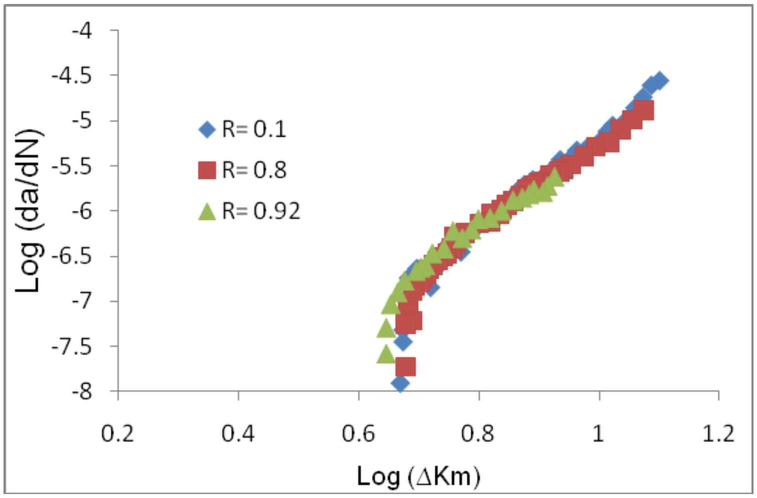

(b)

Figure 4.18 FCGR data of Ti-6Al-4V for different stress ratios depicted based on (a) Huang and Moan model [13]; (b) our modified model

To further illustrate the integrity of our proposed model (i.e., ΔK_m), we also considered the application of the model in consideration of the FCGR data obtained for a similar titanium alloy through the experimental investigation of Ding et al. [26], presented in Figure 4.19. The result of the application of our model in condensing the data is illustrated in Figure 4.20, showing an excellent fit.

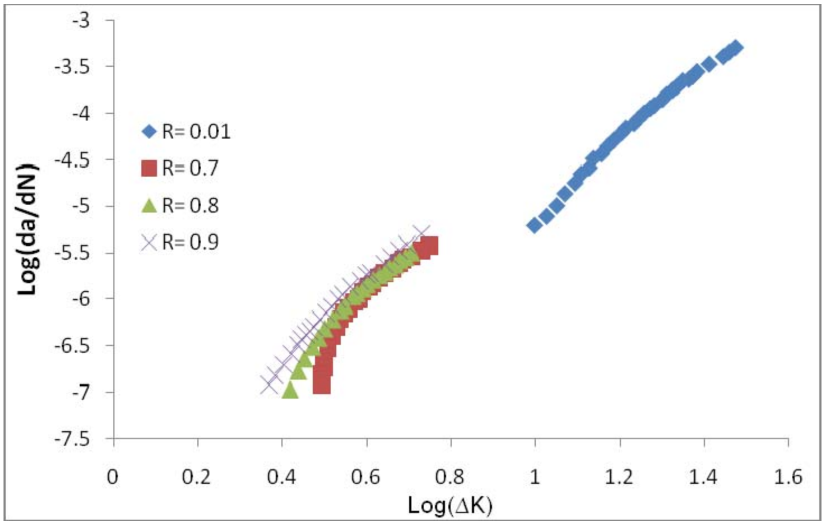

Figure 4.19 FCGR data of Ti-6Al-4V tested under different stress ratios obtained by Ding et al. [26]

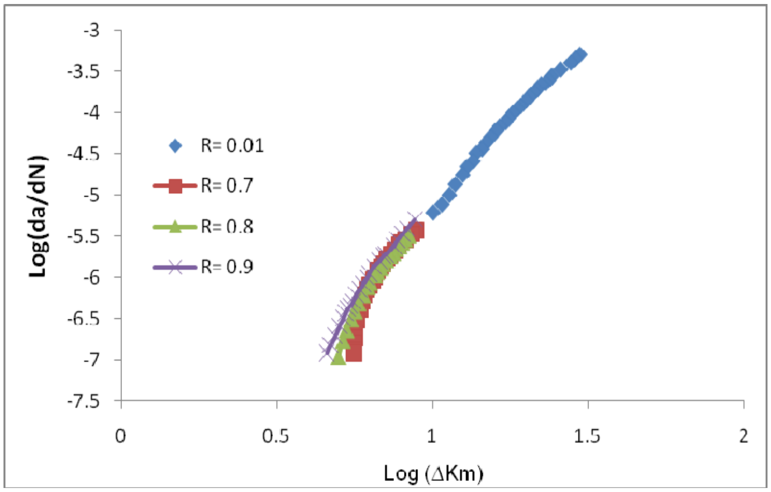

Figure 4.20 Presentation of FCGR data of Ti-6Al-4V obtained by Ding et al. [26] based on our modified model

We also applied our model to the experimental data presented by Kim and Lee [27], who investigated the FCG response of Al 7050-T7451 for the stress ratios of -1 < R < 0.3, as shown in Figure 4.21. The FCGR of this material obtained with respect to our proposed parameter, ΔK_m, as depicted in Figure 4.22, follows a more condensed data band.

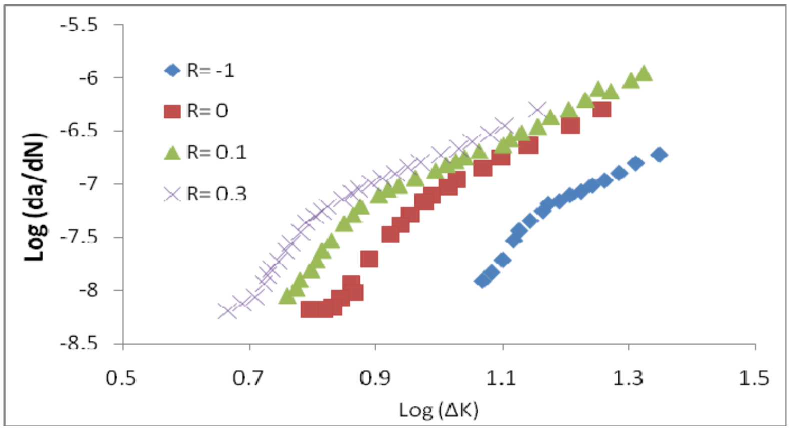

Figure 4.21 Original FCGR data of Al 7050-T7451 obtained experimentally at different stress ratios by Kim and Lee [27]

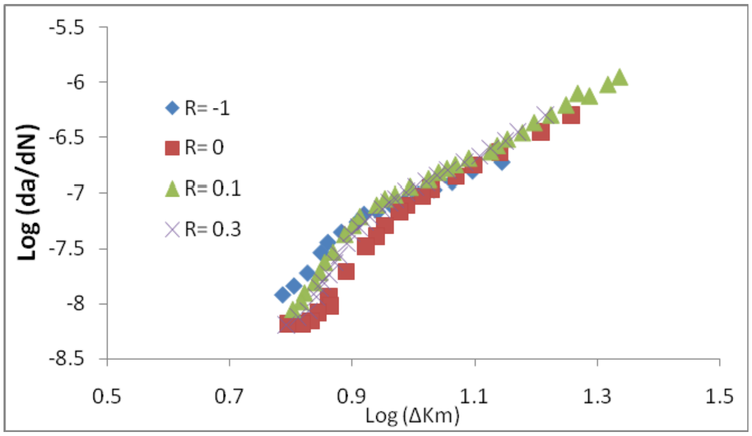

Figure 4.22 Representation of FCGR data of Al 7050-T7451 obtained by Kim and Lee [27] presented by our modified model

4.6 Conclusion

Fatigue crack growth rate is highly dependent on the stress ratio as well as the material and environment. A change in the stress ratio leads to change in the slope of FCGR curve depicted by the commonly used Paris model. Increasing the stress ratio in a positive sense accelerates the growth rate, but its decrease conversely reduces the rate, when only the positive stress intensity range is considered as a driving force.

A relation between the slope of the FCGR in logarithmic scale and the stress ratio could be defined for all stress ratios, since an increase in the stress ratio results in an increase in the slope of the curves when the entire stress cycle is considered in the calculation of the stress intensity range. As well, the compressive portion of the applied stress, which is ignored by most of the commonly used FCGR models, is proven to have a significant effect on crack growth rate and fatigue life; it is therefore highly recommended that the entire stress intensity range be taken into account when evaluating FCGR of a material.

Furthermore, the approaches thus far used for establishing the value of γ_w used in the Walker model have been essentially based on the assumption that the FCGR of a material evaluated at various stress ratios follow a parallel trend with respect to one another in logarithmic scale. We however demonstrated that data at various stress ratios follow a variable trend, highly dependent on the stress ratio. To alleviate this inconsistency when using the Walker model, a new parameter is proposed (i.e., $\Delta K'$) to reduce the slope variation. In addition, the proposed model recommends the use of polynomial function describing the variation of $Log\left[(1-R)^{1-\gamma_w}\right]$ in the Walker model.

Moreover, the use of newly defined parameter, ΔK_m (modified stress intensity range), is proposed, which enables the Walker model to better condense FCGR data around a single line, thus better predicting FCGR of materials when subject to various stress ratios. The integrity of the proposed FCGR model was established in comparison to several other models. The results indicated that the proposed model could produce the most accurate predictions among the models considered.

In conclusion, the proposed FCGR model could effectively and accurately predict the fatigue crack growth response of AM60B Mg alloy, subjected to cyclic loading under a wide range of positive and negative stress ratios.

4.7 Acknowledgement

This research was financially supported by AUT021 Network of Centers of Excellence, an automotive research and development program focusing on issues relating to the automobile in the 21st century. Materials were provided by Meridian Technologies Inc. of Strathroy, Ontario. These supports are gratefully acknowledged.

4.8 References

[1] Watarai, H., Sci. Technol. Trends Quart, Rev. 18, p. 84, 2006.

[2] Lu, Y., Taheri, F. and Gharghourin M., “Monotonic and Cyclic Plasticity Response of Magnesium Alloy. Part II. Computational Simulation and Implementation of a Hardening Model”, Strain (International Journal for Experimental Mechanics), 2008, 47, pp, e25-e33.

[3] Lu, Y., Taheri, F., Gharghouri, M., “Study of Fatigue Crack Incubation and Propagation Mechanisms in a HPDC AM60B Magnesium Alloy”, Journal of Alloys and Compounds, 2008, 466, pp. 214-227.

[4] Nur Hossain, Md. and Taheri, F., "Influence of elevated temperature and stress ratio on the fatigue response of AM60B magnesium alloy”, Accepted for publication in the Journal of Materials Engineering and Performance, July, 2011.

[5] Zheng, J., Powell, B.E., “Effect of Stress Ratio and Test Methods on Fatigue Crack Growth Rate for Nickel Based Superalloy Udimet720”, International Journal of Fatigue, 1999, 21, pp. 507-513

[6] Elber, W., “The Significance of Fatigue Crack Closure”, Damage Tolerance in Aircraft Structures, ASTM STP 486, American Society for Testing and Materials, 1971, pp. 230-242.

[7] Parida, B.K. and Nicholas, T., “Effect of Stress Ratio on Fatigue Crack Growth in a Titanium Aluminide Alloy”, International Journal of Fracture, 1991, 52, pp. R51-R54.

[8] Costa, J. D. M. and Ferreira, J. A. M., “Effect of Stress Ratio and Specimen Thickness on Fatigue Crack Growth of CK45 Steel”, Theoretical and Applied Fracture Mechanics, 1998, 30, pp. 65-73.

[9] James, M. N. and Wenfong, L., “Fatigue Crack Growth in Austempered Ductile and Grey Cast Irons – Stress Ratio Effects in Air and Mine water”, Material Science Engineering, 1999, 265, pp. 129-139.

[10] Kujawski, D., “A New $(\Delta K^{+} K_{max})^{0.5}$ Driving Force Parameter for Crack Growth in Aluminum Alloys”, International Journal of Fatigue, 2001, 23, pp. 733-740.

[11] Kujawski, D., “A Fatigue Crack Driving Force Parameter with Load Ratio Effects”, International Journal of Fatigue, 2001, 23, pp. 239-246.

[12] Dinda, S. and Kujawski, D., “Correlation and Prediction of Fatigue Crack Growth for Different R Ratios Using K_{max} and ΔK^{+} Parameters”, Engineering Fracture Mechanics, 2004, 71, pp. 1779-1790.

[13] Huang, X. and Moan, T., “Improved Modeling of the Effect of R-Ratio on Crack Growth Rate”, International Journal of Fatigue, 2007, 29, pp. 591-602.

[14] Noroozi, A.H., Glinka, G., Lambert, S., “A study of the stress ratio effects on fatigue crack growth using the unified two-parameter fatigue crack growth driving force”, International Journal of Fatigue, 2007, 29, pp. 1616-1633.

[15] Dimitriu, R.C., Bhadeshia, H. K. D. H., “Fatigue crack growth rate model for metallic alloys”, Materials and Design, 2010, 31, pp. 2134–2139.

[16] Mehrzadi, M. and Taheri, F., “Evaluation of Fatigue Damage in HPDC AM60B Magnesium Alloy based on Material’s Dynamic Properties”, 2011, Submitted to International Journal of Fatigue.

[17] ASTM E647-08, “Standard Test Method for Measurement of Fatigue Crack Growth Rates”.

[18] ASTM E1245, “Standard Practice for Determining the Inclusion or Second-Phase Constituent Content of Metals by Automatic Image Analysis”, (Reapproved 2008).

[19] Barsom, J. M. and Rolfe, S. T., “Fracture and Fatigue Control in Structures”, Third Edition, ASTM, PA, USA, 1999.

[20] Paris, P. and Erdogan, F., “A Critical Analysis of Crack Propagation Laws”, Journal of Basic Engineering, 1963, 85, pp. 528-534.

[21] Anderson, T. L., “Fracture Mechanics”, Third Edition, *CRC Press Inc*., USA, 2005.

[22] Broek, D., “The Practical Use of Fracture Mechanics”, *FractuREsearch Inc*., Galena, OH, USA.

[23] Walker, K., “The Effect of Stress Ratio during Crack Propagation and Fatigue for 2024-T3 and 7075-T69 Aluminum”, ASTM STP 462, 1970, pp. 1-14.

[24] Rushton, P.A. and Taheri, F., “Prediction of crack growth in 350WTsteel subjected to constant amplitude with over- and under-loads using a modified wheeler approach”, Journal of marine structures, 2003, 16, pp. 517-539.

[25] Ritchie, RO, Boyce, BL, Campbell, JP, et al. “Thresholds for high-cycle fatigue in a turbine engine Ti–6Al–4V alloy”, International Journal of Fatigue 1999; 21, pp. 653–62.

[26] Ding, J., Hall, R., Byrne, J., “Effects of stress ratio and temperature on fatigue growth in a Ti–6Al–4V alloy”, International Journal of Fatigue, 2005; 27, pp. 1551–1558.

[27] Kim, J. H. and Lee, S. B., “Behavior of plasticity-induced crack closure and roughness- induced crack closure in aluminum alloy”, International Journal of Fatigue, 2001; 23, pp. 247–251.

CHAPTER 5 Influence of Compressive Cyclic Loading on Crack Propagation in AM60B Magnesium Alloy under Random and Constant Amplitude Cyclic Loadings

Morteza Mehrzadi and Farid Taheri
Department of Civil and Resource Engineering, Dalhousie University, 1360 Barrington Street, Halifax, NS, B3J 1Z1, Canada

Published in the Journal of Engineering Fracture Mechanics, 99, 1- 17, 2013.

5.1 Abstract

An experimental investigation is carried out to study the influence of compressive loading cycles on the crack propagation response of AM60B magnesium alloy. Random and constant amplitude loading scenarios with various compressive loading contributions (or stress ratios) are applied on a center-cracked plate, and their fatigue response is examined.

A finite element analysis is also conducted to evaluate the stress distribution around the crack tip at various stages of cyclic loading for various stress ratios for the plates considered in the experimental investigation. The relation between the residual plastic zone size and crack propagation rate is critically examined. It is observed that the size of the residual plastic zone has a significant influence on the crack propagation rate. As a result, new parameter is defined, which captures the influence of the compressive loading on the crack propagation rate.

Keyword: Compressive loading contribution, random amplitude loading, crack propagation, AM60B magnesium alloy, residual plastic zone.

5.2 Introduction

The relatively lower density and high strength-to-weight ratio of AM60B magnesium alloy have attracted designers to use this alloy in various industrial applications. The many applications of AM60B in the auto industry have required more in-depth knowledge on material fracture and fatigue behavior. Several investigations have aimed at characterizing the monotonic and cyclic response of the alloy (for a comprehensive list of such studies see Reference [1] and [2]).

The stress ratio within a cyclic loading, defined as the ratio of the minimum (S_{min}) to maximum (S_{max}) stress amplitude (Equation 1), plays a significant role in crack propagation, especially for AM60B.

$$R = \frac{S_{\min}}{S_{\max}} \tag{5.1}$$

Under a negative stress ratio, the loading cycle will include compressive stress. For many years, the effects of compressive cyclic loading were overlooked. In fact, most research works have presented the crack propagation rate and fatigue response of materials as a function of positive stress intensity range. Even in some standards (e.g., [3]), it has been suggested that the compressive portion of a cyclic loading could be ignored. The dismissal of the compressive cycles in crack propagation calculation have been based on the theory that under compressive loading, the crack faces are closed, so no propagation could occur during the negative part of fatigue loading.

Fleck et al. [4] were probably the first group of researchers to investigate fatigue crack propagation (FCP) under compressive loading. They showed that a crack could be initiated in structural steel under a fully compressive loading. In the same year, Suresh [5] reported that crack propagation could be accelerated as a result of compressive loading. He studied the compressive loading effect on short and long cracks in a relatively low-strength steel, and related this phenomenon to the tensile residual stress formed around the crack tip.

In recent years, a few more investigators have considered this issue as well. For instance, Silva [6] and Shabanov [7] reported that compressive loading would have a significant effect on crack propagation rate. They also concluded that the result of such loading would be different from one material to another, and that the material properties should be incorporated into crack propagation equations. Crack propagation under a fully compressive stress loading has also been reported by other researchers [8-9]. Kasaba et al. [8] described the effect of compressive loading on the crack propagation of stainless steel. They first produced an initial tensile residual stress ahead of the crack tip, and then applied fully compressive stress loading cycles and observed that the crack propagated, even in the absence of tensile loading. Vasudevan and Sadananda [9] introduced the internal stress intensity factor to analyze the crack propagation under compressive loading. They showed that a crack could grow under a fully compressive cyclic loading due to an internal tensile stress state around the crack tip; subsequently, the crack could be decelerated and then arrested after a certain amount of propagation.

Different scenarios have also been used to investigate the influence of variable amplitude loading scenarios by various researchers. The loading scenarios used in most of these investigations included only a small number of overload or underload spikes within otherwise a constant amplitude loading. Yuen and Taheri [10] and Rushton and Taheri [11] reported the retardation and acceleration in crack propagation as a result of the application of an overload and a compressive underload in a polymer and 350WT steel, respectively. They also studied the reduction in the retardation induced as a result of an overload cycle following an underload. Bacila et al. [12] studied the same phenomenon and proposed a modified model describing the effect. Xiaoping et al. [13] performed some modifications on Wheeler's model to capture the effects of overload and underload in cyclic loading. They tested the integrity of their model by comparing their results with the experimental data reported by other researchers and found reasonable agreement.

As stated, thus far, most of the research related to variable amplitude loading has been mainly concentrated on the application of a few over-under loading applied within a constant amplitude loading scenario, while less work has been reported on the inclusion of compressive cycles within a random amplitude loading scenario. The study reported in this paper presents the influence of random variable amplitude tension-compression loading scenario, which includes the contribution of various magnitudes of compressive loading cycles on the fatigue crack growth (FCG) response of AM60B magnesium alloy. The experimental data will be compared with the FCG data obtained under a constant amplitude loading having the same compressive loading contribution or stress ratios. In addition to the experimental data, a series of numerical analyses were conducted to assess the stress field surrounding the crack tip, by which the influence of the compressive loading cycles on FCG could also be discerned.

5.3 Material

Table 5.1 shows the chemical composition of AM60B magnesium alloy used in this study. The material was provided in the form of 3 mm thick cast plates by the Meridian Technologies Inc. (Strathroy, Ontario).

Table 5.1 Chemical composition of the AM60B alloy in weight. % [1]

Mg	**Al**	**Mn**	**Si**	**Zn**	**Fe**	**Cu**	**Ni**	**Other**
Bal.	5.5-6.5	0.25 min	0.1 max	0.22 max	0.005 max	0.01 max	0.002 max	0.003 max (total)

The mechanical properties of the material are summarized in Table 5.2.

Table 5.2 Material properties

Yield stress (σ_y)	150 MPa
Modulus of elasticity (E)	40 GPa
Plastic Modulus (E_T)	2.5 GPa

5.4 Random amplitude loading scenarios

A block of random loading function was generated using the MATLAB, as shown in Figure 5.1. Each block comprised of 144 cycles and was applied over a period of 24 seconds. Each cycle in the random amplitude loading is represented by a sinusoidal curve, whose magnitude of its positive portion is different from that of the negative portion. Therefore, in order to generate a block of 144 cycles, 288 random numbers (from zero to the desired maximum stress value) were generated using the MATLAB. Half of these random numbers were used as stress amplitude of the positive portions and the rest for the negative portions. Therefore the number of cycles for each loading scenario was kept constant. A random amplitude loading contained several of these blocks, back-to-back. The compressive part of the random amplitude loading was scaled with various scaling factors (i.e. 100%, 80%, 60%, 30% and 1%).

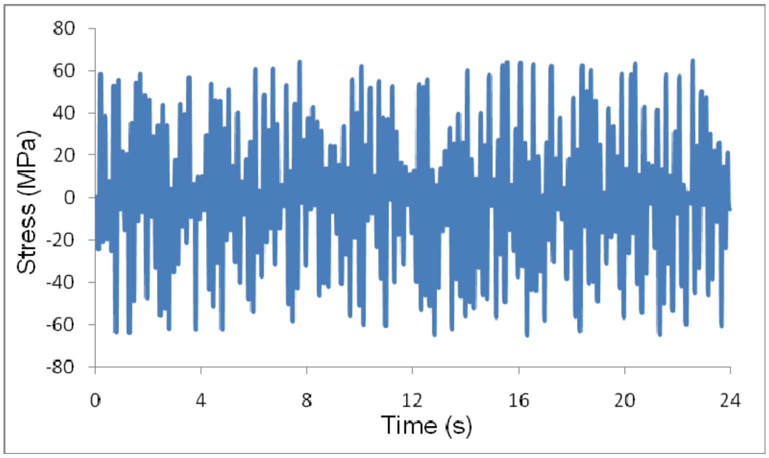

Figure 5.1 block of random amplitude loading history (with 100% compressive loading contribution (CLC))

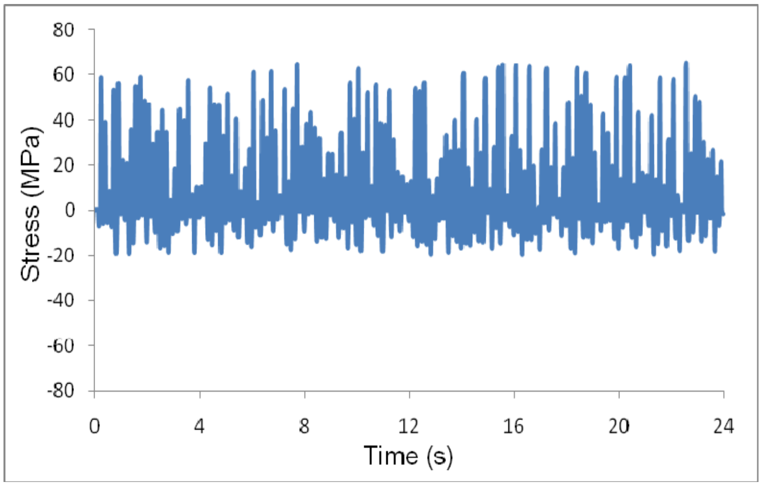

Figure 5.2 A block of random amplitude loading history (with 30% of the compressive loading contribution (CLC))

Figure 5.2 shows a typical loading history with 30% of the magnitude of the original compressive loading cycles. It should be mentioned that in order to maintain a consistent number of cycles in each block, a very small scaling factor (1%) was applied instead of zero. As a part of our study, the crack propagation resulting from the application of the constant amplitude loading (CAL) was compared with the experimental results obtained under the application of CAL scenario, which hosted a few compressive loading spikes.

5.5 Test setup

5.5.1 Specimen preparation

The specimens were configured according to ASTM E647-08 [3], as detailed in Figure 5.3. As illustrated, a 6 mm-long center notch was created using a fine (0.25 mm thick) jeweller's saw. The specimen was then polished, as per ASTM E 1245 recommendations [14], to generate a shiny surface to facilitate more precise measurement of crack length. For this purpose, the specimen was polished with several different fine grit abrasive papers, after which the polishing continued using a rotary pad and a suspension of 3-micron aluminum oxide.

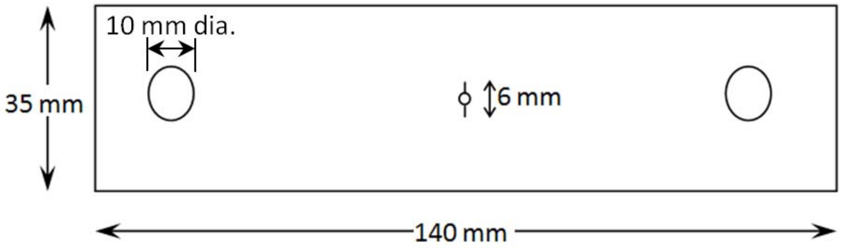

Figure 5.3 Specimen geometry

5.5.2 Cyclic loading and crack measurement

Cyclic loadings (both random and constant amplitude loadings) were applied to the specimens using an Instron servo-hydraulic universal test machine, with a capacity of ±100 kN under dynamic, or 200 kN under static loading conditions, controlled with 8501 digital electronics. In the case of compressive loading, an anti-buckling device was designed and fabricated, which was subsequently used to support the specimen, as shown in Figure 5.4. By using the anti-buckling device, the effective length of the specimen was reduced, thereby preventing premature buckling of the specimen. Four pairs of roller bearings were used to minimize the friction in between the specimen and device. The complete test setup is shown in Figure 5.5.

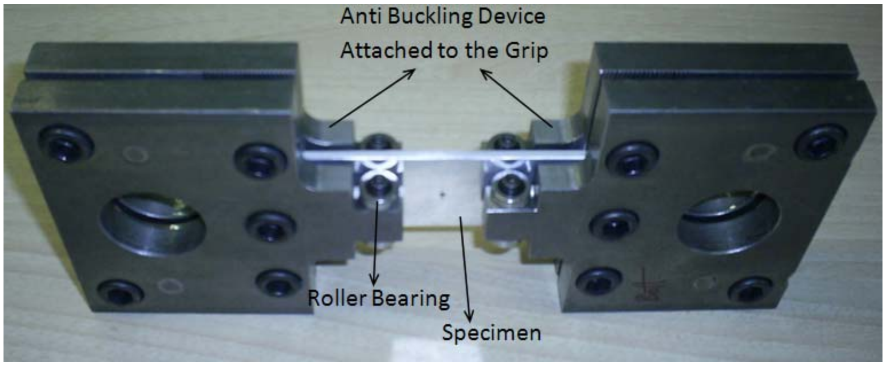

Figure 5.4 Anti-buckling device

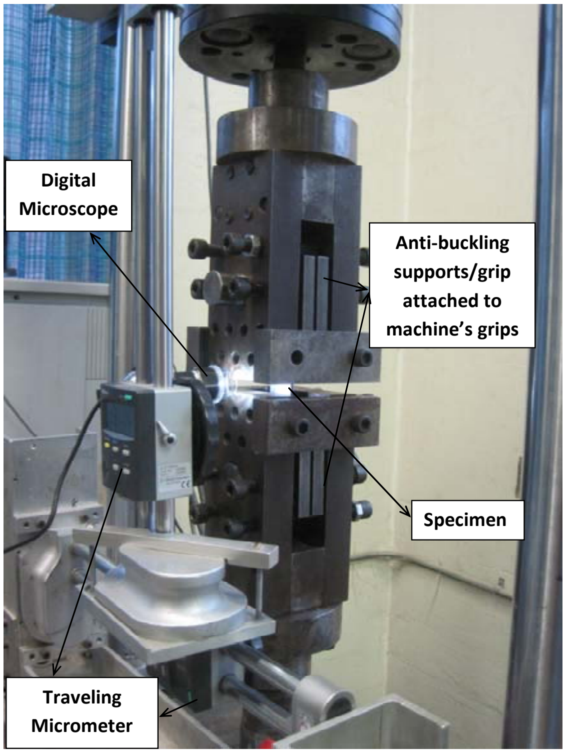

Figure 5.5 Test setup

A digital microscope with a magnification of 92X, mounted on a traveling digital micrometer with an accuracy of 0.01 mm, was used to measure the accurate length of the crack. The microscope had 8 LEDs to illuminate specimens' surface, and was connected to a personal computer to facilitate real-time tracking of crack propagation. After the application of a certain number of cycles, the test was interrupted and the crack length was precisely measured using the microscope. The measurement process was repeated at a set interval, till the complete failure stage of the specimen.

As a first step, the specimen was subjected to constant amplitude (zero-tension) loading cycles with a maximum stress of 55 MPa to form a sharp crack. The pre-cracking cyclic load was continued till an 8 mm-long sharp crack was produced. After generating the sharp crack, the loading scenario was applied and the crack propagation length was measured and recorded from the sharp pre-crack tip. Figure 5.6 shows the notch and the sharp crack.

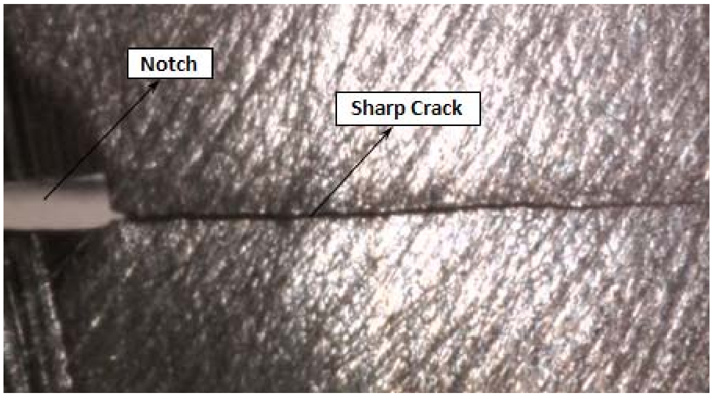

Figure 5.6 Image of a typical notch and crack

5.6 Experimental results

5.6.1 Random amplitude loading

The maximum applied stress contained in the random amplitude loading (RAL) scenario as shown in Figure 5.1, was 70 MPa. The test was carried out at room temperature with various compressive loading contributions (CLC). The plot of crack length versus number of cycles for the specimens tested under RAL containing various levels of CLC are detailed in Figure 5.7. It should be noted that, three specimens were tested for each loading scenarios and the average values are reported here. As seen, the compressive loading cycles produce a significant influence on the FCG of the specimens, by reducing specimens' fatigue life. Even a small amount of CLC (30 %) has a considerable effect and will result in a 25 % reduction in the life of the material. As can be seen, there is a minor deviation in the trend when considering the results of CLC = 60% and 80%. It should be noted that crack length/propagation measurement always involves a certain margin of error, and based on our experience, the error margin is usually relatively much greater at earlier stages of crack propagation. This is mainly due to the fact that it is quite difficult to clearly see/distinguish the crack tip, which is much finer at the early stages of loading; therefore the observed interpenetration of the curves (the crossing of the curves in the early stages) for tests with CLC = 60% and 80% is attributed to the inherent measurement error, and not to the actual material crack propagation response. This can be also justified by noting the otherwise distinct trend in the crack propagation seen in Figure 5.7.

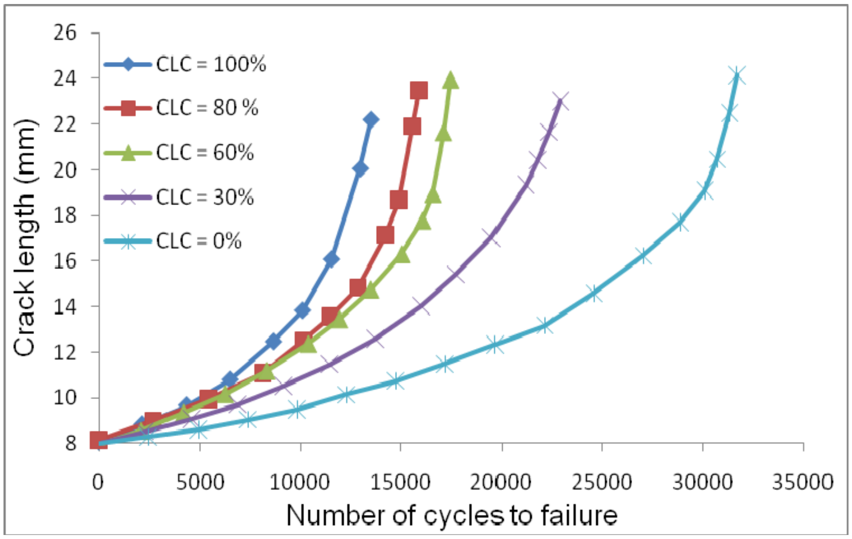

Figure 5.7 Crack propagation versus number of cycles for all the CLCs considered

As mentioned previously, not only the dismissal of the influence of the compressive portion of a cyclic loading has been the norm, but it has also been promoted by some guidelines [3]. It should be noted that a few standards (e.g., the API [15]) indeed recommend taking the influence of the compressive loading into consideration. For instance, the API suggests the consideration of the entire stress range, only when the stress cycles are entirely tensile; however, in case where the stress ratio is negative, it has been suggested that for fatigue life calculation, one could consider the entire tensile portion of a cycle plus 60% of the compressive portion. In other words, according to the API, in essence, 40% of the magnitude of the compressive stress cycles could be overlooked.

To examine the influence of the compressive loading cycles, the variation in the fatigue life as a function of various percentiles of the magnitude of the CLC appearing in the RAL scenario (shown in Figure 5.1) is illustrated in Figure 5.7. As can be seen, the variation in the resulting FCG is much greater when zero to 60% of the CLC has been considered in the calculations, while the variation becomes milder when 60% to 100% of CLCs magnitudes are included in the calculations. This observation could probably rationalize API's suggestion. However, while it is true that the level of change in the fatigue life when including the final 40% margin of the CLC is not as significant as that observed for the first 60% contribution of CLCs, nevertheless, the resulting influence on the FCG is not too insignificant that could warrant the dismissal of the compressive cycles. This issue will be discussed in more detail in the following sections.

As a means to facilitate an easier method for predicting fatigue life cycle of metals subjected to RAL, Barsom and Rolfe [16] suggested the use of the root-mean-square of the stress intensity factor resulting due to the RAL. In this approach, the RAL is converted to an equivalent CAL. By calculating the stress intensity range of the equivalent loading and the use of an appropriate crack propagation model (e.g., Paris' model), the propagation rate and the fatigue life could be effectively ascertained. It should be noted that the integrity of the proposed models (i.e., Paris, Walker, etc.), for evaluating the crack propagation and fatigue life of materials is strongly dependant to the material properties (through the materials constants used to represent the models). Accordingly, the crack propagation behavior of AM60B magnesium alloy was therefore thoroughly investigated in our previous study [17]. The results of that investigation will be briefly reviewed and summarized in the next section.

5.6.2 Constant amplitude loading

The Paris model [18] is a well-known model, used to describe the crack propagation response of materials; it is represented by the following equation:

$$\frac{da}{dN} = C(\Delta K)^m \tag{5.2}$$

where ΔK is the stress intensity range, and C and m are material related parameters. Because the Paris model's coefficients changes from one stress ratio to another, the equation cannot be used for predicting FCG of materials for a wide range of stress ratios. To resolve this issue, Walker [19] proposed a new parameter to account for the effect of stress ratio, and proposed the following equation for estimating the FCG rate:

$$\frac{da}{dN} = C_w \left[\frac{\Delta K}{(1-R)^{1-\gamma_w}} \right]^{m_w} \tag{5.3}$$

where C_w, m_w and γ_w are Walker model's parameters to be established from experimental fatigue tests. The results of our previous study [17] revealed that the model's coefficients are highly stress ratio dependent when applied to AM60B alloy. With this finding, a modified Walker model was developed and proposed, by which one could establish the FCG rate for a wide range of stress ratios; the proposed model is presented by the following equations:

$$\frac{da}{dN} = C_w (\Delta K_m)^{m_w} \tag{5.4}$$

where,

$$\Delta K_m = \begin{cases} \dfrac{\Delta K^{(0.2286R^2 - 0.0495R + 1)}}{10^{(0.2813R^2 - 0.2980R)}} & R \le 0 \\[2ex] \dfrac{\Delta K^{(0.3691R^2 - 0.5674R + 1)}}{10^{(0.5255R^2 - 0.8829R)}} & R \ge 0 \end{cases} \tag{5.5}$$

The crack propagation response of the alloy under constant amplitude loading subject to different stress ratios is shown in Figure 5.8. Comparison of the FCGR under CAL (as illustrated in Figure 5.8), with those generated under random amplitude loading (illustrated in Figure 5.7) reveals a great similarity in fatigue response under both loading scenarios. As seen, the change in FCGR of the specimens tested under stress ratio range of -0.6≤R ≤-1 is not as significant as the change seen for specimens tested under stress ratio range of -0.6≤R ≤0, nonetheless, it should not be overlooked.

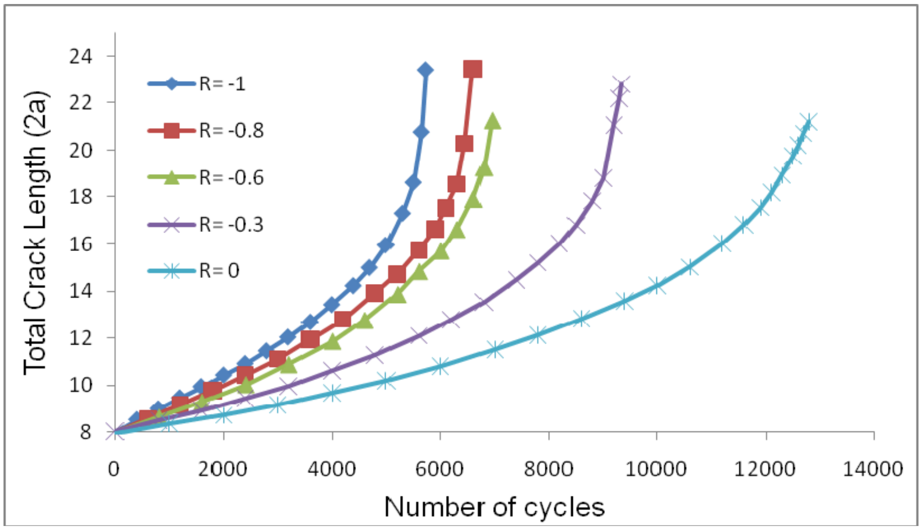

Figure 5.8 Crack propagation versus number of cycles for the CAL with various stress ratios

In Figure 5.9, the fatigue life cycles of the alloy observed under CAL and RAL with different stress ratios (or CLC) are normalized with respect to the fatigue life cycle obtained under a fully compressive (R = CLC = -1) loading scenario. The normalized fatigue life depicted in Figure 5.9 confirms that the compressive loading cycles would generate a consistent effect on alloy’s FCG, regardless of the loading scenario (i.e., being CAL or RAL). It also reveals that the fatigue life can be altered as much as 120% when the compressive cycles’ amplitudes are the same as those of the tensile cycles (i.e., CLC = 100%).

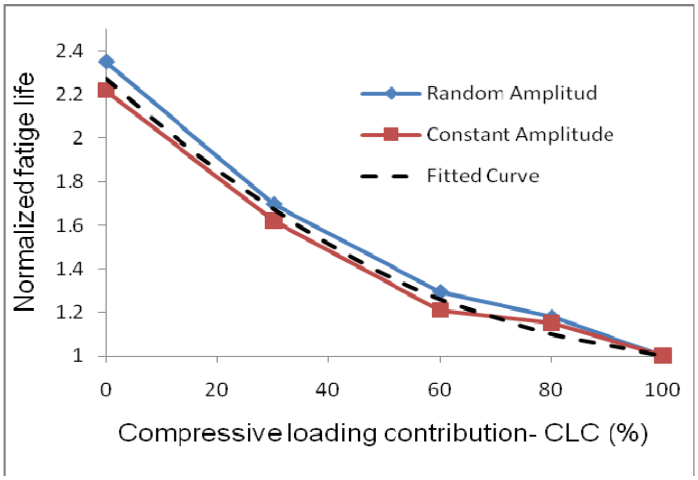

Figure 5.9 Normalized fatigue life as a function of percentage of the compressive loading contribution

In conclusion, therefore, dismissing the compressive portions of a cyclic loading scenario would result in inaccurate fatigue life prediction. The percentile of error as a result of considering only 60% of compressive portion of a cyclic loading (i.e., per API's suggestion [15]) associated with different CLCs is depicted in Figure 5.10. As can be seen, the percent error in FCGR changes nonlinearly as a function of CLC. According to our experimental data, the maximum error occurs when the amplitude of the compressive cycles reaches approximately between 70-80% of the amplitude of the tensile cycles within the loading scenario. From a practical perspective, however, the exact value of CLC within RAL scenarios would not be clearly known. In such cases, one could define a set of equivalent compressive and tensile stresses, following a similar approach as adopted by Barsom and Rolfe [16] for establishing the equivalent stress intensity range.

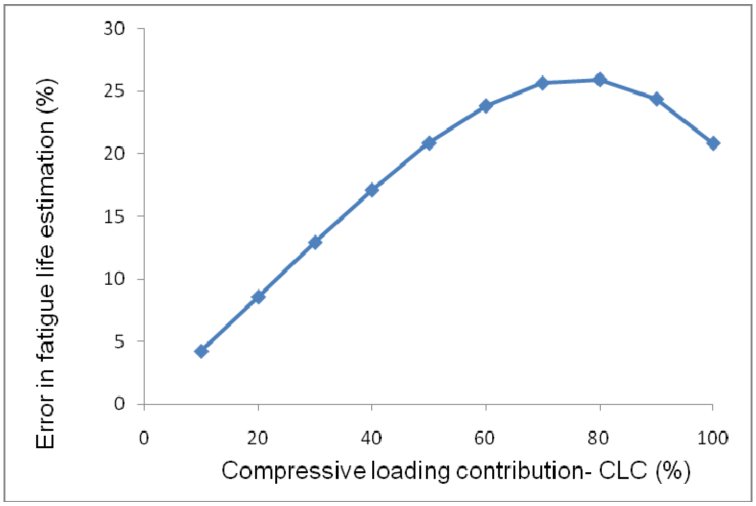

Figure 5.10 Errors resulting in the fatigue life assessment as a result of API's recommendation

5.6.3 Influence of spike loading on FCGR

The other variable amplitude loading type scenario used in this study was the consideration of the spike loading applied within a CAL scenario. Specifically, a numbers of compressive spike loads were applied during the application of zero-tension constant amplitude loading. In other words, after n number of CAL cycles (with R=0 format), one compressive spike was applied, and this sequence was repeated until the specimen failed.

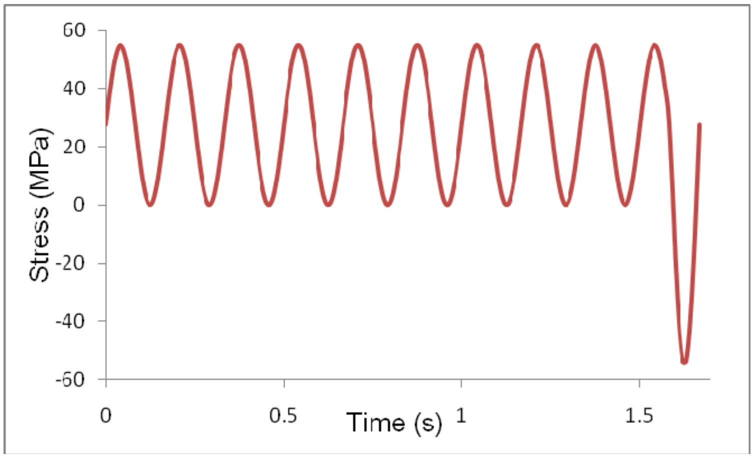

Figure 5.11 A typical loading block with one compressive (underload) loading spike (10-1 Spike)

A representative block of spike loading is shown in Figure 5.11. The maximum amplitude of the CAL section is 55 MPa (with a stress ratio of R = 0). The spike load is applied in the form of a half-cycle load with a maximum stress of -55 MPa. The cyclic loading was applied at a rate of 6 Hz. Different loading blocks, as summarized in Table 5.3, were considered.

Table 5.3 Details of the loading histories that include spike loading

Block Name	Description
3-1 Spike	3 constant amplitude loading cycles + 1 compressive spike
10-1 Spike	10 constant amplitude loading cycles + 1 compressive spike
50-1 Spike	50 constant amplitude loading cycles + 1 compressive spike
500-1 Spike	500 constant amplitude loading cycles + 1 compressive spike
1000-1 Spike	1000 constant amplitude loading cycles + 1 compressive spike

The resulting FCG for the various spike load history considered is shown in Figure 5.12. As can be seen, even an infrequent application of a compressive loading spike (1000-1 Spike) exerts a significant effect on the crack propagation, causing a 15% reduction in the fatigue life of the alloy. As can be seen, the results indicate that only when the number of spikes is very high in a CAL loading scenario (i.e., three constant amplitude cycles and one spike), the resulting fatigue response becomes almost identical to the curve of a CAL with a complete load reversal (i.e., R = -1). In other words, the spikes produce the same influence as the rest of the repeated compressive cycles do.

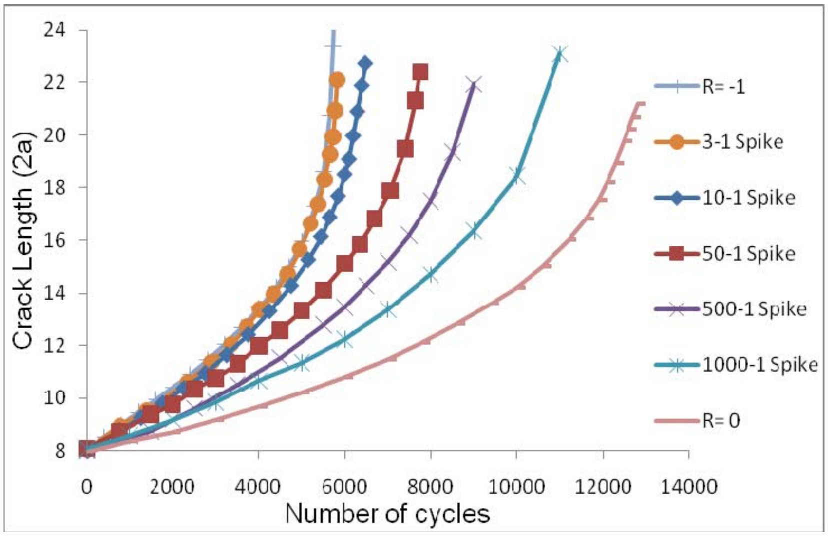

Figure 5.12 Crack propagation for different spike loading

5.6.4 Life estimation

The proposed modified crack propagation model (equations 5.4 and 5.5) has been used to estimate the fatigue life of the specimens and the results are compared with the experimental results.

5.6.4.1 The use of equivalent maximum and minimum stresses

Barsom [16] suggested using the root mean square technique to determine the equivalent stress intensity range (ΔK_{rms}) as shown in equation 5.6, and then apply the Paris-like model to predict the crack propagation rate.

$$\Delta K_{rms} = \sqrt{\frac{\sum_{i=1}^{n} \left(\Delta K_i\right)^2}{n}} \tag{5.6}$$

This method does not account for the influence of stress ratios. Hudson [20] proposed the equivalent maximum and minimum stresses and stress ratio to predict the crack propagation under variable amplitude loading. The relations for these equivalent parameters are as follows:

$$S_{\max,rms} = \sqrt{\frac{\sum_{i=1}^{n} \left(S_{\max,i}\right)^2}{n}} \quad and \quad S_{\min,rms} = \sqrt{\frac{\sum_{i=1}^{n} \left(S_{\min,i}\right)^2}{n}} \tag{5.7}$$

$$R_{rms} = \frac{S_{\min,rms}}{S_{\max,rms}} \tag{5.8}$$

where $\sigma_{\max,rms}$, $\sigma_{\min,rms}$ and R_{rms} are the equivalent maximum stress, minimum stresses and stress ratio, respectively. The proposed equation for evaluating the crack propagation rate was used along with the equivalent parameters defined by Barsom and Hudson to predict the fatigue life of the specimens that were subjected to the random amplitude loading, which included 100% compressive loading contribution. The results are compared with the experimental results as illustrated in Figure 5.13. It should be noted that when applying the Barsom model, the stress ratio was set to R = -1. As can be seen, both models produced results with significant error margins.

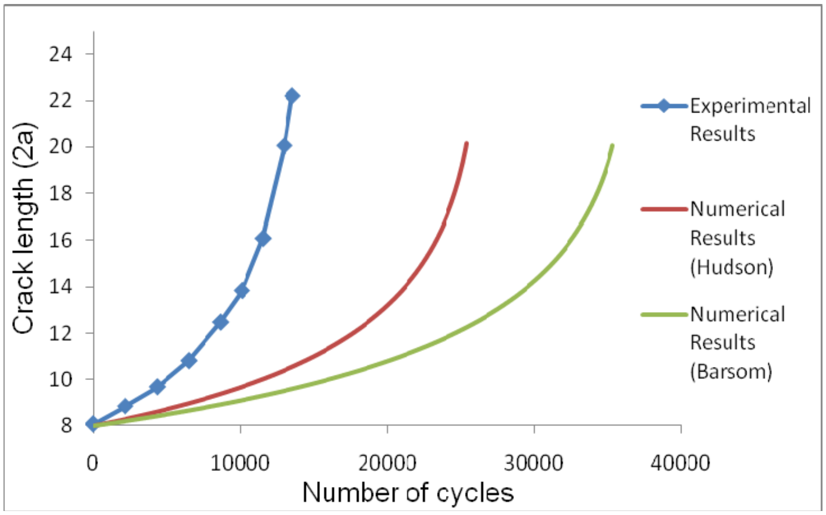

Figure 5.13 Life estimation using Barsom and Hudson equivalent parameters (CLC = 100%)

5.6.4.2 Cycle by cycle method

In this method the increase in crack length is calculated as a result of the individual crack growth increment due to each individual cycle, using the proposed crack propagation rate model. In this method the crack length would be allowed to propagate until reaching the critical value. The predicted results for the loading scenarios having various contributions of CLCs are shown in Figure 5.14. As can be seen, the estimated results are in reasonably good agreement with the experimental results. It is only for the case of CLC = 0 that the model slightly overestimates the crack propagation rate. The overestimation could be attributed to the retardation effect that is produced by some of the overloads embedded within the applied loading scenario. Similar observation, that is, a reduction in crack propagation retardation, has also been reported in the works of other researchers (see for instance references 10 and 11), where a compressive underload was applied following an overload. However, in the case of the investigated alloy the retardation is minimized in cases when the loading scenario included compressive stress cycles (i.e., those with CLC contributions of 30% to 100%). It is therefore concluded that the cycle-by-cycle method can estimate the fatigue life with a reasonable accuracy.

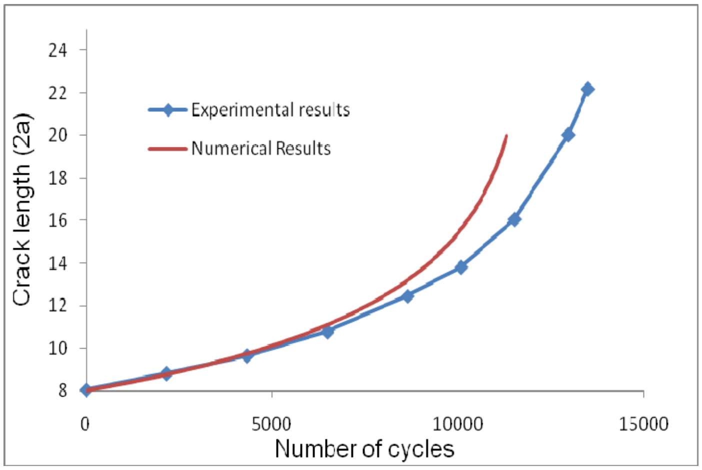
Crack length (2a)
24
22
20
18
16
14
12
10
8
Experimental results
Numerical Results
0
5000
10000
15000
Number of cycles

(a)

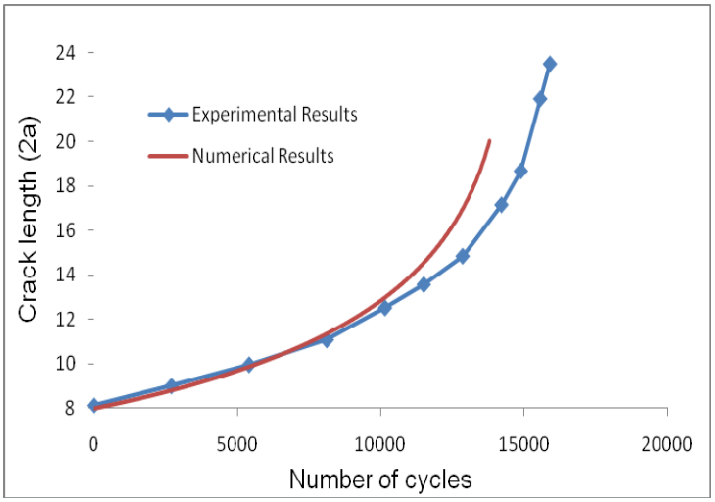
Crack length (2a)
24
22
20
18
16
14
12
10
8
Experimental Results
Numerical Results
0
5000
10000
15000
20000
Number of cycles

(b)

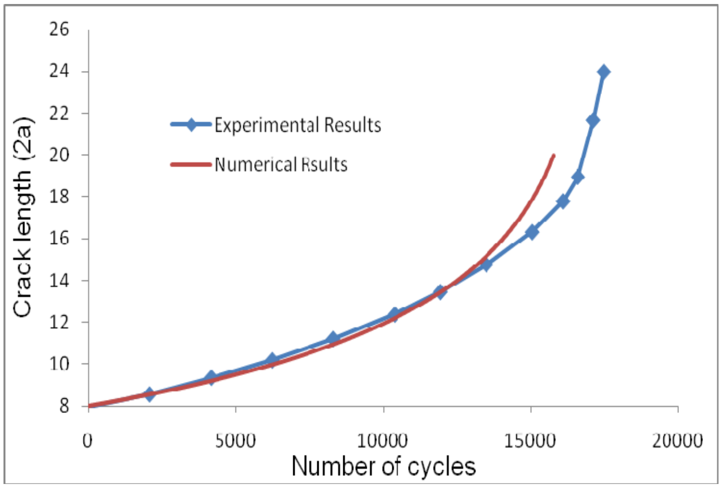
Crack length (2a)
26
24
22
20
18
16
14
12
10
8
Experimental Results
Numerical Rsults
0
5000
10000
15000
20000
Number of cycles

(c)

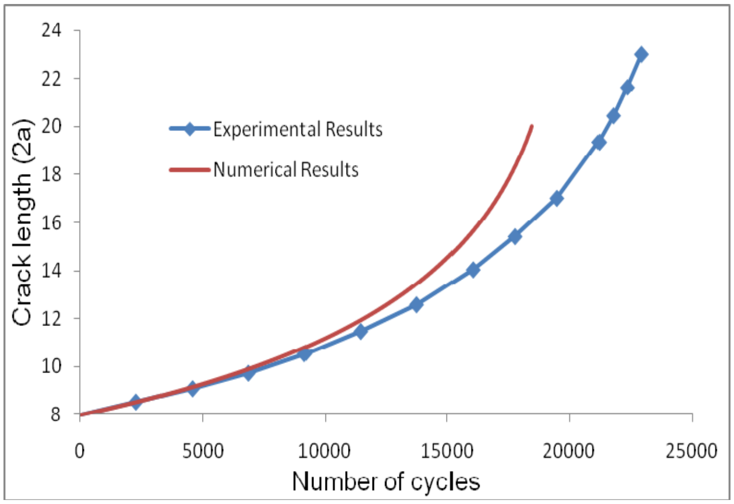

(d)

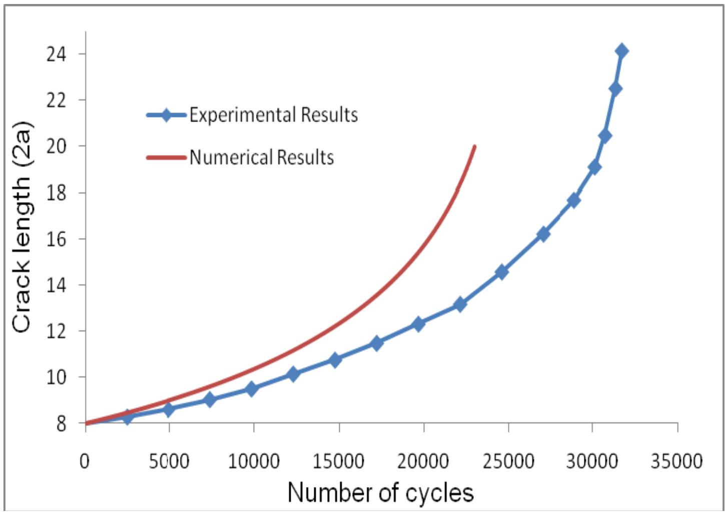

(e)

Figure 5.14 Fatigue life estimation under RAL loading when a) CLC = 100%, b) CLC = 80%, c) CLC = 60%, d) CLC = 30%, e) CLC = 0

Moreover, to investigate the limitation of the proposed model, the model was applied to estimate the fatigue life of the alloy undergoing constant amplitude loading scenarios that include compressive (underload) loading spikes. For that, a series CAL scenarios (at stress ratio of R=0) that included a series of compressive loading spikes (with a stress ratio of R=-1), applied at a set intervals were used to investigate the influence of the loading spikes. For instance, Figures 5.15 illustrates the prediction of the model against the experimental results for two of the loading scenarios. In the first case the compressive loading spikes are applied after every 1000 CAL cycles, while in the second scenario, the spike is applied at after every three-cycle increment. As seen, the proposed method underestimates the fatigue crack propagation rate and cannot account for the acceleration developed as a result of the applied compressive underloads.

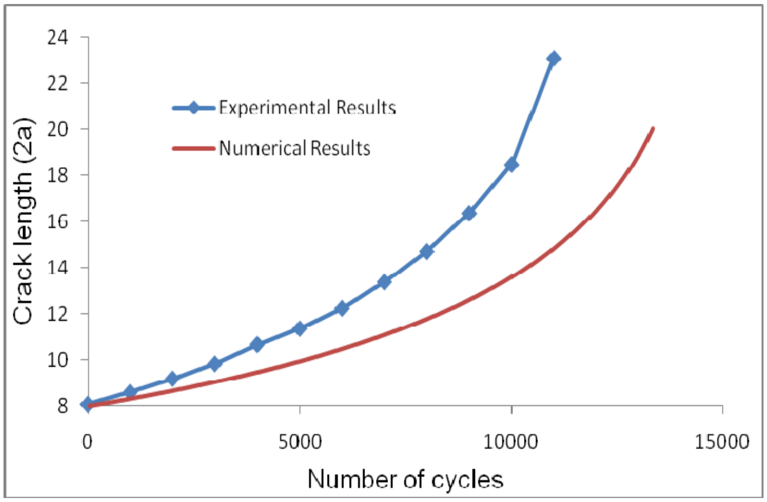

(a)

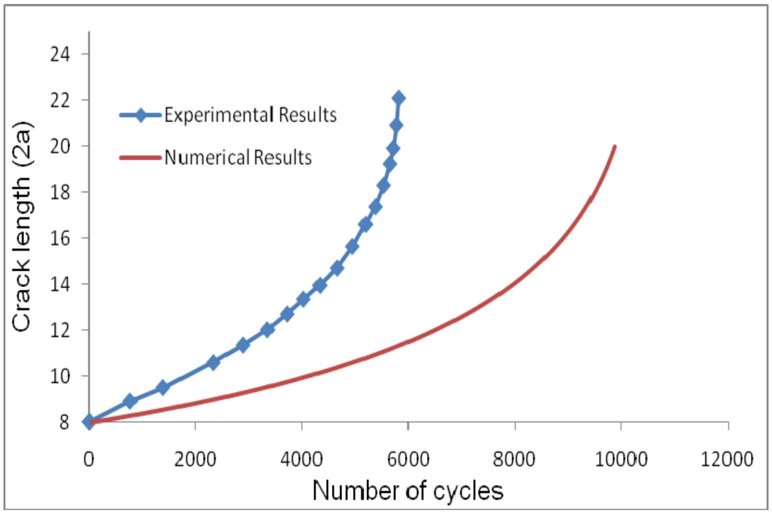

(b)

Figure 5.15 Fatigue life estimation under spike loading scenarios a) 1000-1, b) 3-1

To summarize all the results, the difference between the predicted and experimental results as a function of the total number of underload spikes applied within the total number of cycles that was consumed to propagate a crack from 8 mm to 20 mm was calculated and shown in Figure 5.16. In essence, in the figure, the horizontal axis represents the total number of the accelerated cycles per underload spike. The results indicate that the existence of the compressive loading spikes could impose a significant interaction effect as the number of underloads is increased.

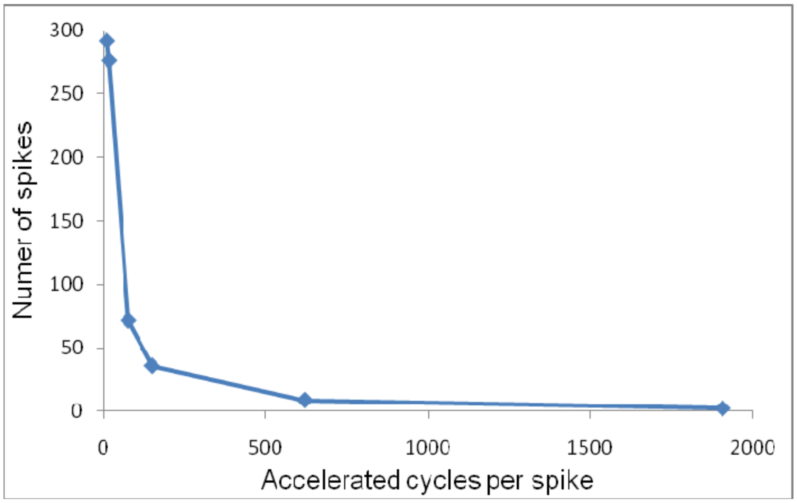

Figure 5.16 Fatigue life reduction per spike for different loading scenarios

5.7 Finite element modeling

Finite element method was also used to study the influence of compressive loading on the stress distribution ahead of the crack tip. Some researchers [10, 11, 21 and 22] have reported that a tensile residual stress is formed ahead of the crack tip upon the completion of cyclic loadings that include a negative stress ratio, and that this positive stress state would be responsible for the acceleration in crack propagation. Zhang et al. [21] carried out an elastic-plastic finite element analysis on a center-cracked plate, hosting a crack with three different lengths. The loading histories were designed in such a way as to produce a constant state of maximum stress intensity for the tensile portion of the cyclic loading and a constant maximum compressive state for the negative portion of the loading. They also used the isotropic hardening rule in modeling material's plasticity response. Finally, they concluded that the stress distribution at different stages of the loading history was identical when different crack lengths were considered. They further stated that the maximum stress intensity factors corresponding to the maximum tensile and maximum compressive stress were therefore the driving parameters governing the crack propagation rates. Zhang and his colleagues furthered their research [22], by changing the hardening rule from isotropic to kinematic and arrived at the same conclusion. In all of these works, the researchers related the crack propagation acceleration to the positive (tensile) residual stress state formed ahead of the crack tip. Nevertheless, literature on the influence of crack length and stress ratio on the residual stress is almost non-existent.

In summary, the finite element analysis was carried out to further examine the cause of the acceleration that would result in crack propagation due to the application of the compressive underloads. The increase in the tensile residual plastic zone size is hypothesized as a cause for the observed crack growth acceleration. It will be shown that a greater residual plastic zone size would cause faster crack propagation. As will be seen, the FE results will demonstrate that a residual plastic zone of a significant size would not be developed when the magnitude of the applied compressive loading cycle is relatively small; therefore, a new parameter is introduced, which in our opinion, would better represent the influence of all levels of the compressive loading cycles.

The NISA (Numerically Integrated System Analysis) finite element software was employed to conduct the numerical investigation. Center-crack plates with three different crack lengths (a = 6, 8 and 10 mm, where 'a' represents half of crack length) were investigated. The geometry and boundary conditions of the specimen were symmetric, so only half of the plate was modeled. The crack mouth opening at the center of the plate was set to 0.25 mm, which is equal to the thickness of a jeweler's saw blade.

The material was modeled as bilinear elastic-plastic material, with the properties shown in Table 5.2. The kinematic hardening rule was applied to define the material's cyclic hardening behaviour. Generally, two types of hardening models can be used in an elastic-plastic finite element modeling; these are: (i) the isotropic and (ii) kinematic.

The isotropic hardening [23, 24] assumes identical yield surface when the material is subject to tensile or compressive stress, and that the locus of the yield surface on the stress plane remains at the same position as the load varies. Moreover, the Bauschinger effect is not considered in the isotropic hardening. In the kinematic hardening rule, an increase in the tensile yield stress results in a reduction of the compressive yield stress, while the summation of the yield stress in compression and tension remains always consistent. Therefore, the shape and size of the yield surface will remain consistent; however, its locus would be shifted in the stress space. Moreover, the Bauschinger effect is also considered in this hardening model. As reported by Lu et al [1], since the Bauschinger effect is relatively large in AM60B magnesium alloy under cyclic loading, the kinematic hardening rule should be employed when analyzing the fatigue response of this alloy by finite element method.

The eight-node quadrilateral plane stress element was used to model the specimens. The crack tip singularity was achieved by moving the mid-side node of the elements surrounding the crack tip to the quarter location nearer to the crack tip [25]. To maximize computational accuracy, a very fine mesh was used to model the crack tip region (see Figure 5.17); the element size in that zone was 0.001 mm (i.e., a ratio of approximately 1/10000 of the crack length).

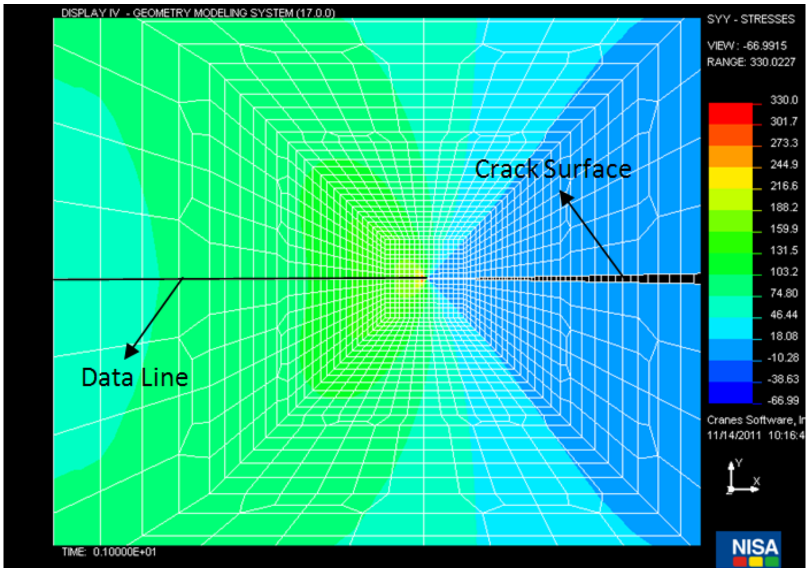

Figure 5.17 The FE mesh and data line used for presenting the stress distribution ahead of the crack tip

Since the application of the compressive loading cycle would cause crack faces to come in contact, a two-dimensional frictionless gap element was employed to connect the nodes on two opposite crack surfaces. From the numerical perspective, the stiffness of the gap element undergoing tension should be different from that under compression. Since crack surfaces do not have any resistance against opening under a tensile stress, the tensile stiffness of the gap element should be zero (or, in order to insure numerical stability, it should be of a very small value compared to the compressive stiffness); however, when subject to a compressive load, those elements should be adequately stiff to prevent the surfaces from overlapping. The NISA user's manual suggests employing a compressive stiffness of one to three orders of magnitude higher than the stiffness of adjacent elements. The compressive stiffness of the gap element could be estimated by observing the vertical distance between the two faces of the crack.

Three cycles of constant amplitude loading with different stress ratios, similar to that used in out experimental work were modeled and the stress distribution along a line ahead of the crack tip during the loading history was monitored. It should be noted that each cycle was divided into 80 load steps. The location of the line (or plane) on the FE mesh on which the data was extracted and the loading history are shown in Figures 5.17 and 5.18, respectively.

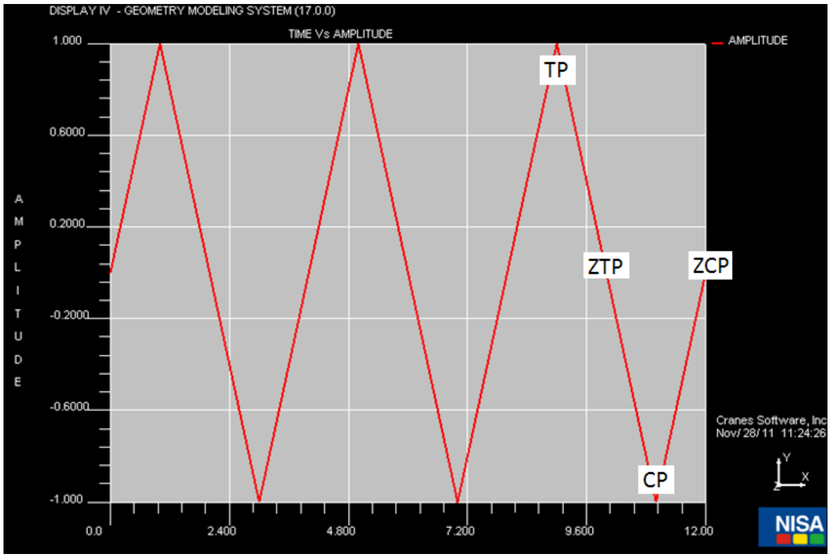

Figure 5.18 Sampling location of the stress values on the loading history for R = -1

As shown in Figure 5.18, the stress distribution will be presented at four loading levels of the last loading cycle. A description of these four loading levels can be found in Table 5.4.

Table 5.4 Description of different loading stages

TP	The tensile peak load
ZTP	Zero load after the tensile loading cycle
CP	The compressive peak load
ZCP	Zero load after completion of the compressive loading cycle

5.7.1 Results and discussion

As mentioned previously, specimens with various crack lengths subject to different stress ratios were analyzed using the finite element method. Figure 5.19 shows the stress distribution normal to the surface of the data line (plane) ahead of the crack tip. In this case, the half crack length is 8 mm and the stress ratio is -1. As can be seen, the application of the maximum tensile load (TP) will cause a singular behavior around the crack tip, while removing the tensile loading (ZTP) will result in a compressive plastic zone. Increasing the compressive load to the peak value (CP) will increase the compressive plastic zone. After removing the compressive stress portion (ZCP), the tensile residual stress, was hypothesized as a reason for crack growth acceleration. Accordingly, therefore, the acceleration in crack propagation as a result of the application of compressive loading cycles is related to the “tensile” residual stress formed at the crack tip, while the application of a tensile overload results in compressive residual stress ahead of the crack tip. Therefore, in addition to the size of the plastic zone, which clearly influences the propagation of the crack, the sign of the residual stress (tensile or compressive) would determine whether the crack would accelerate or decelerate/retard. For the case when the applied compressive loading cycles have different magnitudes (i.e., different scaling factors), the residual stress becomes tensile; as a result, the crack will propagate at a faster rate, while the magnitude of the resulting propagation would be governed by the plastic zone size, thereby varying based on the level of the scaling factor.

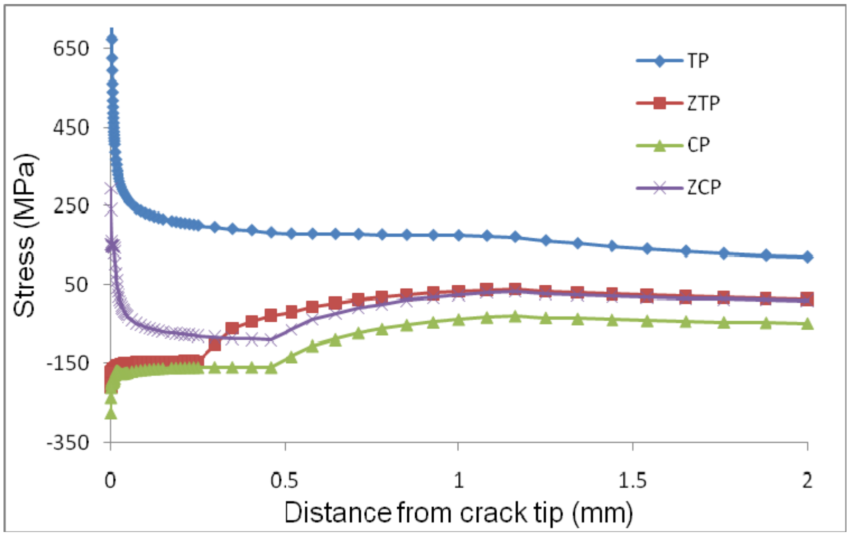

Figure 5.19 Distribution of the Longitudinal (vertical) stress (S_{yy}), at different loading stages, for the plate hosting a crack with a = 8 mm (See Fig. 5.18)

The stress distribution at the three different loading stages (ZTP, CP and ZCP), for a plate hosting different crack lengths, but subject to the same stress ratio (R = -1) are depicted in Figures 5.20 – 5.22, respectively. The results in these figures show that the plastic zone size increases as a function of the crack length. If one assumes that the plastic zone is equivalent to the damaged zone, then the application of the same loading scenario should develop a larger damaged zone in the plate hosting a longer crack length. This would also justify the higher crack propagation rates observed for the longer cracks in our previous study [17]. The resulting residual stress distribution developed after the removal of the entire loading cycle (ZCP), as illustrated in Figure 5.22, evidences a residual plastic zone that is much smaller than the plastic zone sizes observed at the other loading stages. The graph in Figure 5.22 is magnified to show only a distance of 0.05 mm ahead of the crack tip. The results indicate that in order to accurately capture the residual plastic zone, a very fine mesh should be used to model the crack tip region. It should be noted that most of the researchers who have investigated the influence of cyclic loading on FCG of materials, presented their results in the form of the distribution of the tensile stress formed ahead of the crack tip, not the plastic residual stress state. The state of the plastic residual stress for different crack lengths is presented in Figures 5.23 – 5.25.

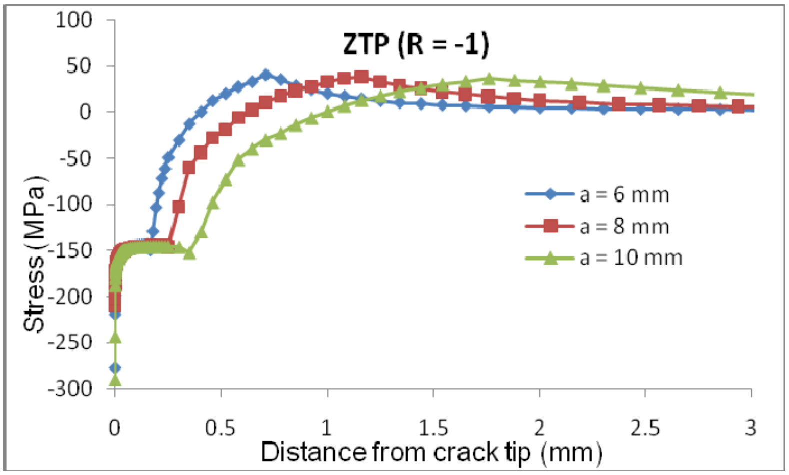

Figure 5.20 Distribution of the Longitudinal (vertical) stress (S_{yy}), at loading stage-ZTP (See Fig. 5.18), for plates with different crack lengths, subject to R = -1

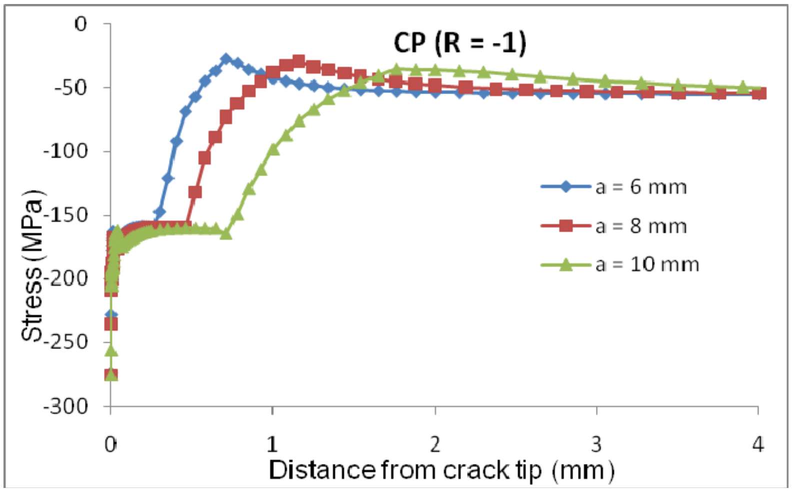

Figure 5.21 Distribution of the Longitudinal (vertical) stress (S_{yy}), at loading stage-CP (See Fig. 5.18), for plates with different crack lengths, subject to R = -1

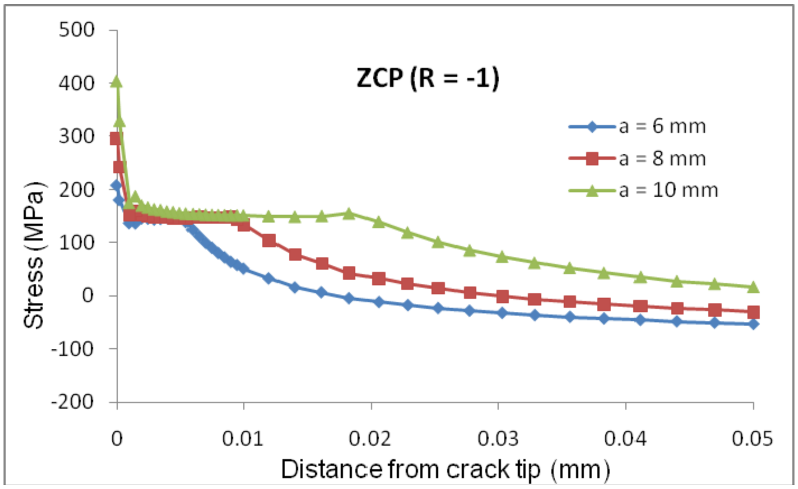

Figure 5.22 Distribution of the Longitudinal (vertical) stress (S_{yy}), at loading stage-ZCP (See Fig. 5.18), for plates with different crack lengths, subject to R = -1

The results shown in the figures clearly illustrate that the residual plastic zone associated to all the three crack lengths increases by increasing the compressive loading contribution. Moreover, no plastic zone was developed in the case of plates with short crack lengths, which were subject to small magnitudes of CLC (e.g., CLC = 30%).

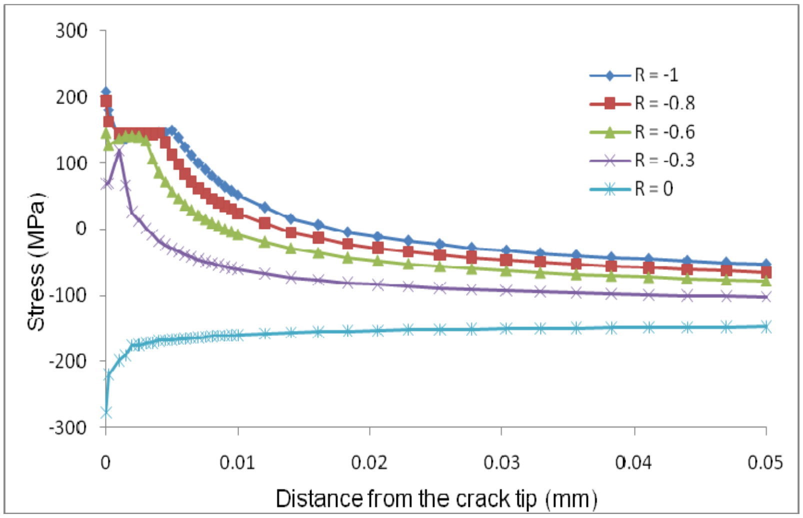

Figure 5.23 Distribution of the Longitudinal (vertical) stress (S_{yy}), at loading stage-ZCP (See Fig. 5.18), for plates with crack lengths a=6 mm, subject to different stress ratios

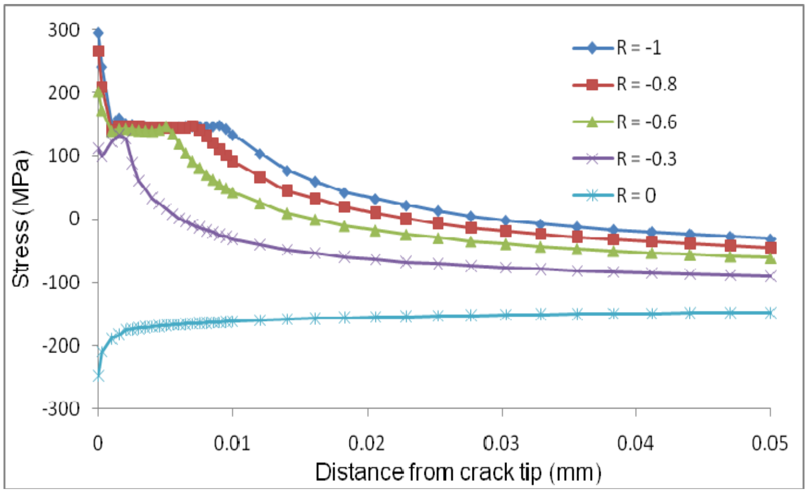

Figure 5.24 Distribution of the Longitudinal (vertical) stress (S_{yy}), at loading stage-ZCP (See Fig. 5.18), for plates with crack lengths a=8 mm, subject to different stress ratios

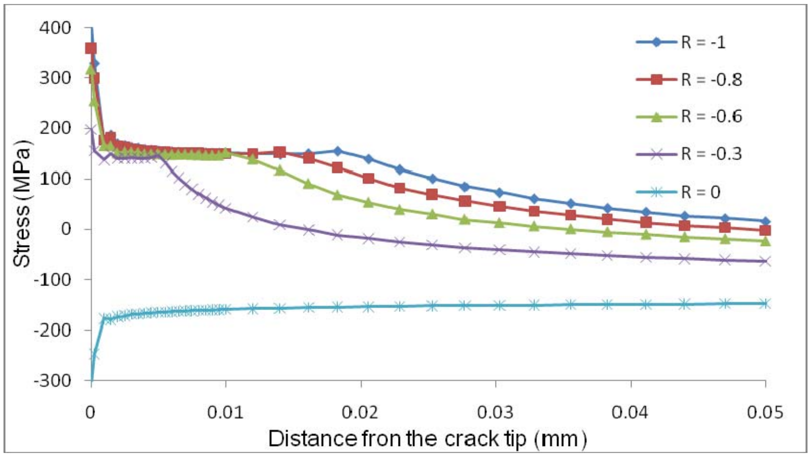

Figure 5.25 Distribution of the Longitudinal (vertical) stress (S_{yy}), at loading stage-ZCP (See Fig. 5.18), for plates with crack lengths a=10 mm, subject to different stress ratios

The variation of the residual plastic zone size with respect to the variation in CLC for different crack lengths is shown in Figure 5.26. Figure 5.26 shows a linear increase in the residual plastic zone size as a function of variation in the compressive loading contribution. Therefore, one can conclude that the application of a compressive loading cycle on a crack could increase the damage zone, thereby creating the opportunity for the crack to grow in a faster rate. If one considers the residual plastic zone as a criterion governing the crack propagation rate, it is clear that the influence of relatively small CLCs on certain crack lengths could not be accounted for; therefore, another criterion should be sought by which one could account for various crack lengths and levels of compressive loading contributions.

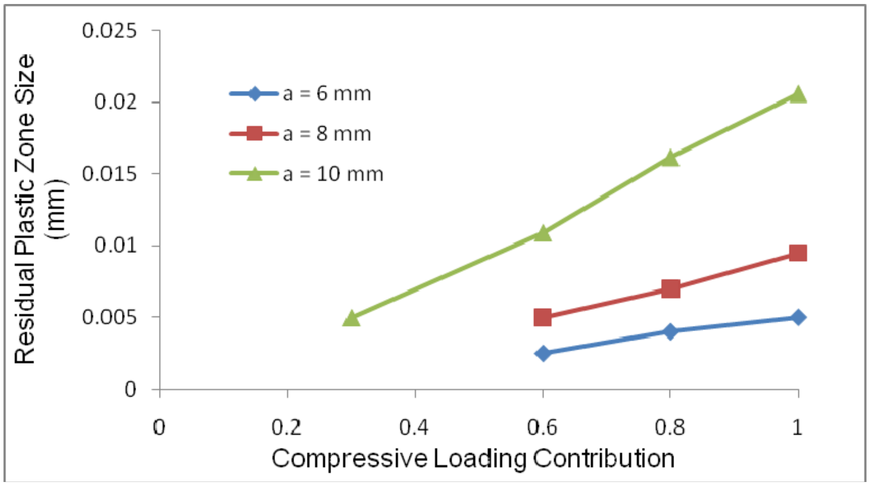

Figure 5.26 Estimated residual plastic zone size for different stress ratios

As a potential effective criterion, here we consider the effective force over an area in close proximity to the crack tip, expressed mathematically by the following integral:

$$F_e = \int_0^l S_{yy}\, t\, dx \tag{5.9}$$

where Fe, Syy, t and l are, respectively, the effective force, the normal stress value ahead of the crack tip, thickness of the plate and the length along which the integration would be carried out. This length would be an arbitrary length; however, it should be greater than the residual plastic zone developed at the loading stage ZCP (end-point of compressive portion) and less than the residual plastic zone size that is developed under a cyclic loading without any compressive cycles. In our study, this length was determined to be 0.05 mm. The variation of the calculated effective force versus different CLCs and crack lengths are shown in Figure 5.27. In essence, this parameter is introduced to mainly qualify the potential of acceleration in crack propagation as a function of a given loading scenario. It is postulated that the comparison of the effective force of a specimen that is subjected to a cyclic loading with stress ratio of R = 0 and that undergoing a different loading scenario, could give us a sense as to whether the crack would accelerate or not. It should be noted, however, that this parameter could not quantify the resulting crack propagation rate.

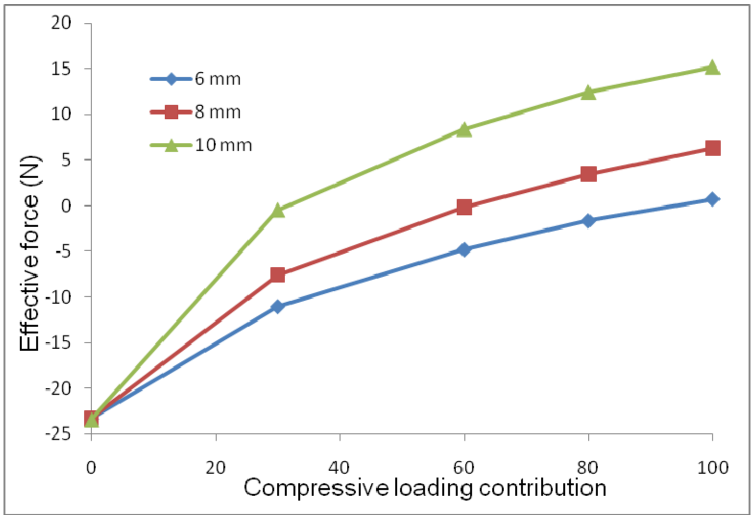

Figure 5.27 Variation of the effective force as a function of the compressive loading contribution and crack lengths

Results shown in Figure 5.27 confirm that higher crack propagation rates would occur in cases where the contribution of the compressive loading cycles is relatively large. Moreover, it is observed that the proposed approach could also capture the influence of relatively small compressive loading contributions that in actuality would not create a residual plastic zone. The magnitude of the effective force is also consistent for various crack lengths when the stress ratio or CLC is zero. The reason is believed to be due to the fact that the residual stress distributions in such cases are compressive, occupying a much larger region ahead of the crack tip. On the other hand, the stress through the entire length of the integration is taken equal to the yield strength of the material (with a negative sign), thus resulting in a consistent integration value. This observed consistency would also indicate that no crack propagation acceleration would be observed in the case when the loading includes no compressive cycles, which also corroborates with our experimental data.

5.8 Conclusion

Compressive loading cycles exert a significant influence on the fatigue crack propagation rate of most metals. In the case of the alloy considered in this study, even a small contribution of compressive loading (e.g., equal to 30% of the maximum compressive cycle) would have a marked influence, thus should not be overlooked. However, some guidelines (e.g., API) state that for cyclic loading cases involving compressive stress cycles, one could dismiss 40% of the magnitude of the compressive loads in a fatigue analysis. It has been shown that the adaptation of such a recommendation could result in 25% error in fatigue life estimation, and that the extent of the error would differ from one stress ratio to another. Therefore, standards and guidelines should revisit the importance of the compressive loading cycles, especially when considering the fatigue life of materials that are subject to real-life random amplitude loading scenarios.

In random amplitude loading scenarios, the contribution of the compressive stress cycles (or the stress ratio) is not as clear as that in the case of a constant amplitude loading scenario. It is therefore recommended that, as a first step, one should define an equivalent stress ratio, using a suitable approach (such as that proposed by Barsom and Rolfe's), and then for the cases where the stress ratio is negative, based on the magnitude of the equivalent stress ratio, one makes a judicious decision as to whether the influence of the compressive cycles could be overlooked.

Our experimental investigation also revealed that the influences of compressive cycles occurring within both random and constant amplitude loading scenarios on crack propagation response were similar, and the same amount of reduction was observed by applying a consistent stress ratio. When the cycle-by-cycle method was used to estimate the fatigue life of the specimens that were subjected to the variable amplitude loading, the results showed no sensitivity to the retardation effect. This would indicate that the method would be suitable for estimating the fatigue life of the alloy when the alloy is subjected to RAL that includes compressive loading contribution.

Moreover an increase in the compressive loading contribution resulted in an increase in the residual plastic zone size, which is believed to be the reason for the higher crack propagation rate. The residual plastic zone size developed under a cyclic loading that includes compressive loading cycles, is much smaller than the residual plastic zone size that is developed under a CAL scenario with no compressive loading cycles. As a result, when simulating the stress distribution at a crack tip subject to such loading scenarios, one should model the crack tip region with a very fine mesh (e.g., element size ≈ 1/10000 of the crack length), so that accurate results could be obtained.

Since the residual plastic zone was not observed in the case of plates with small crack lengths subject to the loading scenarios that included compressive loading contributions, a new parameter was defined (i.e., the effective force) by which the influence of the compressive loading could be more accurately idealized.

5.9 Acknowledgement

This project is financially supported by Auto21 and the AM60B plates were provided by Meridian Technologies Inc.; the supports are gratefully appreciated.

5.10 References

[1] Lu, Y., Taheri, F. and Gharghouri, M., “Monotonic and Cyclic Plasticity Response of Magnesium Alloy. Part II. Computational Simulation and Implementation of a Hardening Model”, Strain (International Journal for Experimental Mechanics), 2008, 47, pp. e25-e33.

[2] Nur Hossain, Md. and Taheri, F., "Influence of elevated temperature and stress ratio on the fatigue response of AM60B magnesium alloy”. Accepted for publication in the Journal of Materials Engineering and Performance, July 2011.

[3] ASTM E647-08, “Standard Test Method for Measurement of Fatigue Crack Growth Rates”.

[4] Fleck, N. A., Shin, C. S. and Smith, R. A., "Fatigue Crack Growth under Compressive Loading", Engineering Fracture Mechanics, Vol. 21, No. 1, pp. 173-185, 1985.

[5] Suresh, S., "Crack Initiation in Cyclic Compression and Its Application", Engineering Fracture Mechanics, Vol. 21, Issue 3, pp. 453-463, 1985.

[6] Silva, F. S., "The Importance of Compressive Stress on Fatigue Crack Propagation Rate", International Journal of Fatigue, Vol. 27, pp. 1441-1452, 2005.

[7] Shabanov, A. P., "Mechanism of Fatigue Crack Growth under Compressive External Stresses", Journal of Applied Mechanics and Technical Physics, Vol. 46, No. 6, pp. 861-866, 2005.

[8] Kasaba, K., Sano, T., Kudo, S., Shoji, T., Katagiri, K. and Sato, T., "Fatigue Crack Growth under Compressive Loading", Journal of Nuclear Materials, pp. 258-263, 1998.

[9] Vasudevan, A. K., Sadananda, K., "Analysis of Fatigue Crack Growth under Compression-Compression Loading", International Journal of Fatigue, Vol. 23, S365-S374, 2001.

[10] Yuen, B. C. K. and Taheri, F., "The Effect of Loading Frequency, Tensile Overload and Compressive Underload on the Fatigue Crack Propagation Behavior of Polymethyl Methacrylate", Polymer testing, Vol. 23, pp. 491-500, 2004.

[11] Rushton, P. A. and Taheri, F., "Prediction of Variable Amplitude Crack Growth in 350 WT Steel Using a Modified Wheeler Approach", Marine Structures, Vol. 16, No. 7, pp. 517-539.

[12] Bacila, A., Decoopman, X., Mesmacque, G., Voda, M. and Serban, V. A., “Study of underload effects on the delay induced by an overload in fatigue crack propagation”, International Journal of Fatigue, Vol. 29, pp. 1781-1787, 2007.

[13] Xiaoping, H., Moan T. and Weicheng, C.. “An Engineering Model of Fatigue Crack Growth under Variable Amplitude Loading”, International Journal of Fatigue, Vol. 30, pp. 2-10, 2008.

[14] ASTM E1245, “Standard Practice for Determining the Inclusion or Second-Phase Constituent Content of Metals by Automatic Image Analysis”, (reapproved 2008).

[15] API 2RD, “Design of Risers for Floating Production Systems (FPSs) and Tension Leg Platforms (TLPs)”, American Petroleum Institute, Washington D.C., USA, 1998.

[16] Barsom, J. M. and Rolfe, S. T., “Fracture and Fatigue Control in Structures-Application of Fracture Mechanics”, Third Edition, ASTM, PA, USA, 1999.

[17] Mehrzadi, M. and Taheri, F., “The Influence of Negative and Positive Stress Ratios on Crack Growth Rate in AM60M Magnesium Alloy”, Journal of Material Science and Engineering A, Vol. 545, pp. 68-77, 2012.

[18] Paris, P. and Erdogan, F., “A Critical Analysis of Crack Propagation Laws”, Journal of Basic Engineering, 1963, 85, pp. 528-534.

[19] Walker, K., “The Effect of Stress Ratio during Crack Propagation and Fatigue for 2024-T3 and 7075-T69 Aluminum”, ASTM STP 462, 1970, pp. 1-14.

[20] Hudson, C.M., “A root-mean-square approach for predicting fatigue crack growth under random loading”. In: Chang JB, Hudson CM, editors. Methods and models for predicting fatigue crack growth under random loading. American Societyfor Testing and Materials; 1981. p. 41–52. ASTM STP 748.

[21] Zhang, J., He, X. D., Suo, B. and Du, S.Y., "Elastic- Plastic Finite Element Analysis of the Effect of Compressive Loading on Crack Tip Parameters and Its Impact on Fatigue Crack Propagation Rate", Engineering Fracture Mechanics, Vol. 75, pp. 5217-5228, 2008.

[22] Zhang J., He, X. D., Sha, Y. and Du, S. Y., "The Compressive Stress Effect on Fatigue Crack Growth under Tension-Compression Loading", International Journal of Fatigue, Vol. 32, pp. 361-367, 2010.

[23] Hoffman, O. and Sachs, G., "Introduction to the Theory of Plasticity for Engineers", *McGraw-Hill,* 1953.

[24] Mendelson, A., "Plasticity: Theory and Application", *Macmillan, New York,* 1968.

[25] Anderson, T. L., "Fracture Mechanics; Fundamental and Applications", Third edition, CRC Press, 2005.

CHAPTER 6 A Modified Wheeler Model for Predicting the Retardation in Fatigue Response of AM60B Magnesium Alloy Based on Material's Sensitivity to an Overload

Morteza Mehrzadi and Farid Taheri
Department of Civil and Resource Engineering, Dalhousie University, PO Box 15000,
1360 Barrington Street, Halifax, NS, B3H 4R2, Canada

Submitted to International Journal of Fatigue, 2012.

6.1 Abstract

Application of an overload within an otherwise constant-amplitude loading scenario causes retardation in crack propagation, resulting in longer fatigue life. Several models have been proposed for predicting retardation in crack propagation due to an overload cycle. Among them, the Wheeler model, a widely used model, assumes the "affected zone dimension" to be a function of the current and overloaded plastic zone radii. When one considers the actual shape of the plastic zone, however, one realizes that the affected zone dimension does not agree with that assumed by Wheeler. As a result, several effective plastic zone radius coefficients have been proposed by various researchers, so that the equation's prediction would better fit the experimentally obtained retardation data.

In this paper, the influence of a single overload (but by considering three different overload ratios) on the fatigue crack growth retardation of center-cracked AM60B magnesium alloy plates is experimentally investigated. The retardation effect on crack growth due to an applied overload within a random-amplitude loading scenario, using various "clipping levels", is also investigated. The sensitivity of this material to overload is compared with the response of some other materials.

The results indicate that depending on the material, the affected zone would be sometimes larger or smaller than that produced by Wheeler's model. The actual radius of the plastic zone is also evaluated for various stress intensity factors, using the finite element method. Subsequently, a new parameter, hereafter referred to as the "sensitivity parameter" (β), is introduced that enables one to evaluate the affected zone dimension more accurately. It is shown that the proposed modified model is more effective than the original one in predicting the retardation response of the alloy. The integrity of the modified model is also investigated by evaluating the retardation in some other materials.

Keywords: Overload, sensitivity parameter, retardation, Wheeler model, clipping level.

6.2 Introduction

High-pressure die-cast (HPDC) magnesium alloys are increasingly being used in automobile and light-truck industries, mainly due to their lower density, higher specific strength and excellent castability and machinability. A few investigations have been carried out to study the monotonic and cyclic mechanical response of the alloy at room, elevated and sub-zero temperatures [1 & 2]. Due to the wide application of these alloys in auto industry however, cyclic loading is considered as one of the more dominant loading conditions. Therefore investigation of fatigue and fracture behavior of these alloys is of importance.

Application of overload in a cyclic loading is known to produce retardation in crack propagation [3 & 4]. Kumar et al. [3] studied the fatigue crack growth retardation in IS-1020 steel plate due to application of a single overload (with various overload ratios) applied within a constant-amplitude cyclic loading. They also attempted to formulate the number of delayed cycles as a function of overload ratio. The same experimental studies have been carried out on 6082-T6 aluminum alloy by Borrego et al. [4], in which the crack closure concept was applied to analyze the crack propagation retardation. The crack closure concept was initially introduced by Elber [5]; this procedure however requires a large body of experimental data in order to establish the stress intensity factor at the onset of crack opening. Shuter and Geary [6] showed that the degree of retardation would depend on specimen's thickness, stress intensity level and stress ratios. Tur and Vardar [7] studied the influence of a periodic tensile overload on crack growth retardation. They claimed that the maximum interaction was observed when the overload spacing was approximately half of the delayed cycles. Sander and Richard [8] showed that the amount of retardation would depend on the overload ratio, baseline stress intensity range and stress ratio, number of overload and fraction of mixed mode. Crack arresting, due to the application of overload with ratios greater than two, was also observed in their research.

Several models have been proposed for predicting the retardation of crack propagation due to application of an overload. Some modeling efforts [9 & 10] led to the introduction of various equivalency parameters into the constant-amplitude loading fatigue crack growth (FCG) models for predicting the crack propagation rate under variable-amplitude loading. For instance; Barsom [9] applied the root-mean-square technique to define the equivalent stress intensity factor, and Hudson [10] defined the equivalent minimum and maximum stress, using the same technique. These equivalent parameters were applied along with a Paris-like model [11] to determine the crack propagation rate. In one of our previous works [12], it was demonstrated that these models could not accurately predict the crack propagation rate in AM60B plates under variable amplitude loading. Some other models [13 & 14] have also been developed with focus on the plastic zone radius developed ahead of the crack tip. At this juncture, it should be acknowledged that the shape of the plastic zone is not a perfect circular shape; therefore, the word "radius" used throughout this paper refers to the distance from the track tip to the boundary of the zone ahead of the crack.

Wheeler [13] assumed that as soon as an overload is applied, a larger plastic zone (than that developed in the previous loading cycle) would develop ahead of the crack tip. This larger plastic zone becomes active in suppressing (or retarding) the crack growth; as a result, the crack tip would grow in a slower rate during the subsequent cycles. Wheeler then assumed that the retardation in FCG would continue until the boundary of the current plastic zone reaches the boundary of the large plastic zone developed as a result of the overload. He developed the following equation for the evaluation of the FCG rate:

$$\frac{da}{dN} = \Phi_R \left(\frac{da}{dN} \right)_{CAL} \tag{6.1}$$

where:
$$\Phi_R = \begin{cases} \left[\dfrac{r_{p,i}}{a_{OL} + r_{p,OL} - a_i} \right]^m & when \quad a_i + r_{p,i} \langle a_{OL} + r_{p,OL} \\ 1 & when \quad a_i + r_{p,i} \rangle a_{OL} + r_{p,OL} \end{cases} \tag{6.2}$$

In the above equations, Φ_R is the retardation factor, which is a function of the current plastic radius, $r_{p,i}$, the overload plastic radius, $r_{p,\,OL}$, the current crack length, a_i, and the crack length at which the overload is applied, a_{OL}, and m is a shaping exponent obtained through curve-fitting, which controls the magnitude of retardation. This model has been used widely due to its simplicity. Using this approach, Taheri et al. [15] attempted to estimate the fatigue life of a 350WT steel plate subjected to some overloads applied within a constant amplitude loading scenario. They used the plane strain assumption to model the plastic zone region and reported a good agreement with the experimental results. Khan et al. [16] used both the Wheeler and Elber models to predict the fatigue life of specimens subjected to variable amplitude loading. They obtained better prediction when the Wheeler model was incorporated in comparison to Elber's model. Rushton and Taheri [17] modified the Wheeler model in order to better predict the crack propagation rate when a compressive underload was applied following a tensile overload. For this purpose, they introduced an effective plastic zone radius and modified the shaping exponent. Kim and Shim [18] studied the crack retardation and variability of the results on a 7075-T6 aluminum alloy. Their model, similar to the Wheeler model, is characterized by a retardation coefficient, the affected zone and one extra parameter, which tracks the retardation in crack-growth. They have also shown that the affected zone is a function of the overload plastic zone radius.

In this paper, the influence of a single overload (having various overload ratios), on the crack propagation rate of AM60B magnesium alloy plates hosting a centre-crack is studied. A modified Wheeler model is developed to improve the original model's accuracy in assessing the retardation in FCG due the applied overload.

6.3 Experimental investigation (Constant amplitude loading baseline)

The material used in our investigation was AM60B magnesium alloy that was provided by Meridian Technologies Inc. (Strathroy, Ontario). The specimens, with the as received thickness of 3 mm, were configured according to ASTM E647-08 recommendations [19].

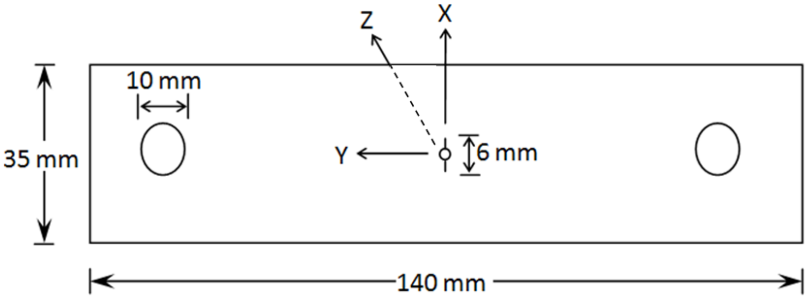

Figure 6.1 Specimen geometry

As shown in Figure 6.1, a 6 mm long center notch was incorporated using a jeweler's saw (having thickness of 0.25 mm). Specimens were drilled at both ends so they could be attached to the fixtures. The alloy manifests a bilinear elastic-plastic behavior; its mechanical properties are summarized in Table 6.1.

Table 6.1 Material properties

Yield stress (σ_y)	150 MPa
Modulus of elasticity (E)	40 GPa
Plastic Modulus (E_T)	2.5 GPa

Cyclic loading was applied using the Instron servo-hydraulic universal test machine, with a capacity of ±100 kN under dynamic, or 200 kN under static loading conditions, controlled with 8501 digital electronics. In order to generate sharp crack tips, a constant amplitude cyclic loading with the maximum stress of 45 MPa and stress ratio of R = 0.1 was applied to grow the notch tips to sharp cracks in the specimens. This pre-cracking procedure continued to increase the crack length to 2a = 8 mm (where "a" is half of the crack length). Then, the loading scenarios were applied and the crack length, measured from the sharp pre-crack tips, was recorded against the number of cycles. The fixtures were designed such that any unwanted planer bending (potentially generated as a result of misalignment) could be cancelled out, thus enabling to crack tips to grow in equal lengths.

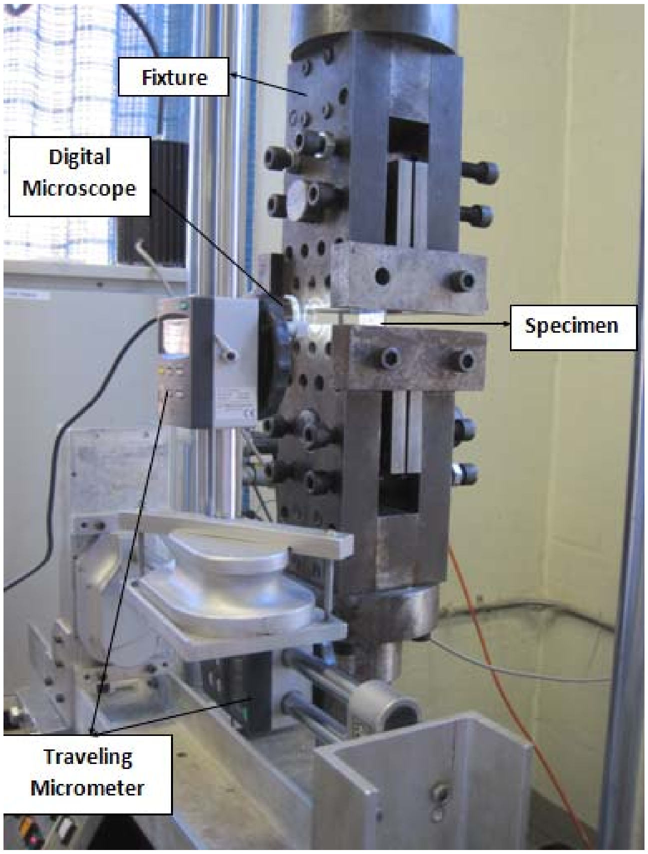

Figure 6.2 Test setup

The specimens' surfaces were polished as per ASTM 1245 [20] recommendations, using various grits of fine abrasive papers and finalized with a rotary pad and a suspension of 3-micron aluminum oxide. A 92X magnifying power digital microscope, mounted on a travelling micrometer, was used to measure the crack length accurately. The microscope was equipped with 8 LEDs to illuminate the crack surface. The test setup is shown in Figure 6.2.

6.3.1 Loading scenarios

A single overload with different overload ratios (i.e., OLR = 1.5, 1.75 and 2) was applied within an otherwise constant amplitude loading scenarios. The baseline loading consisted of a cyclic loading with the maximum stress of 45 MPa and stress ratio of R = 0.1. All baseline loadings were applied at 10 Hz frequency, while the overload was applied very slowly. Each overload was applied at crack length of 2a = 11.5 mm. Figure 6.3 shows the crack tip after the application of the largest overload (i.e., OLR = 2). The dark area surrounding the crack tip represents the bean shape plastic zone.

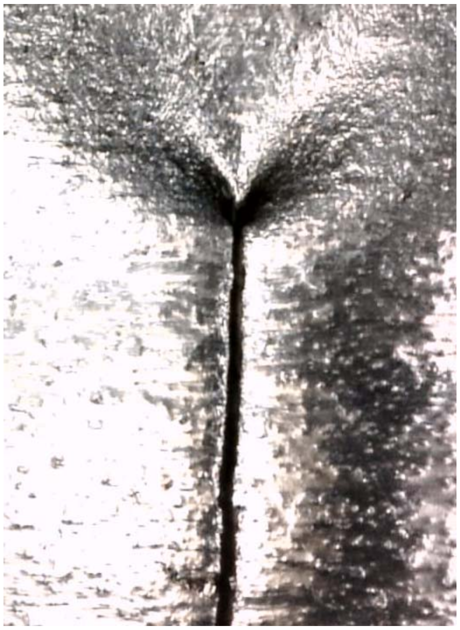

Figure 6.3 Crack tip under the applied overload (OLR = 2)

Two specimens were tested at each overload ratio and the crack propagation versus the number of cycles was recorded and shown in Figure 6.4. As can be seen, the application of overload ratio of OLR = 2 significantly increased the fatigue life of the specimens. Attempts were made to apply smaller OLR (for instance, OLR = 1.25), but no substantive increase in fatigue life was observed as a result; therefore, the results are not reported.

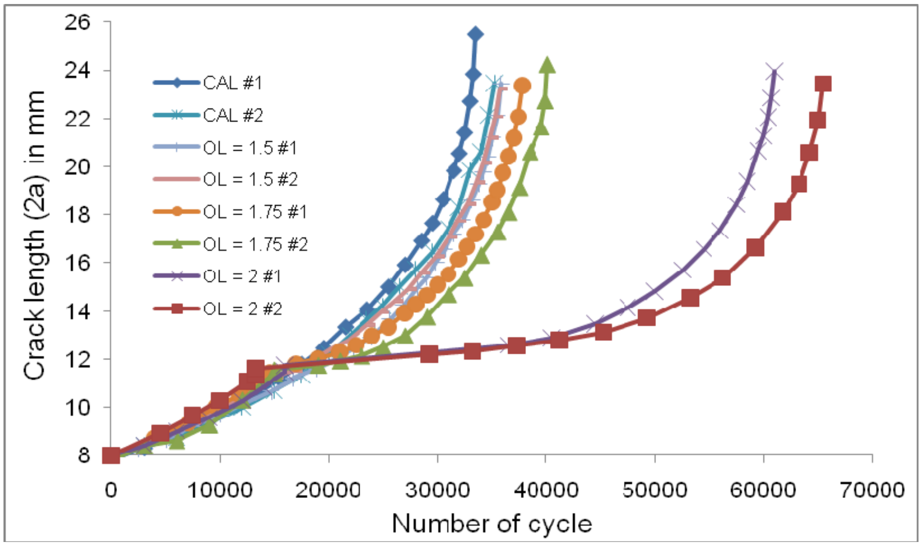

Figure 6.4 Crack propagation versus the number of cycles

6.4 Wheeler model

Wheeler [13] proposed a distinct model that defined a reduction factor for the crack propagation rate when an overload is applied within an otherwise constant amplitude cyclic loading. As graphically illustrated in Figure 6.5, when the current plastic zone radius, $r_{p,i}$, reaches the overload plastic zone radius, $r_{p,OL}$, the FCGR returns back to the steady state crack propagation rate.

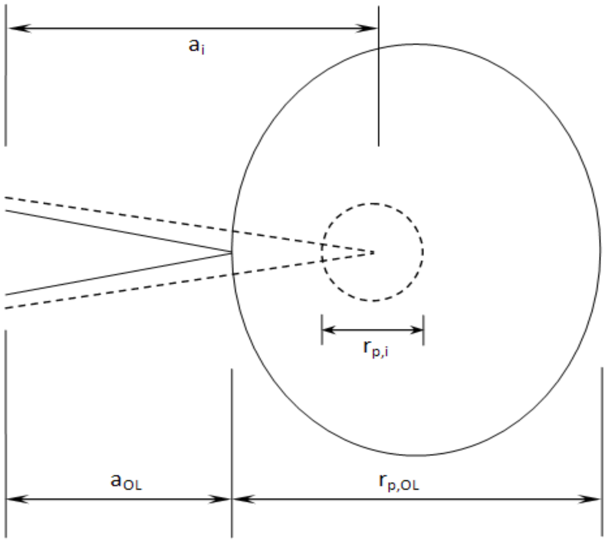

Figure 6.5 Parameters considered in Wheeler's model

Wheeler assumed that the retardation would occur immediately upon the application of an overload; nevertheless, several researchers have observed acceleration in crack growth before the retardation [4, 6, 15 & 21]. A typical retardation in crack growth rate is shown schematically in Figure 6.6. As can be seen, FCG is accelerated following the application of the overload and then decelerated to the minimum FCG rate, returning back to the steady state crack propagation. Two main parameters would have to be determined when using Wheeler's model; (i) the distance (a_r), which is affected by the overload, and (ii) the retardation magnitude, which is governed by the shaping exponent, m (as shown in equation 6.1). Since the affected zone (a_r) depends on the overload and current plastic zone radii, the variation in the plastic zone radius could significantly affect the retardation induced affected zone dimension.

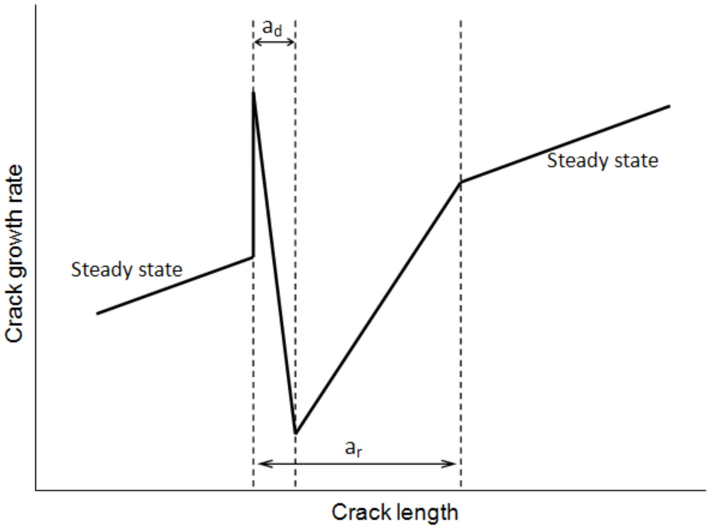

Figure 6.6 Schematic retardation of FCG following tensile overload

The plastic zone radius is basically a function of the stress intensity factor, K, and material's yield strength σ_y, as represented by the following relation.

$$r_p = \alpha \left(\frac{K_{\max}}{\sigma_y} \right)^2 \tag{6.3}$$

where α is the plastic zone coefficient. Several values have been suggested for α, which depends on the thickness of the plate and the maximum stress intensity factor.

Some modifications on Wheeler's model have also been reported to reflect a material's FCG behaviour in response to an overload. Song et al. [22] applied an experimental investigation on 5083-O aluminum alloy to study overload's effect on FCG. They found that the evaluation of the plastic zone radius (using Irwin's equations) would result in a conservative prediction of the crack propagation rate. They also suggested the use of the effective overload plastic zone radius, $r'_{P,OL}$, for predicting the retardation response of the material. The effective overload plastic zone radius, $r'_{P,OL}$, is evaluated based on the experimental data for each overload ratio, separately. On the other hand, when the crack propagation reaches to length of $a = a_{OL} + a_r$, the plastic zone radius at that stage should be added to a_r and the new dimension be assumed as $r'_{P,OL}$.

Sheu et al. [23] carried out a similar investigation and formulated the plastic zone coefficient and shaping exponent as a function of the overload ratio and initial crack length. Two different aluminum alloys were studied under several overload ratios and the affected zones were experimentally measured. Then, they used the following equation for establishing the effective plastic zone radius:

$$a_r = r_{P,OL} - r_{p,d} = \alpha \left[\left(\frac{K_{OL}}{\sigma_y} \right)^2 - \left(\frac{K_d}{\sigma_y} \right)^2 \right] \tag{6.4}$$

where $r_{p,d}$ and K_d are the plastic zone radius and stress intensity factor when the crack propagates to the length of $a_{OL} + a_r$, respectively. A similar formulation was presented for evaluating the shaping exponent as a function of various overload ratios and initial crack lengths. Yuen and Taheri [24] proposed two extra coefficients to be included in Wheeler's retardation model. The purpose of these coefficients is to account for the delay in retardation and the overload interaction. Similarly the affected zone and the plastic zone coefficient were established using the experimental data.

As mentioned above, the plastic zone radius has a significant influence on the retardation-affected zone in Wheeler's model, and it does not follow the condition that was assumed by Wheeler when developing his model. Therefore, the actual dimension of the plastic zone has rarely been incorporated in the models used for predicting FCG retardation under different loading scenarios in various materials. Most of the experimentally evaluated plastic zone radii (also referred to as the effective plastic zone radius), do not have any tangible physical meaning; they have been essentially developed by best fitting the experimental data to the Wheeler equation, so that a better match to the retarded FCG data could be obtained.

6.4.1 Plastic zone radius

The plastic zone radius is usually related to $\left(\frac{K}{\sigma_y}\right)^2$, by the coefficient (α). Irwin [25] proposed an analytical approach for establishing α, by equating the longitudinal stress (perpendicular to the crack direction) to the yield strength of the material. Considering linear-elastic material behavior, he analytically obtained α to be 1/2π for plane stress and 1/6π for plane strain. When considering an elastic perfectly plastic material behavior; however, α would increase to 1/π and 1/3π, respectively, for plane stress and plane strain conditions. The values of π/8 and $(1\text{-}2\nu)^2\pi/8$ have also been suggested by Guo [26] for plane stress and plane strain conditions, respectively. Voorwald et al. [27] proposed a different set of equations for α for plates with various thicknesses as shown in the following relation;

$$\alpha = \begin{cases} \dfrac{1}{6\pi} & t > 2.5\left(K_{\max}/\sigma_y\right)^2 \\ \dfrac{1}{\pi} & t < \dfrac{1}{\pi}\left(K_{\max}/\sigma_y\right)^2 \\ \dfrac{1}{6\pi} + \dfrac{5}{6\pi}\dfrac{2.5 - t\left(K_{\max}/\sigma_y\right)^{-2}}{2.5 - \pi^{-1}} & \dfrac{1}{\pi}\left(K_{\max}/\sigma_y\right)^2 < t < 2.5\left(K_{\max}/\sigma_y\right)^2 \end{cases} \tag{6.5}$$

A finite element analysis was also carried out by Xiaoping et al. [28] to establish the plastic zone coefficient for various thicknesses and stress intensity factors. They developed the following equation for evaluating α.

$$\alpha = 0.35 - \frac{0.29}{1 + \left[1.08\, K_{\max}^2 / \left(t\, \sigma_y^2\right)\right]^{2.15}} \tag{6.6}$$

As mentioned earlier, several equations have been proposed for evaluation of α, with the assumption that the material response is elastic-perfectly plastic. In our investigation, a three-dimensional finite element analysis was carried out to determine the plastic region for the AM60B magnesium alloy specimens. The actual bilinear material response of the alloy, as tabulated in Table 6.1 was used in our finite element model.

For that, the center-cracked plate, with the dimensions described earlier, was modeled in the NISA (Numerically Integrated System Analysis) finite element environment, subjected to a far field tensile stress that increased gradually from 0 to 90 MPa in ten equal increments. Due to the symmetric geometry and boundary conditions (see Figure 6.1), one-eighth of the plate (one half thickness of the quarter symmetry in the x-y plane) was modeled using 20-node higher-order solid elements (NKPT 4). Ten layers of elements were used to model the plate through its 1.5 mm half thickness. After running a nonlinear analysis, the plastic zone's boundary was established along the thickness (z-axis of the specimen; see Figure 6.1). The results for the relatively small and large applied far-field stresses of 30 MPa and 90 MPa are shown in Figure 6.7. It should be noted that for illustration purposes, the results obtained for the quarter plate were projected on the plane of symmetry to generate the graph.

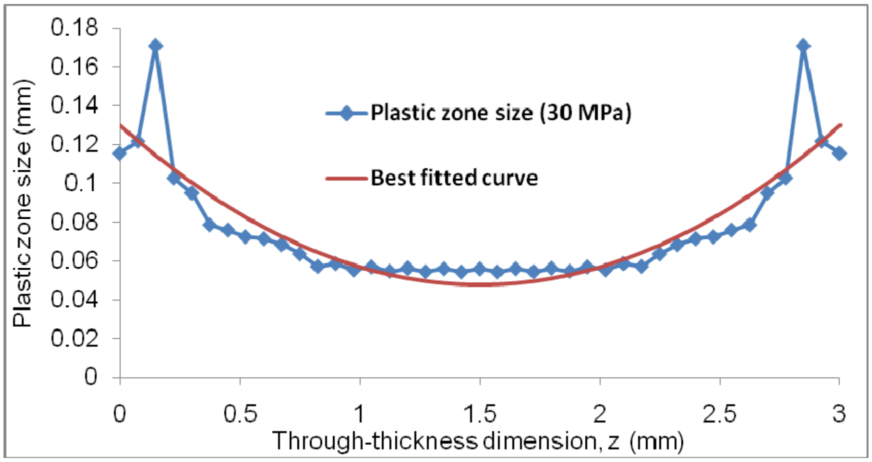

(a)

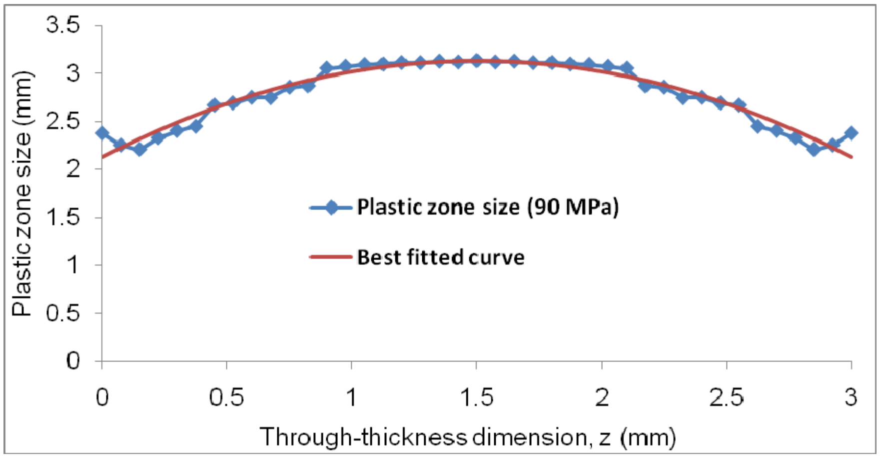

(b)

Figure 6.7 Plastic zone size when the plate is subjected to far field tensile stress of (a) 30 MPa and (b) 90MPa

As shown, the plastic zone's boundary through the thickness of the plate varies as a function of the far-field stress. Moreover, at the lower applied stress (i.e., 30 MPa, see Figure 6.7(a)), the plastic zone is relatively larger near the free surfaces and smaller at the mid-plane, while the application of the larger far-field stress (i.e., 90 MPa, see Figure 6.7(b)), results in a larger plastic zone at the mid-plane. The plastic zone configuration shown in Figure 6.7(b) confirms the experimentally obtained overload marking line clearly visible on the fatigue-fractured surface of the specimen (shown in Figure 6.8). Similar marking line has been reported by Borrego et al. [4].

Figure 6.8 Overload marking line on fractured surface

Since the plastic zone radius is usually presented as a function of the stress intensity factor (K), the variation of the stress intensity factor throughout the thickness was also investigated. A linear three-dimensional finite element analysis was carried out and the resulting through-thickness variation of the stress intensity factor, K, is illustrated in Figure 6.9. As can be seen, K is almost constant and equal to its theoretical value across plate's thickness (with less than 3% error in the mid-thickness of the plate). A sudden change in the stress intensity factor is also observed over small regions near free surfaces of the plate. The findings reveal that the theoretical equation can be used to establish the plastic zone radius.

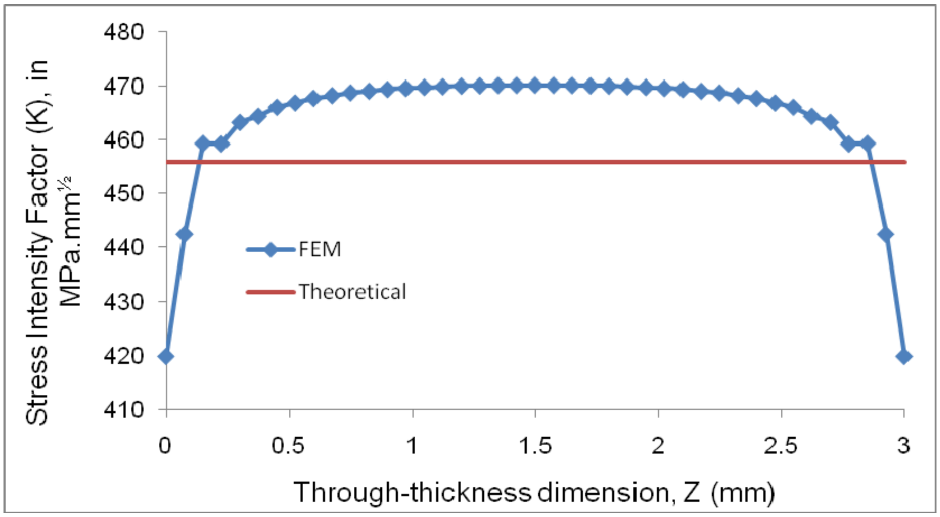

Figure 6.9 Variation of stress intensity factor (K) over specimen's thickness

Having established the variation of plastic zone's dimension through the specimen thickness, its average value could be determined by:

$$r_p = \frac{1}{t}\int_0^t \rho dz \tag{6.7}$$

where t and ρ are the thickness and plastic zone radius across the thickness, respectively. The plastic zone coefficient (α) established based on the finite element (FE) results are compared with the equations developed by others [27 & 28] and shown in Figure 6.10. In order to show the influence of plane stress/stain assumption on the plastic zone radius, two other two-dimensional models (i.e., using the plane stress and plane strain assumptions), were constructed in addition to the three-dimensional model.

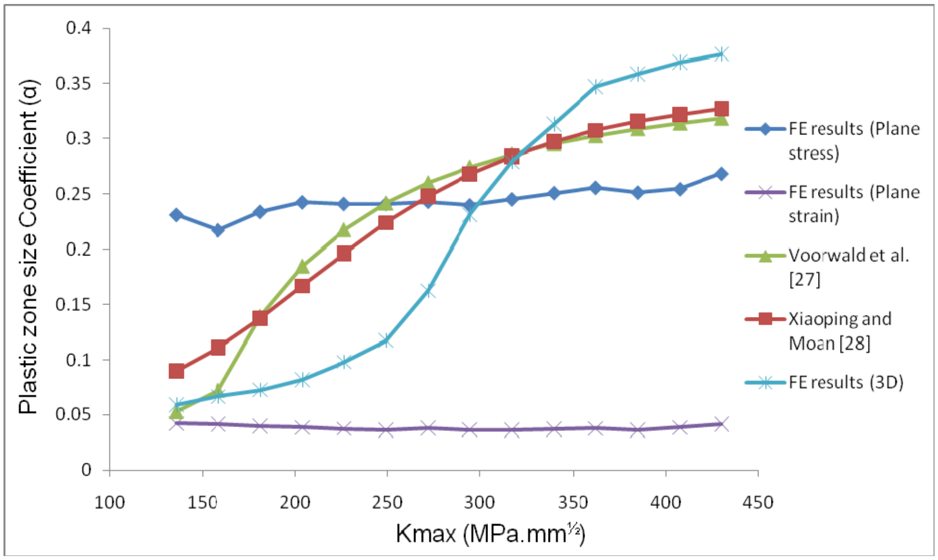

Figure 6.10 Plastic zone size coefficient

As can be seen from the results exhibited in Figure 6.10, as anticipated, the incorporation of the plane stress assumption resulted in a larger plastic zone than when the plane strain assumption was used. The comparison of the results revealed that the plastic zone coefficient varied in its value, ranging from that obtained from the plane strain analysis (when subjected to lower stress intensity factor), and then approaching the results obtained from the plane stress analysis (especially when subjected to a higher stress field).

6.5 Retardation of crack growth in AM60B magnesium plates

As illustrated in Figure 6.6, the crack growth would accelerate upon the application of an overload, and then subsequently be retarded. Considering the fact that the acceleration in crack propagation occurred within a very small crack increment, and that it is physically very difficult to measure such crack's advancement, the acceleration in crack growth is neglected. Therefore, the deceleration has been shown to start immediately after the application of an overload, thereby taking the FCG to its lowest value and subsequently returning back to the steady state.

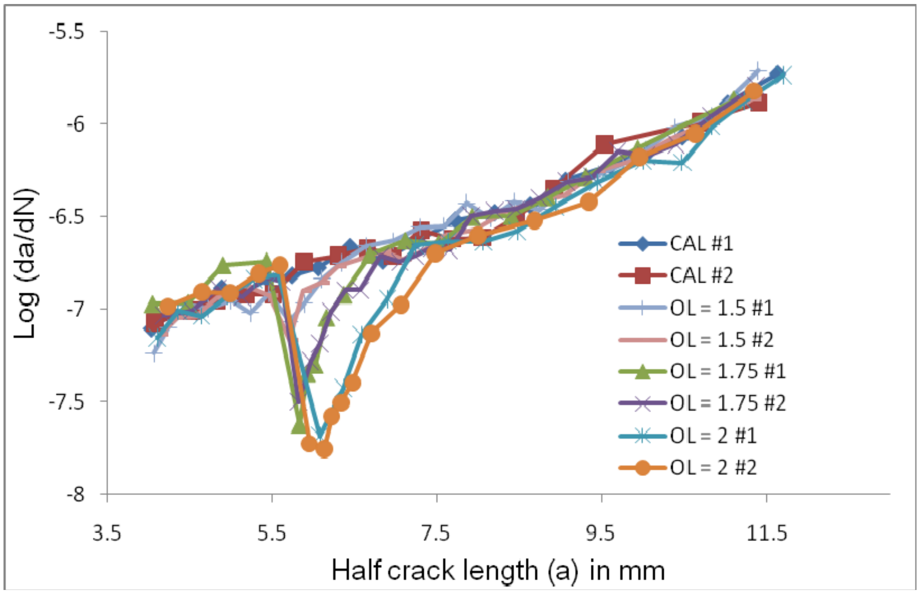

Figure 6.11 Crack propagation versus the crack length for various overload ratios

The crack propagation rate versus the crack length for AM60B magnesium plates subjected to various OLRs are shown in Figure 6.11. The affected zone begins from the crack length at which the overload was applied (a_{OL}), to the crack length at which the propagation rate returns back to the steady state; these values are reported in Table 6.2. The results indicate that the affected zone was enlarged when higher OLR was applied. It should be noted that the average value for each OLR is reported in the table. As also seen, the experimentally measured affected zone values for AM60B plates are considerably smaller than those calculated using the Wheeler model, while some other materials (e.g., 350WT steel, as reported in [24], and 6082-T6 aluminum alloy [4]) have exhibited larger affected zone compared to the values obtained by Wheeler's model.

Table 6.2 Affected zone size (experimental and those based on Wheeler model) (mm)

OLR	a_{OL}	$a_{OL} + a_r$ (Experimental)	$a_{OL} + a_r$ (Wheeler model)
1.5	5.65	6.15	6.58
1.75	5.68	6.7	7.55
2	5.7	7.24	8.35

Wheeler also assumed that the crack propagation rate would return back to the steady state when the affected zone parameter $[r_{p,i}/(a_{OL}+r_{p,OL}-a_i)]$ reaches unity. This parameter has been evaluated at the end of experimentally-measured affected zones and illustrated with respect to the overload ratios in Figure 6.12. The chart shows that the affected zone parameter is significantly lower than unity when the retardation process is completed.

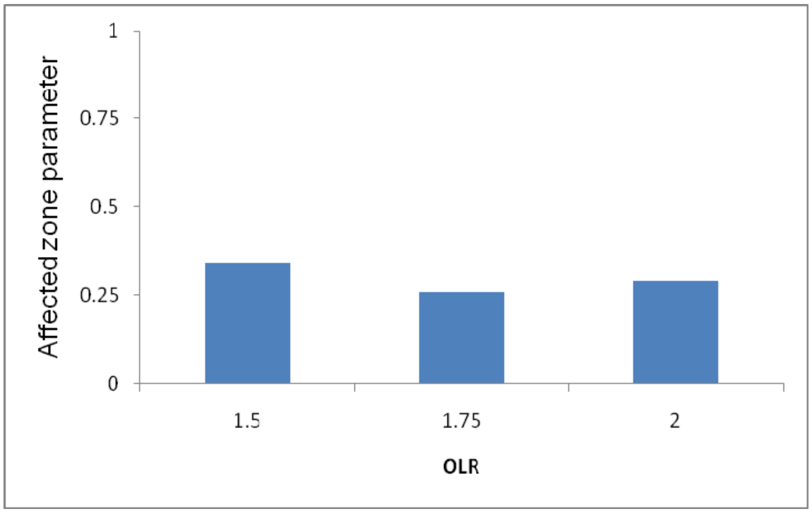

Figure 6.12 Affected zone parameter for various overload ratio

6.6 Modification of Wheeler model

It has been demonstrated by several researchers that due to the variation of the actual plastic zone from that assumed by Wheeler, the affected zone parameter defined by Wheeler could not predict the crack propagation in an accurate manner. As a result, various approaches have been proposed by several researchers for establishing the effective plastic zone radius. In actuality, however, none of the plastic zone dimensions established by the proposed approaches matches the actual plastic zone. Moreover, it has been shown that in some materials, the actual affected zone would be either larger or smaller than that assumed by Wheeler. It could be therefore concluded that the sensitivity of materials to overload cycles varies from one material to another. The aim of the proposed modified Wheeler model discussed below is to account for the delay in crack growth retardation and to address the sensitivity of the material to overload in an effective manner.

6.6.1 The modified reduction factor

To evaluate the retardation due to application of an overload within an otherwise CAL, the Wheeler model (as represented by equation (6.1)), is modified in the following format:

$$\frac{da}{dN} = \Phi_D \Phi'_R \left(\frac{da}{dN} \right)_{CAL} \tag{6.8}$$

where Φ_D is the delay parameter and Φ'_R is the proposed modified reduction factor. As can be seen, the reduction factor used in the original Wheeler model is modified, and one extra parameter, Φ_D, is added to the original model.

In order to evaluate the modified reduction factor (Φ'_R), a portion of the overload plastic zone is considered. In other words, the reduction factor is modified to account for material's sensitivity to overload, described by the following equation:

$$\Phi'_R = \begin{cases} \left[\dfrac{r_{p,i}}{a_{OL} + \beta r_{p,OL} - a_i} \right]^m & when \quad a_i + r_{p,i} \langle \, a_{OL} + r_{p,OL} \\ 1 & when \quad a_i + r_{p,i} \rangle \, a_{OL} + r_{p,OL} \end{cases} \tag{6.9}$$

Comparing equations 6.9 and 6.2 reveals that an additional parameter (β) is included in the original Wheeler model. This parameter accounts for material's sensitivity to overload. It should be noted that this modified reduction factor acts over the crack length from $a_{OL} + a_d$ to $a_{OL} + a_r$, while it would be equal to unity for any other crack lengths. The parameters β and m were determined based on the experimental data obtained for various overload ratios, as presented in Table 6.3.

Table 6.3 The parameters for the modified reduction factor

Overload ratio	m	β
1.5	0.524	0.58
1.75	0.948	0.575
2	1.044	0.585

As can be seen, the sensitivity parameter (β) seems to be independent of the overload ratio. The observed minor variation for different overload ratios is believed to be due to the experimental errors.

6.6.2 Delay parameter

Yuen and Taheri [24] assumed that each fatigue loading produces an effective delay zone (r_d) as per equation 6.10.

$$r_d = \gamma \left(\frac{K}{\sigma_y} \right)^2 \tag{6.10}$$

where γ is the effective delay zone coefficient. The delay in retardation would continue until the current effective delay radius ($r_{d,i}$) reaches the overload effective delay zone radius ($r_{d,OL}$), where the crack propagation at the end of the delay zone reaches its minimum value. Having established the delay zone dimension (a_d) through the experimental results, the value of γ could be calculated using the following equation [24].

$$a_d = r_{d,OL} - r_{d,d} = \gamma \left[\left(\frac{K_{OL}}{\sigma_y} \right)^2 - \left(\frac{K_d}{\sigma_y} \right)^2 \right] \tag{6.11}$$

where K_d and $r_{d,d}$ are the stress intensity factor and effective delay zone radius at crack length of $a = a_{OL} + a_d$. The values of the delay zone coefficients (γ) and a_d for various overload ratios are presented in Table 6.4. The delay parameter should be a decreasing function, reaching its minimum value at the end of a_d. Yuen and Taheri [24] postulated that the delay parameter would be a function of $(a_{OL} + r_{d,OL} - a_i) / r_{d,i}$ and defined an additional shaping exponent (m_{mod}). Moreover, the stress intensity factor was also modified to obtain a better fit of the experimental data, making their modified model somewhat complicated.

Table 6.4 Delay zone size coefficients (γ) and a_d

Overload ratio	γ	a_d (mm)
1.5	0.0265	0.07
1.75	0.03135	0.14
2	0.0591	0.4

Crack propagation rate in the delay zone is believed to be a decreasing linear function of the baseline stress intensity factor in the logarithmic scale. Since the delayed zone crack length (a_d) is small in comparison to the affected zone (a_r), a linear relation between the crack propagation rate (in the logarithmic scale) and crack length in the delayed zone has been assumed. It should be noted that, the delay parameter should decrease from unity at $a_{OL,}$ to its minimum value at $a_{OL} + a_d$; therefore, it could not be presented as a function of $(a_{OL} + r_{d,OL} - a_i) / r_{d,i}$. The modified delay parameter is presented in the following equation.

$$\begin{cases} Log\left(\Phi_D\right) = \left(\dfrac{a_i - a_{OL}}{a_d}\right) Log\left(\Phi'_{R,\min}\right) & a_i + r_{d,i} \langle\, a_{OL} + r_{d,OL} \\ \Phi_D = 1 & a_i + r_{d,i} \,\rangle\, a_{OL} + r_{d,OL} \end{cases} \qquad (6.12)$$

where $\Phi'_{R,min}$ is the minimum value of the modified reduction factor, which occurs at $a_{OL} + a_d$, established using equation 6.9. A comparison between the original and modified Wheeler model for overload ratio of 1.75 is shown in Figure 6.13. As can be seen, the proposed modified Wheeler model can predict the affected zone dimension with more accuracy.

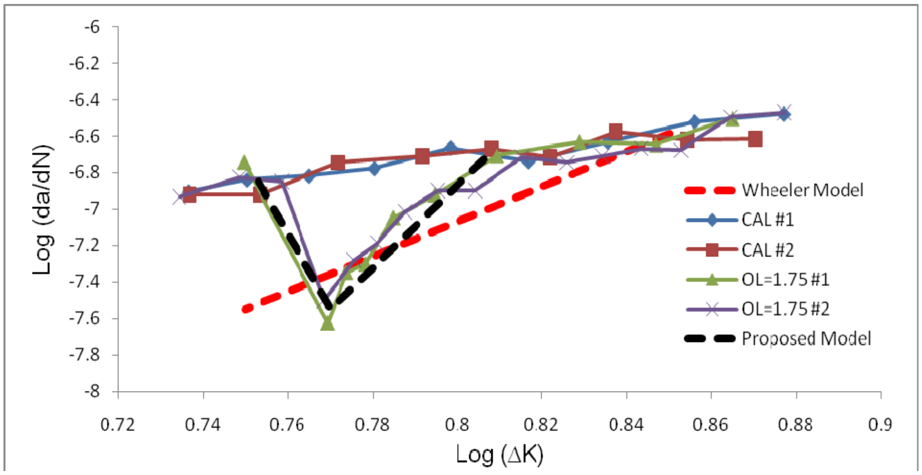

Figure 6.13 Comparison of retardation in crack propagation evaluated by Wheeler's original and the proposed modified models (OLR = 1.75)

6.6.3 Verification of the model for predicting the affected zone in other materials

The integrity of the proposed modified model is evaluated by considering its predictions when applied to two other materials. In these case studies, the coefficient of sensitivity (β), and capability of the model to predict the affected zone dimension are verified. The first set of the experimental data were taken from the investigation that was carried out by Yuen and Taheri [24] on 350WT steel plates. In their tests, an overload was applied on each specimen hosting a crack with the length of 2a = 30 mm. Three overloads with the ratio of OLR = 1.33, 1.5 and 1.67 (with respect to the baseline constant amplitude cyclic loading, which had a stress ratio of R = 0.1 and maximum stress of 120 MPa) were investigated. The results of these experiments are summarized in Table 6.5.

Table 6.5 Experimental results reported by Yuen and Taheri [24]

Overload ratio	a_{OL} (mm)	$a_{OL} + a_d$ (mm)	$a_{OL} + a_r$ (mm)	α (Effective plastic zone size coefficient)
1.33	15.13	16.67	20.85	5.91
1.5	15	16.03	22.10	3.11
1.67	14.94	16.45	24.43	2.99

It should be noted that in the results obtained by Yuen and Taheri [24] (tabulated in Table 6.5), a different effective plastic zone coefficient (instead of the actual one) was considered in order to fit the experimental results to the model for each overload ratio. Their effective plastic zone coefficients are indeed much larger than those shown in Figure 6.10, and varies significantly from one overload ratio to another. Moreover, this parameter could not be established through a finite element analysis. Therefore, in order to calculate the effective zone coefficient for a given material, one must always have a set of experimental data for each overload ratio for that particular material.

In order to evaluate the sensitivity parameter (β) for 350WT steel plate under the abovementioned baseline loading condition, a three dimensional finite element analysis was performed using the NISA, and the plastic zone coefficients were established (similar to the results presented in Figure 6.10). Then Wheeler model's parameter ($r_{p,i}$ / $a_{OL} + r_{p,OL} - a_i$), which controls the affected zone's dimension, was also evaluated. The variation of this parameter as a function of crack length, for different OLRs is presented in Figure 6.14.

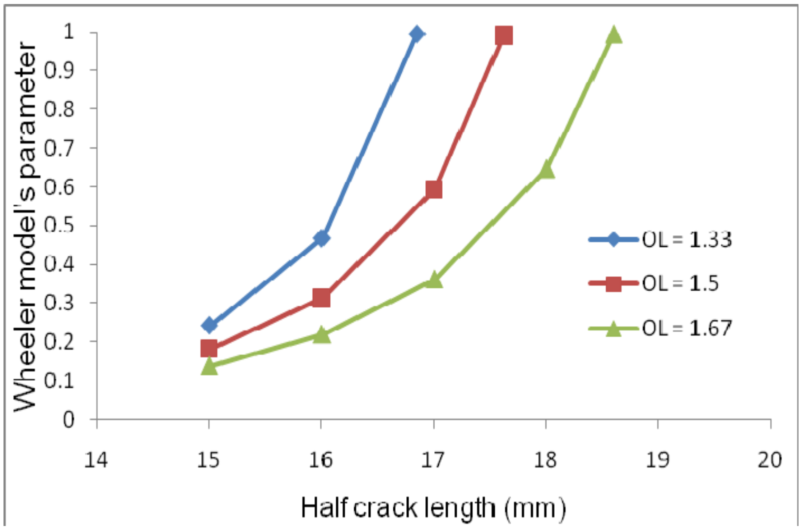

Figure 6.14 Variation of Wheeler model's parameter with respect to the crack length

The results indicate that the Wheeler parameter reaches to unity (which signifies the termination of retardation influence) at a crack length that is much smaller than those reported by Yuen & Taheri [24], as tabulated in Table 6.5. Using the plastic zone radii and the experimentally reported affected zone dimensions, the sensitivity parameter (β) is determined to be 2.5 for all three overload ratios. The consistency in the value of β for various overload ratios confirms the independency of this parameter to the overload ratios. Comparing the $\beta = 2.5$ for 350WT steel with $\beta = 0.58$ for AM60B magnesium alloy reveals the fact that 350WT steel is much more sensitive to the application of an overload than AM60B magnesium alloy.

Additionally, the integrity of the proposed modified model has been verified by considering the experimental data reported by Kumar et al. [3] on IS-1020 steel plates. In their investigation, overloads with various ratios of 1.4, 1.6, 1.8 and 2 were applied on edge-cracked specimens. The initial crack length at which the overload was applied was

12 mm. After conducting a finite element analysis to establish the plastic zone coefficient, and using the affected zone dimension calculated in their report, β value was determined to be 1.33, consistent for all the overload ratios.

6.7 Influence of overload in random amplitude loading

Most structural components are subjected to random amplitude loading during their service life. In order to study the influence of an overload in a random amplitude loading, one can use the clipping level technique [29 & 30]. In this method, all stress amplitudes that are greater than a certain percentage of the highest loading cycle amplitude in the loading history are truncated (clipped) in their magnitude to that certain level. The presumption is that some levels of truncation would produce shorter fatigue life, or may accelerate the crack propagation.

Kim et al. [29] investigated the influence of two different clipping levels (i.e., 90% and 80%) on a random amplitude loading applied on 7050-T7451 aluminum alloy plates. They reported that the application of 90% clipping level significantly reduced the fatigue life (by more than 50% reduction), while 80% clipping level resulted in lesser amount of fatigue life reduction. Iranpour and Taheri [30] studied the clipping level's influence on 6061-T651 aluminum alloy plates. Maximum crack growth acceleration was observed at 70% clipping level, while application of 55% clipping level resulted in no acceleration. Clipping levels less than 55% caused the cyclic loading to move into lower stress amplitude; therefore, the crack was observed to have grown slower, leading to longer fatigue life.

In this investigation, similar center-cracked AM60B magnesium alloy plates, as previously noted, were subjected to a random amplitude loading scenario. Each block of the random amplitude loading consisted of 144 zero-to-tension loading cycles, with cycles having various amplitudes. The random amplitudes were generated using the MATLAB. Two clipping levels of 85% and 70% were investigated in our experimental studies. A typical block of random amplitude loading and a truncated one with 70% clipping level are shown in Figure 6.15.

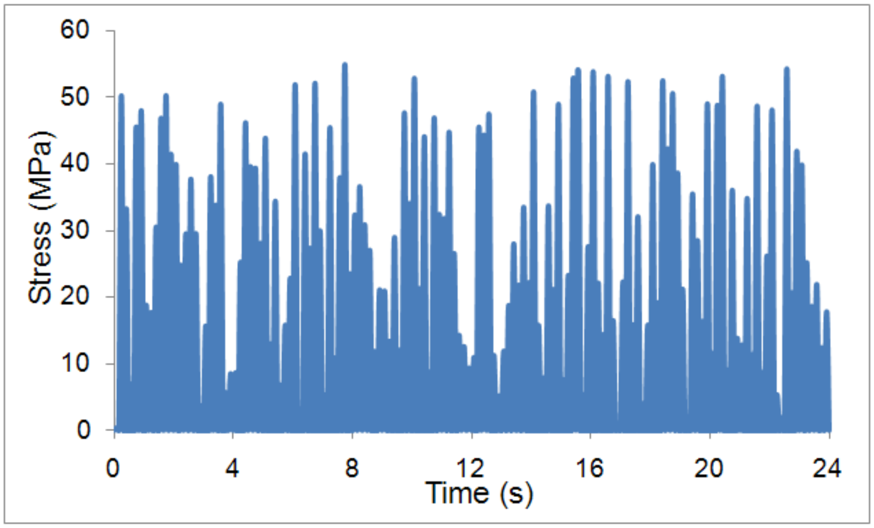

(a)

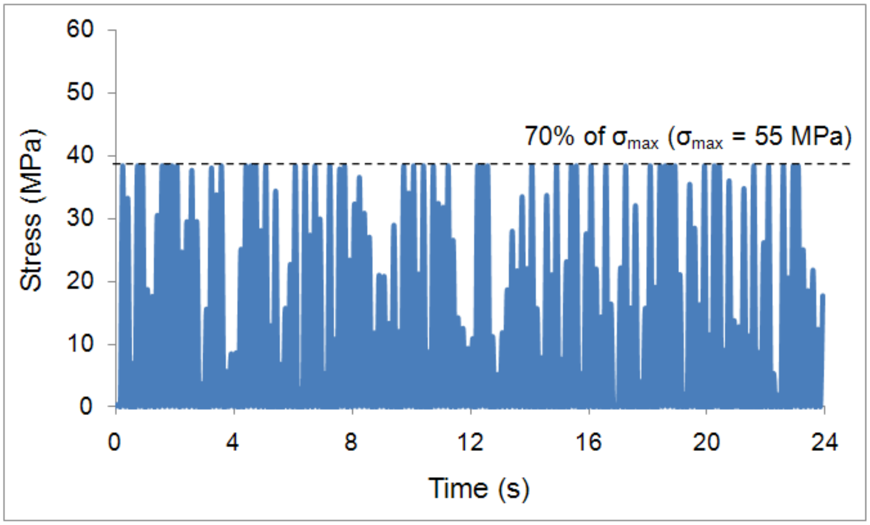

(b)

Figure 6.15 Typical block of (a) random and (b) 70% clipped random amplitude loading scenarios

The results (crack length versus the number of cycle) for different clipping levels are shown in Figure 6.16. It should be noted that three specimens were tested at each clipping level; due to consistency of the results, only the average values are reported. As can be seen, the application of 85% clipping level resulted in the same fatigue life as the case with no clipping, while further decrease in clipping level (i.e., to 70%) yielded slower crack propagation, thus longer fatigue life.

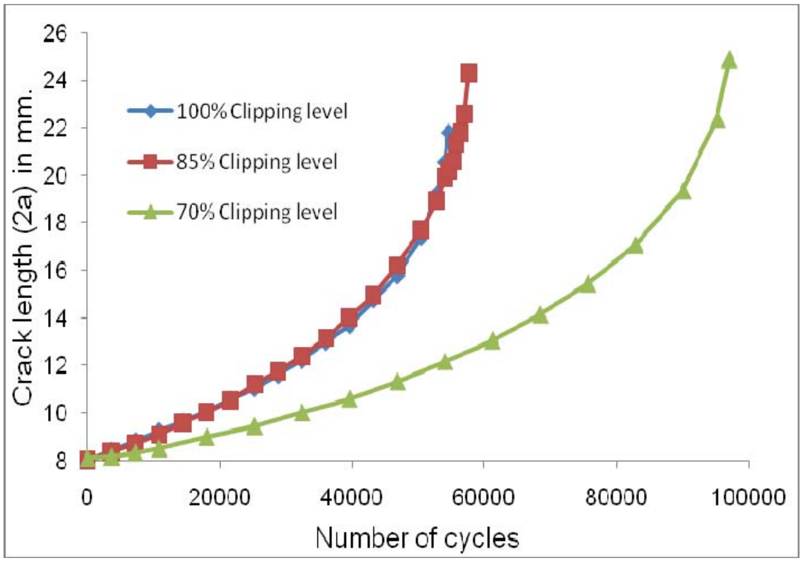

Figure 6.16 Crack length versus the number of cycles for various clipping levels

The results observed for AM60B magnesium alloy revealed different response than those observed for aluminum alloys by other researchers [29 & 30]. In the case of the Mg alloy considered here, the application of the clipping levels (or removing the overloads), did not produce any acceleration in crack growth. This phenomenon could be attributed to the sensitivity of this material to overload. Moreover, as shown earlier, the value of β coefficient for this material is significantly lower than those obtained for other materials.

6.8 Conclusion

Application of an overload applied within a CAL scenario resulted in retardation in crack propagation in AM60B magnesium alloy plates investigated experimentally. The retardation due to overload could be characterized by consideration of the affected zone and the amount of increased life cycles.

The Wheeler model uses the plastic zone radius to establish the affected zone's dimension that is used for life-cycle assessment. When the actual plastic zone radius is considered in the model, the model falls short of predicting the affected zone radius with an acceptable accuracy. Therefore, effective plastic zone coefficients were evaluated and proposed for several materials, and various overload ratios. It is also concluded that a separate set of detailed experimental data is required for each overload ratio if one wishes to accurately establish the value of the effective plastic zone coefficient.

Furthermore, the Wheeler model was modified to include the actual plastic zone radius in evaluating the affected zone dimension. A new parameter (β) was also proposed to be included in the model; this parameter accounts for material's sensitivity to overload. It was shown that this sensitivity parameter would be constant for all overload ratios; however, its value would vary from one material to another.

The affected zone dimension calculated for AM60B magnesium alloy was found to be smaller than that produced by the Wheeler model. Moreover, the magnitude of the sensitivity parameter, β, calculated for AM60B magnesium alloy, revealed that this material is not very sensitive to the application of an overload when compared with the other materials considered in our investigation. The investigation conducted to consider the influence of overload cycles within a random amplitude loading scenario, demonstrated that clipping level's influence is not unified across all alloys.

6.9 Acknowledgement

The research was financially supported by Auto21. The AM60B plates were provided by Meridian Technologies Inc. The supports are gratefully appreciated.

6.10 References

[1] Lu, Y. & Taheri, F., "Monotonic and Cyclic Plasticity Response of Magnesium Alloy. Part II. Computational Simulation and Implementation of a Hardening Model", *Strain (International Journal for Experimental Mechanics)*, 47, pp.e25-33, 2008.

[2] Nur Hossain, M. & Taheri, F., “Influence of Elevated Temperature and Stress Ratio on the Fatigue Response of AM60B Magnesium Alloy”, *Journal of Materials Engineering and Performance*, 21, pp.1395-404, 2011.

[3] Kumar, R., Kumar, A. & Kumar, S., “Delay Effect in Fatigue Crack Propagation” *Int. J. Pres. Ves. & Piping*, 67, pp.1-5, 1996.

[4] Borresgo, L.P., Ferreira, J.M., Pinho da Cruz, J.M. & Costa, J.M., “Evaluation of Overload Effects on Fatigue Crack Growth and Closure”, *Engineeing Fracture Mechanic*, 70, pp.1379- 1397, 2003.

[5] Elber, W., “The Significance of Fatigue Crack Closure” *Damage Tolerance in Aircraft Structures, ASTM STP 486, American Society for Testing and Materials*, pp.230-42, 1971.

[6] Shuter, D.M. & Geary, W., “Some Aspects of Fatigue Crack Growth Retardation Behaviour Following Tensile Overloads in a Structural Steel”, *Fatigue Fract Eng Mater Struct* , 19, pp.185–99, 1996.

[7] Tur, Y.K. & Vardar, O., “Periodic Tensile Overloads in 2024-T3 Al-Alloy”, *Eng Fract Mech*, 53, pp.69-77, 1996.

[8] Sander, M. & Richard, H.A., “Fatigue Crack Growth Under Variable Amplitude Loading, Prt I: Experimental Investigation”, *Fatigue Fract Engng Mater Struct*, 29, pp.291-301, 2006.

[9] Barsom, J.M., “Fatigue Crack Growth under Variable Amplitude Loading in Various Bridge Steel., In Fatigue Crack Growth under Spectrum Loads”, *ASTM STP 595, Amercian Society for Testing and Materials*, pp.217-35, 1976.

[10] Hudson, C.M., "A Root-Mean-Square Approach for Predicting Fatigue Crack Growth under Random Loading, Methods and Models for Predicting Fatigue Crack Growth under Random Loading", *ASTM STP 748. J. B. Chang and C. M. Hudson, Eds., American Society for Testing and Materials*, pp.41-52, 1981.

[11] Paris, P.C. & Erdogan, F., "A Critical Analysis of Crack Growth Laws", *Journal of Basic Engineering*, 85, pp.528-34, 1965.

[12] Mehrzadi, M. & Taheri, F., "Influence of Compressive Cyclic Loading on Crack Propagation in AM60B Magnesium Alloy under Random and Constant Amplitude Cyclic Loadings", *Submitted to Engineering Fracture Mechanics,* August 2012.

[13] Wheeler, O.E., "Spectrum Loading and Crack Growth", *Journal of Basic Engineering*, 94, pp.181-86, 1972.

[14] Willenborg, J., Engle, R.M. & Wood, H.A., "A Crack Growth Retardation Model Using an Effective Stress Concept", *Air Force Flight Dynamics Laboratory, Report AFFDL-TR-71-FB,* 1971.

[15] Taheri, F., Trask, D. & Pegg, N., "Experimental and Analytical Investigation of Fatigue Characteristics of 350WT Steel Under Constant and Variable Amplitude Loadings", *J Marine Struct*, 16, pp.69-91, 2003.

[16] Khan, Z., Rauf, A. & Younas, M., "Prediction of Fatigue Crack Propagation Life in Notched Members under Variable Amplitude Loading", *Journal of Materials Engineering and Performance*, 6, pp.365-37, 1997.

[17] Rushton, P.A. & Taheri, F., "Prediction of Crack Growth in 350WT Steel Subjected to Constant Amplitude with Over- and Under- Loads Using a Modified Wheeler Approach", *Journal of Marine Structures*, 16, pp.517-39, 2003.

[18] Kim, J.K. & Shim, D.S., “A Statistical Approach for Predicting the Crack Retardation Due to Single Tensile Overload”, *International Journal of Fatigue*, 25, pp.335-42, 2003.

[19] ASTM E647-08, “Standard Test Method for Measurement of Fatigue Crack Growth Rates”, ASTM International, PA, USA.

[20] ASTM E1245, “Standard Practice for Determining the Inclusion or Second-Phase Constituent Content of Metals by Automatic Image Analysis”, (reapproved 2008), ASTM International, PA, USA.

[21] Skorpua, M. & Skorpua, A., “Experimental Results and Predictions on Fatigue Crack Growth in Structural Steel”, *International Journal of Fatigue*, 27, pp.1016-28, 2005.

[22] Song, P.-S., Sheu, B.-C. & Chang, L., “A Modified Wheeler Model to Improve Predictions of Crack Growth Following a Single Overload”, *JSME International Journal*, 44, pp.117-22, 2001.

[23] Sheu, B.C., Song, P.S. & Hwang, S., “Shaping Exponent in Wheeler Model Under a Single Overload”, *Engineering Fracture Mechanics*, 51, pp.135-45, 1995.

[24] Yuen, B.C.K. & Taheri, F., “Proposed Modification to the Wheeler Retardation Model for Multiple Overloading Fatigue Life Prediction”, *International Journal of Fatigue*, 28, pp.1803-19, 2006.

[25] Irwin, G., “Linear Fracture Mechanics, Fracture Transition, and Fracture Control”, *Engineering Fracture Mechanics*, 1, pp.241-57. 1968.

[26] Guo, W., “Three Dimensional Analysis of Plastic Constraint for Through-Thickness Cracked Bodies”, *Engineering Fracture Mechanics*, 1, pp.383-407, 1999.

[27] Voorwald, H. & Torres, M., “Modeling of Fatigue Crack Growth Following Overloads”, *International Journal of Fatigue*, 13, pp.423-27, 1991.

[28] Xiaoping, H., Moan, T. & Weicheng, C., “An Engineering Model of Fatigue Crack Growth Under Variable Amplitude Loading”, *International Journal of Fatigue*, 30, pp.2-10, 2008.

[29] Kim, J.-H., Lee, S.-B. & Hong, S.-G., “Fatigue Crack Growth Behavior of Al7050-T7451 Attachment Lugs Under Fight Spectrum Variation”, *Journal of Theoretical and Appied Fracture Mechanics*, 40, pp.135-44, 2003.

[30] Iranpour, M. & Taheri, F., “Influence of the Peak Tensile Overload Cycles and Clipping Level on the Fatigue Crack Growth of Aluminum Alloy under Spectrum Loading”, *Conditionally accepted, Journal of Material Engineering and Performance,* 2012.

CHAPTER 7 Influence of Compressive Cycles on Retardation of Crack Propagation in AM60B Magnesium Alloy Plates Due to Application of Overload

Morteza Mehrzadi and Farid Taheri
Department of Civil and Resource Engineering, Dalhousie University, PO Box 15000,
1360 Barrington Street, Halifax, NS, B3H 4R2, Canada

Submitted to the Journal of Engineering Fracture Mechanics, 2013.

7.1 Abstract

Application of a tensile overload within an otherwise constant amplitude cyclic loading scenario is known to retard the resulting crack propagation in metals, thus resulting in longer fatigue life. The magnitude of retardation and crack length increment that would be affected by such an overload would depend on the overload ratio and the nature of baseline loading. However, the influence of an overload within a baseline loading with negative stress ratio on crack propagation has not been extensively investigated. Consequently, the influence of overload (with various overload ratios), applied within various baseline loadings consist of both positive and negative stress ratios, is considered in our experimental investigation. It is shown that the retardation response of AM60B magnesium alloy varies when the stress ratio of the baseline loading changes. Wheeler model's parameters are evaluated separately for positive and negative stress ratios. For a positive stress ratio, the affected zone was modified based on the baseline loading's stress ratios.

The experimental results reveals that the retardation trend in crack propagation would be affected significantly by negative stress ratios; therefore, Wheeler's model would have to be modified to account for this important issue. Moreover, the influence of loading sequence (i.e., when the overload is followed by a compressive underload) on retardation of crack propagation is also investigated.

Finally, surface roughness of the fractured specimens is carefully examined by a profilometer and its variation with respect to stress ratio is reported in this paper.

Keywords: Overload, baseline loading, stress ratio, retardation, Wheeler model.

7.2 Introduction

In order to increase the application of high pressure die casting (HPDC) AM60B magnesium alloys in auto industry, more knowledge about the mechanical properties of the alloy is required. Some investigators [1-5] have reported the monotonic and cyclic response, crack initiation and propagation mechanisms, influence of porosities and casting defects on fatigue response of the alloy. The influence of cold and elevated temperature on fatigue response of the alloy was also investigated by Nur Hossain and Taheri [6, 7]. Nevertheless, due to the increase in the application of the alloy in auto industry, and considering the fact that cyclic loading is a dominant loading type in those applications, more investigation on the characterization of fatigue and fracture responses of the alloy are required.

In general, any cyclic loading could be characterized by the stress range (Δσ) and stress ratio (R) as defined by the following equation.

$$R = \frac{\sigma_{\min}}{\sigma_{\max}} \tag{7.1}$$

In the case of negative stress ratios, a portion of each cycle would be compressive. Ironically however, some standards [8, 9] and investigators have either recommended the complete dismissal of the compressive loading cycles' amplitudes, or partial consideration of the compressive amplitudes when estimating fatigue life of metallic materials. For instance, Kujawski [10, 11] proposed the positive stress intensity range (ΔK^{+}) and maximum stress intensity (K_{max}) in a cyclic loading as driving forces for crack propagation under such loading scenarios. It has however been shown that cracks could propagate even under fully compressive cyclic loading due to tensile residual stress around the crack tip and progressively decreases to be arrested [12- 14]. It should also be noted that dismissal of the compressive portion of a cyclic loading in fatigue life estimation has been based on the hypothesis that the crack faces would be closed under a compressive loading cycle, and that the crack would not propagate under the compressive loading.

The importance of the compressive stress cycles (CSC) within a constant amplitude loading scenario has been thoroughly investigated in last decade. It has been proven that a crack would indeed propagate faster when subject to a negative stress ratio. In some of the recent works [15-17], the finite element analysis has been employed to show that the maximum stress intensity factor (K_{max}) and the maximum compressive stress ($\sigma_{c,max}$) govern the crack propagation rate when the stress ratio is negative. Huang and Moan [18] proposed a modification parameter to the Paris model [19] in order to predict the crack propagation resulting due to both positive and negative stress ratios. Some modification of Walker's model [20] has also been suggested by the authors [21] in order to increase the predictive accuracy of Walker's equation for estimating crack propagation in AM60B magnesium alloy under a wide range of stress ratios. Silva [22] showed experimentally that the influence of compressive cycles would vary from one material to the other. He performed experimental studies on materials considering three different aspects; that is: cyclic hardening, cyclic softening and cyclic neutral. Due to the varied responses of those materials to the presence of compressive stress portion within a cyclic loading, he suggested that the intrinsic properties of the material should be considered within crack propagation models.

In most industrial applications, however, structural components are rarely subjected to constant amplitude cyclic loading (CAL) and are usually subject to a random amplitude loading (RAL). In order to study the material response under real fatigue loading conditions, some simplified scenarios, such as the inclusion of an overload or underload within an otherwise CAL have been investigated.

The application of an overload has also been known to produce retardation in crack propagation and several models have been proposed to predict the crack propagation in such a circumstance. Among them, Wheeler [23] characterized the retardation by the affected zone, and suggested the use of the following equation for evaluating the magnitude of the crack propagation retardation.

$$\frac{da}{dN}=\Phi_R\left(\frac{da}{dN}\right)_{CAL},\ \Phi_R=\begin{cases}\left[\dfrac{r_{p,i}}{a_{OL}+r_{p,OL}-a_i}\right]^m & when \quad a_i+r_{p,i}\langle a_{OL}+r_{p,OL}\\ 1 & when \quad a_i+r_{p,i}\rangle a_{OL}+r_{p,OL}\end{cases} \tag{7.2}$$

where Φ_R, (da/dN) and $(da/dN)_{CAL}$ are the reduction factor, the retarded and steady state crack propagation rates, respectively. The reduction factor is a function of the current and overload plastic zone radii (i.e., $r_{p,i}$ and $r_{p,OL}$, respectively), and the shaping factor (m). It has been shown however that the affected zone in some materials would be larger or smaller than what was originally stated by Wheeler [21]. Therefore Wheler's model was modified by adding a sensitivity parameter.

The crack closure concept was originally introduced by Elber [24] and has been used by other researchers to predict the crack propagation rate. Elber observed that the crack faces may stay closed during a cyclic loading, even under the application of some levels of tensile stress. He proposed the "effective stress intensity range" as a driving force for crack propagation. Nevertheless, Silva [25] has shown that the crack closure is not adequate to predict the crack propagation at negative stress ratios. He also reported that under some specific negative stress ratios, the crack opening stress level could be compressive.

It has been observed that investigations considering the influence of overload on crack propagation rate in baseline loadings with negative stress ratio have been quite scarce. The lack of such practical data motivated us to study the response of AM60B magnesium alloy to an overload within an otherwise constant amplitude loading subject to various stress ratios (both positive and negative). Moreover the fracture surface of the specimens was also carefully analyzed to investigate their potential influence as a driving force.

7.3 Experimental setup

The AM60B magnesium alloy plates used in our investigation were cast by Meridian Technologies Inc. (Strathroy, Ontario). The specimens were configured according to ASTM E647-08 [8] specifications with the same as received thickness (3 mm), as shown in Figure 7.1. A small hole was drilled at the center of the specimen in order to be able to make a 6 mm notch using a jeweler's saw (having thickness of 0.25 mm). Another hole was drilled at each end of the specimen for attaching it to the grip system.

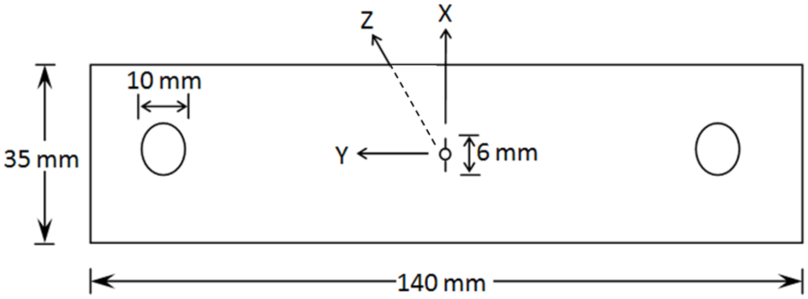

Figure 7.1 Geometry of the specimens

Since the specimen would be subjected to both tensile and compressive stresses cycles, an anti-buckling device was designed and fabricated to prevent pre-mature buckling of the specimens. The configuration of the anti-buckling device is shown in Figure 7.2. As can be seen, two roller bearings were used at four specific locations to provide the required lateral-support, yet minimizing the traction between the specimen and the anti-buckling device.

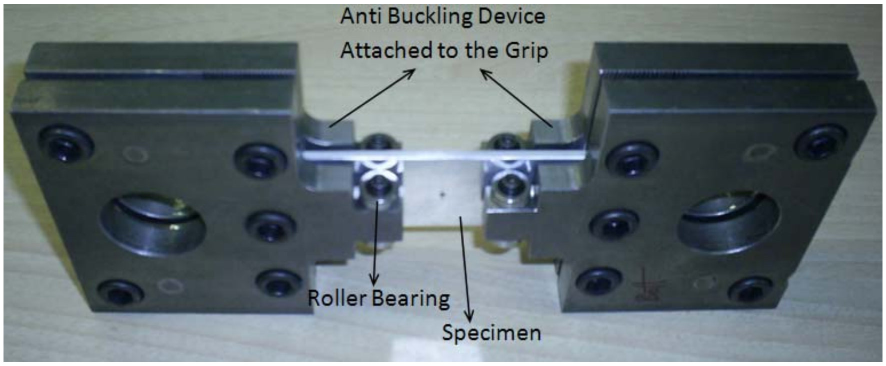

Figure 7.2 Configuration of the anti buckling device

In order to make sharp crack tips, specimens were pre-cracked by applying a constant amplitude cyclic loading with the maximum stress of 45 MPa (30% of yield strength) and stress ratio of 0.1, until a sharp crack with a length of 2a = 8 mm (where "a" is the half crack length). Then, the actual cyclic loading scenarios were applied and the crack lengths were recorded at certain intervals. An Instron servo-hydraulic universal test machine was used to apply the cyclic loading. The maximum capacity of the machine was ±100 kN under dynamic, or 200 kN under static loading conditions, controlled with 8501 digital electronics. The entire test setup is shown in Figure 7.3. A digital microscope with 92X magnification was used to measure the crack length accurately. As shown in Figure 7.3, the microscope was mounted on a travelling digital micrometer. The surface of the specimens were polished using various fine grade abrasive papers and subsequently with a suspension of aluminum oxide particles applied with a rotary pad to produce a shiny surface.

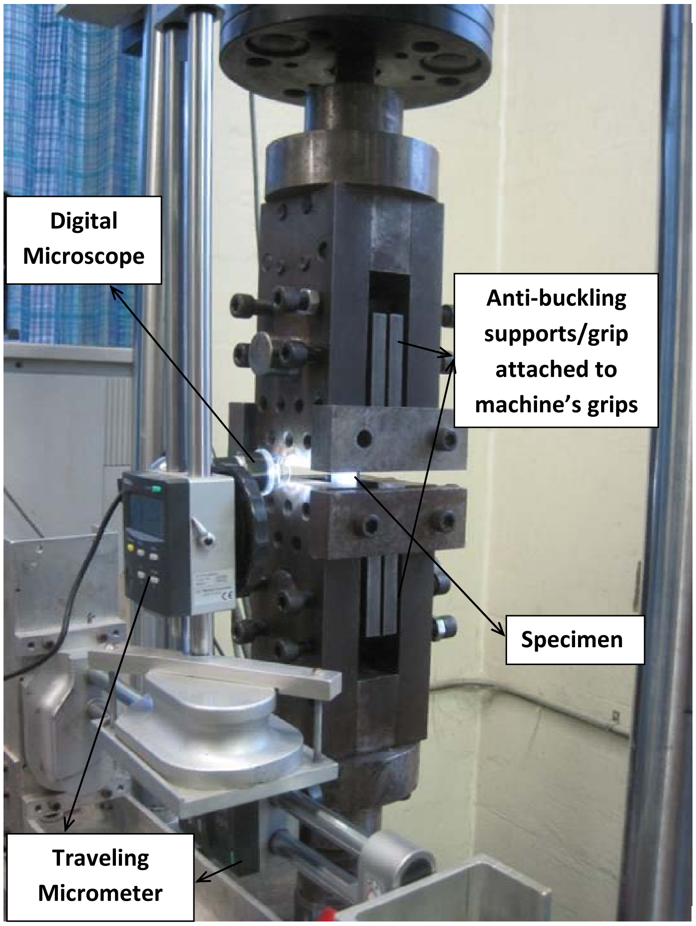

Figure 7.3 Test setup

Overloads with the ratios of 1.5, 1.75 and 2 were applied at the total crack length of 2a = 11.5 mm at each baseline loading scenarios. Both positive (R = 0.1 and 0.5) and negative (R = -0.5 and -1) stress ratios were considered as the constant amplitude baseline loadings.

7.4 Experimental results

7.4.1 Constant amplitude loading

At each stress ratio, two specimens were subjected to constant amplitude loading (CAL), so that their response could be compared with those specimens whose loading scenarios included an overload. The cyclic CAL was applied with a sinusoidal curve format with the maximum stress of 45 MPa. The selection of such relatively low number of specimens was justified by the fact that test results obtained from two were in very close agreement. The crack length (incremental growth), due to application of CALs with various stress ratios is shown in Figure 7.4 versus the number of cycles. It should be noted that each curve represents the average value of two curves, obtained at each stress ratio.

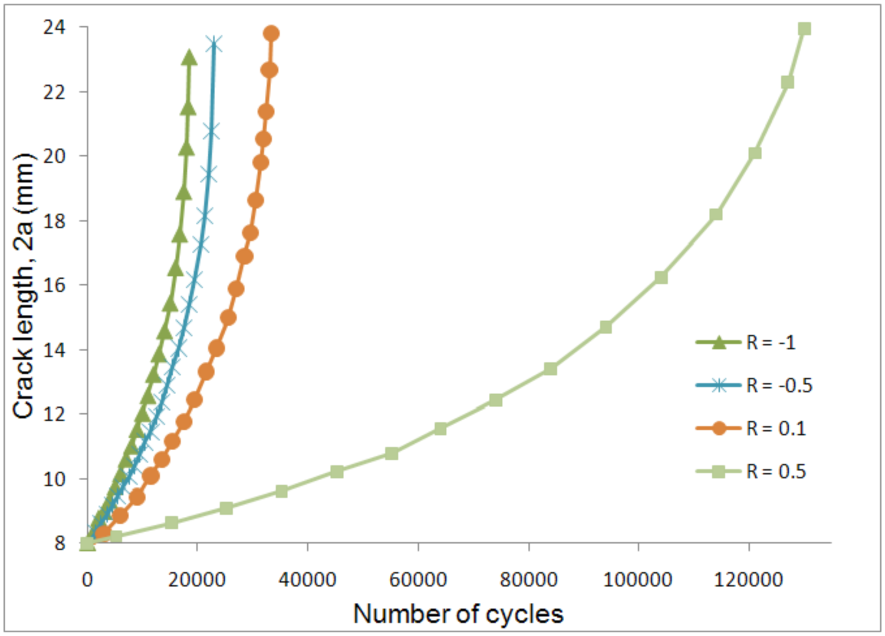

Figure 7.4 Crack length versus the number of cycles for different stress ratios

As can be seen, the presence of compressive cycles significantly accelerates the crack propagation and shortens the fatigue life. Comparison of the results for R = -1 with that of R = 0.1 reveals that the number of cycles to failure reduces by 50% when completely reversed cyclic loading was applied. Figure 7.5 presents the crack propagation rate versus the stress intensity range in the logarithmic scale. It should be mentioned that the entire stress range was considered in calculation of the stress intensity ranges, while as stated earlier, some standards and guidelines suggest dismissal of the compressive portion of the loading scenarios.

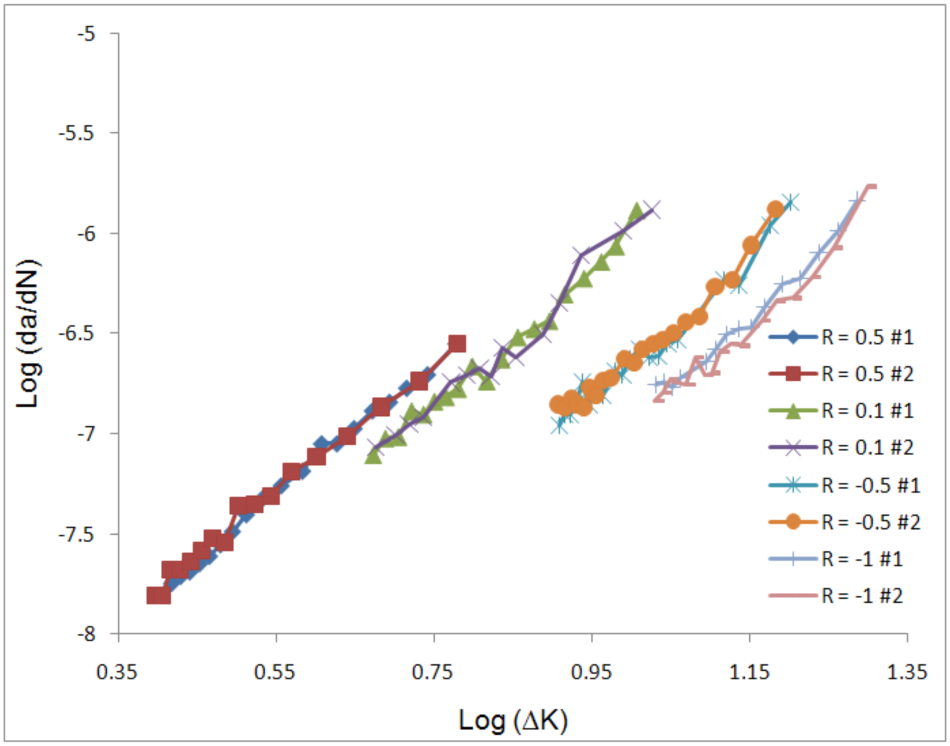

Figure 7.5 Variation of crack propagation rate as a function of stress intensity range

The graph shows that any increase in the stress ratio would in turn shift the crack propagation rate curves to the left, corroborating with previously observed results [26]. Moreover the trend is rather interesting; as it appears, the slope of the curves increase as the stress ratio decreases and the rate of change becomes nonlinear at negative stress ratios. Several models have been proposed to account for the influence of stress ratio on crack propagation.

All the models are based on the use of a modified stress intensity range with the aim of defining the crack propagation rate with a single line (in the logarithmic scale). For instance, Walker [20] related the crack propagation rate to stress ratio by adding a new parameter, with the assumption that crack propagation curves (lines) remain parallel to one another (when plotted in the logarithmic scale). Considering the fact that the slope of the crack propagation curves varies with respect to stress ratios, the Walker model was modified in our previous study, and a new modified stress intensity range was introduced by which the experimental data could be condensed into a single line (for more details refer to [26]).

7.4.2 Variable amplitude loading

Industrial components are rarely subjected to constant amplitude loading and may experience overloads and underloads within a more or less constant amplitude loading scenario. In this part of the experimental study, one overload is applied within each constant amplitude loading scenario, at the stage when the total crack length reaches 2a = 11.5 mm. The overload ratio (OLR) is defined as the ratio of the maximum stress at the overload stage to the maximum stress of the baseline loading; as such, three overload ratios were considered (OLR = 1.5, 1.75 and 2).

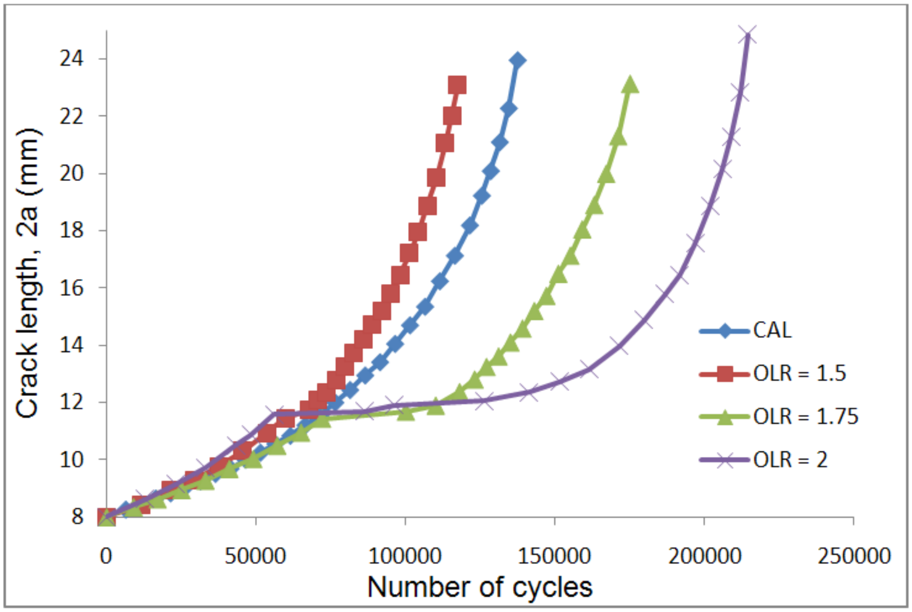

Figure 7.6 Influence of overload applied in a constant amplitude loading with R = 0.5

The resulting crack propagations as a function of the number of applied cycles are shown in Figure 7.6 for the case when the stress ratio of the baseline CAL was R = 0.5. As can be seen, the application of an overload with the ratio of OLR = 2 significantly increased the fatigue life of the specimen. For the same baseline loading, the logarithm of the crack propagation rate versus crack length is plotted in Figure 7.7, which reflects the fact that the crack propagation rates reach their lowest values upon the application of the OL, and then return back to their steady state.

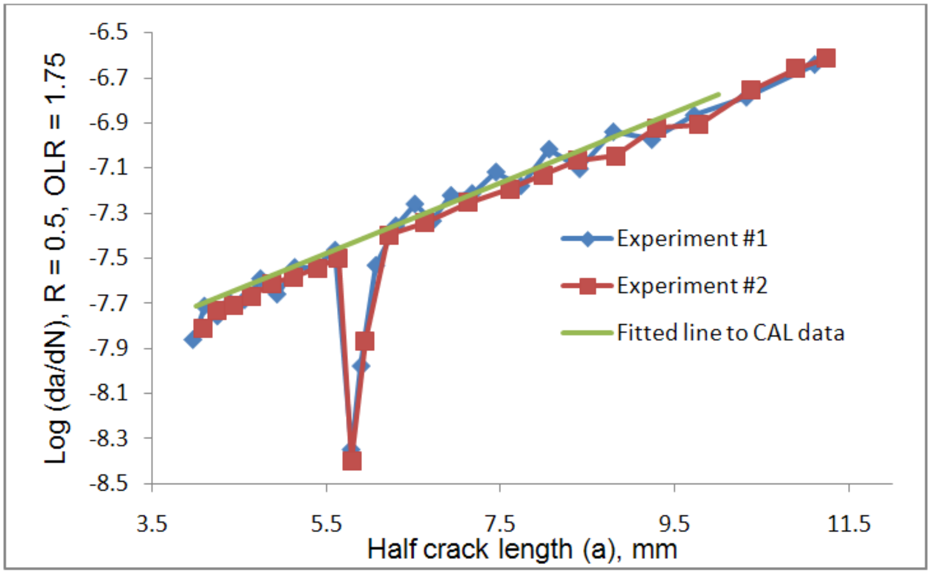

Figure 7.7 Variation of crack propagation rate versus the crack length when R = 0.5 and OLR = 1.75

7.5 Application of the Wheeler model for predicting retardation in crack propagation

Wheeler [23] proposed his model in 1972 (as noted in equation 7.2), depicting the retardation response of a crack upon the application of an overload (OL). He characterized this phenomenon by the introduction of the "affected zone" and incorporation of the magnitude of retardation. The affected zone was assumed to be a function of the current plastic zone, as well as the plastic zone developed as a result of the

OL. It was postulated that the crack propagation would return to its steady state rate when the boundary of the plastic zone developed under a given CAL reaches the boundary of the plastic zone developed due to the OL; or when the ratio $r_{p,i}/(a_{OL}+r_{p,OL}-a_i)$ reaches to the unity. The magnitude of the retardation is also governed by the shaping exponent, m, included in the Wheeler model, a parameter that depends on the overload ratio and the nature of the baseline loading. It has also been shown that [21] the affected zone in some materials would be larger than that predicted by Wheeler's model, and that it would be smaller in some other materials. Therefore, Wheeler's model would have to be modified to include a sensitivity parameter, β, as proposed by the following equation.

$$\frac{da}{dN}=\Phi_D\Phi'_R\left(\frac{da}{dN}\right)_{CAL}, \quad \Phi'_R=\begin{cases}\left[\dfrac{r_{p,i}}{a_{OL}+\beta r_{p,OL}-a_i}\right]^m & when \quad a_d+r_{p,i}\langle a_{OL}+r_{p,OL} \\ 1 & when \quad a_d+r_{p,i}\rangle a_{OL}+r_{p,OL}\end{cases} \tag{7.3}$$

In the above equation, a_d is the crack length at which the propagation rate reaches its minimum (see Figure 7.7). The sensitivity parameter (β) was found to be less than one for AM60B magnesium alloy, which indicates that the sensitivity of this alloy to overload is less in comparison to other materials.

The plastic zone size is usually presented as a function of the stress intensity factor and yield strength of the material, represented by equation 7.4.

$$r_p=\alpha\left(\frac{K_{\max}}{\sigma_y}\right)^2 \tag{7.4}$$

where α is the plastic zone coefficient, for which several values have been suggested. For instance, 1/2π and 1/6π have been suggested by Irwin [27] for plane stress and plane strain conditions, respectively (assuming the material responds elastically). In the case of an elastic perfectly-plastic material response, Irwin's parameters would increase to 1/π and 1/3π, respectively. Other researches [28, 29] have proposed various equations for establishing the coefficient, mostly developed based on the finite element analysis. These equations relate α to the maximum stress intensity factor, material yield strength and plate's thickness. Furthermore, virtually all such equations have been developed based on the assumption that the material behaves elastic-perfectly plastic, while the actual response of a metallic alloy is rarely elastic-perfectly plastic. Therefore, carrying out an accurate finite element analysis and evaluating the actual plastic zone coefficient is considered to be a more accurate means for establishing the value as opposed to the use of the simplified equations.

Therefore, a three dimensional nonlinear finite element analysis was carried out to evaluate the plastic zone size along the thickness (z-axis, see Figure 7.1) of the specimen for various stress intensity factors. The material was modeled using a bilinear elastic-plastic stress-strain response with the properties shown in Table 7.1.

Table 7.1 Material properties

Yield stress (σ_y)	150 MPa
Modulus of elasticity (E)	40 GPa
Plastic Modulus (E_T)	2.5 GPa

The NISA (Numerically Integrated System Analysis) was used to carry out the numerical analysis. NISA's 20-node isoparametric solid element was used to model the specimen. The average value of the plastic zone radius along the z-axis (see Figure 7.1), was evaluated using equation 7.5.

$$r_p = \frac{1}{t}\int_0^t \rho dz \tag{7.5}$$

where ρ is the plastic zone radius along the thickness of the specimen, and t is the thickness of the specimen.

7.6 Retardation in crack propagation due to various stress ratios

The retardation of crack propagation due to application of an overload is schematically shown in Figure 7.8. As illustrated in that figure, acceleration in crack propagation could be observed immediately upon the application of an overload, but for a very small increment of crack growth. It should be noted that the Wheeler model is not capable of predicting this initial crack acceleration. The experimental results of crack propagation rate when an overload with the ratio of 1.75 is applied within constant amplitude baseline loadings with various stress ratios are illustrated in Figure 7.9. It is clear that for a baseline CAL with a positive stress ratio, the crack would start to retard immediately after the application of an overload with no acceleration following it. On the other hand, the application of an overload within a baseline CAL with a negative stress ratio would result in a significant initial acceleration, followed by small amount of retardation. The magnitude of the retardation occurring within baseline CALs with negative stress ratios is much lower than those with positive stress ratios.

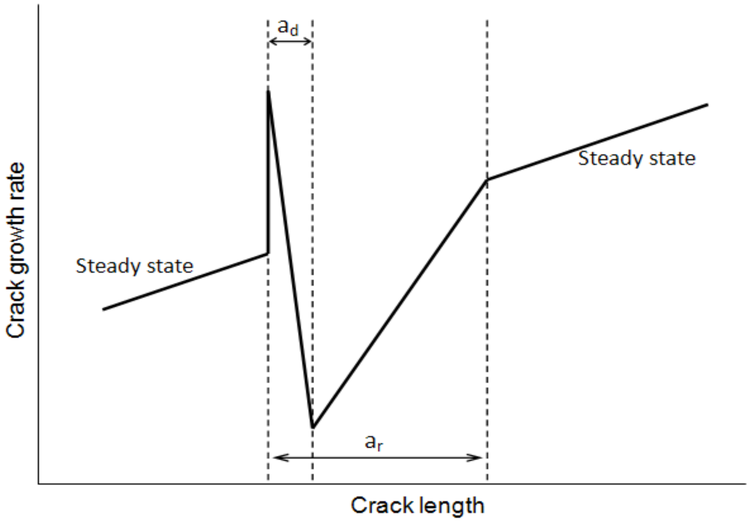

Figure 7.8 Schematic of the resulting retardation in crack propagation due to an applied overload

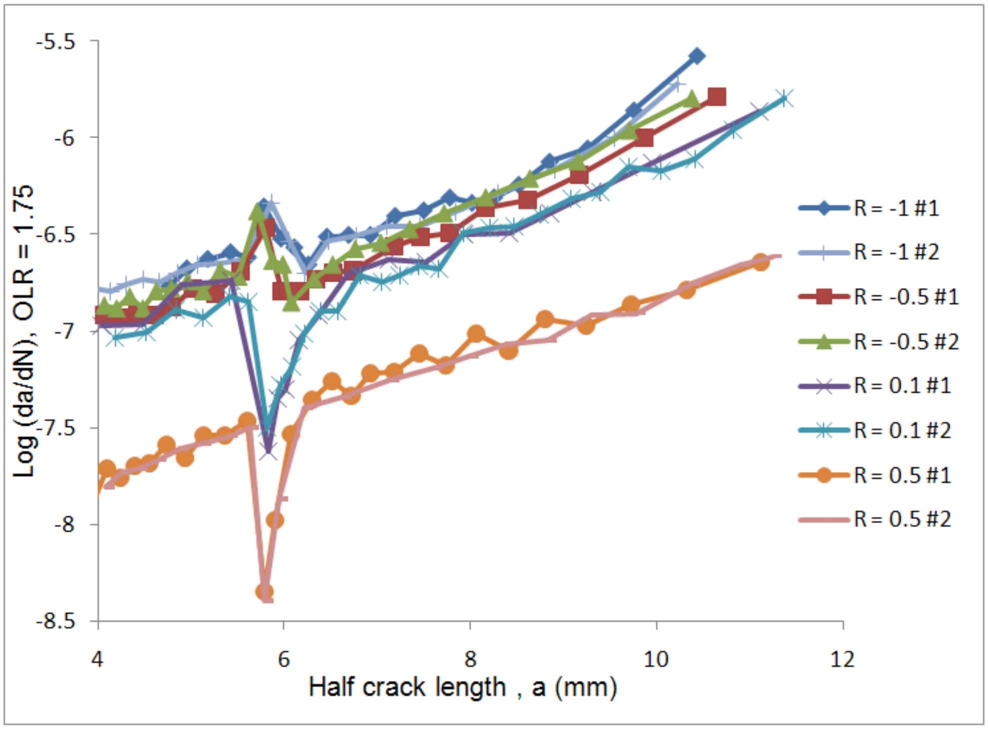

Figure 7.9 Retardation in crack propagation (OLR = 1.75) for various baseline's stress ratios

As can be seen in Figure 7.9, the acceleration portion does not assume an infinite slope as was illustrated schematically in Figure 7.8. This observation indicates that the acceleration in crack propagation would continue for finite increment in crack length, which should not be neglected in cases where the stress ratios of the baselines CAL are negative. Therefore, three different characteristic crack lengths should be defined in the case of CALs with negative stress ratios, namely: a_{acc}, a_d and a_r; those parameters will be described in the following section.

The affected zone dimension evaluated for various CAL baselines and overload ratios are presented in Table 7.2. The results presented in Table 7.2 reveal that the affected zone dimensions obtained for the negative stress ratios and the positive stress ratio of R = 0.1 are consistent and the minimal variation observed in their values could be attributed to the experimental related anomalies. On the other hand, the affected zone for the stress ratio of R = 0.5 is relatively significantly smaller. It indicates that the compressive stress cycles do not affect the affected zone dimension; however, it could not be concluded that their influence on the whole retardation process is nullified.

Table 7.2 Affected zone dimension for various baseline loadings and overload ratios

OLR	R	Affected Zone Dimension (mm)
1.5	-1	0.68375
	-0.5	0.61875
	0.1	0.63375
	0.5	0.51
1.75	-1	0.87
	-0.5	0.9075
	0.1	0.95
	0.5	0.64
2	-1	1.72
	-0.5	1.78375
	0.1	1.775
	0.5	1.31875

Silva [30] assumed that the crack propagation rate is governed by cyclic plastic zone instead of a monotonic plastic zone under negative stress ratios. The cyclic plastic zone radius was defined by Rice [31] with the following equation.

$$r_{p,c} = \alpha \left(\frac{\Delta K}{2\sigma_y} \right)^2 \tag{7.6}$$

where $r_{p,c}$, α and ΔK are the cyclic plastic zone radius, plastic zone coefficient and stress intensity range. Comparison of equations 7.4 and 7.6 indicates that the monotonic plastic zone radius is a function of the maximum stress intensity factor, hence, not affected by the stress ratio. On the other hand, the cyclic plastic zone radius would vary with varying the stress ratio and would be always smaller than the monotonic plastic zone radius.

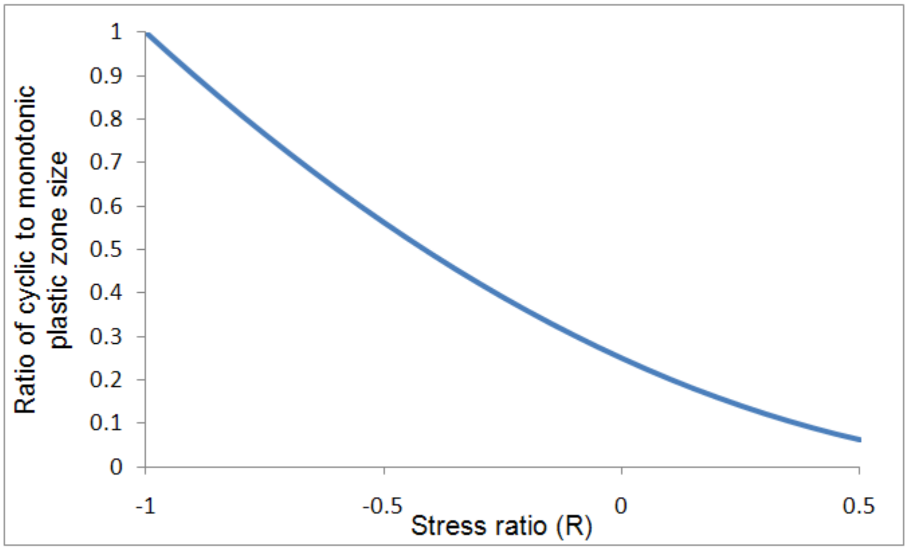

Figure 7.10 Ratio of cyclic to monotonic plastic zone size with respect to stress ratio

The variation in the ratio of cyclic to monotonic plastic zone radii is shown in Figure 7.10. As can be seen, the ratio would reach unity for a completely reverse cyclic loading (i.e., R = -1). The affected zone dimensions for various stress ratios tabulated in Table 7.2 are also consistent in value for R = -1 to R = 0, while the cyclic plastic zone radii vary significantly over this range of stress ratios. Therefore, the use of the evaluated monotonic plastic zone radius and incorporation of the sensitivity parameter in the Wheeler equation are highly recommended.

7.7 Retardation model for baseline CALs with positive stress ratios

Due to the shortfall of Wheeler's model in predicting the affected zone size, the model was modified in previous work by the authors [21] and a sensitivity parameter was added to the equation. The model was modified to the format shown in equation 7.3. Wheeler originally reduced the crack propagation rate in the affected zone by adding a reduction factor Φ_R; this factor was also modified to Φ'_R in consideration of the sensitivity of alloys to overload. As can be seen, another parameter, Φ_D, was also incorporated (see equation 3) in consideration of the delay in retardation. The delay parameter, Φ_D, governs the crack propagation from crack length at which the overload is applied, (i.e., a_{OL}), to the crack length at which the propagation rate reaches its minimum value, (i.e., $a_{OL} + a_d$). The delay parameter, Φ_D, is a decreasing parameter, reported in the following equation.

$$\begin{cases} Log\left(\Phi_D\right) = \left(\dfrac{a_i - a_{OL}}{a_d}\right) Log\left(\Phi'_{R,\min}\right) & a_i + r_{d,i} \langle\, a_{OL} + r_{d,OL} \\ \Phi_D = 1 & a_i + r_{d,i} \,\rangle\, a_{OL} + r_{d,OL} \end{cases} \tag{7.7}$$

In the above equation, $\Phi'_{R,\min}$ is the reduction factor at crack length of a = $a_{OL} + a_d$. Equation 7.7 is based on the assumption that each loading cycle would produce a delay zone with radius of $r_{d,i}$. When the boundary of this (the current) delay zone reaches the boundary of the delay zone produced by the overload, $r_{d,OL}$, thus the propagation rate would attain its minimum level.

The sensitivity parameter evaluated for the baseline CAL with the stress ratio of R = 0.1 is 0.58, which is less than unity, thereby indicating lower sensitivity of this alloy to overloads. Similar analysis was carried out on the experimental data obtained for the baseline CAL with the stress ratio of R = 0.5, leading to the sensitivity parameter of 0.39, a consistent value for all tested overload ratios. The consistency in values of the sensitivity parameter indicates that β is independent of the overload ratio. Moreover, it reveals that the sensitivity parameter would vary with respect to the stress ratios in the positive range. Higher positive stress ratios would produce smaller affected zone and would exhibit lower sensitivity to overloads.

Table 7.3 Modified Wheeler's model parameters

OLR	R	$\Phi'_{R,\min}$	m
1.5	0.1	0.596774	0.524
	0.5	0.339749	0.447
1.75	0.1	0.179108	0.948
	0.5	0.114242	0.78
2	0.1	0.112134	1.044
	0.5	0.053003	0.883

The evaluated reduction factor ($\Phi'_{R,\min}$) and shaping exponent (m) for various stress and overload ratios are presented in Table 7.3. As seen, at each overload ratio, the higher stress ratio (i.e., R = 0.5) produces lower reduction factor, but also along with a smaller crack length increment.

7.8 Retardation model for negative stress ratio baseline loading

As shown in Figure 7.9, negative stress ratios significantly affect the trend in retardation response of the alloy. Application of an overload within baseline CALs with negative stress ratios would produce substantive initial acceleration in crack propagation, while in the cases of baseline CALs with positive stress ratios, no initial acceleration would be expected. Moreover, the retardation in crack propagation is significantly greater when the stress ratio of the baseline loading is positive. Therefore, the retardation model should be capable of predicting the three stages of crack propagation in the affected zone; that is: (i)The initial acceleration (i.e., the portion from a_{OL} to a_{acc}, where a_{acc} is the crack length at which the maximum acceleration occurs), (ii) when the crack propagation rate decreases to its minimum value (i.e., from a_{acc} to a_d, where a_d is the crack length at which the minimum crack propagation rate occurs); and (iii) when the crack attains its steady state propagation rate (i.e., from a_d to a_r, where a_r is the crack length at which the crack propagation returns back to the steady state). Therefore, three modification factors would need to be developed and included in the Wheeler model; that is:

$$\frac{da}{dN} = \Phi_{acc}\Phi_D\Phi'_R\left(\frac{da}{dN}\right)_{CAL} \qquad (7.8)$$

In the above equation, Φ_{acc}, Φ_D and Φ'_R are the modification factors that govern the initial acceleration, the deceleration in the delay zone and the final increase in the crack propagation stage, respectively. The crack propagation rates are linear at each stage (in the logarithmic scale). One can therefore define a shaping exponent for each stage, using the least square method. As a result, the maximum value of Φ_{acc} and minimum value of Φ_D, as tabulated in Table 7.4, for various overload ratios are recommended for obtaining relatively conservative results.

Table 7.4 Model parameters for negative stress ratio baseline loading

R	OLR	$\Phi_{acc,\max}$	$\Phi'_{R,\min}$
-1	1.5	1.515021	0.708059
	1.75	1.78195	0.742205
	2	1.802264	0.53498
-0.5	1.5	1.457573	0.947746
	1.75	1.751805	0.635435
	2	2.414601	0.539509

The results noted in Table 7.4 reveal that the application of larger overloads would result in lower retardation in crack propagation while for positive stress ratios, higher overloads produce higher retardation. Moreover, higher overloads also produce higher initial acceleration in crack propagation.

7.8.1 Proposed modified Wheeler model's parameters

As stated, Wheeler's original model is not capable of predicting the initial acceleration in crack propagation. As can be seen in Figure 7.9, the initial acceleration is not observed in baseline CAL with a positive stress ratio, while the acceleration for baseline CAL with a negative stress ratio is significant. The acceleration parameter, Φ_{acc}, is found to be an increasing parameter, starting from unity and linearly increasing to $\Phi_{acc,\max}$, as represented by equation 7.9.

$$\begin{cases} Log\left(\Phi_{acc}\right)=\left(\dfrac{a_i-a_{OL}}{a_{acc}-a_{OL}}\right)Log\left(\Phi_{acc,\max}\right) & a_{OL}\langle\, a\,\langle a_{acc} \\ \Phi_{acc}=1 & a\,\langle\, a_{OL}\;\; or\;\; a\,\rangle\, a_{acc} \end{cases} \tag{7.9}$$

The delay parameter is a decreasing parameter, starting from $\Phi_{acc,\max}$ at a$_{acc}$, reaching to $\Phi'_{R,\min}$ at a$_{d}$, as formulated in the following equation.

$$\begin{cases} Log\left(\Phi_D\right) = Log\left(\Phi_{acc,\max}\right) - \left(\dfrac{a_i - a_{acc}}{a_d - a_{acc}}\right)\left[Log\left(\Phi_{acc,\max}\right) - Log\left(\Phi'_{R,\min}\right)\right] & a_{acc} \langle\, a \,\langle a_d \\ \Phi_d = 1 & a \,\langle\, a_{acc} \;\; or \;\; a \,\rangle\, a_d \end{cases} \tag{7.10}$$

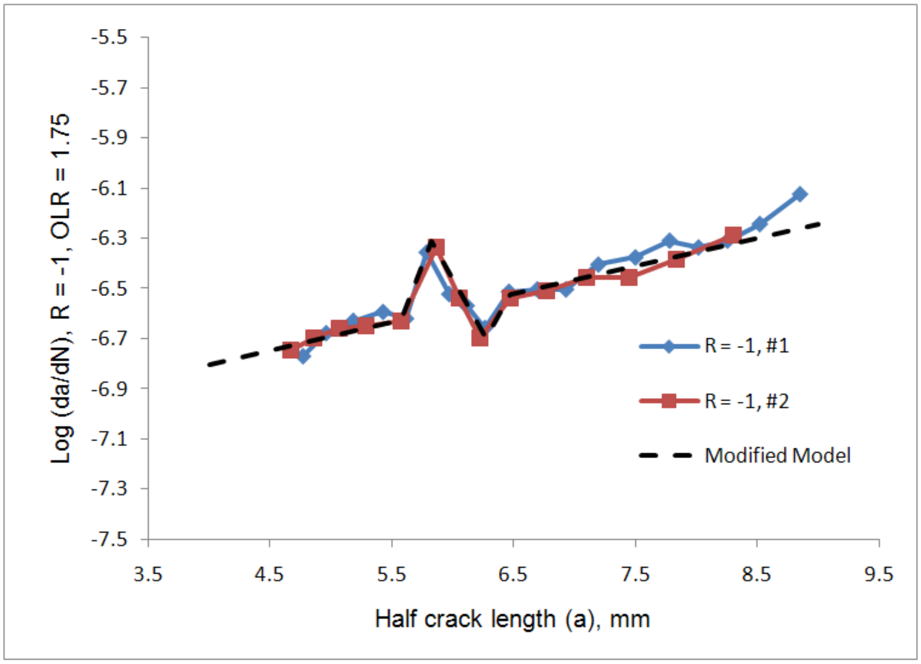

Figure 7.11 Prediction of retardation process in crack propagation (R = -1 and OLR = 1.75)

The same parameter (Φ'_R), as shown in equation 7.3, can be used to define the crack propagation in the last region of retardation process. Since the affected zone dimensions created under negative stress ratios are similar to that created under the stress ratio of R = 0.1, the same sensitivity parameter could be used in evaluating the reduction factor. Using the parameters evaluated in Table 7.4 and the equations proposed for negative stress ratios, the retardation process is predicted and depicted in Figure 7.11.

7.9 Influence of loading sequence on retardation in crack propagation

Opposite to the retardation influence of a tensile overload described earlier, the application of a compressive underload (UL) within an otherwise constant amplitude loading is known to accelerate the crack propagation. The retardation in crack propagation could also be influenced by the sequence of the overload and underload. As a part of this experimental investigation, one compressive underload is applied after the application of an overload with the ratio of OLR = 1.75, applied within a constant amplitude loading with the stress ratio of R = 0.1. Two underload ratios (ULR = -1 and -1.75) were considered in this investigation. The results are compared with similar loading scenarios, but without the application of a compressive underload, as presented in Figure 7.12. Comparing the results illustrated in Figure 7.12 with those in Figure 7.9 reveals that the application of the compressive UL did not change the affected zone dimension.

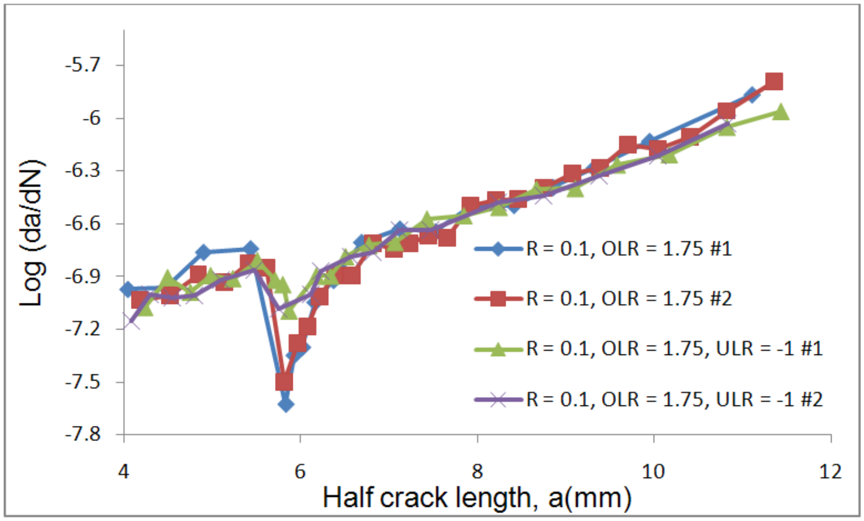

(a)

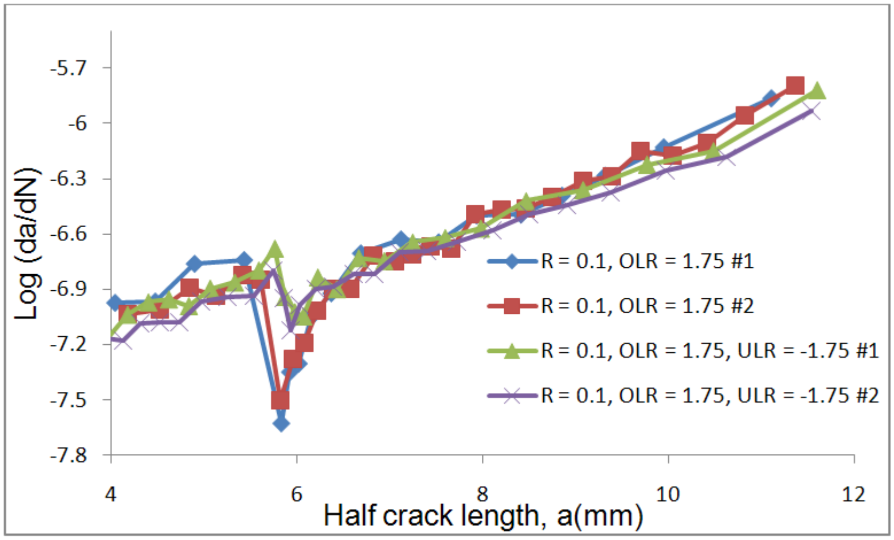

(b)

Figure 7.12 Retardation in crack propagation when the overload is followed by a compressive underload when the ratio of the underload is (a) -1 and (b) -1.75

The initial acceleration in crack propagation was attributed to the applied compressive cycles, however, the application of just one compressive underload did not produce noticeable initial acceleration. The results show a slight acceleration in crack propagation when the higher underload (ULR = -1.75) was applied. The level of retardation in crack propagation was significantly reduced due to application of the compressive underload. Reduction in retardation due to application of one underload (compressive cycle) has been reported by other researchers as well. For instance, Rushton and Taheri [32] suggested the adaptation of the radius of the plastic zone due to cyclic loading instead of the one produced as a result of a monotonic loading to accurately account for the influence of compressive cycle. Considering the fact that the affected zones are consistent in dimension for negative and zero stress ratios, and that the compressive cycles do not produce any influence on them, as a result the incorporation of the monotonic plastic radius is preferred. The reduction of retardation in crack propagation due to loading sequence can be accounted for by increasing the value of the modified reduction factor and reducing the value of the shaping exponent (m) as tabulated in Table 7.5.

Table 7.5 Model parameters when an underload was applied

R	OLR	ULR	$\Phi'_{R,\min}$	m
0.1	1.75	**	0.179108	0.948
		-1	0.531633	0.330642
		-1.75	0.5088	0.325014

7.10 Roughness of fracture surface

Walker [33] suggested the fracture surface roughness as a parameter that controls crack closure and it has also been postulated to govern the crack propagation rate. Walker postulated that in essence, the roughness would wedge the crack faces, hence forcing them to be opened, therefore the minimum stress intensity factor would be increased, thereby producing smaller stress intensity range. As a result, one would expect a slower crack propagation when the roughness amplitude of the fracture surfaces are larger. This concept was used by some researchers (e.g., [34, 25]) to predict more accurate crack propagation rates. Chen and Lawrence [34] concluded that the roughness induced crack closure (RICC) may be used to predict more accurate crack propagation rate when the material is subjected to positive stress ratio loading, but it would not be applicable to crack propagation under negative stress ratio. Silva [25] also reported that neither crack closure nor RICC are relevant to crack propagation rate at negative stress ratios. The same observations in crack propagation response for aluminum alloy have also been reported by Iranpour and Taheri [35].

The profile of the fracture surfaces of the specimens tested under the various stress ratios were scanned using a profilometer. The arithmetic mean of the roughness (R_a) was measured along seven lines running along the fracture surface's length (see Figure 7.13) and their average values are reported as the roughness value of the surface. The roughness parameter (R_a) was evaluated according to DIN 4768, using the following equation:

$$R_a = \frac{1}{L\int_0^L |z|\,dx} \tag{7.11}$$

where L is the length of the reference line and z is the height of the asperities. A 3D profile of the fracture surface and the lines along which R_a were calculated are shown in Figure 7.13.

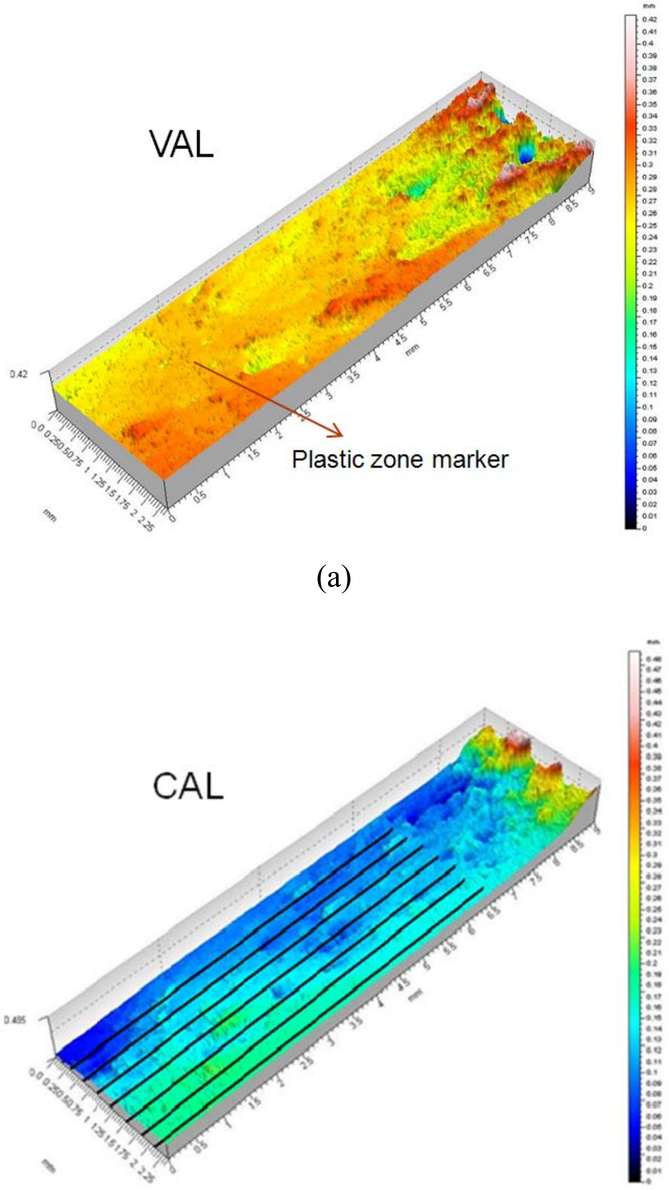

(a)

(b)

Figure 7.13 3D profile of the fracture surface of specimens subjected to (a) variable amplitude loading (b) constant amplitude loading

As can be seen in Figure 7.13(a), the application of an overload produces a marking line on the fracture surface, which indicates the extent of the plastic zone. Moreover, some metallurgical defects could be detected within the 3D profile that could affect the values of the evaluated roughness. In other words, all the observed asperities may not be due to the applied cyclic loading.

The analysis of the surface roughness of the specimens reveals that the application of a single overload does not produce any considerable change in the magnitude of the surface roughness. In addition, considering the fact that the surface roughness is comprised of scattered data also due to metallurgical defects, nevertheless, it appears that it has an increasing trend when the stress ratios are decreased. The magnitudes of R_a for various stress ratios are reported in Table 7.6.

Table 7.6 Surface roughness under various stress ratios

R (Stress Ratio)	R_a (Roughness, μm)
0.5	3.39
0.1	4.38
-0.5	5.365
-1	6.5

As widely known, a crack would propagate faster under a CAL that is applied with a relatively lower stress ratio; thus, based on Walker's assumption, a lower (smoother) surface roughness profile should be expected. In contrast, in these experiments, higher roughnesses (R_a) were observed for the lower stress ratios. It could therefore be concluded that surface roughness might be a consequence of cyclic loading as opposed to be purely a cause for altering the crack propagation rate.

7.11 Summary and conclusion

In this section a summary of the work presented in this paper is offered, as well as the key observations and conclusions.

- The stress ratio of baseline constant amplitude loading was observed to have a significant influence on retardation in crack propagation when an overload was applied within an otherwise constant amplitude loading. The crack propagation retardation's trend under a baseline CAL with a negative stress ratio was also markedly different from that when the stress ratio of baseline CAL was positive. Wheeler model was used in this work to describe the retardation response of the alloy. This model is characterized by the affected zone size and the magnitude of retardation.

- As for positive stress ratios, the increase in the stress ratio could result in a smaller affected zone, and produce larger retardation magnitudes. Considering the fact that for some materials the affected zone is either larger or smaller than the Wheeler model's prediction, a new parameter, referred to as the "sensitivity parameter", (β), was introduced and implemented to the Wheeler model. The value of this parameter was evaluated to be 0.58 and 0.39 for the baseline stress ratio of 0.1 and 0.5, respectively.

- Cyclic loads with negative stress ratios (i.e., those with compressive stress cycles), were observed to promote crack propagation rate and reduce the fatigue life. Moreover, such loading scenarios would also change the trend of retardation in crack propagation in the Mg alloy tested. The result of an applied overload within baseline loadings with a negative stress ratio could be characterized into three stages: (i) initial acceleration, (ii) deceleration of the crack propagation rate to its minimum, and (iii) the return of the propagation rate to its steady state. In comparison to the baseline loading with positive stress ratios, the magnitude of the retardation would be significantly reduced. The affected zone size for baseline CAL with negative and zero stress ratios were found to be similar, thus indicating that the magnitude of the compressive cycles do not have influence on the affected zone's dimension; as a result, the same sensitivity parameter (β) could be used for calculating the retardation in crack propagation rate with the proposed modified Wheeler model.

- In addition to those effects, the application of a larger overload within a baseline CAL with negative stress ratio was observed to increase the magnitude of crack propagation acceleration and decrease the magnitude of the subsequent retardation, which is completely reverse of what was observed when the material underwent baseline CAL with positive stress ratio. On the other hand, the application of relatively higher overloads may result in acceleration in crack propagation instead of deceleration.

- When the applied overload was followed by a compressive underload, then the magnitude of retardation was observed to be reduced significantly, without imposing any change on the affected zone dimension.

- The radius of the cyclic plastic zone decreases when the stress ratio increases. Since the dimension of the affected zone was observed to be similar for baseline CAL with negative and zero stress ratios, the incorporation of the cyclic plastic zone radius into the Wheeler retardation model would not improve the accuracy of the results.

- Finally it was observed that the roughness induced crack closure (as hypothesized by Walker) would not have the same effect on crack propagation rate in CALs with positive or negative stress ratios. This parameter seems to be affected by the applied cyclic loading, and do not govern the acceleration or retardation of crack propagation. Moreover, the application of an overload did not produce a significant influence on the roughness of fracture surface.

7.12 Acknowledgement

This project was financially supported by AUTO21 and the specimens were kindly provided by Meridian Technologies Inc. All their supports and cooperation are appreciated.

7.13 References

[1] Lu, Y., Taheri, F. & Gharghouri, M., “Monotonic and Cyclic Plasticity Response of Magnesium Alloy. Part I. Experimental Response of a High-Pressure Die Cast AM60B”, Strain (International Journal for Experimental Mechanics), 47, pp.e15- e24, 2008.

[2] Lu, Y., Taheri, F. & Gharghouri, M., “Monotonic and Cyclic Plasticity Response of Magnesium Alloy. Part II. Computational Simulation and Implementation of a Hardening Model”, Strain (International Journal for Experimental Mechanics), 47, pp.e25- e33, 2008.

[3] Lu, Y., Taheri, F. & Gharghouri, M., “Study of Fatigue Crack Incubation and Propagation Mechanisms in a HPDC AM60B Magnesium Alloy”, Journal of Alloys and Compounds, 466, pp.214- 227, 2008.

[4] Lu, Y., Gharghouri, M., Taheri, F. & Han, H., “Numerical Study of the Casting Features on the Fracture and Debonding of Mg17Al12 in AM60B Mg Alloy Under High Cycle Fatigue Condition”, Materials and Design, 30, pp.1994- 2005, 2009.

[5] Lu, Y., Taheri, F., Gharghouri, M. & Han, H.P., “Experimental and Numerical Study of the Effects of Porosity on Fatigue Crack Initiation of HPDC Magnesium AM60B Alloy”, Journal of Alloys and Compounds, 470, pp.202- 213, 2009.

[6] Nur Hossain, M. & Taheri, F., “Fatigue and Fracture Characterization of HPDC AM6OB Magnesium Alloy at Cold Temperature”, Journal of Materials Engineering and Performance, 20, pp.1684- 1689, 2011.

[7] Nur Hossain, M. & Taheri, F., “Influence of Elevated Temperature and Stress Ratio on the Fatigue Response of AM60B Magnesium Alloy”, Journal of Materials Engineering and Performance, 21, pp.1395- 1404, 2011.

[8] ASTM E647-08, "Standard Test Method for Measurement of Fatigue Crack Growth Rates”, ASTM International, PA, USA, 2009.

[9] API 2RD, “Design of Risers for Floating Production Systems (FPSs) and Tension Leg Platforms (TLPs)”, American Petroleum Institute, Washington D.C., USA, 1998.

[10] Kujawski, D., “A Fatigue Crack Driving Force Parameter with Load Ratio Effects”, International Journal of Fatigue, 23, pp.S239- S246, 2001.

[11] Kujawski, D., “A New $(\Delta K^{+} Kmax)^{0.5}$ Driving Force Parameter for Crack Growth in Aluminum”, International Journal of Fatigue, 23, pp.733- 740, 2001.

[12] Fleck, N.A., Shin, C.S. & Smith, R.A., “Fatigue Crack Growth Under Compressive Loading”, Engineering Fracture Mechanics, 21, pp.173- 185, 1985.

[13] Suresh, S., “Crack Initiation in Cyclic Compression and Its Application”, Engineering Fracture Mechanics, 21, pp.453- 463. 1985.

[14] Kasaba, K., Takashiro, S., Souichi, K., Tetsuo, S., Kazumune, K., Tadashi, S., “Fatigue Crack Growth Under Compressive Loading”, Journal of Nuclear Materials, 258, pp.2059-2063, 1998.

[15] Zhang, J., He, X.D. & Du, S.Y., “Analysis of the Effects of Compressive Stresses on Fatigue Crack Propagation Rate”, International Journal of Fatigue, 29, pp.1751- 1756, 2007.

[16] Zhang, J., He, X.D., Suo, B. & Du, S.Y., “Elastic- Plastic Finite Element Analysis of the Effect of Compressive Loading on Crack Tip Parameters and Its Impact on Fatigue Crack Propagation Rate”, Engineering Fracture Mechanics, 75, pp.5217- 5228, 2008.

[17] Zhang, J., He, X.D., Sha, Y. & Du, S.Y., “The Compressive Stress Effect on Fatigue Crack Growth under Tension-Compression Loading”, International Journal of Fatigue, 32, pp.361- 367, 2010.

[18] Huang, X. & Moan, T., “Improved Modeling of the Effect of R-ratio on Crack Growth Rte”, International Journal of Fatigue, 29, pp.591- 602, 2007.

[19] Paris, P. & Erdogan, F., “A Critical Analysis of Crack Propagation Laws”, Journal of Basic Engineering, 85, pp.528- 534, 1963.

[20] Walker, K., “The Effect of Stress Ratio during Crack Propagation and Fatigue for 2024-T3 and 7075-T69 Aluminum”, ASTM STP 462, pp.1-14, 1970.

[21] Mehrzadi, M. & Taheri, F., “A Modified Wheeler Model Based on the Material Sensitivity to the Overload for Predicting the Retardation in AM60B Magnesium alloy”, Submitted to International Journal of Fatigue, 2012.

[22] Silva, F.S., “The Importance of Compressive Stresses on Fatigue Crack Propagation Rate”. International Journal of Fatigue, 27, pp.1441- 1452, 2005.

[23] Wheeler, O.E., “Spectrum Loading and Crack Growth”, Journal of Basic Engineering, 94, pp.181-86, 1972.

[24] Elber, W., “The Significance of Fatigue Crack Closure. Damage Tolerance in Aircraft Structures”, ASTM STP 486, American Society for Testing and Materials, pp.230-42, 1971.

[25] Silva, F.S., “Crack Closure Inadequacy at Negative Stress Ratios”, International Journal of Fatigue, 26, pp.241- 252, 2004.

[26] Mehrzadi, M. & Taheri, F., “The Influence of Negative and Positive Stress Ratios on Crack Growth Rate in AM60B Magnesium Alloy”, Materials Science and Engineering A, 545, pp.68- 77, 2012.

[27] Irwin, G., “Linear Fracture Mechanics, Fracture Transition, and Fracture Control”, Engineering Fracture Mechanics, 1, pp.241-57, 1968.

[28] Guo, W., “Three Dimensional Analysis of Plastic Constraint for Through-Thickness Cracked Bodies”, Engineering Fracture Mechanics, 1, pp.383-407, 1999.

[29] Voorwald, H. & Torres, M., “Modeling of Fatigue Crack Growth Following Overloads”, International Journal of Fatigue, 13, pp.423-27, 1991.

[30] Silva, F.S., “Fatigue Crack Propagation After Overloading and Underloading at Negative Stress Ratios”, International Journal of Fatigue, 29, pp.1757- 1771, 2007.

[31] Rice, J.R., “Mechanics of Crack Tip Deformation and Extension by Fatigue”, ASTM STP 415, pp.247- 311, 1967.

[32] Rushton, P.A. & Taheri, F., “Prediction of Crack Growth in 350WT Steel Subjected to Constant Amplitude with Over- and Under- Loads Using a Modified Wheeler Approach”, Journal of Marine Structures, 16, pp.517-39, 2003.

[33] Walker, N. & Beevers, C.J., “A Fatigue Crack Closure Mechanism in Titanium”, Fatigue of Engineering Materials and Structures, 1, pp.135- 148, 1979.

[34] Chen, N. & Lawrence, F.V., “A Comparison of Two Total Fatigue Life Prediction Methods”, ASTM STP 1343, pp.351- 366, 1999.

[35] Iranpour, M. & Taheri, F., “On the Effect of Stress Intensity Factor in Evaluating the Fatigue Crack Growth Rate of Aluminum Alloy Under the Influence of Compressive Stress Cycles”, International Journal of Fatigue, 43, pp.1- 11, 2012.

CHAPTER 8 Summary and conclusion

8.1 Summary

Fatigue response of AM60B magnesium alloy has been investigated in the present dissertation. The investigation was initiated by monitoring the progressive damage in alloy specimens with various levels of porosity due to applied cyclic loading. The variation of the alloy's natural frequency and damping capacity on the specimens configured for fatigue testing (per ASTM E-466), were evaluated and reported.

The crack propagation of the alloy under constant amplitude loading with various stress ratios was also studied. A modified model has been proposed for predicting the crack propagation under a wide range of stress ratios. It has been shown that the presence of compressive stress cycles within a cyclic loading would accelerate the crack propagation and shorten the fatigue life. Moreover, the influence of a spiked compressive loading cycle (underload) was also presented in this thesis.

As it is commonly known, the application of a tensile overload in an otherwise constant amplitude loading scenario would retard the crack propagation. Retardation in crack propagation would be characterized by the affected zone and magnitude of retardation. The affected zone is a function of the overload plastic zone radius. The radius is also governed by the nature of the applied loading and the stress intensity factor. Therefore, using the finite element analysis, a coefficient, referred to as the "plastic zone coefficient", was evaluated for various stress intensity factors for the AM60B magnesium alloy as well as other materials. It was shown that the affected zone was different from what was assumed by other widely used FCGR models (e.g. Wheeler's model) and would vary from one material to another. In addition, the influence of baseline loading stress ratio on retardation in crack propagation due to overload was studied and reported.

8.2 Conclusions

The results of this investigation as well as the conclusions could be summarized as follows:

- Degradation in material properties due to application of a cyclic loading could be monitored by evaluating the natural frequency and damping capacity. A 5% degradation in natural frequency and 60% to 100% increase in damping capacity have been observed at the end of the fatigue life of the specimens.

- The experimental values of the natural frequency and damping capacity were found to be highly scattered. Variation of the results at the same stage of fatigue life is attributed to the casting induced defects and the nature of the methods used for evaluating the dynamic properties of the specimens. The density of casting defects was found to seemingly have an inverse relation with the thickness of the specimens, such that the variance of the results is significantly decreased when thinner plates were considered.

- As anticipated, the stress ratio of applied cyclic loading has a significant influence on crack propagation rate. Negative stress ratios would result in a shorter fatigue life and would accelerate the crack propagation in contrast to that under positive ratios.

- The compressive portion of a cyclic loading should not be dismissed or partially considered as suggested by standards, since it was observed that compressive loading cycles would have a significant influence on FCGR.

- Contrary to the assumption made by Walker and many other researchers, it was demonstrated that the slope of FCGR versus the stress intensity factor range curves plotted on a logarithmic scale would not be parallel to one another when fatigue tests are conducted under different stress ratios. In fact, the slope would actually decrease as a function of increasing stress ratio.

- As per the above observation, modification to the Walker model has been proposed, such that the model would be admissible for predicting FCGR for specimens subjected to a wide range of stress ratios (negative or positive). Moreover, the integrity of the proposed model was verified by the experimental results in this study as well as those reported for other alloys. The modified model effectively condenses the experimental FCGR results obtained for various stress ratios onto a single line on a logarithmic scale. Consequently, FCGR could be predicted using a single equation for all stress ratios.

- Application of compressive loading cycles in both constant and random amplitude cyclic loadings would accelerate the crack propagation rate in a similar manner. It has been shown that even the application of compressive spikes applied within constant amplitude loading scenarios would shorten the fatigue life. This is attributed to the increased size of the residual plastic zone.

- A new parameter referred here as “the effective force” has been defined, thereby indicating the potential of acceleration in crack propagation due to the presence of compressive loading cycles within a cyclic loading.

- It has been shown that the retardation affected zone due to the application of a tensile loading spike (i.e. overload) would depend on the nature of the material, as well as the overload and baseline loading. A parameter (β) was therefore defined to account for the sensitivity of the material to the application of an overload. Moreover, the Wheeler model was modified to include this parameter, accordingly.

- The sensitivity parameter of the AM60B magnesium alloy was evaluated to be less than unity, indicating that the sensitivity of the alloy to overload is lower than other materials.

- The influence of a tensile overload applied within a random amplitude loading scenario was also investigated using the “clipping level” approach. It has been demonstrated that the clipping level would produce different outcomes on crack propagation rates on different materials due to material’s sensitivity to overload.

- The affected zone, magnitude of retardation and even the retardation trend would be affected by the nature of the baseline loading. Increase of the stress ratio in a positive sense, would result in lower sensitivity to overload.

- Application of a tensile overload within a baseline loading with a negative stress ratio was observed to produce noticeable initial acceleration, while that response could not be observed when the stress ratio of baseline loading was positive.

- Application of an overload within a baseline loading with a positive stress ratio would produce a higher magnitude of retardation in comparison to a baseline loading with a negative stress ratio.

- When the overload is followed by a compressive underload the magnitude of the resulting retardation would decrease, however the affected zone dimension would remain unchanged.

- The roughness of the fracture surface was observed to develop as a result of the nature of the applied cyclic loading, and not a governing parameter that could influence the crack propagation rate.

8.3 Recommendation for future work

The following suggestions are recommended for further investigations in order to gain a better understanding of the fatigue response of this alloy and its response in comparison to other metallic alloys.

- Materials with various cyclic responses could be tested under constant and random amplitude loading to investigate the influence of the material nature on crack propagation rate.

- All of these experimental investigations were conducted at room temperature, while materials usually present different responses in various environmental conditions (e.g. temperature). It is strongly recommended to investigate the influence of the parameters noted above on the fatigue response of the alloy within various environmental conditions.

- It has been shown that the stress ratio of baseline loading could significantly affect the proposed "sensitivity parameter". It would be worthwhile to study the influence of other parameters that may affect the sensitivity parameter.

BIBLIOGRAPHY

Anderson, T. L., “Fracture Mechanics, Fundamentals and Applications”, Third Edition, CRC Press, Taylor & Francis Group, Boca Raton, FL 33487-2742, 2005.

API 2RD, “Design of Risers for Floating Production Systems (FPSs) and Tension Leg Platforms (TLPs)”, American Petroleum Institute, Washington D.C., USA, 1998.

ASTM E1245, “Standard Practice for Determining the Inclusion or Second-Phase Constituent Content of Metals by Automatic Image Analysis”, (reapproved 2008), ASTM International, PA, USA.

ASTM E466-07, “Standard Practice for Conducting Force Controlled Constant Amplitude Axial Fatigue Tests of Metallic Materials”.

ASTM E647-08, "Standard Test Method for Measurement of Fatigue Crack Growth Rates”, ASTM International, PA, USA, 2009.

Bacila, A., Decoopman, X., Mesmacque, G., Voda, M. and Serban, V. A., “Study of underload effects on the delay induced by an overload in fatigue crack propagation”, International Journal of Fatigue, Vol. 29, pp. 1781-1787, 2007.

Bannantine, J. A., Commer, J. J., Handrock, J. L., “Fundamental of Metal Fatigue Analysis”, Prentice Hall, Englewood Cliffs, New Jersey, 07632, 1989.

Barsom, J. M. & Rolfe, S. T., “Fracture and Fatigue Control in Structures, Application of Fracture Mechanics”, Third Edition, ASTM, 100 Bar Harbor Drive, West Conshohocken, PA, 1999.

Barsom, J. M., “Fatigue Crack Growth under Variable Amplitude Loading in Various Bridge Steels”, In Fatigue Crack Growth under Spectrum Loads, ASTM STP 595, American Society for Testing and Materials, Philadelphia, PA, pp.217-235, 1976.

Borresgo, L.P., Ferreira, J.M., Pinho da Cruz, J.M. & Costa, J.M., “Evaluation of Overload Effects on Fatigue Crack Growth and Closure”, *Engineeing Fracture Mechanic*, 70, pp.1379- 1397, 2003.

Broek, D., “The Practical Use of Fracture Mechanics”, FractuREsarch Inc., Galena, OH, USA, Kluwer Academic Publisher, P. O. Box 17, 3300 AA Dordrecht, The Netherland, 1988.

Chen, N. & Lawrence, F.V., “A Comparison of Two Total Fatigue Life Prediction Methods”, ASTM STP 1343, pp.351- 366, 1999.

Costa, J. D. M. and Ferreira, J. A. M., “Effect of Stress Ratio and Specimen Thickness on Fatigue Crack Growth of CK45 Steel”, Theoretical and Applied Fracture Mechanics, 1998, 30, pp. 65-73.

Dimitriu, R.C., Bhadeshia, H. K. D. H., “Fatigue crack growth rate model for metallic alloys”, Materials and Design, 2010, 31, pp. 2134–2139.

Dinda, S. and Kujawski, D., “Correlation and Prediction of Fatigue Crack Growth for Different R Ratios Using K_{max} and ΔK^+ Parameters”, Engineering Fracture Mechanics, 2004, 71, pp. 1779-1790.

Ding, J., Hall, R., Byrne, J., “Effects of stress ratio and temperature on fatigue growth in a Ti–6Al–4V alloy”, International Journal of Fatigue, 2005; 27, pp. 1551–1558.

Dowling, N. E. and Begley, J. A., "Fatigue Crack Growth during Gross Plasticity and the J-Integral", Mechanics of Crack Growth, ASTM STP 590, American Society for Testing and Materials, Philadelphia, PA, pp. 82- 105, 1976.

Dowling, N. E., "Mechanical Behavior of Materials, Engineering Methods for Deformation, Fracture and Fatigue", Second Edition, PRENTICE HALL, Upper Saddle River, New Jersey 07458, 1999.

Elber W., "Fatigue Crack Closure under Cyclic Tension", Engineering Fracture Mechanics, 2, pp. 37- 45, 1970.

Elber, W., "The Significance of Fatigue Crack Closure. Damage Tolerance in Aircraft Structures", ASTM STP 486, American Society for Testing and Materials, pp.230-42, 1971.

Fleck, N. A., Shin, C. S. and Smith, R. A., "Fatigue Crack Growth under Compressive Loading", Engineering Fracture Mechanics, Vol. 21, No. 1, pp. 173-185, 1985.

Forman, R. G., "Study of Fatigue Crack Initiation from Flaws Using Fracture Mechanics Theory", Engineering Fracture Mechanics, 4, pp. 333- 345, 1972.

Frost, N. E., Pook, L. P. and Denton, K., "A Fracture Mechanics Analysis of Fatigue Crack Growth Data for Various Materials", Engineering Fracture Mechanics, 3, pp. 109-126, 1971.

Funchs, H. O. and Stephens, R., "Metal Fatigue in Engineering", John Wiely and Sons, New York, 1980.

Gallagher, J. P., "A Generalized Development of Yield-zone Models", AFFDL-TM-74-28, Air Force Flight Dynamics Laboratory, Wright-Patterson Air Force Base, Ohio, 1974.

Guo, W., “Three Dimensional Analysis of Plastic Constraint for Through-Thickness Cracked Bodies”, Engineering Fracture Mechanics, 1, pp.383-407, 1999.

Hartman, A. and Shijve, J., “The Effect of Environment and Load Frequency on the Crack Propagation Law for Macro Fatigue Crack Growth in Aluminum Alloys”, Engineering Fracture Mechanics, 1, pp. 615- 631, 1970.

Hoffman, O. and Sachs, G.*, “*Introduction to the Theory of Plasticity for Engineers”*, McGraw-Hill,* 1953.

Hsieh, S.-C., Lee, S.- Y., Ciou, C.- Y., Huang, H.- M., “Non-Destructive Natural Frequency Tests of Cyclic Fatigue-Loaded Nickel–Titanium Rotary Instruments”, Med Biol Eng Comput, 48, pp. 555–560, 2010.

Huang, X. & Moan, T., “Improved Modeling of the Effect of R-ratio on Crack Growth Rte”, International Journal of Fatigue, 29, pp.591- 602, 2007.

Hudson, C. M., “A Root-Mean-Square Approach for Predicting Fatigue Crack Growth under Random Loading”, Methods and Models for Predicting Fatigue Crack Growth under Random Loading, ASTM STP 748. J. B. Chang and C .M. Hudson, Eds., American Society for Testing and Materials, pp. 41-52, 1981.

Hutchinson, J. W., “Singular Behavior at the End of a Tensile Crack Tip in a Hardening Material”, Journal of the Mechanics and Physics of Solids, 16, pp. 13- 31, 1968.

Iranpour, M. & Taheri, F., “Influence of the Peak Tensile Overload Cycles and Clipping Level on the Fatigue Crack Growth of Aluminum Alloy under Spectrum Loading”, *Conditionally accepted, Journal of Material Engineering and Performance,* 2012.

Iranpour, M. & Taheri, F., “On the Effect of Stress Intensity Factor in Evaluating the Fatigue Crack Growth Rate of Aluminum Alloy Under the Influence of Compressive Stress Cycles”, International Journal of Fatigue, 43, pp.1- 11, 2012.

Irwin, G., “Linear Fracture Mechanics, Fracture Transition, and Fracture Control”, Engineering Fracture Mechanics, 1, pp.241-57, 1968.

James, M. N. and Wenfong, L., “Fatigue Crack Growth in Austempered Ductile and Grey Cast Irons – Stress Ratio Effects in Air and Mine water”, Material Science Engineering, 1999, 265, pp. 129-139.

Kasaba, K., Sano, T., Kudo, S., Shoji, T., Katagiri, K. and Sato, T., “Fatigue Crack Growth under Compressive Loading”, Journal of Nuclear Materials, pp. 258-263, 1998.

Khan, Z., Rauf, A. & Younas, M., “Prediction of Fatigue Crack Propagation Life in Notched Members under Variable Amplitude Loading”, *Journal of Materials Engineering and Performance*, 6, pp.365-37, 1997.

Kim, J. H. and Lee, S. B., “Behavior of plasticity-induced crack closure and roughness-induced crack closure in aluminum alloy”, International Journal of Fatigue, 2001; 23, pp. 247–251.

Kim, J.-H., Lee, S.-B. & Hong, S.-G., “Fatigue Crack Growth Behavior of Al7050-T7451 Attachment Lugs Under Fight Spectrum Variation”, *Journal of Theoretical and Appied Fracture Mechanics*, 40, pp.135-44, 2003.

Kim, J.K. & Shim, D.S., “A Statistical Approach for Predicting the Crack Retardation Due to Single Tensile Overload”, *International Journal of Fatigue*, 25, pp.335-42, 2003.

Kujawski, D., "A Fatigue Crack Driving Force Parameter with Load Ratio Effects", International Journal of Fatigue, 23, pp.S239- S246, 2001.

Kujawski, D., "A New $(\Delta K^{+} Kmax)^{0.5}$ Driving Force Parameter for Crack Growth in Aluminum", International Journal of Fatigue, 23, pp.733- 740, 2001.

Kumar, R., Kumar, A. & Kumar, S., "Delay Effect in Fatigue Crack Propagation" *Int. J. Pres. Ves. & Piping*, 67, pp.1-5, 1996.

Lal, D. N. and Wiess, V., "A Notch Analysis of Fracture Approach to Fatigue Crack Propagation", Metallurgical Transactions, 9A, pp. 413- 425, 1978.

Lu, Y., Gharghouri, M., Taheri, F. & Han, H., "Numerical Study of the Casting Features on the Fracture and Debonding of Mg17Al12 in AM60B Mg Alloy Under High Cycle Fatigue Condition", Materials and Design, 30, pp.1994- 2005, 2009.

Lu, Y., Taheri, F. & Gharghouri, M., "Monotonic and Cyclic Plasticity Response of Magnesium Alloy. Part I. Experimental Response of a High-Pressure Die Cast AM60B", Strain (International Journal for Experimental Mechanics), 47, pp.e15- e24, 2008.

Lu, Y., Taheri, F. & Gharghouri, M., "Monotonic and Cyclic Plasticity Response of Magnesium Alloy. Part II. Computational Simulation and Implementation of a Hardening Model", Strain (International Journal for Experimental Mechanics), 47, pp.e25- e33, 2008.

Lu, Y., Taheri, F., Gharghouri, M. & Han, H.P., "Experimental and Numerical Study of the Effects of Porosity on Fatigue Crack Initiation of HPDC Magnesium AM60B Alloy", Journal of Alloys and Compounds, 470, pp.202- 213, 2009.

Lu, Y., Taheri, F., Gharghouri, M., “Study of Fatigue Crack Incubation and Propagation Mechanisms in a HPDC AM60B Magnesium Alloy”, Journal of Alloys and Compounds, 2008, 466, pp. 214-227.

Mehrzadi, M. & Taheri, F., “A Modified Wheeler Model Based on the Material Sensitivity to the Overload for Predicting the Retardation in AM60B Magnesium alloy”, Submitted to International Journal of Fatigue, 2012.
Mehrzadi, M. & Taheri, F., “The Influence of Negative and Positive Stress Ratios on Crack Growth Rate in AM60B Magnesium Alloy”, Materials Science and Engineering A, 545, pp.68- 77, 2012.

Mehrzadi, M. and Taheri, F., “Evaluation of Fatigue Damage in HPDC AM60B Magnesium Alloy based on Material’s Dynamic Properties”, Submitted to International Journal of Fatigue, 2011.

Mendelson, A., “Plasticity: Theory and Application”, *Macmillan, New York,* 1968.

Newman, J. C., “A Crack Opening Stress Equation for Fatigue Crack Growth”, International Journal of Fracture, 24, pp. R131- R135, 1984.

Noroozi, A.H., Glinka, G., Lambert, S., “A study of the stress ratio effects on fatigue crack growth using the unified two-parameter fatigue crack growth driving force”, International Journal of Fatigue, 2007, 29, pp. 1616-1633.

Nur Hossain, M. & Taheri, F., “Fatigue and Fracture Characterization of HPDC AM6OB Magnesium Alloy at Cold Temperature”, Journal of Materials Engineering and Performance, 20, pp.1684- 1689, 2011.

Nur Hossain, M. & Taheri, F., “Influence of Elevated Temperature and Stress Ratio on the Fatigue Response of AM60B Magnesium Alloy”, Journal of Materials Engineering and Performance, 21, pp.1395- 1404, 2011.

Parida, B.K. and Nicholas, T., "Effect of Stress Ratio on Fatigue Crack Growth in a Titanium Aluminide Alloy", International Journal of Fracture, 1991, 52, pp. R51-R54.

Paris, P. & Erdogan, F., "A Critical Analysis of Crack Propagation Laws", Journal of Basic Engineering, 85, pp.528- 534, 1963.

Rice, J. R. and Rosengren, G. F., "Plane Strain Deformation near a Crack Tip in a Power Law Hardening Material", Journal of the Mechanics and Physics of Solids, 16, pp. 1-12, 1968.

Rice, J. R., "A Path Independent Integral and the Approximate Analysis of Strain Concentration by Notches and Cracks", Journal of Applied Mechanics, 35, pp. 379- 386, 1968.

Rice, J.R., "Mechanics of Crack Tip Deformation and Extension by Fatigue", ASTM STP 415, pp.247- 311, 1967.

Ritchie, RO, Boyce, BL, Campbell, JP, et al. "Thresholds for high-cycle fatigue in a turbine engine Ti–6Al–4V alloy", International Journal of Fatigue, 21, pp. 653–62, 1999.

Rushton, P.A. & Taheri, F., "Prediction of Crack Growth in 350WT Steel Subjected to Constant Amplitude with Over- and Under- Loads Using a Modified Wheeler Approach", Journal of Marine Structures, 16, pp.517-39, 2003.

Salawu, O.S., "Detection of Structural Damage through Change in Frequency; A Review", Engineering Structures, 19, pp. 718-723, 1997.

Sander, M. & Richard, H.A., "Fatigue Crack Growth Under Variable Amplitude Loading, Prt I: Experimental Investigation", *Fatigue Fract Engng Mater Struct*, 29, pp.291-301, 2006.

Shabanov, A. P., "Mechanism of Fatigue Crack Growth under Compressive External Stresses", Journal of Applied Mechanics and Technical Physics, Vol. 46, No. 6, pp. 861-866, 2005.

Shang, D.- G., Barkey, M. E., Wang, Y., Lim, T. C., "Effect of Fatigue Damage on the Dynamic Response Frequency of Spot-Welded Joints", International Journal of Fatigue, 25, pp. 311– 316, 2003.

Shang. D.-G. and Barkey, M.E., "Analysis of Fatigue Crack Behavior Based on Dynamic Response Simulations and Experiments for Tensile-Shear Spot-Welded Joints", Fatigue Fract Engng Mater Struct, 29, 23–30, 2006.

Sheu, B.C., Song, P.S. & Hwang, S., "Shaping Exponent in Wheeler Model Under a Single Overload", *Engineering Fracture Mechanics*, 51, pp.135-45, 1995.

Shuter, D.M. & Geary, W., "Some Aspects of Fatigue Crack Growth Retardation Behaviour Following Tensile Overloads in a Structural Steel", *Fatigue Fract Eng Mater Struct* , 19, pp.185–99, 1996.

Silva, F. S., "The Importance of Compressive Stress on Fatigue Crack Propagation Rate", International Journal of Fatigue, Vol. 27, pp. 1441-1452, 2005.

Silva, F.S., "Crack Closure Inadequacy at Negative Stress Ratios", International Journal of Fatigue, 26, pp.241- 252, 2004.

Silva, F.S., "Fatigue Crack Propagation After Overloading and Underloading at Negative Stress Ratios", International Journal of Fatigue, 29, pp.1757- 1771, 2007.

Skorpua, M. & Skorpua, A., “Experimental Results and Predictions on Fatigue Crack Growth in Structural Steel”, *International Journal of Fatigue*, 27, pp.1016-28, 2005.

Smith, C. B. and Werely, N. M., “Composite Rotorcraft Flex Beams with Viscoelastic Damping Layers for Aeromechanical Stability Augmentation”, In M^3D III: Mechanics and Mechanisms of Material Damping, Edited by Volfenden and V.K.Kinra. American Society for Testing and Materials, ASTM STP 1304, West Conshohoken, Pa, pp. 62-67, 1997.

Song, P.-S., Sheu, B.-C. & Chang, L., “A Modified Wheeler Model to Improve Predictions of Crack Growth Following a Single Overload”, *JSME International Journal*, 44, pp.117-22, 2001.

Stephens, R. L., Fatemi, A., Stephens, R. R., and Funchs, H. O., “Metal Fatigue in Engineering”, Second Edition, WILEY-INTERSCIENCE, John Wiley & Sons, Inc., Professional/Trade Division, 605 Third Avenue, New York, NY, 10158-0012, 2001.

Suresh, S., “Crack Initiation in Cyclic Compression and Its Application”, Engineering Fracture Mechanics, 21, pp.453- 463. 1985.

Tada, H., Paris, P. C. & Irwin, G. R., “The Stress Analysis of Crack Handbook”, Second Edition, Paris Productions Inc., St. Louis, 1985.

Taheri, F., Trask, D. & Pegg, N., “Experimental and Analytical Investigation of Fatigue Characteristics of 350WT Steel Under Constant and Variable Amplitude Loadings”, *J Marine Struct*, 16, pp.69-91, 2003.

Tur, Y.K. & Vardar, O., “Periodic Tensile Overloads in 2024-T3 Al-Alloy”, *Eng Fract Mech*, 53, pp.69-77, 1996.

Vasudevan, A. K., Sadananda, K., “Analysis of Fatigue Crack Growth under Compression-Compression Loading”, International Journal of Fatigue, Vol. 23, S365-S374, 2001.

Voorwald, H. & Torres, M., “Modeling of Fatigue Crack Growth Following Overloads”, *International Journal of Fatigue*, 13, pp.423-27, 1991.

Walker, K., “The Effect of Stress Ratio during Crack Propagation and Fatigue for 2024-T3 and 7075-T69 Aluminum”, ASTM STP 462, pp.1-14, 1970.

Walker, N. & Beevers, C.J., “A Fatigue Crack Closure Mechanism in Titanium”, Fatigue of Engineering Materials and Structures, 1, pp.135- 148, 1979.

Wason, J. and Heier, E., “Fatigue Crack Growth Threshold- The Influence of Young’s Modulus and Fracture Surface Roughness”, International Journal of Fatigue, 20, pp. 737- 742, 1998.

Watarai, H., Sci. Technol. Trends Quart, Rev. 18, p. 84, 2006.

Wheeler, O.E., “Spectrum Loading and Crack Growth”, Journal of Basic Engineering, 94, pp.181-86, 1972.

Willenborg, J., Engle, R. M. and Wood, H. A., 1971. “A Crack Growth Retardation Model Using an Effective Stress Concept”. Air Force Flight Dynamic Laboratory, Dayton, Report AFFDL-TR71-1, 1971.

Xiaoping, H., Moan, T. & Weicheng, C., “An Engineering Model of Fatigue Crack Growth Under Variable Amplitude Loading”, *International Journal of Fatigue*, 30, pp.2-10, 2008.

Yuen, B. C. K. and Taheri, F., "The Effect of Loading Frequency, Tensile Overload and Compressive Underload on the Fatigue Crack Propagation Behavior of Polymethyl Methacrylate", Polymer testing, Vol. 23, pp. 491-500, 2004.

Yuen, B. K. C. and Taheri, F., "Proposed Modification to the Zheng and Hirt Fatigue Model", Journal of Material Engineering and Performance, 13, pp. 226- 231, 2004.

Yuen, B.C.K. & Taheri, F., "Proposed Modification to the Wheeler Retardation Model for Multiple Overloading Fatigue Life Prediction", *International Journal of Fatigue*, 28, pp.1803-19, 2006.

Zhang J., He, X. D., Sha, Y. and Du, S. Y., "The Compressive Stress Effect on Fatigue Crack Growth under Tension-Compression Loading", International Journal of Fatigue, Vol. 32, pp. 361-367, 2010.

Zhang, J., He, X. D., Suo, B. and Du, S.Y., "Elastic- Plastic Finite Element Analysis of the Effect of Compressive Loading on Crack Tip Parameters and Its Impact on Fatigue Crack Propagation Rate", Engineering Fracture Mechanics, Vol. 75, pp. 5217- 5228, 2008.

Zhang, J., He, X.D. & Du, S.Y., "Analysis of the Effects of Compressive Stresses on Fatigue Crack Propagation Rate", International Journal of Fatigue, 29, pp.1751- 1756, 2007.

Zhang, J., He, X.D., Sha, Y. & Du, S.Y., "The Compressive Stress Effect on Fatigue Crack Growth under Tension-Compression Loading", International Journal of Fatigue, 32, pp.361- 367, 2010.

Zheng X., "A Simple Formula for Fatigue Crack Propagation and a New Method for Determining of ΔK_{th}", Engineering Fracture Mechanics, 27, pp. 465- 475, 1987.

Zheng, J., Powell, B.E., “Effect of Stress Ratio and Test Methods on Fatigue Crack Growth Rate for Nickel Based Superalloy Udimet720”, International Journal of Fatigue, 21, pp. 507-513, 1999.

Zheng, X. and Hirt, M. A., “Fatigue Crack Propagation in Steels”, Engineering Fracture Mechanics, 18, pp. 965- 973, 1983.

APPENDIX A Copyright Permission Letters

A.1. Copyright permission for Chapter 4.

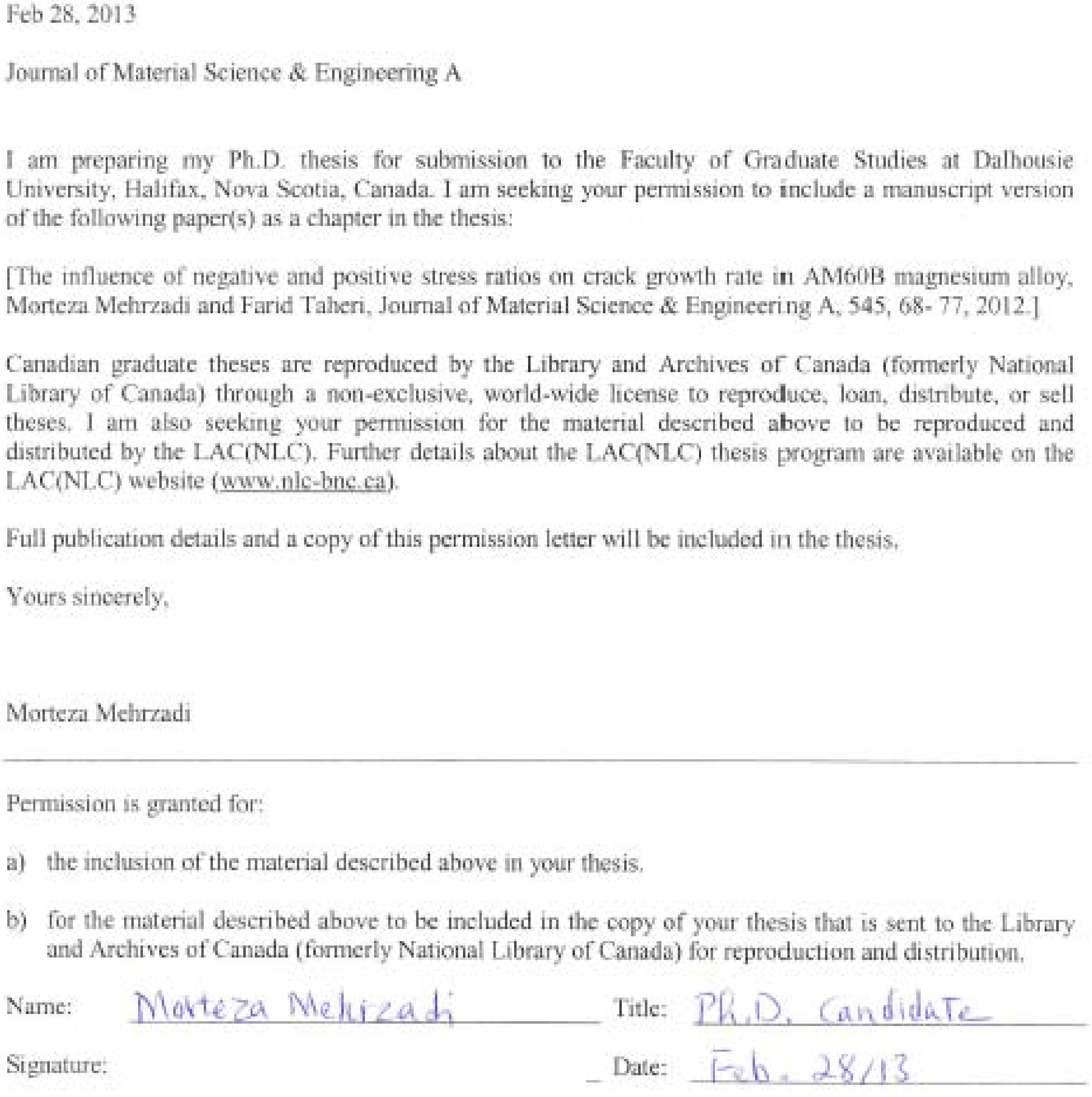

Feb 28, 2013

Journal of Material Science & Engineering A

I am preparing my Ph.D. thesis for submission to the Faculty of Graduate Studies at Dalhousie University, Halifax, Nova Scotia, Canada. I am seeking your permission to include a manuscript version of the following paper(s) as a chapter in the thesis:

[The influence of negative and positive stress ratios on crack growth rate in AM60B magnesium alloy, Morteza Mehrzadi and Farid Taheri, Journal of Material Science & Engineering A, 545, 68- 77, 2012.]

Canadian graduate theses are reproduced by the Library and Archives of Canada (formerly National Library of Canada) through a non-exclusive, world-wide license to reproduce, loan, distribute, or sell theses. I am also seeking your permission for the material described above to be reproduced and distributed by the LAC(NLC). Further details about the LAC(NLC) thesis program are available on the LAC(NLC) website (www.nlc-bnc.ca).

Full publication details and a copy of this permission letter will be included in the thesis.

Yours sincerely,

Morteza Mehrzadi

Permission is granted for:

a) the inclusion of the material described above in your thesis.

b) for the material described above to be included in the copy of your thesis that is sent to the Library and Archives of Canada (formerly National Library of Canada) for reproduction and distribution.

Name: Morteza Mehrzadi
Title: Ph.D. Candidate
Signature:
Date: Feb. 28/13

Dear Dr. Mehrzadi,

We hereby grant you permission to reprint the material below at no charge **in your thesis** subject to the following conditions:

1. If any part of the material to be used (for example, figures) has appeared in our publication with credit or acknowledgement to another source, permission must also be sought from that source. If such permission is not obtained then that material may not be included in your publication/copies.

2. Suitable acknowledgment to the source must be made, either as a footnote or in a reference list at the end of your publication, as follows:

"This article was published in Publication title, Vol number, Author(s), Title of article, Page Nos, Copyright Elsevier (or appropriate Society name) (Year)."

3. Your thesis may be submitted to your institution in either print or electronic form.

4. Reproduction of this material is confined to the purpose for which permission is hereby given.

5. This permission is granted for non-exclusive world **English** rights only. For other languages please reapply separately for each one required. Permission excludes use in an electronic form other than submission. Should you have a specific electronic project in mind please reapply for permission.

6. Should your thesis be published commercially, please reapply for permission.

This includes permission for the Library and Archives of Canada to supply single copies, on demand, of the complete thesis. Should your thesis be published commercially, please reapply for permission.

This includes permission for UMI to supply single copies, on demand, of the complete thesis. Should your thesis be published commercially, please reapply for permission.

Kind regards
Laura

Laura Stingelin
Permissions Helpdesk Associate
Global Rights Department
Elsevier
1600 John F. Kennedy Boulevard
Suite 1800
Philadelphia, PA 19103-2899
T: (215) 239-3867
F: (215) 239-3805
E: l.stingelin@elsevier.com
Questions about obtaining permission: whom to contact? What rights to request?
When is permission required? Contact the Permissions Helpdesk at:

+1-800-523-4069 x 3808 *permissionshelpdesk@elsevier.com*

A.2. Copyright permission for Chapter 5.

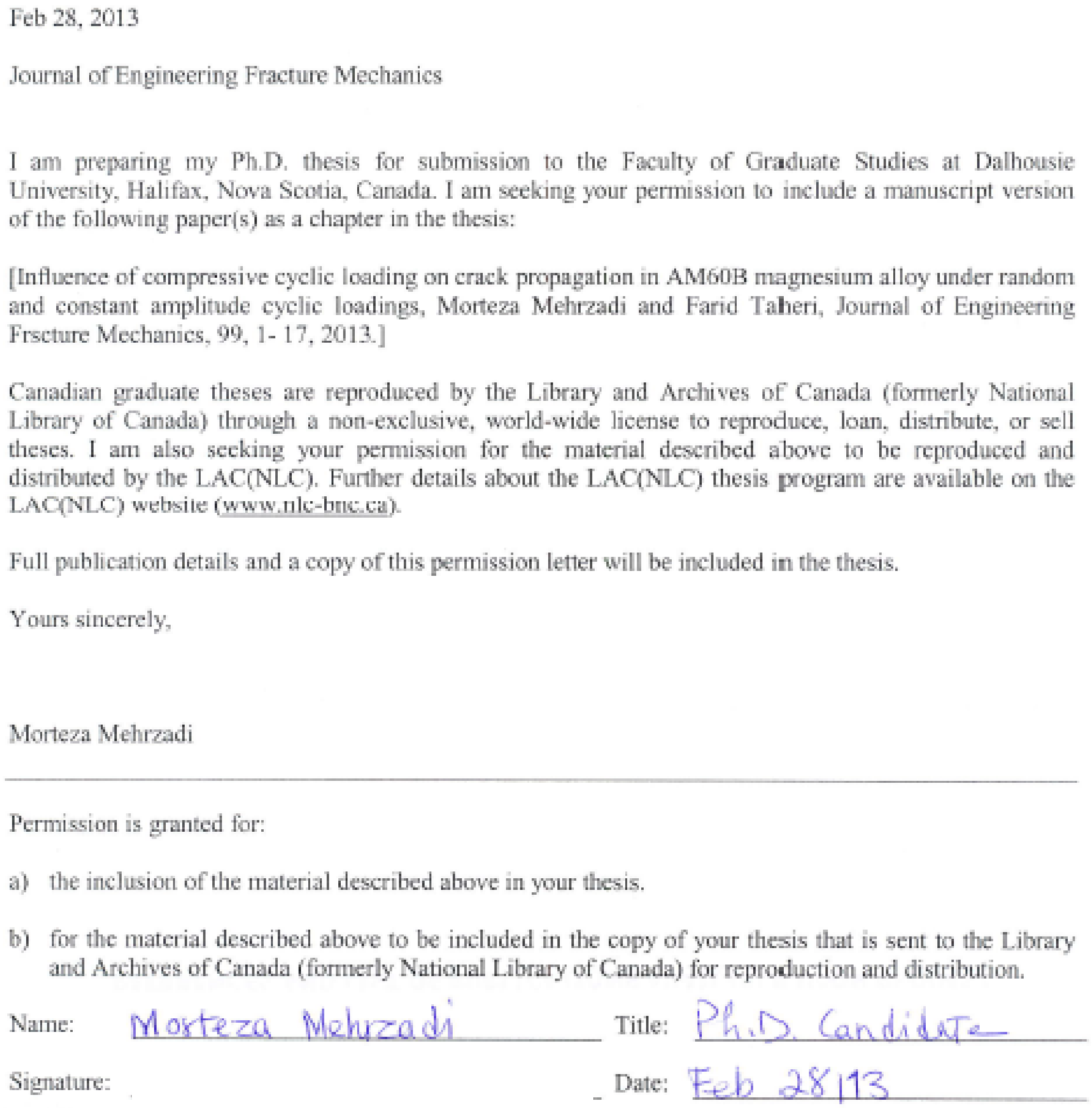

Feb 28, 2013

Journal of Engineering Fracture Mechanics

I am preparing my Ph.D. thesis for submission to the Faculty of Graduate Studies at Dalhousie University, Halifax, Nova Scotia, Canada. I am seeking your permission to include a manuscript version of the following paper(s) as a chapter in the thesis:

[Influence of compressive cyclic loading on crack propagation in AM60B magnesium alloy under random and constant amplitude cyclic loadings, Morteza Mehrzadi and Farid Taheri, Journal of Engineering Frscture Mechanics, 99, 1- 17, 2013.]

Canadian graduate theses are reproduced by the Library and Archives of Canada (formerly National Library of Canada) through a non-exclusive, world-wide license to reproduce, loan, distribute, or sell theses. I am also seeking your permission for the material described above to be reproduced and distributed by the LAC(NLC). Further details about the LAC(NLC) thesis program are available on the LAC(NLC) website (www.nlc-bnc.ca).

Full publication details and a copy of this permission letter will be included in the thesis.

Yours sincerely,

Morteza Mehrzadi

Permission is granted for:

a) the inclusion of the material described above in your thesis.

b) for the material described above to be included in the copy of your thesis that is sent to the Library and Archives of Canada (formerly National Library of Canada) for reproduction and distribution.

Name: Morteza Mehrzadi Title: Ph.D. Candidate

Signature: Date: Feb 28/13

Dear Dr. Mehrzadi,

We hereby grant you permission to reprint the material below at no
charge **in your thesis** subject to the following conditions:

1. If any part of the material to be used (for example, figures) has appeared in our publication with credit or acknowledgement to another source, permission must also be sought from that source. If such permission is not obtained then that material may not be included in your publication/copies.

2. Suitable acknowledgment to the source must be made, either as a footnote or in a reference list at the end of your publication, as follows:

"This article was published in Publication title, Vol number, Author(s), Title of article, Page Nos, Copyright Elsevier (or appropriate Society name) (Year)."

3. Your thesis may be submitted to your institution in either print or electronic form.

4. Reproduction of this material is confined to the purpose for which permission is hereby given.

5. This permission is granted for non-exclusive world **English** rights only. For other languages please reapply separately for each one required. Permission excludes use in an electronic form other than submission. Should you have a specific electronic project in mind please reapply for permission.

6. Should your thesis be published commercially, please reapply for permission.

This includes permission for the Library and Archives of Canada to supply single copies, on demand, of the complete thesis. Should your thesis be published commercially, please reapply for permission.

This includes permission for UMI to supply single copies, on demand, of the complete thesis. Should your thesis be published commercially, please reapply for permission.

Kind regards
Laura

Laura Stingelin
Permissions Helpdesk Associate
Global Rights Department
Elsevier
1600 John F. Kennedy Boulevard
Suite 1800
Philadelphia, PA 19103-2899
T: (215) 239-3867
F: (215) 239-3805
E: l.stingelin@elsevier.com

Questions about obtaining permission: whom to contact? What rights to request?
When is permission required? Contact the Permissions Helpdesk at:

+1-800-523-4069 x 3808 *permissionshelpdesk@elsevier.com*

A.3. Copyright permission for Chapter 6.

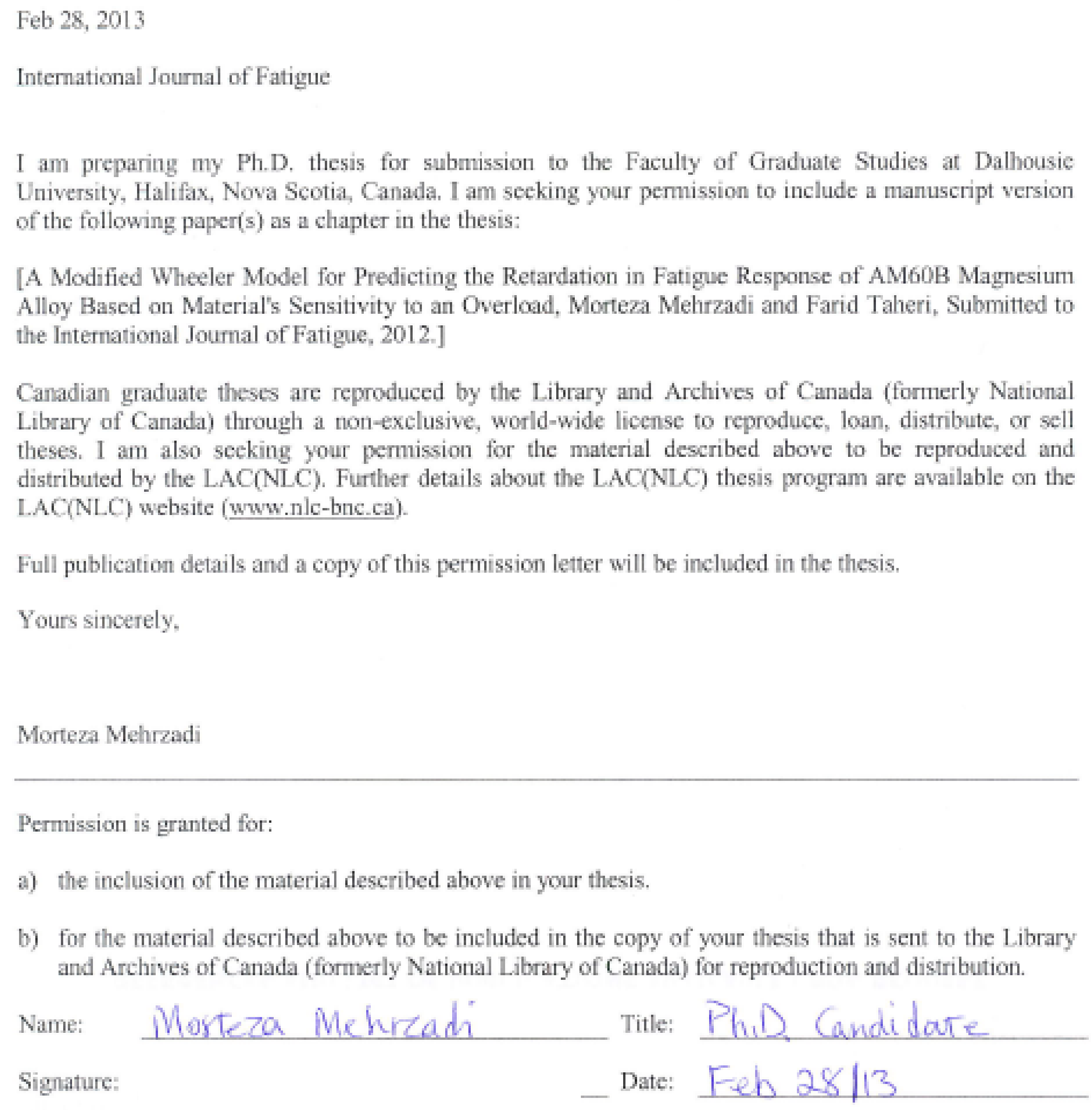

Feb 28, 2013

International Journal of Fatigue

I am preparing my Ph.D. thesis for submission to the Faculty of Graduate Studies at Dalhousie University, Halifax, Nova Scotia, Canada. I am seeking your permission to include a manuscript version of the following paper(s) as a chapter in the thesis:

[A Modified Wheeler Model for Predicting the Retardation in Fatigue Response of AM60B Magnesium Alloy Based on Material's Sensitivity to an Overload, Morteza Mehrzadi and Farid Taheri, Submitted to the International Journal of Fatigue, 2012.]

Canadian graduate theses are reproduced by the Library and Archives of Canada (formerly National Library of Canada) through a non-exclusive, world-wide license to reproduce, loan, distribute, or sell theses. I am also seeking your permission for the material described above to be reproduced and distributed by the LAC(NLC). Further details about the LAC(NLC) thesis program are available on the LAC(NLC) website (www.nlc-bnc.ca).

Full publication details and a copy of this permission letter will be included in the thesis.

Yours sincerely,

Morteza Mehrzadi

Permission is granted for:

a) the inclusion of the material described above in your thesis.

b) for the material described above to be included in the copy of your thesis that is sent to the Library and Archives of Canada (formerly National Library of Canada) for reproduction and distribution.

Name: Morteza Mehrzadi Title: PhD Candidate

Signature: Date: Feb 28/13

Dear Dr. Mehrzadi,

We hereby grant you permission to reprint the material below at no charge **in your thesis** subject to the following conditions:

1. If any part of the material to be used (for example, figures) has appeared in our publication with credit or acknowledgement to another source, permission must also be sought from that source. If such permission is not obtained then that material may not be included in your publication/copies.

2. Suitable acknowledgment to the source must be made, either as a footnote or in a reference list at the end of your publication, as follows:

"This article was published in Publication title, Vol number, Author(s), Title of article, Page Nos, Copyright Elsevier (or appropriate Society name) (Year)."

3. Your thesis may be submitted to your institution in either print or electronic form.

4. Reproduction of this material is confined to the purpose for which permission is hereby given.

5. This permission is granted for non-exclusive world **English** rights only. For other languages please reapply separately for each one required. Permission excludes use in an electronic form other than submission. Should you have a specific electronic project in mind please reapply for permission.

6. Should your thesis be published commercially, please reapply for permission.

This includes permission for the Library and Archives of Canada to supply single copies, on demand, of the complete thesis. Should your thesis be published commercially, please reapply for permission.

This includes permission for UMI to supply single copies, on demand, of the complete thesis. Should your thesis be published commercially, please reapply for permission.

Kind regards
Laura

Laura Stingelin
Permissions Helpdesk Associate
Global Rights Department
Elsevier
1600 John F. Kennedy Boulevard
Suite 1800
Philadelphia, PA 19103-2899
T: (215) 239-3867
F: (215) 239-3805
E: l.stingelin@elsevier.com

Questions about obtaining permission: whom to contact? What rights to request?
When is permission required? Contact the Permissions Helpdesk at:

+1-800-523-4069 x 3808 *permissionshelpdesk@elsevier.com*

A.4. Copyright permission for Chapter 7.

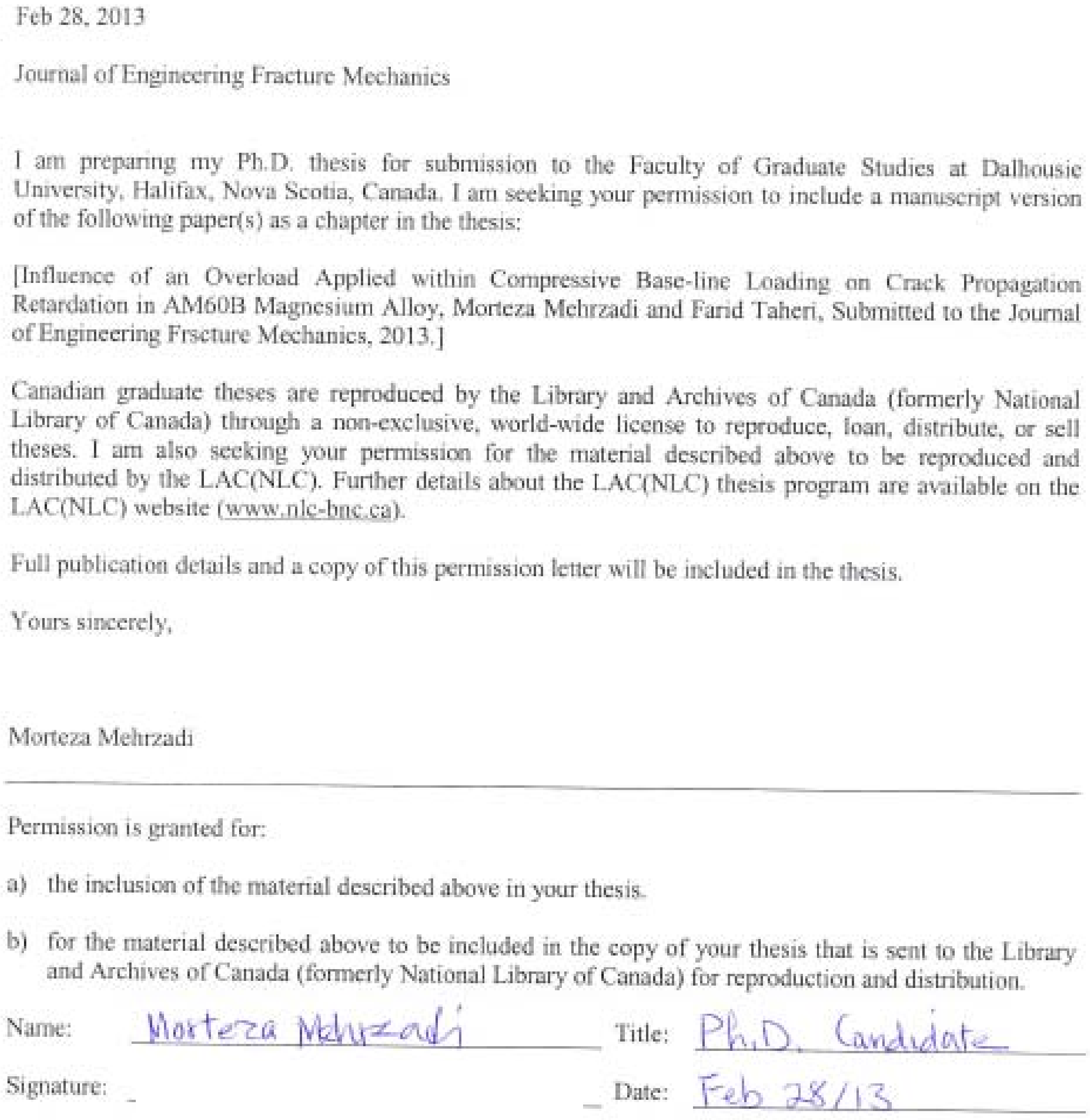

Feb 28, 2013

Journal of Engineering Fracture Mechanics

I am preparing my Ph.D. thesis for submission to the Faculty of Graduate Studies at Dalhousie University, Halifax, Nova Scotia, Canada. I am seeking your permission to include a manuscript version of the following paper(s) as a chapter in the thesis:

[Influence of an Overload Applied within Compressive Base-line Loading on Crack Propagation Retardation in AM60B Magnesium Alloy, Morteza Mehrzadi and Farid Taheri, Submitted to the Journal of Engineering Frscture Mechanics, 2013.]

Canadian graduate theses are reproduced by the Library and Archives of Canada (formerly National Library of Canada) through a non-exclusive, world-wide license to reproduce, loan, distribute, or sell theses. I am also seeking your permission for the material described above to be reproduced and distributed by the LAC(NLC). Further details about the LAC(NLC) thesis program are available on the LAC(NLC) website (www.nlc-bnc.ca).

Full publication details and a copy of this permission letter will be included in the thesis.

Yours sincerely,

Morteza Mehrzadi

Permission is granted for:

a) the inclusion of the material described above in your thesis.

b) for the material described above to be included in the copy of your thesis that is sent to the Library and Archives of Canada (formerly National Library of Canada) for reproduction and distribution.

Name: Morteza Mehrzadi Title: Ph.D. Candidate

Signature: Date: Feb 28/13

Dear Dr. Mehrzadi,

We hereby grant you permission to reprint the material below at no charge **in your thesis** subject to the following conditions:

1. If any part of the material to be used (for example, figures) has appeared in our publication with credit or acknowledgement to another source, permission must also be sought from that source. If such permission is not obtained then that material may not be included in your publication/copies.

2. Suitable acknowledgment to the source must be made, either as a footnote or in a reference list at the end of your publication, as follows:

"This article was published in Publication title, Vol number, Author(s), Title of article, Page Nos, Copyright Elsevier (or appropriate Society name) (Year)."

3. Your thesis may be submitted to your institution in either print or electronic form.

4. Reproduction of this material is confined to the purpose for which permission is hereby given.

5. This permission is granted for non-exclusive world **English** rights only. For other languages please reapply separately for each one required. Permission excludes use in an electronic form other than submission. Should you have a specific electronic project in mind please reapply for permission.

6. Should your thesis be published commercially, please reapply for permission.

This includes permission for the Library and Archives of Canada to supply single copies, on demand, of the complete thesis. Should your thesis be published commercially, please reapply for permission.

This includes permission for UMI to supply single copies, on demand, of the complete thesis. Should your thesis be published commercially, please reapply for permission.

Kind regards
Laura

Laura Stingelin
Permissions Helpdesk Associate
Global Rights Department
Elsevier
1600 John F. Kennedy Boulevard
Suite 1800
Philadelphia, PA 19103-2899
T: (215) 239-3867
F: (215) 239-3805
E: l.stingelin@elsevier.com

Questions about obtaining permission: whom to contact? What rights to request?
When is permission required? Contact the Permissions Helpdesk at:

+1-800-523-4069 x 3808 *permissionshelpdesk@elsevier.com*